DOCTOR OF PHILOSOPHY

From reaction injection moulding to microdevices

Almanza Arjona, Yara Cecilia

Award date:
2008

Awarding institution:
Bangor University

From Reaction Injection Moulding to Microdevices

A study of the feasibility of intensification of polyurethane synthesis by the use of Ink Jet Printing technology

By

Yara Cecilia Almanza Arjona

Thesis submitted to Bangor University in candidature for the degree of Doctor of Philosophy

Bangor University

2008

Preface

The genesis of the work reported in this thesis is slightly unusual. As a graduate Chemical Engineer my interests were in reaction engineering which can be broadly described as that part of chemical engineering which focuses on chemical reactors. On obtaining a British Council/Mexican Government grant to study in the UK my choice was to study polymerisation reaction engineering with the group that specialised in that field in the Interdisciplinary Research Centre in Polymer Science and Technology at the University of Leeds. However, that group was in the process of planning a move to North Wales, the OpTIC Technium and the School of Informatics at Bangor University (BU) where there was a strong research interest in the use of ink jet printing (IJP) technology for the printing of polymer-based microelectronic devices. In anticipation of the arrival of the facilities of the group from Leeds, an interdisciplinary programme was suggested which built on the superficial resemblance between the computer controlled reagent pumping techniques used in polymerisation reaction processes and reactive processing on the macroscopic scale, and the pumping of fluids using piezo electric and other types of pumps in the case of IJP to see whether reactive polymer chemistry could be done on the micro-scale of the IJP Technology. In essence, the proposal was to examine the scale-down of chemical processes rather than scale-up, which is the normal task faced by chemical engineers.

This initial plan became the substance of the work reported in the thesis. Although some macroscopic polymerisation reaction methods were examined, notably, reactive injection techniques, and products were analysed using the facilities in the new laboratories at the OpTIC Technium, the dominant theme of the study has been an attempt to bring together electronics, chemistry and engineering for the development of a micro-scale reactive processing technology.

In order to accommodate the many very different facets of the work carried out, the thesis is divided into six chapters which are self-contained and constructed around specific topics. However, the underlying theme of the thesis as a whole is that of process intensification.

Chapter 1 is devoted to an explanation of what process intensification (PI) is i.e. what does it mean, what is required to achieve it, and why it is important in the

field of chemical engineering. As PI can be applied in numerous processes, the synthesis of polyurethane materials was selected as the focus of PI considerations.

In **Chapter 2** polyurethanes are placed in context, what they are, what their relevance is and what possible applications can arise if their synthetic process is miniaturised. The details of their chemistry and properties are described. This chapter also contains a description of conventional polyurethane synthesis and reaction injection moulding (RIM), a macroscopic scale process with strong similarities to IJP methods.

It is as necessary to quantify the reaction kinetics for the scaling down of process technology as it is for scale-up. **Chapter 3** describes the analytical techniques used to measure the reaction kinetics of polyurethane formation. Obviously, in investigating a process it is crucial to understand the process and the features which might lend themselves to intensification e.g. mixing, reaction kinetics, fluid dynamics, and molecular diffusion. Basic polyurethane synthesis requirements are explored and formulations for micro-scale processes are examined and developed.

The next steps in the scaling down process, the main body of the work carried out, are presented in **Chapter 4.** All the different strategies developed and tested for micro scale reactive polymer production are described and IJP technology is fully explored. This section contains the different IJP systems tested.

As the conventional IJP system available was not well suited for handling reactive polymer chemistry, a new system was designed and built and became the main tool for the generation of the data reported. The description of all considerations taken into account in the design and construction of the new IJP system are contained in **Chapter 5**.

Finally, the whole process of scaling down of PU synthesis is discussed in **Chapter 6**, highlighting the key new information generated in each of the main facets of the work. Conclusions are drawn and compared and the achievements considered in relation to the initial objectives. It became evident that further studies would be desirable and suggestions for further work are presented.

Abstract

Process Intensification (PI) is an aspect of Chemical Engineering devoted to the design of new processes and techniques to reduce equipment size for more efficient product output. This thesis reports the first investigation directed at establishing whether ink jet printing (IJP) technology can be adapted for downscaling the direct reactive processing of polyurethanes (PU). Reaction Injection Moulding (RIM) technology represents an important step in downscaling so that a brief exploration of the RIM approach was undertaken first to identify PI features relevant to IJP technology.

As a prelude to developing the IJP processing technology, the kinetics of the chemical reactions leading to the synthesis of PUs were characterised using a range of methods including gel permeation chromatography (GPC), FTIR and Raman spectroscopy, differential scanning calorimetry (DSC) and dynamic mechanical analysis (DMA). The impact of the initial formulation and process conditions on the microstructure of PU was established. These data served as a guide to the design of PU formulations suitable for both the RIM and IJP experiments.

The Reynolds and Weber numbers of the polypropylene glycol/isopropanol solutions proved to be unsuited to dispensing using the commercial Microdrop Inkjet Printer so that a new, IJP-type, two-stream micro-dispensing system using solenoid valves and incorporating a high-voltage electrode was designed and built. This system allowed the possibility of making two droplets collide in mid-air and to coalesce forming a spherical surface-free microreactor. This novel approach to PI produced good quality droplets of 70%w/w diisocyanate prepolymer solution in tetrahydrofurane (THF) in one stream and 60% w/w of polypropylene glycol in isopropanol in the second, albeit that droplets of the latter were some 30% larger than the former. By simultaneously triggering the reactant streams polyol droplets some 30% larger than the prepolymer droplets were formed. The resulting differences in velocities made it difficult to achieve droplet collision with simultaneous triggering of the two solenoids. However, relatively little further work will be necessary to achieve this final goal.

The reaction between two colliding droplets was simulated by adding a droplet of prepolymer to a polyol droplet in a microassay plate and monitored by FTIR (bulk measurement) and Raman spectroscopy (interfacial measurement) techniques. The half-life for conversion was found to be between 30 and 50 mins. A significant observation was that upon contact, a homogeneous reaction occurred at the interface leading to PU film formation. A mass and heat balance model of the PU chemistry was solved numerically. For equimolar quantities of the reactants in two drops of 100 μm diameter, it was shown that 50% conversion should be achieved in the first 2 s and 98% in approximately 60 s, which is consistent with the spectroscopic data.

Although the final goal of synthesising PU by the mid-air collision of two precursor droplets was not achieved, nevertheless, the study represents significant progress in the process intensification of PU. Key parameters have been identified and new opportunities created for further research in this direction.

Contents

Acknowledgements

This research was sponsored by the British Government through the British Council's Chevening Scheme and the Mexican Government through CONACYT (Consejo Nacional de Ciencia y Tecnología).

I gratefully acknowledge Professor D.M. Taylor for his supervision and support. The assistance received from Dr. Paul Sayers, Mr. Donald Poirot, Mr. John Cambridge and Mr. Iwan Jones in the experimental development of the project at the Electronic Engineering department, has been greatly appreciated. Thanks to Penny Easter for her valuable discussion about spectroscopy.

Thanks to Professor Tony Johnson from the Centre for Advanced Polymers for his supervision and support. I also thank the collaboration of his team in the different locations: Dr. Prasert Khunkamchoo in the Llandygai Unit, Dr. Steve Wong, Mr Rob Ashworth and Ms Sian Roberts at Kinmel Bay Unit and Mr. Jose Juan Mendoza Martinez in the Analytical Services Laboratory at OpTIC Technium.

I want to show gratitude to Penny Dowdney for her support in the writing up of the thesis, to Mr. Alan Kleiman from University of California Santa Barbara for his cooperation in the bibliographic and literature search. Also thanks to Mr. Adrian Walker from EPSRC for the high-speed camera loan and to the LECHE Trust for its financial support.

Finally but not less important, thanks to my family and friends who encouraged me and gave me all their love during this marathon.

I want to show special thankfulness to my husband Jose Juan, who I dedicate this PhD to: thanks for believing in this dream, Maktub!.

Thanks to all for their generous support in this research.

Chapter 1. Introduction

1.1. Process Intensification

Process Intensification (PI) is a relatively new area of research in the field of Chemical Engineering. The first PI concept was originally defined by Ramshaw from the New Science Group, part of Imperial Chemical Industries (ICI), Runcorn. It was based on the design and generation of new techniques to reduce process plant size by "reconsidering the concepts upon which the individual unit operations are based" (Ramshaw, 1983). At the opening of the 1st International Conference on PI Ramshaw stated that PI "is the strategy of making dramatic reductions in the size of a chemical plant in order to reach a given production objective" (Ramshaw, 1995). At this early stage, PI was aiming to reduce the reactor volume by a factor >100, to be able to secure the planned impact on cost. Basically, PI is the evolution of the methods that chemical engineers have developed over the last century to improve the efficiency of processes. Even though the driving force for "shrinking" the process at the outset was mainly cost reduction. Other potential benefits included significantly safer, compact processes that would bring reduced energy use and sustainability. It would also decrease capital expenditure and result in environmental advantages such as reduced waste production. Several authors suggest that more research needs to be conducted in order to assess the real economic feasibility of PI and to ascertain the benefits and challenges that PI brings to the chemical and materials industry (Etchells, 2005; Gogate, 2008; Deshmukh et al., 2007).

Nevertheless, more interest was paid to the application of PI by the chemical industry and many authors suggested wider definitions that are not only expressed in terms of miniaturisation. On the one hand, Stankiewicz et al. (2000) offered the concept of PI as "the development of novel apparatuses and techniques … that are expected to bring dramatic improvements in manufacturing and processing, substantially decreasing equipment-size/production-capacity ratio, energy consumption, or waste production, and ultimately resulting in cheaper, sustainable technologies". In short "any chemical engineering development that leads to a substantially smaller, cleaner, and more energy-efficient technology is Process

Intensification" (Stankiewicz, 2000). On the other hand, Moulijn et al. (2008), make a distinction between PI as an objective and as a scientific skill area. Although the meaning of process intensification has been evolving and authors have added more attributes to the concept, this thesis focuses on the original Ramshaw idea. Within this definition, this research agrees that PI entails the development of new equipment design and methods by understanding and rethinking the process as a whole.

PI was primarily created to describe the intensification of mass transfer characteristics of rotating packed beds used to perform distillation and absorption (Ramshaw, 1983). With time, PI has widened its applications in numerous directions, guiding important developments of novel equipment and methods (Figure 1.1).

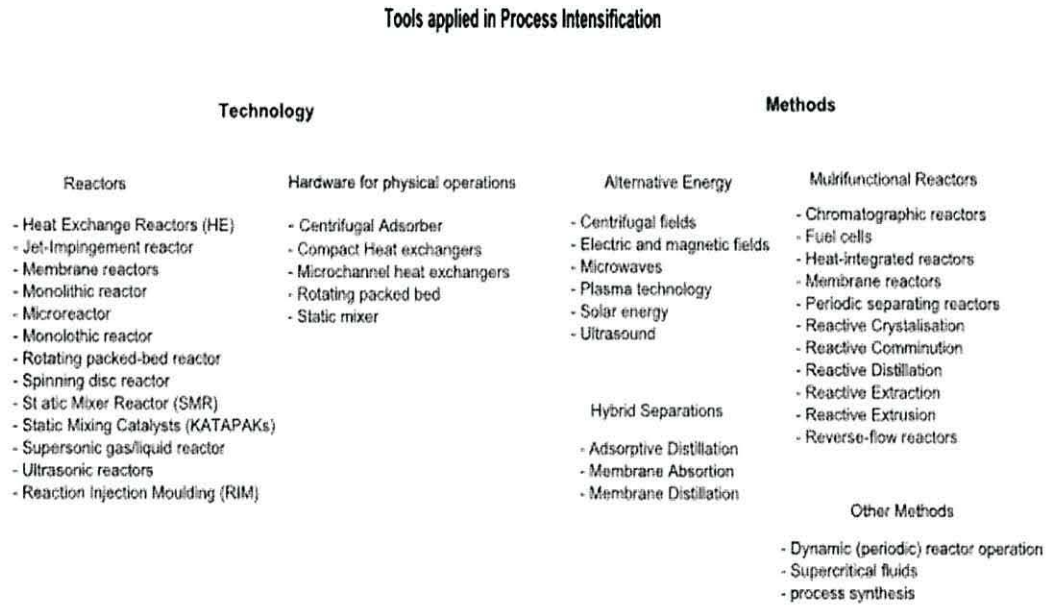

Figure 1.1 Novel technology and methods used as tools in Process Intensification. Based on (Keil, 2007; Stankiewicz, 2000).

Process Intensification pays attention to processes especially involving chemical reactions, separations, heat and mass transfer and phase transition (Jachuck et al., 1997). The matter of this thesis focuses on how PI can be applied in polymerisation reaction engineering and the technology that can contribute to it, e.g. microreactors.

Microreactor was a term that at first referred to small tubular reactors used in research, but with new technology advances, it now refers to microfabricated systems comprising of several micro-channels with diameters in the order of 10 – 100 μm

(Jensen, 2003) . Microreactors are the most extreme application of PI. On a very small scale, different processes take place, such as heat exchange, mixing, separation or catalytic reactions. The developments in microreactors are increasing dramatically, and several methods for increasing their productivity have been tested.

For example, Okamoto et al. (2004) explored a planar pumping microreactor for an addition reaction of phenylisocyanate and ethyl alcohol in toluene at equimolar concentrations. The reaction field was 200 μm thick, 50 mm wide and 110 mm long and composed of two layers. A 10 μm thick stainless steel splitter plate was inserted to stabilise the laminar flow from the inlet. The reaction yield using the microreactor was 10% greater for the same residence time than that in conventional batch process using a mechanical stirrer. The reactants were diffusively mixed in laminar flow by the large surface to volume ratio. The authors argued that the time required for mixing based on molecular diffusion, is proportional to the square of the characteristic length scale. Reducing the reactor size to half, the mixing time is a quarter of that originally required. Therefore, the quick homogenisation would make possible the production of high quality chemical products (Okamoto et al., 2004).

Obviously, microreactors have selected applications, mainly in research and in the production of speciality chemicals (e.g. relatively low production volume with high added-value end-products).

Other relevant tools for the intensification of polymerisation reactions include spinning disc reactors (SDRs) and Reaction Injection Moulding (RIM). In traditional processes, the efficiency of conventional stirred tank reactors drops off as the polymerisation proceeds, because the viscosity of the reactive mixture increases. Subsequently, mixing and mass transfer difficulties arise, but dilution with solvents and increasing reacting mixture temperature in the reactor to reduce viscosity are unattractive solutions. This is when SDRs and RIM become important tools for Process Intensification in polymerisation reaction engineering.

On the one hand, the rotational disc reactor synchronises the chemical kinetics of a reaction and the fluid dynamic intensity within the reaction space. This type of reactor generates a highly-sheared thin liquid film on the surface of a rotating disc, where the heat and mass transfer rates are accelerated. This enhancement is due to the short conduction and diffusion path lengths, which is a key attribute for processing

viscous liquids (Ramshaw and Cook, 2006). However, it is necessary to employ extremely accurate feed pumps to dispense the precise, optimum stoichiometry across the whole disc surface where the reaction takes place. This technology has been applied in the manufacture of polystyrene, where higher mass and heat transfer than a conventional batch reactor have been achieved (Boodhoo et al., 1995). However, the formulations employed had to be re-designed for the disc conditions because formulations for batch reactors were designed for different process conditions. On this basis, polymerisation reactions can be designed to be efficiently processed in SDRs.

On the other hand, Reaction Injection Moulding is a well established reactive method for processing polymers. It is based on the precise injection of reactants into a device where jet impingement mixing takes place. Then the reactive mixture is delivered into a mould where polymerisation takes place. This process is the starting point of this research work and it is explained in more detail in Chapter 2. RIM has been mainly applied to produce polyurethanes (PU), (Dawood, 1994), and the relevance of downscaling even more their synthesis is discussed in the following section.

1.2. Polyurethanes

The PU industry was created in the late 1930's when Otto Bayer developed polyurethanes suitable for coatings, fibres, adhesives and foams. In the late 1950's PU applications moved to the production of foams and the building of aircraft parts and seating. Elastomeric fibres, known as Spandex and Lycra, were introduced to the market in the 1960's (Reisch, 1999), whereas rigid foams were used for isolation in refrigerators and in buildings on the 1970's. At that time, the industry was led by Bayer and BASF in Germany, ICI in the UK, Dow Chemical and Upjohn Polymer Chemicals in the USA, and Mitsui in Japan (Grieve, 2003). In 2002, Bayer Polymers claimed to be the principal supplier in the polyurethane industry with sales worth €10.8 M in 2003. Currently, the most common industrial applications of polyurethanes include production of interior parts for cars such as spare wheel covers, sliding roofs and the trunk floors of the Audi A4 and Daimler Chrysler E Class station wagon (Bayer, 2003), adhesives, binders, coatings, paints, cushion materials, construction insulating

materials, soles and uppers of footwear, and computer housings to mention some (Woods, 1990).

Commodity polymers were being produced from simple starting compounds and were inexpensive and used in large amounts. The market for commodity polymers faced difficult conditions at the beginning of the 1980's (Allen, 1987), and drove the industry to refine their specifications in order to gain competitiveness. Research led to the emergence of new products with better control of properties and microstructure. For instance, fibre-reinforced polymer composites incorporated polyurethane foamed structures to improve the control of their macroscopic structure. By that time, it was forecast that future research and development of polymers was going to be focused on self-orienting polymers, thin films with new optical and electronic properties for applications in microelectronics and conducting polymers.

This was the beginning of the development and evolution of more advanced products, with good engineering properties and new applications. These speciality polymers, even though produced in low volume, contributed 25% of profits in 1984 and from then on, the growth of speciality polymers doubled that of commodity polymers (Allen, 1987). In 2003, Bayer Polymers reported that approximately two-thirds of its portfolio was commodity products and one third speciality products. In the past five years, it has been recognised that the chemical commodity industry in the UK has come under rising pressure from competition by economies like China and India. There are reports that confirm that the UK based industry is moving away from commodity products towards the production of low volume but high added-value speciality chemicals. It has been reported that "major industry players believe that if the UK industry is to survive then companies need to move on from this traditional approach to manufacturing and thus imbue the industry value streams with increased agility" (Burgess et al., 2002).

Speciality polyurethane products have been developed, and some special applications include the fabrication of membranes and coatings which are biocompatible with living tissues and body fluids such as blood (Król and Pilch-Pitera, 2003b). Since PUs have good physical and mechanical properties, and because they have good tissue and blood compatibility, they have been widely used in optics, electronics and biomaterials (Liu et al., 2005; Reynolds et al., 2004). They are capable

of housing micro-sensors and biosensors, able to detect (bio)molecules and be implantable inside the human body (Acharya et al., 2004; Joung et al., 2001). This type of polyurethane is essentially a pharmacologically inert material designed for implantation in the living system and is continuously or intermittently exposed to body fluids, the ultimate aim being restoration of natural living tissues and organs in the body (Acharya et al., 2004). After almost 50 years of use in the health field, this polymer family remains one of the most popular groups of biomaterials used in medical devices. Their popularity has been sustained as a direct result of their segmented block copolymeric character which endows them with a wide range of versatility in terms of tailoring their properties including blood and tissue compatibility. Biomedical applications are blood-contacting and involve implantable devices such as catheters, blood pumps, heart valves, insulation of pacemakers, vascular grafts, artificial heart-assisting devices, vascular prostheses, and *in-vivo* sensors (Reynolds et al., 2004).

Moreover, polyurethanes have been found to be suitable for the construction of miniaturized sensors, as a polymeric matrix or as membranes. Recent publications confirmed the success of the use of these materials as ion-selective electrode (ISE) membranes in sensors, for example in the construction of fluoride-selective sensors with membranes using a polyurethane as the polymeric matrix (Górski and Malinowska, 2005). To date, polyurethanes have attracted particular interest in the manufacture of all-solid state electrode (ASSE) type disposable pH sensors, where the polymeric membrane matrix is PU based (Joung et al., 2001). Other pH sensors are fibre-optic-based fabricated using a PU resin which entraps a pH indicator that undergoes a colour change in the presence of ammonia (Moreno et al., 2005).

It is now evident that all these new advances in sensors and devices based on polyurethanes are leading to the design of novel applications, and more research is needed to contribute to the fabrication of microdevices based on polyurethane materials.

1.3. Motivation

Initially microreactor research focused on ascertaining suitable fabrication/assembly techniques and adequate materials, based on the success in fabricating microdevices such as Microelectromechanical (MEM) Systems (Kock et al., 2007).

Microfabrication techniques play a crucial role in the properties and cost of devices. Furthermore, it is vital that the properties of the microdevices lie within the specified quality standards in order to provide good performance for which they have been designed. Of particular concern in the fabrication of micro and nano devices, are the accuracy and reproducibility of the technology used for their fabrication. These processes are known to include lithography, photolithography, etching techniques (including plasma, wet and reactive ion), physical and chemical vapour deposition, laser micromachining, moulding, and many others (Saliterman, 2006; McCreedy, 2000; Ziaie et al., 2004). In the past few years Ink Jet Printing (IJP) technology has also been employed for the fabrication of microdevices and printing of functional materials (Chou et al., 2007; Calvert, 2001b; Sirringhaus and Shimoda, 2003; Xue et al., 2006; Pede et al., 1998). This type of microfabrication technique was chosen as the tool for the miniaturisation of polyurethane synthesis in this research, and a detailed description can be found in Chapter 4.

Materials used for the fabrication of microdevices are as important as the microfabrication techniques because the properties of the materials will determine how they will be processed. Commonly used materials include metals such as gold, silver and aluminium. Also materials like silicon, glass, ceramics and a variety of polymers, such as hydrogels have been employed (Saliterman, 2006; Biswal and Hilt, 2006). Microreactors have been fabricated of wafer-grade silicon and a special-purpose photo-structured glass (known as FOTURAN). It is lithium-aluminium-silicate based and is useful for creating microchannels (Mills et al., 2007).

Microfabrication techniques and materials are essential tools for the fabrication and development of devices and their performance for specific applications. For instance, since the late 1970s when silicon technology expanded to include the machining of MEMs, the development of micro-actuator devices such as micro pumps, microvalves and sensors has become possible (Nguyen and Werely, 2002).

Furthermore, polymer-based electronic parts such as solar cells, transistors, microgrippers, springs, microspacers, micropositioners, microrappers, microswitches and microrelays have been reported (Fu et al., 2004). Certainly, microdevice-development and new microtechnologies, are emerging rapidly. Areas such as electronics, optics (Chou et al., 2007; Yang et al., 2007), life sciences (Tanaka et al., 2007; Chovan and Guttman, 2002; Willner et al., 2007; Elman et al., 2008), chemistry (Ghafar-Zadeh et al., 2008; Biswal and Hilt, 2006) and medicine (Vo-Dinh et al., 2001; Stieglitz, 2001; Cheung and Renaud, 2006; Meyer, 2002) are benefited the most. Also, precise drug delivery is achievable by implantable and transdermal techniques by the use of microdevices (Nisar et al., 2008; Hilt and Peppas, 2005; Ahmed et al., 2002).

Figure 1.2 shows different examples of microdevices. Image (a) illustrates TiNi/Si microgrippers with cantilever structure with out-of-plane bending mode that has been fabricated using ultra-fast pulsed excimer laser micromachining. In Figure 1.2b, a packed-bed microreactor is shown, where the gas-liquid inlet sections are on the left, and the catalyst support grid and exit are on the right. In this microreactor, the catalyst is introduced through the large wing sections. Optical fibres are the vertical lines used for species monitoring. Micrographs inserted on the right and left-hand side depict the inlet and exit sections, respectively, with openings 30 μm wide and 300 μm deep. Figure 1.2c is a photograph of a multichannel reactor and Figure 1.2d is a photograph of an electrokinetic plate with fluidic chambers.

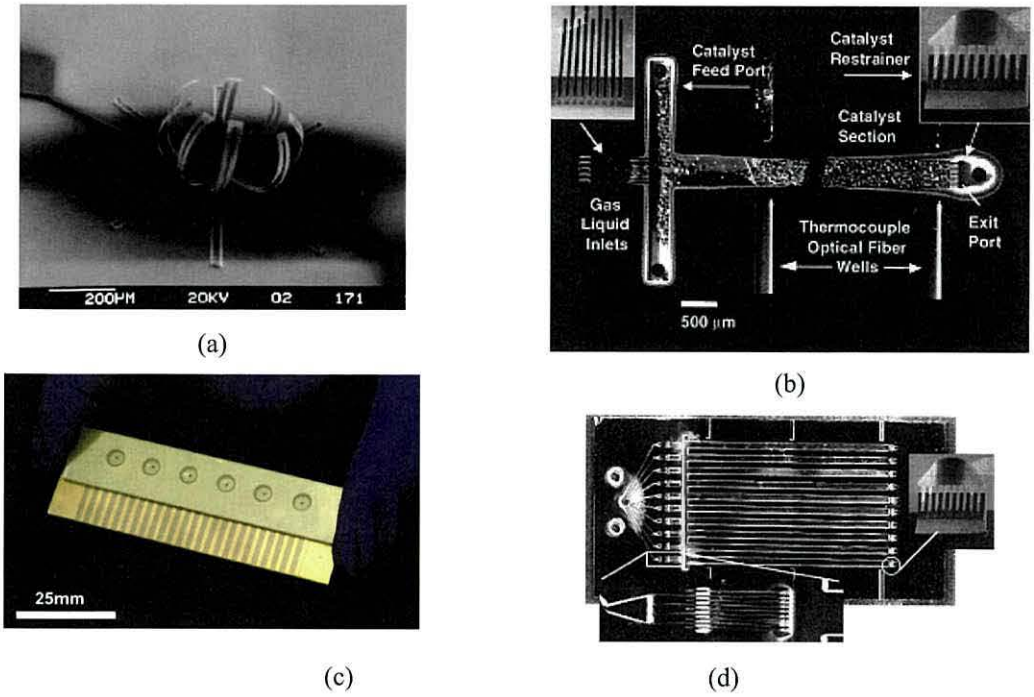

Figure 1.2 (a) microgripper (Fu et al., 2004), (b) packed bed reactor with active carbon catalyst (Jensen, 2001), (c) photograph of a completed electrokinetic microtitre plate with fluidic chambers (Burt et al., 2007) and (d) photograph of a multichannel reactor (Jensen, 2001).

From all these innovative applications, commercial success and financial benefits are expected. Figure 1.3 shows estimated sales of microfluidic devices and MEMs in 1999 (Nguyen and Werely, 2002).

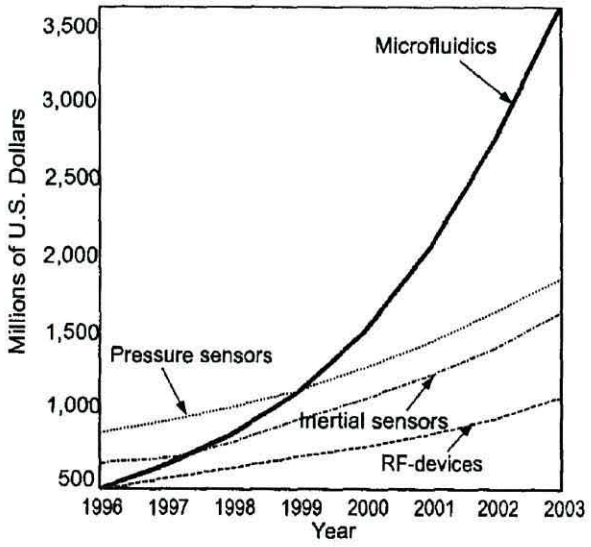

Figure 1.3 Estimated sales of microfluidic components, 1999 (Nguyen and Werely, 2002).

The progress and innovation achieved in the polyurethane field leads now to the development of smart multi-layered micro-sensors composed of functionalized polyurethane (PU) layers. For implantable drug delivery and diagnosis devices, it is essential to use materials compatible with human blood and tissue. Polymers such as hydrogels and polyurethanes (PU) are polymers with properties that make them suitable for implantation in the human body. As such, they have excellent potential for the fabrication of implantable sensors and devices for biomedical applications (Liu et al., 2005; Hwang and Meyerhoff, 2008; Schwartz and Bahadur, 2007; Tuominen et al., 2007). The possibility that the miniaturisation of PU synthesis can lead to the development of new polyurethane-based microdevices motivates the research presented in this thesis.

In order to achieve this end, the in-situ micro-synthesis of PUs is essential. A few studies have been undertaken in this direction (Ramanathan et al., 1998; Okamoto et al., 2004; Hessel et al., 2005; Becker and Locascio, 2002), but more work is required in order to scale-down the polymerisation process. As mentioned in section 1.1, one of the main requirements for the miniaturization of reactive systems is the extremely precise pumping and efficient mixing of the reactants. What is needed is a technology capable of dispensing accurately small quantities (~μL), and to ensure at the same time the reproducible deposition of several spots of reacting material in a small area (few mm^2), that will allow the fabrication of microdevices. Hence, the aim of this research is to evaluate the feasibility of down scaling polyurethane synthesis using Ink Jet Printing Technology. Several questions arise from this idea:

- ◊ Can IJP technology be used to miniaturise PU synthesis?
- ◊ What are the processes involved?
- ◊ What are the key factors that control the micro-scale chemistry?
- ◊ Is IJP robust enough to be tailored to the chemistry of PU?

The answers to these questions drive the exploratory studies conducted in this research and create an opportunity for novel application of polyurethanes e.g. to build smart-devices such as wound dressing materials or multilayer sensors as depicted in Figure 1.4.

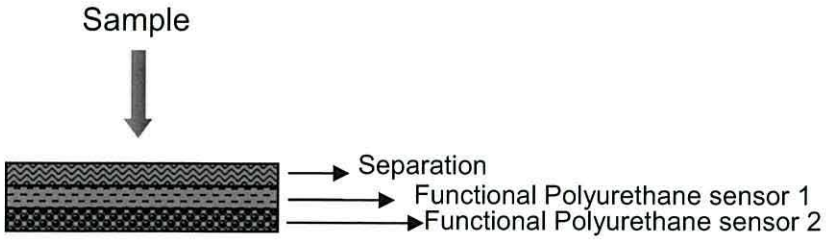

Figure 1.4 Potential multilayered sensor with functionalized PU layers which will react and produce a change in properties (e.g. colour).

The suggested smart sensor is comprised of several layers, which can be functionalised or designed to have different properties. The different polyurethane-film layers are required to separate the sample, and in subsequent layers several detection mechanisms can take place, such as a physical or chemical change that could work as a sensor.

1.4. Aims and Objectives

This thesis seeks to study if a further step can be achieved by moving from the current RIM technology to an even smaller scale production of speciality polyurethane products. Ink Jet Printing Technology is potentially an important tool for achieve it. As little research has been conducted in this direction, an outstanding opportunity has opened up for the intensification of this step-polymerisation reaction. For that, it is necessary to undertake interdisciplinary research because the different fundamental sciences bring new angles and ideas.

Within the adopted concept of Process Intensification, the ultimate aim of this research was to explore the feasibility of the miniaturisation of PU synthesis using IJP technology, with an interdisciplinary approach. This aim was achieved by focusing on the following specific objectives:

› Characterise and monitor traditional polyurethane chemistry using state-of-the-art technology to understand polyurethane synthesis and ascertain the impact of any changes in process conditions and formulations.

- Examine the relevance and impact of stoichiometry and mixing requirements in polyurethane formulations.
- Compare the traditional batch reactor process with the already intensified process of Reaction Injection Moulding.
- Identify process practicalities, similarities and differences between Reaction Injection Moulding and Ink Jet Printing.
- Adapt polyurethane formulations of known properties suitable for Reaction Injection Moulding and Ink Jet Printing processes.
- Investigate reaction kinetics needed to obtain fast polyurethane reactions when using IJP.
- Suggest possible behaviour in microscale polyurethane synthesis in terms of mass and energy balances.
- Gain sufficient understanding of Ink Jet Printing fundamentals and evaluate the drop formation mechanism of the reactive liquids needed for the polyurethane synthesis.
- Identify limitations of available IJP technology for its use in the polyurethane reactive process, and examine alternative methodologies.
- If necessary, build and evaluate a new IJP system.
- Ascertain the effect of the IJP microprocess in the control of stoichiometry and mixing in the reactive process of PU.

Chapter 2. Polyurethanes

In this chapter is presented a brief review of the theoretical concepts needed to fully understand the synthesis and processing of polyurethanes (PUs). The step-grow polymerisation mechanism and the kinetics of PU formation are described. The importance of reactant stoichiometry for the synthesis of high molecular weight PUs is highlighted.

2.1. Polymerisation Chemistry

2.1.1. Reaction Mechanism: Step-growth polymerisation

Polyurethanes (PUs) can either be thermoplastic or thermoset materials that form a class of industrially useful materials due to the range and excellence of the properties which can be achieved (Rajendran et al., 1982). This type of polymer contains urethane (carbamate) linkages in the main polymer chain. The carbamate repeat unit shown below is the defining characteristic of PUs.

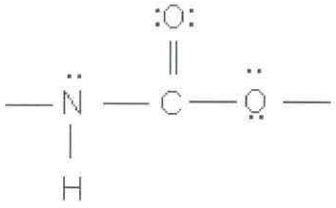

Polyurethanes are formed by the exothermic reaction of di-isocyanates and polyfunctional compounds containing several hydroxy-groups shown in Scheme 2.1:

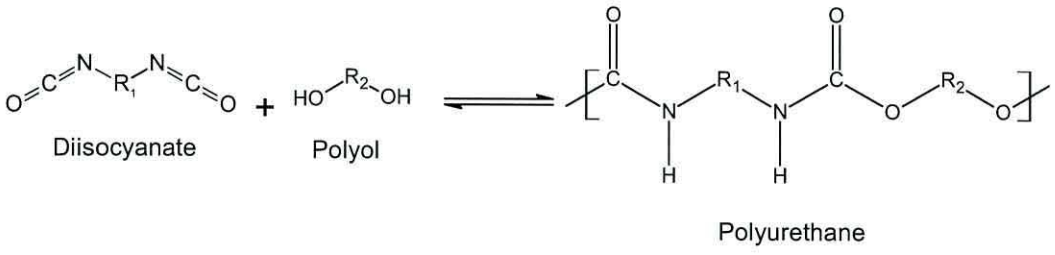

Scheme 2.1

It is a spontaneous addition reaction, chemically efficient because no un-wanted by-products are given off and the raw materials react completely (when the equilibrium is in favour of polymer formation). In principle, no other cure treatment by post reaction heating is necessary but the reactions are often quenched as a result of phase

separation arising from the high viscosity developed during reaction. Isocyanate groups are susceptible to side reactions if the reaction temperature is taken much above 100^0C. The reactivity of the isocyanate group depends on the electronic charge distribution, which in turn is dependent as well on the groups attached to the isocyanate moiety. The resonance structure of the isocyanate is shown in Scheme 2.2:

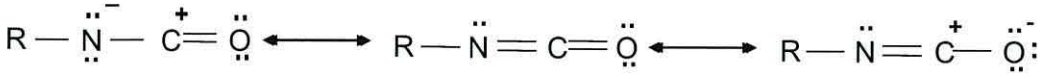

Scheme 2.2

The NCO group is reactive due to the carbon-nitrogen double bond, a feature which leads to a large number of possible ionic addition reactions with several reagents containing active hydrogen atoms such as water, amines, alcohols, phenols, carboxylic acids and thiols. Scheme 2.3 shows that the reaction between water and diisocyanate produces carbon dioxide, which is liberated and forms foams. In some cases, this reaction is promoted with controlled stoichiometry to produce polyurethane foams.

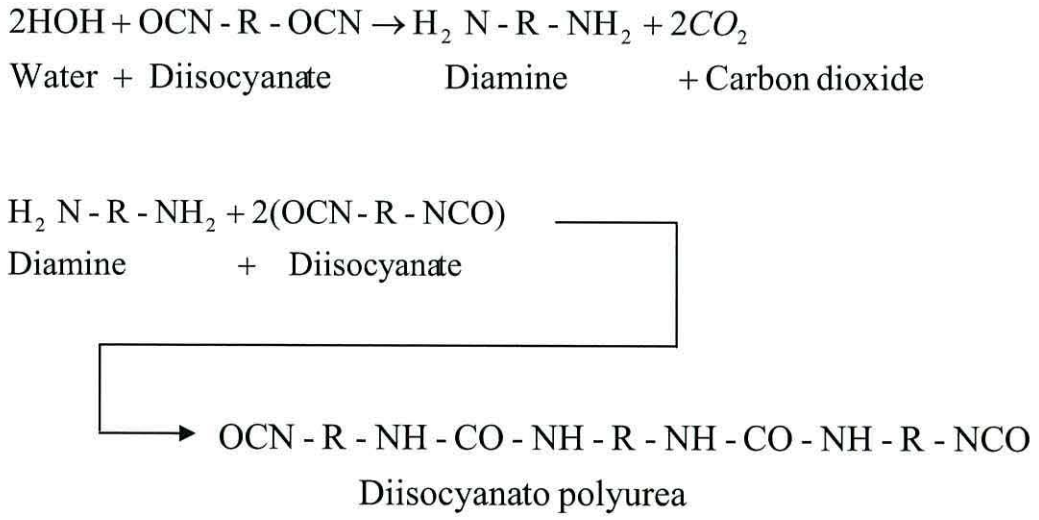

Scheme 2.3

Consequently, to avoid contamination with water and ambient moisture the reactants should be dried and be free of other contaminants. Most polyols employed in PU manufacture are hygroscopic, so any contact of the material with moisture should be prevented. It is important to emphasise that the precise control of water content in polyols and diisocyanates is crucial, because even a small variation will lead to major

damage to the properties of the end product (1 part of water will react with 10-14 parts of diisocyanate approximately).

2.1.2. Thermodynamics

The polymerization reaction will only proceed if it reduces the Gibbs free energy G of the system, i.e. if the change in Gibbs free energy ΔG is negative, where:

$$\Delta G = G_{pol} - G_{mon} \quad (2.1)$$

and G_{pol} and G_{mon} are the Gibbs free energy of the polymer and monomer respectively. Thus a spontaneous chemical reaction will occur while G goes to a minimum value. As the reaction progresses, there is a change in composition of the reaction mixture that changes the Gibbs energy of the system. This change is commonly written as a function of the chemical potential (μ) of the species in the reactive mixture (Atkins, 1994). Accordingly, polymerisation will occur spontaneously as long as the chemical potential of the monomer is larger than that of the polymer formed (i.e. the reaction product).

At constant absolute temperature T, it is further known that: $\Delta G = \Delta H - T\Delta S$, where ΔH and ΔS denote the changes in enthalpy and entropy, respectively, upon conversion of a monomer into a polymer base unit. The enthalpy change ΔH equals the negative of the heat of reaction. If $\Delta G > 0$, depolymerization will occur, while $\Delta G=0$ denotes chemical equilibrium, where the rates of polymerization and depolymerization are equal. Based on these facts, there will be different situations depending on the sign of ΔH:

If $\Delta H < 0$, an exothermic polymerization will take place:

for $\Delta S < 0$, polymerization is possible if $T|\Delta S| < |\Delta H|$

for $\Delta S < 0$, polymerization is not possible if $T|\Delta S| > |\Delta H|$

for $\Delta S < 0$, the polymerization exhibits a so-called ceiling temperature $T_c=\Delta H/\Delta S$

As a rule, $\Delta S < 0$ upon polymerization, because *n* separate monomer molecules can be arranged in a larger number of distinguishable ways than *n* monomer residues connected together in a single chain. This means that most polymerisations must be exothermic and should be performed below T_c. If the temperature rises above T_c, then

depolymerisation starts from reactive chain ends. So, when polymerizing just below T_c care should be taken to remove the heat of reaction.

2.1.3. Reaction Kinetics and Catalysis

As explained in section 2.1.1 the synthesis of PUs takes place as a step-growth polymerisation. So far the reaction has been described without considering the time scale in which the process occurs. The reaction kinetic model predicts the length of time required for the reaction to proceed to a particular extent.

The essential assumption of equal reactivity needed to explain step-growth polymerisation kinetics in a simple model, was proposed by Flory (1971). The principle introduced, namely "the reactivities of all like functional groups are equal to each other, irrespective of the size of the polymer molecules to which they belong". Thus it is sufficient to consider only one rate constant k for all propagation steps and possibly also one value k' for the depolymerization in reversible reactions. Hence, the reactivity of a functional group does not change if a neighbouring group has reacted, and that the reactivity becomes independent of the presence of a second group in the same molecule if the groups are separated by at least three CH_2- units. So, considering the reaction of polyurethanes shown in Scheme 2.1, the reaction rate can be expressed in terms of the concentration of NCO groups and OH groups as follows:

$$-\frac{d[NCO]}{dt} = k[NCO]^a[OH]^b \qquad \textbf{(2.2)}$$

where NCO and OH are the concentration of isocyanate and hydroxyl groups, respectively. Accordingly, the exponents a and b are the order of the reaction with respect to NCO and OH components respectively. If the reactants are initially present in stoichiometric ratio (e.g. $[NCO]_o = [OH]_o$), the fraction of functional groups which has reacted is given by:

$$\alpha = \frac{[NCO]_O - [NCO]_t}{[NCO]_O} = \frac{[OH]_O - [OH]_t}{[OH]_O} \quad . \qquad \textbf{(2.3)}$$

The subscripts o and t indicate the time at which the concentrations are considered, i.e. at times 0 and t. Combining equations 2.2 and 2.3:

$$\frac{d\alpha}{dt} = \frac{k}{[NCO]_o}\{[NCO]_o(1-\alpha)\}^a\{[OH]_o(1-\alpha)\}^b \quad . \qquad \textbf{(2.4)}$$

Considering a stoichiometric ratio of 1, and that the exponents a=b=1, e.g. an overall second order reaction, then equation 2.4 can be simplified to yield:

$$\frac{d\alpha}{dt} = \frac{k}{[NCO]_o}([NCO]_o(1-\alpha))^2 \quad . \qquad \textbf{(2.5)}$$

Integrating subject to the boundary condition that $\alpha = 0$ at time $t = 0$ yields:

$$\frac{1}{[NCO]} - \frac{1}{[NCO]_O} = kt \quad . \qquad \textbf{(2.6)}$$

If the constant k is known, then equation 2.6 provides a simple approach for calculating the time required to achieve a specific degree of polymerisation in any specified system. For instance, the half-life is given by:

$$t_{1/2} = \frac{1}{[NCO]_O k} \quad . \qquad \textbf{(2.7)}$$

It is important to highlight here the fact that reactions used to produce PUs are usually catalysed. Aliphatic and aromatic tertiary amines, organo-metallic compounds (tin, mercury and lead) and alkali metal salts of carboxylic acids and phenols can all be used to accelerate the reaction between polyols and diisocyanates. In such cases, the rate constant k is proportional to the catalyst concentration.

Diverse kinetic models have been developed which are different to that presented above, essentially just in the assumptions made, such as different reaction order (e.g. exponents a and $b \neq 1$) or different boundary conditions. Numerical simulations can be undertaken to calculate changes in the concentrations of reacting substances during the process. Also it is possible to compute the number average molecular weight of polyurethanes in relation to the reaction conditions adopted i.e. molar ratio of functional groups, temperature, thus allowing adjustments to be made in order to achieve a tailored synthesis.

2.1.4. Stoichiometry Requirements

The relevance of reactant stoichiometry in the synthesis of PUs can be understood if the impact it has on the molecular weight of the final polymer is considered. The polyurethane step-growth polymerisation reaction proceeds by the slow increase of the molecular weight. Two monomers firstly form a dimer that will subsequently react to form a trimer and then a tetramer and so on, so that the molecular weight of the polymer is continuously increasing. The product obtained by this mechanism will be determined by the average number of reactive functional groups per reacting molecule. For instance, a low-molecular weight product will be obtained when at least one of the reactants is a monofunctional molecule, whereas bifunctional starting materials will lead to linear polymers and polyfunctional monomers will give rise to branched and cross-linked polymers (Billmeyer, 1984). It has been demonstrated (Król and Pilch-Pitera, 2003b) that the progress of step-growth polymerisations can be controlled to some extent by means of the initial NCO/OH ratio. This is based on the average degree of polymerisation $\overline{DP}$ (Flory, 1971), which is expressed as:

$$\overline{DP} = \frac{1+r}{1-r} \tag{2.8}$$

with r given by:

$$r = \frac{NCO}{OH} \tag{2.9}$$

where NCO and OH are the molar concentrations of the isocyanate and hydroxyl groups respectively. Equation 2.8 predicts an infinite degree of polymerisation when the molar ratio of functional groups equals 1. In order to avoid the production of a high-molar-mass polymer that could be difficult to process, a precisely controlled imbalance of stoichiometry can provide control of the molecular weight. Therefore, the equimolar ratio of the functional groups facilitates the formation of high-molecular-weight products, while the molecular weight distribution of such materials will have high polydispersity. When an excess of any of the functional groups is present, polydispersity can be reduced, but there will be an unconverted excess of that specific reactant.

It is important to emphasize that there are several factors that may limit the degree of polymerization, for example: imbalance in the stoichiometry, impurity of monomers, and establishment of equilibrium. As a result, the degree of polymerisation, and therefore the molecular weight of the polymer, is directly affected by the stoichiometry of the reaction.

This is a key variable that can be adjusted in order to tailor the synthesis of a PU to achieve the desired molecular weight. A common practice in industry to control the molecular weight of a PU, is to stop the reaction by cooling the mixture, or by adjusting the composition of the reaction mixture away from stoichiometric quantities (Woods, 1990). The latter is achieved by adding a slight excess of one of the bifunctional reactants or by adding a small proportion of monofunctional component (chain extender). When one component is in excess then after some time, the functional group present in the lesser quantity will become exhausted so that all the polymer chains will be terminated in the functional group in excess. The degree of polymerisation can be calculated for this case, in a similar fashion to that presented above (Odian, 1970; Billmeyer, 1984).

In the case of adding a chain extender, the molecules react with diisocyanate to form a PU in the urethane polymer. It is added to allow the hard segment parts to segregate. This results in an increase of the glass transition temperature, Tg, of the hard-segment part of the polymer.

2.1.5. Structure-property Relationships

The properties of polyurethane polymers (and therefore their final application) vary depending on their molecular structures. Polyurethanes are materials that have the versatility to be manufactured in an extremely wide range of grades, in densities varying from 1220 kg/m^3 to 6 kg/m^3 if they are foams. Polymer stiffness also varies, ranging from very flexible elastomers to hard plastics. Consequently, the use of these materials is very broad. It has been recognised that properties such as elasticity, abrasion resistance, flexibility and clarity of films is attributed to the polymer chain structure. There is a wide variety of structure-property relationships classified by the extent of deformation of the molecular arrangement of the polymer chains. For example, electrical and optical behaviour, mechanical properties such as stiffness and yield point, and the glass and crystalline melting transitions are properties that involve

only small deformations (i.e. in chemical level). For instance, these properties are influenced by the interaction of atoms at small distances e.g. symmetry and steric effects, flexibility of chain bonds and spacing of polar groups (Billmeyer, 1984). Properties such as tensile strength, involve large deformation of the polymer chain configuration (i.e. architectural level), and are influenced by the molecular weight and its distribution, and whether the polymer is linear, branched or crosslinked.

On this basis, the properties of polyurethanes based on polyol and diisocyanates (Scheme 2.1) are influenced by the nature of the starting materials. For instance, if aromatic diisocyanates are employed, the polymer chain stiffness is larger due to the limited rotation of the bonds in the backbone. Therefore, the isocyanate monomer unit is known as the "hard" segment. In contrast, when a polyol of high molecular weight is employed (i.e. long CH_2 section length), the flexibility of the chain is increased because the easy rotation of bonds is possible. Hence, the polyol forms the "soft" segment.

For example, Spandex™ is a long-chain synthetic polymeric fibre with soft and hard segments of polyester or polyether polyols (See Figure 2.1). These structures permit the fibre to stretch by up to 600% and yet recover its original shape. The urethane segments comprise the hard block that endow the polymer with rigidity and hence high tensile strength. They also limit plastic flow in the material (Reisch, 1999).

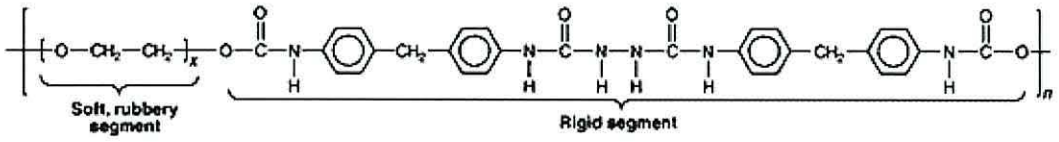

Figure 2.1 Structure of polyurethane chains present in Spandex™ (Reisch, 1999).

It is generally accepted that for polyurethanes, better properties are achieved as the microphase segregation between the soft and hard blocks is increased (Zia et al., 2008). All these relationships have been reported in more detail elsewhere (Nicholson, 1991; Woods, 1990; Billmeyer, 1984).

2.2. Polyurethane Synthesis and Processing

2.2.1. Typical raw materials

Even though many different isocyanates are available, about 95% of polyurethanes produced commercially are based on the following aromatic diisocyanates:

- Toluene diisocyanate (TDI)

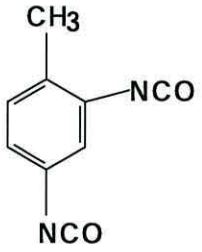

2, 4 – TDI

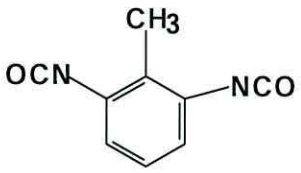

2,6 - TDI

- Diphenylmethane diisocyanate (MDI) and its derivatives

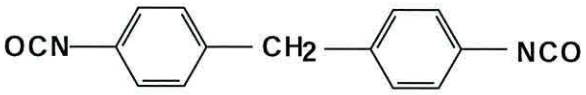

4,4' – MDI

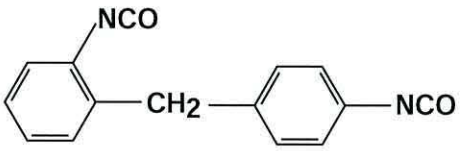

2,4' – MDI

The self-polymerisation of some diisocyanates such as 4,4'- diphenylmethane dyiisocyanate (MDI) can occur spontaneously when they are left standing at room temperature. When heated they can also form isocyanurates. The various side reactions of the NCO group make it difficult to obtain a stoichiometric balance of the reactants. For that reason it is a common practice to add a small excess of the diisocyanate. The aromatic isocyanates are generally more reactive than the aliphatic ones. The adjacent

substituents tend to lower the reactivity due to steric impediment. Isocyanates are toxic materials and need careful handling; once they have been allowed to react, they undergo complete conversion and appear to leave no toxic residues. However, recently due to safety reasons, there has been a tendency to avoid using TDI which is a volatile reactant. Pure MDI is a solid that tends to form dimers when stored, so it is difficult to handle. Therefore modified MDI's have been developed in order to reduce this tendency to dimerise. The modified MDI's are liquids at room temperature and are obtained by different processes. One approach is to react some of the NCO groups with a linear diol to give a low molecular weight diurethane with isocyanate end groups. The modified MDI will be a relatively low viscosity fluid (e.g. in the range of 200 - 2700 mPa s at 25°C) with the functionality of the modified MDI varying from 2.0 to 3.0.

About 90% of the polyols used in PU synthesis are polyethers. The rest are usually polyesters for achieving special properties particularly in rigid foams (Woods, 1990). Aliphatic polyols with primary hydroxyl end-groups (which are the most reactive) are fully saturated and have relative molar masses in the range 1000-2000. Such substances are viscous liquids or low melting-point solids. The choice of the polyol is important because its size, flexibility of the molecular structure and the functionality controls to a large extent the degree of cross-linking of the polymer which determines mainly the properties of the finished polyurethane and their ultimate application. For example rigid foam requires a stiff polymer network and a high degree of cross linking. If the starting material is an aliphatic diol with Mn = 1000 – 5000, the resulting foam is soft, whereas a diol with Mn = 300 – 700 yields a hard foam.

2.2.2. Conventional Synthetic Process

Polyurethane syntheses are usually carried out in bulk; it is a simple process that only requires the reactants, and catalyst if necessary. The process is conventionally carried out in batch reactors. The viscosity of the reactive mixture is relatively low initially and the mixing of reactants is easily accomplished because high molecular weight product is produced in the final stages. Thermal control of the process is simpler in step-growth polymerisations compared to radical polymerisation. Conventionally, the batch production processes of these materials comprises simple components: the reactor, the pumping and mixing systems and, if required, the heating-

cooling system (Kendagannaswamy and Siddaramaiah, 2002; Król and Pilch-Pitera, 2003b; Król and Pilch-Pitera, 2003a). Solution polymerisation and dispersed systems are used occasionally as well, especially in the paint industry, for microelectronics and cosmetics. The reaction can be carried out on different scales ranging from the small (g/min) to the large (kg/min). In the former, the required ratios of the reactants are placed in a small container and hand-mixed. On a large scale, industrial machinery is used to dispense and mix reactants. Whether the batch or continuous processing is used, there are some basic requirements in order to achieve a satisfactory manufacturing process. These include (Woods, 1990):

1. Accurate metering, weighing and dispensing of the chemicals.
2. Accurate dispensing system.
3. Temperature control and conditioning of the ingredients. The reaction rate can be modified and important properties of the raw materials such as viscosity and density can change with temperature.
4. Complete and reproducible mixing.
5. Freedom from contaminants.
6. Curing.
7. Safety.

All these requirements must be studied in detail for the intensification of the synthetic process. For instance, mixing is a key phenomenon and a vital step in achieving uniformity in the reaction blend. The description of mixing is normally by an average striation thickness or the magnitude of the interfacial area between fluids (Mohr et al., 1957). It has been recognised that the quality of the mixing affects directly not only the properties of the end product, but also alters the dynamics of the reaction. In other words, the mixing rate controls the conversion rate at the beginning of the reaction process. This effect is due to the fact that with mechanical mixing, the striation thickness decreases until the reaction mixture reaches a homogeneous stage. "Perfect" mixing has been achieved when no concentration gradients and no diffusion occurs during the mixing-reaction process. Then the reaction is controlled by the chemical kinetics (Ou and Ranz, 1983).

In polyurethane production there are two main kinds of mixers: mechanical and static. Mechanical mixers consist of a rotor that rotates at ~2000 rpm in a mixing chamber and come in different sizes, geometries and materials. Static mixers on the other hand, use high-pressure jet concepts. The streams of metered components are mixed together by the turbulence that results from the directly opposed impingement of the high speed jets that results from forcing the component through small orifices in a mixing chamber of low volume. This type of mixing is restricted to systems of low viscosity and ratios of 1:1. The reactants have to be accurately dispensed, so that the pumping systems are a key factor in the overall process. Most machines used for pumping are electrically driven and can be for example gear pumps, diaphragm pumps or piston pumps. By varying the pump speed, it is possible to control the feed rate and therefore fulfil the stoichiometry requirements.

Regardless of the method employed in the synthesis of PUs, the process used for the fabrication of the actual end product is of paramount importance. Moreover, the processing of the polymer is as essential as its synthesis, especially if it is desired to obtain an added-value product. Methods available for the processing of polyurethanes are based primarily on the rheological properties of the polymer, as well as on the softening temperature, stability and evidently the size and shape of the end-product.

As is the case for other polymers, polyurethanes can be processed by several different processing methods such as moulding, extrusion, calendaring, casting and foaming (Tadmor and Gogos, 1979). All these processes operate on the same basic principles: handling of solids in order to melt them, application of high pressure for subsequent dispensing (pumping) and mixing. The differences relate to the final step, which is where the ultimate shape is given.

Reaction Injection Moulding (RIM) is a versatile fabrication method widely used in the polyurethane industry. This process is different from those mentioned above because it starts with the un-reacted materials and leads directly to a polymer end-product. In other words, the polymerisation reaction takes place during the shaping process i.e. in the mould.

2.2.3. Reaction Injection Moulding

RIM processing methods became important in the early 1970's when the simplest member of the family of techniques was used to fabricate shoe soles (Fan et al., 1997; Woods, 1990). It is a simple high speed process for the synthesis of PU directly from relatively low viscosity reactants, which are pumped in prearranged quantities into a mixing chamber. Inside this chamber they undergo efficient impingement mixing after which the reaction mixture is injected into a mould at a medium temperature (e.g. 60°C) under pressures in the range of 50 -100 bars.

Mixing in RIM processes is the most important part of the synthesis, and is obtained by different means than in an ordinary polymerisation process. The physical and chemical mixing forces are sufficient to achieve high molecular-level mixing of species in microseconds. RIM mixing occurs in the chamber by the opposed encounter of the two monomer high speed jet streams (e.g. between 10 and 100 m/s). The mixing chamber is cleaned by a fitting ram that also works as a valve to stop the flow. Figure 2.2 shows the basic RIM process.

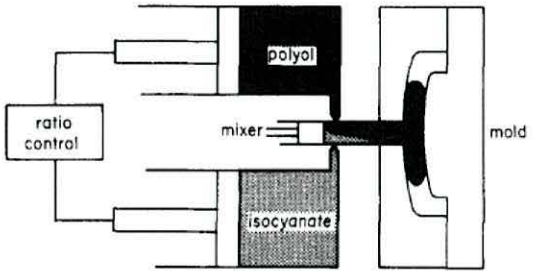

Figure 2.2 The schematic representation of the reaction injection moulding process (Lee et al., 1980).

The streams come from nozzles of diameters between 2-4 mm, at Reynolds numbers typically between 100 and 500. The Reynolds number (Re) is defined as:

$$\mathrm{Re} = \frac{Dv\rho}{\mu} \tag{2.10}$$

where D is the diameter of the orifice from which the fluid is ejected, v is the average flow velocity, ρ and μ are the density and viscosity of the fluid respectively. The low Re values of the streams injected, indicate that the flow is laminar. However, the impingement velocity is so high that chaotic mixing occurs (Erkoc et al., 2007) due to

chaotic advection (Aref, 1994). The latter phenomenon is defined as the motion of a fluid particle that visits rapidly different regions of the fluid and follows a complex (i.e. chaotic) trajectory (Aref, 2002). This physical type of mixing considers the fluid particle as light, inert and passive so that it follows the fluid movement (Stremler et al., 2004). This rapid fluid motion reduces the striation thickness to a value in the range of 15 μm, and forms a lamellar structure (see Figure 2.3).

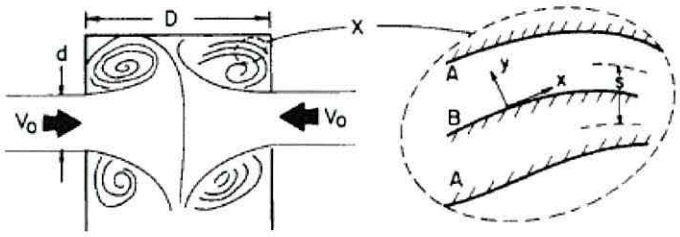

Figure 2.3 Lamellar structure formed during impingement, showing striation thickness (Kolodziej et al., 1982).

It has been reported that in order to accomplish homogeneous mixing in a reaction taking place in a RIM process, a striation thickness in the range of 15 μm is required (Rauwendaal, 1991).

Wickert et al. (1987) studied small scale mixing of reactants. The experiments undertaken by them consisted of observing the interfacial zone between two reactant drops that yielded polyurethanes by means of a light microscope. The authors found that, even without the added effect of high velocity impingement mixing, when a drop of liquid MDI and a drop of polyether diol of molecular weight 2300 g/mol mixed, there was a tendency for the MDI to disperse into the polyol phase (Figure 2.4a). The dispersion phenomenon started upon contact between the two reactant phases. Similarly, a dispersion of the MDI in the polyol containing 0.1%w of dibutyltin dilaurate as a catalyst was observed (Figure 2.4b).

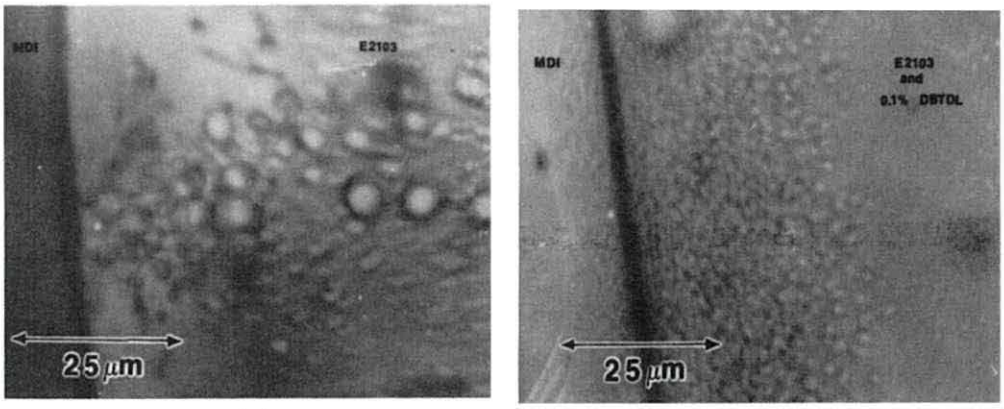

(a) (b)

Figure 2.4 (a) Dispersion of liquid MDI into polyether diol; (b) Dispersion of liquid MDI into polyether diol containing 0.1% w catalyst (Wickert et al., 1987).

The authors indicated that the main difference between the catalysed and the non-catalysed systems was that the dispersion size in the first case was smaller, with a diameter of 1.5 μm, whereas the second case showed a dispersion diameter of 3 μm.

Based on these findings, it becomes evident that more research needs to be undertaken in order to determine if similar phenomena will be observed when down-scaling the reactive process of polyurethane formation. As mentioned in the introduction of this thesis, the aim of this research was to study the feasibility of moving from the current RIM technology to an even smaller scale by means of Ink Jet Printing technology. The following chapters are devoted to the study of the polyurethane chemistry involved and the exploration of IJP as a tool for downscaling PU synthesis.

Chapter 3. Characterisation of PU synthesis as a basis for Intensification

3.1. Process Intensification as a challenge for Chemical Engineers

A key factor for achieving desired properties in an end-use polyurethane is its microstructure, which is reliant on the product formulation, process equipment and operating conditions (Edwards, 2006).

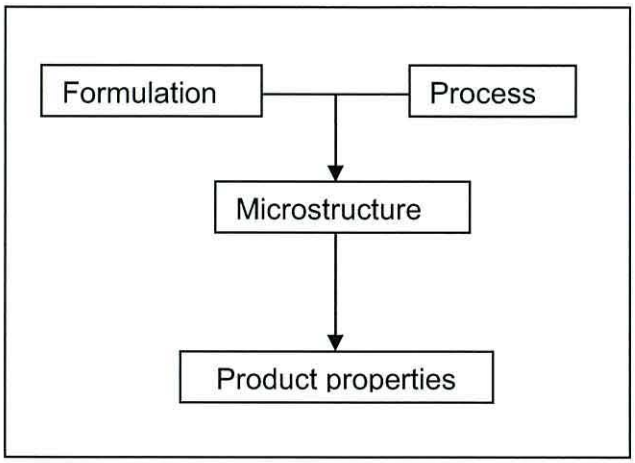

Figure 3.1. Effect of the formulation and process on end-product properties, based on (Edwards, 2006).

The first step towards the intensification of polyurethane synthesis is to understand the polymerisation chemistry, process dynamics and the interaction between them (Moggridge and Cussler, 2000).

Conventional chemical engineers are familiar with the design of equipment and processes on a length scale 1–10 m (for instance reactors and heat exchangers) used in the commodity chemical industry. A chemical engineer is also capable of scaling up the processes and to integrate multiple processes into a single plant on the scale between 100 and 1000 m (Edwards, 2006). However, chemical engineers face important challenges when it comes to their integration in the speciality-polymers industry. The new approach of scaling-down and intensifying processes entails crossing the boundaries of chemical engineering and multi-disciplinary research is often needed.

Polyurethane materials are still the subject of research because they can be used to produce high added-value products and smart materials, as presented in section 2.1. The shift from commodity to speciality polyurethanes has been achieved by Reaction Injection Moulding. In this already efficient process, mixing is intensified and the end-product is shaped during the polymerisation reaction. It is believed that down-scaling this process (miniaturisation) can bring new applications. To achieve such an ambitious challenge, new ways of thinking and studying the polyurethane synthetic process is needed.

The new approach that this study suggests for the miniaturisation of PU synthesis is based on the dynamics of the Reaction Injection Moulding process and conventional polyurethane chemistry. The new process that was investigated comprised the accurate micro-dispensing of 2 micro-droplets of reactants (e.g. diisocyanate and polyol) onto a specific location and their *in-situ* polymerisation. In order to miniaturise the PU polymerisation process in such a way, it has been essential to understand the dynamics of the synthetic process of PU and to test basic and well-understood formulations of the material. Analytical methods have been adopted to monitor syntheses and for the characterisation of the materials produced. The following section (3.2) contains a brief description of the analytical techniques used in this research.

3.2. Characterisation of polyurethanes

Some of the fundamentals of polyurethane chemistry were reviewed in Chapter 2, but it is necessary to establish how the chemistry and the polymerisation process become convolved. i.e. it is necessary to design the chemistry and the reaction dynamics to match the dynamics of the miniaturised process whilst retaining the capacity to produce materials with the desired physical properties.

The reaction kinetics were explored using differential scanning calorimetry (DSC), a commonly adopted method for such measurements (Fan et al., 1997; Lan et al., 1996; John et al., 1991; Hugo et al., 1993). DSC and dynamical mechanical analysis (DMA) are thermal techniques employed to measure the physical behaviour of polymers i.e. their glass transition temperature (Tg) and melting temperature (Tm).

The apparent molecular weight was quantified using gel permeation chromatography (GPC) (Król and Pilch-Pitera, 2001). As discussed in sections 2.2.4 and 2.2.5, there are two main reasons why it is necessary to monitor the molecular weight of the polymer. The first reason is that mean molecular weight of the end product determines its properties. The second is that, in step-growth polymerisation, the mean molecular weight of the product and its molecular weight distribution change with time so determining these properties during the progress of the reaction is important in order to control the process.

Raman microscopy and Fourier-transform infra red spectroscopy (FTIR) were chosen to determine the final product structure, e.g. composition and in some cases the extent of reaction (Lan et al., 1996; Fan et al., 1997; Rajendran et al., 1982; Wilhelm et al., 1998; Ferry and Jacobsson, 1996).

These analytical techniques are standard methods in the field of study and their detailed description will not be discussed in this thesis. However, the way in which they were employed is described in some detail in order to place in context the data generated (see sections 3.2.1, 3.2.2 and 3.2.3).

3.2.1 Thermal analysis

Thermal analysis comprises many different techniques including differential thermal analysis, thermogravimetric analysis, dilatometry, X-ray diffraction, calorimetry, conductivity and differential calorimetry just to mention some (Garn, 1965). It is the properties of materials that are measured by these methods rather than the elemental species comprising the compound.

3.2.1.1. Differential Scanning Calorimetry

DSC measures the energy (e.g. enthalpy or heat capacity changes) needed to maintain a nearly zero temperature difference between the sample and a standard reference material while heating or cooling. From such thermal data it is possible to identify changes in morphology, structure or the course of a reaction.

a) Thermal transitions in polymers

Crystalline melting temperature, Tm, and glass transition temperature, Tg, are the most important transition temperatures in polyurethanes. Tm is the temperature at which the crystalline domain of a polymer sample melts i.e. the temperature range

over which there is a phase change from a crystalline solid to the amorphous state (Bhadeshia, 2002). Tg is the temperature at which the brittle amorphous solid polymer changes to a rubbery soft material when the polymer is heated. Both states are amorphous but each has a different heat capacity (C_p) which is why a DSC instrument can detect the transition (Odian, 1970). However, on some occasions, when the Tg value is low (i.e. -20 °C) DSC is not sensitive enough due to poor control of low temperatures. In such cases, DMA can be used for the determination of Tg as explained in the following section.

b) Determining the reaction kinetics of an exothermic polymerisation

Polyurethane formation from appropriately functionalized co-reactants is an exothermic process. It can be measured readily by DSC provided the reaction rate is such that the dynamic characteristics of the instrument are capable of measuring the rate of heat output. In other words, that the reaction is not so fast or so slow that it is beyond the capabilities of the instrument. It has to be assumed that the rate of heat output is directly related to polymerization and not to any other thermal event which might take place concurrent with polymerization. Reactions may be followed under isothermal conditions or by using a constantly increasing temperature ramp. DSC has been employed by many in these different modes to study the curing kinetics and thermal properties of reacting systems (Wagner et al., 1993; Kenny et al., 1995; Dimier et al., 2004; Rodrigues et al., 2005).

Isothermal DSC results are employed to calculate the heat of reaction, whereas dynamic DSC results are commonly used to calculate the activation energy of the reaction (Rodrigues et al., 2005). In calculations based on the dynamic DSC method, it is assumed that the reaction rate is given by the expression:

$$\frac{d\alpha}{dt} = k(T) f(\alpha) \qquad \textbf{(3.1)}$$

where α is the fraction converted, k(T) the specific rate constant at themperature T and $f(\alpha)$ some function of α. k(T) is given by the Arrhenius equation (John et al., 1991), i.e.

$$k(T) = A_o \cdot \exp\left(\frac{-E_a}{RT}\right) \tag{3.2}$$

where A_o is the Arrhenius frequency factor, E_a the activation energy, R the ideal gas constant and T the absolute temperature.

The extent of reaction can be calculated using isothermal experiments if it is assumed that, the number of moles reacting during an interval of time is directly proportional to the heat H liberated in that time at a given temperature T. The reaction rate is given by:

$$\frac{d\alpha}{dt} = \left(\frac{\left|\frac{dH}{dt}\right|_{T=cons\tan t}}{\Delta H_o}\right) \tag{3.3}$$

where α is the fraction converted and ΔH_o is the total heat of reaction. As can be seen in Figure 3.2, the fractional conversion is the ratio between the partial area at a specific time t_p, $\Delta H_{partial}$ and the total area under the peak:

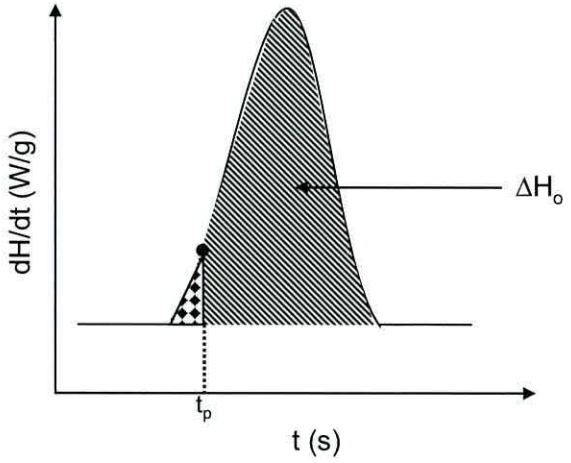

Figure 3.2 Diagram of the output from isothermal DSC experiment for calculation of reaction conversion.

The activation energy can be calculated by non-isothermal experiments. Several methods have been proposed (Brown et al., 2000; Chen et al., 1993; Kissinger, 1956). The Kissinger method has been applied for the calculation of kinetic parameters (Starink, 2003; Taylor and Fryer, 1992; Wagner et al., 1993). The Kissinger method is based on equation 3.1 and 3.2, and is for non-isothermal experiments at a constant heating rate, β. For various heating rates, the determination

of the temperature $T_f(\beta)$ is required. This temperature is taken at an equivalent extent of reaction (e.g. isoconversion method). In the calculations done in this specific research, T_f was assigned to be the exotherm peak temperature. The Kissinger method for which the detailed mathematical derivation has been described (Starink, 2003), suggests that plots of $\ln(\beta/T_f^2)$ versus $1/T_f$ should be straight line plots with a slope which equals E_a/R. This method does not make any assumption about the nature of the function $f(\alpha)$ i.e. it is a model-free method.

Since the DSC method has the advantage of simultaneously providing kinetic and thermal data, it was the technique selected to study the polyurethane reaction in this work.

3.2.1.2. Dynamic Mechanical Analysis

DMA is an important tool for the characterisation of polyurethanes. It measures the deformation (modulus) of a sample when an oscillatory constant load is applied. On the one hand the storage modulus E' is a measure of how elastic the material acts under specific conditions of temperature, load and frequency. On the other hand, the loss modulus E'' is an indication of energy loss. The ratio of the loss modulus to the storage modulus is known as tan δ, which is called damping. This is a property that indicates how well the material can dissipate energy. This is relevant information to determine the elastic, viscous or viscoelastic behaviour of a material (Billmeyer, 1984). DMA can also give Tg as a function of deformation frequency and is more sensitive to glass transition changes than DSC. In this study, the peak of the tan δ curve is regarded as the Tg of the material as it is shown in section 3.4.1.1.2.

DMA cannot provide Tm data but does allow the onset of melting to be seen. In this research DMA analysis was employed to determine the glass transition temperature Tg.

3.2.2 Gel Permeation Chromatography

GPC is a chromatographic technique that has successfully been employed to determine the apparent molecular weight of polyurethanes (Lan et al., 1996; Król and Pilch-Pitera, 2003b; Król and Pilch-Pitera, 2001). This technique is based on the exclusion or separation of polymer molecules by their size in chromatographic columns with designed pore structures. The polymer is dissolved in the eluent and

injected into an appropriate series of columns for the material being analysed, so that separation occurs without total exclusion of molecular species occurring. Small polymer molecules permeate deep inside the packed material and their residence time in the column set will be long. Large molecules are not able to permeate as deeply and have a shorter residence time (Cowie, 1991). Many detector systems can be used including refractive index devices, light scattering, evaporative light scattering, viscometers and various spectroscopic devices including UV/visible instruments. A refractive index detector was using in the work reported here.

With this technique it is possible to quantify the separation of the molecules on the basis of their size (eluting largest first) and to obtain a molecular weight distribution provided the column set used can be calibrated with appropriate standards. Since the polyurethanes produced in the work are linear segmented copolymers, the hydrodynamic volume of the molecules in solution is a function of the chemical units in the polymer chain, the copolymer composition, and the refractive index gradient differences with molecular weight and composition. In this work, the column set was calibrated using polystyrene standards in a good solvent (tetrahydrofuran). This approach only provides an apparent molecular weight and care is needed in using such data if there are differences in chemical type and composition in the samples being compared.

3.2.3 Spectroscopy: FTIR and Raman

Both Raman and FTIR are powerful tools for the quantitative and qualitative analysis of PU (Ferry and Jacobsson, 1996; Parnell et al., 2003; Recalde et al., 2005; Wilhelm et al., 1998). These spectroscopic techniques give important information about the structure of the polymer, and can be used to explore the chemistry of polymerisation by revealing specific functional group activity. This information, used in conjunction with data obtained by thermal analysis and chromatography, can add much to the mechanistic understanding of the polymerisation chemistry, and end-product. Raman and FTIR are complementary molecular spectroscopic techniques since it is often the case that some bands which are weak in infrared (IR) (for instance, stretching of C=C, N=N and O-O functional groups and the stretching of symmetrical groups) may be strong in Raman. The opposite is also true, Raman inactive bands such as polar groups show a strong signal in IR. However, the covalent character of bonds tends to be clearly observed in Raman. Additionally, if a sample shows activity

in regions where band signals overlap, the use of an alternative technique (Raman or FTIR) frequently offers the opportunity to observe the bands under study in regions where there is no interference (Socrates, 2001).

FTIR is the most commonly used spectroscopy technique for monitoring PU polymerisation chemistry on the macro-scale (Fan et al., 1997; Król and Pilch-Pitera, 2001). Micro-scale analyses are also possible (Wilhelm et al., 1998; Recalde et al., 2005). The benefits of using this technique are that considerable information relating to fundamental absorption frequencies has been published over the years, and there is a vast literature available for the interpretation of the spectra (Socrates, 2001; Coates, 2000) .

Even though it is not the same for Raman, this technique is gaining in importance due to the significant technological developments in recent years. For instance, illumination, dispersion and detection components have evolved rapidly as have new rapid digital data processing and microscopy. This has resulted in the availability of small, robust instruments for bench work and for rapid on-line measurement purposes (Kip et al., 2000). The use of laser Raman microscopy in microscale studies is highly efficient because it combines the versatility and benefits of microscopy with the rapid recording of spectra in the range from 100 to 4000 cm^{-1} , which makes possible *in situ* analysis (Brookes et al., 1997; Mestl, 2000).

3.3. Polyurethane Synthesis: Experimental

3.3.1 Batch System

3.3.1.1 Solution Polymerisation and on-line monitoring of PU reaction: Materials and Method

The reactant ratio for the initial, un-catalysed batch solution polymerisation reactions carried out was set at 1NCO:1OH and comprised 1 mole of solid diphenylmethane-4,4'-diisocyanate (MDI), 0.5 mole of poly(1,4-butanediol) with a molecular weight of 2000 g/mol and 0.5 mole of 1,4 butanediol (BDO) as a chain extender. The polyol and chain extender (Sigma Aldrich) were dried at 60°C under vacuum for four hours before use. The solid diisocyanate (Desmodur 44M, Industrial Copolymers Ltd) was employed as received. The synthesis of the polyurethane was carried out in a 250 ml jacketed glass reactor, with a 5-neck lid. The system included a mechanical stirrer, nitrogen input line, recirculation line, and a condenser. The solution polymerisation was carried out in 100 ml of dried THF at room temperature, under a nitrogen atmosphere, and with a stirring rate of 200 rpm. A 20 mg sample was taken every 15 minutes and analysed in the PL GPC 50. The concentration of the solution employed for GPC analysis was around 0.2%w in 4 ml of THF. A drop of dried methanol was added to stop the reaction and avoid any damage to the column which might be caused by further reaction in the columns.

For the GPC analysis, firstly a calibration run was undertaken in a High Resolution Integrated GPC/SEC System; Polymer Laboratories model PL-GPC 50, comprising a precision solvent delivery system, a sample injection system, a high performance differential refractive index detector, UV detector and an auto-sampler. The equipment included one PLgel 5μm MIXED-C column, for polymer analysis up to 2 million weight average molecular weight, M_w, (linear range of 200 to 2,000,000). Two kinds of standards were used to run the calibration, the first one called Polystyrene EasiCal PS, with a range of 580 – 7,500,000 Mp, and mainly used for routine samples, constituted a mixture of 5 polymer calibrants deposited in a spatula. They were prepared in a vial with 3 ml of THF and 3 μl of toluene as a Flow Rate Marker. The second kind of standard, called EasiVial PS, with a range of 162 – 6,035,000 Mp, is basically used for more accurate measurements. The kit contains three colour-coded vials, each one containing a mixture of four narrow-polydispersity polystyrene standards deposited in the vials. 4 ml of THF were added as the solvent,

and 4 ml of toluene were added as a Flow Rate Marker. The eluent used for the GPC analysis was THF with 250 ppm of BHT, at a rate of 1 ml/min, and 15 min of residence time for each determination.

The reaction was monitored for 22 hours, and the final polymer was precipitated and subsequently analysed by GPC. A second approach was made by changing the reactant ratio to 1 mole of MDI, 0.2 mole of poly(1,4-butanediol) 2000 and 0.8 mole of 1,4 butanediol. The reaction was carried out as before with samples now being taken every 20 minutes but each prepared as above before for GPC analysis.

In a third approach, an attempt was made to monitor the polymerisation using a Process Monitoring System developed by Polymer Laboratories Ltd. In this case, no column separation was used but the composition of the reaction mixture was monitored using the GPC detectors alone. To achieve an optimum response from the detectors and a constant flow through the pumping system, it was necessary to set a baseline before running the reaction. For this purpose, a solution of the polyol and butanediol in THF was placed in the reactor at 30°C recirculated through the detector system for about 20 minutes. When the detector signals reached a plateau, a 500 g/L solution of MDI in dried THF was added and the reactor and the reaction monitored for three hours. The reaction time could not be extended beyond three hours as the viscosity of the reaction mixture increased and it was feared that this would de-stabilize the flow controller.

The PL process monitoring system is shown in Figure 3.3. It comprises a 250 ml jacketed glass reactor with a 5-neck lid. The system included a mechanical stirrer, nitrogen input line, recirculation line and a condenser. The recirculation line is attached to the sample-pumping system which extracts 0.2 ml/min of the reactor content and prepares the samples for injection into the detection system. The solvent used to prepare the samples was a mixture of dried THF and dried methanol. The detection system is composed of a series of detectors for light scattering, refractive Index, two UV spectrometers and viscosity detector. The final product was analysed by GPC.

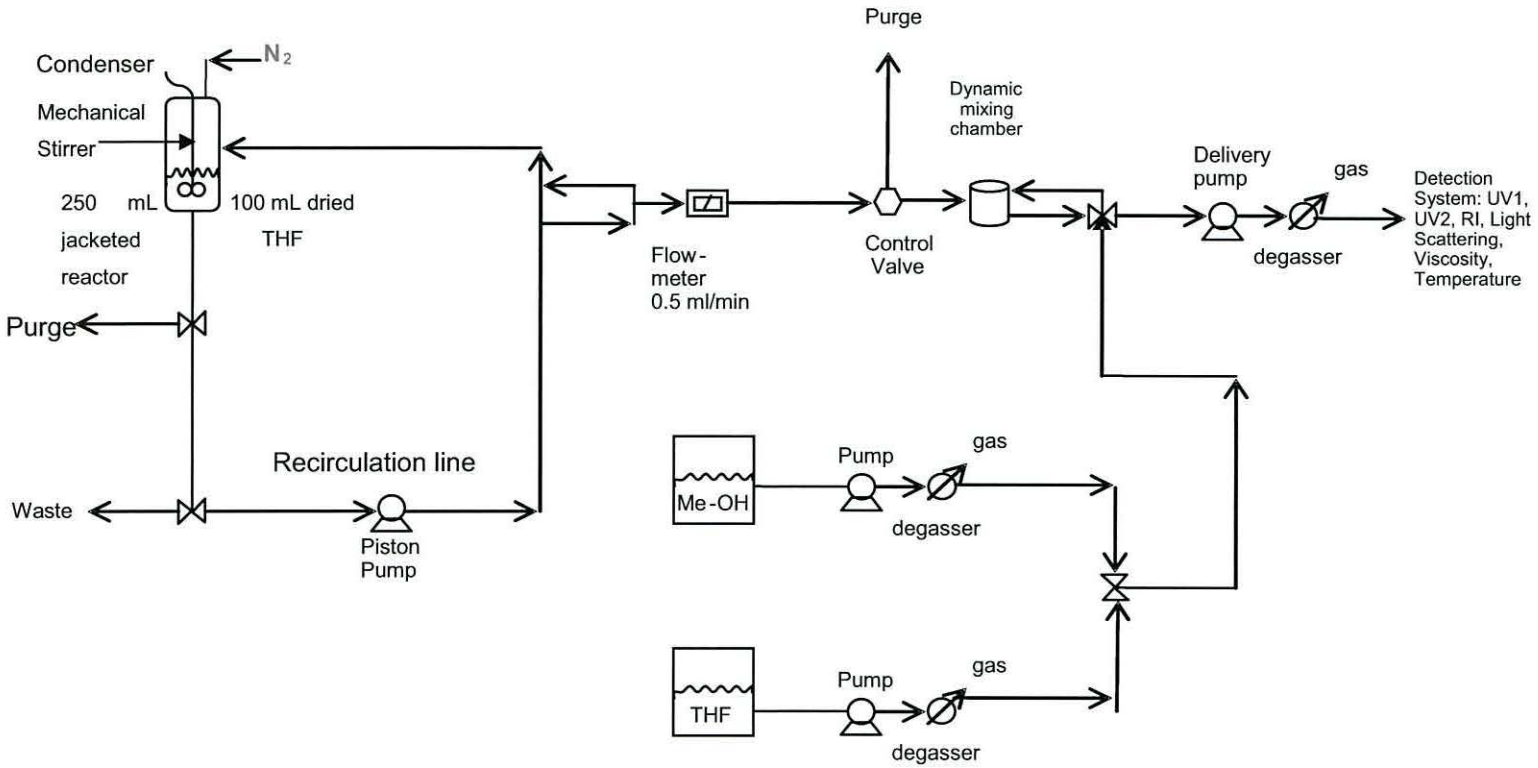

Figure 3.3 Flow diagram of the Process Monitoring System

3.3.1.2 Effect of different formulations: materials and methods

3.3.1.2.1 *Different NCO:OH ratios*

In order to scale down the PU synthesis, it was necessary to design an adequate formulation that would essentially comprise two streams. Both streams should preferably be in a liquid state, in order to be pumped accurately and precisely by the RIM machine and IJP system. Even though there are commercially available PU formulations which consist of two low-viscosity components, insufficient information about their composition was available. Furthermore, the commercial formulations often yielded cross-linked polyurethanes that did not lend themselves to characterisation using GPC. For this reason, an in-house formulation was sought which led to a linear polyurethane by the reaction of a prepolymer formed from a diisocyanate and polyol with an excess of NCO groups, and the subsequent reaction of the prepolymer with a polyol. This approach was taken to ensure the safe handling of the isocyante reactant with the RIM and IJP technologies.

Firstly, the effect of varying the stoichiometry on thermal behaviour and molecular weight of PU was studied. The NCO:OH ratio was set to the following values: 0.18, 0.40, 0.60, 2 and 3. The molar ratio of the OH groups in the polyol 2000 and chain extender was kept constant at 4 mols of polyol to 1 mol of chain extender. The un-catalysed system employed for prepolymer synthesis comprised solid MDI (Desmodur 44M), poly(1,4-butanediol) with a molecular weight of 2000 g/mol and 1,4 butanediol as a chain extender. The materials were prepared as described in section 3.3.1.1.

The synthesis of the polyurethane was carried out in glass vials. 0.31 g of solid MDI and 2 g of polyol were weighed and placed in an oil bath at 50°C for 15 mins and removed. The chain extender was added to the melted MDI/polyol vial and stirred for 15 s. Similarly, the rest of the reacting mixtures were prepared by weighing the appropiate amount of reactants. 5 mg of the reaction mixture were placed in self-sealing DSC pans. The DSC employed was a Perkin Elmer Pyris 1, using dynamic scan at 30°C/min. The residual reaction mixture was left for 24 hours to complete the curing after which the sample was analysed by GPC. The exprerimental GPC setup was similar to that described in section 3.3.1.1.

Secondly, the variation of stoichiometry on the physical state of the prepolymer was investigated. The excess of NCO groups was varied in the following ratios: 1.11, 1.33, 1.53, 1.66, 1.86, 2, and 3 using a polypropylene glycol (PPG) with molecular weight of 1000 g/mol. Additionally, the use of a PPG with molecular weight of 2000 g/mol at NCO/OH of ratios 2, 3 and 4 was explored and the samples were analysed using the same GPC system. Finally the prepolymer synthesis with a molar ratio NCO:OH 8:1 (named Prepol-12) was also investigated, and in this case the polymerisation was catalysed using dibutyltin dilaurate at a concentrion of 0.1%w as studied by Wickert (1987). To produce a Prep-12 prepolymer batch of 200g, 100 grams of MDI were weighed and put into a five-orifice glass reactor. Then 100 grams of dried polyol 2000 and 100 mg of dibutyltin dilaurate were added. The reactor was placed inside a fume cupboard and held from one of the mouths (closed with a stopper) in a stand using nut clips. A stopper with a hole in it was placed on the left-hand side mouth of the reactor, as a ventilation tube. A mechanical stirrer was fitted in the middle orifice, and on the right-hand side orifice, a stopper with a hole in it was introduced to create a nitrogen atmosphere inside the reactor. The remaining orifice was closed except when extracting samples. Approximately 60mg samples were taken using a glass micropipette every 5 minutes during the first half hour, and then one sample after 60 minutes. The molecular weight was monitored by GPC. Also, this prepolymer structure was analysed using a Spectrum One FTIR system from Perkin Elmer (with Golden Gate accessory, which allows the direct analysis of the sample without any special preparation).

3.3.1.2.2 *NCO excess content in PU prepolymers*

The NCO content of the prepolymers was determined by a titration based on the fact that the reaction between an excess of dibutylamine with MDI produces an amine. The excess of amine is assessed by back titration with HCl (see Scheme 3.1).

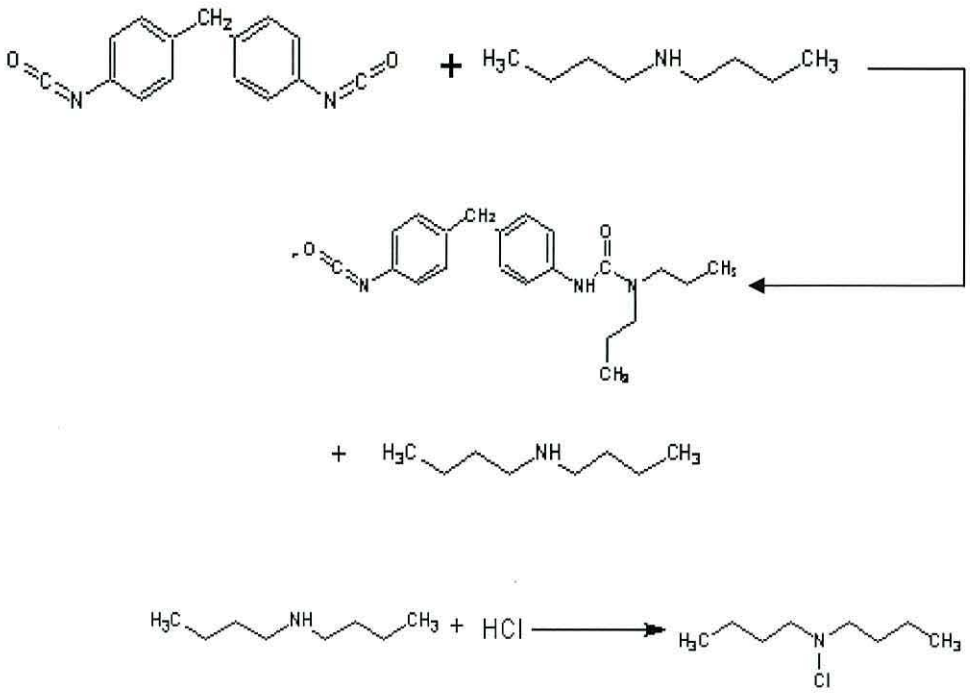

Scheme 3.1 Reaction for determining the NCO content in the prepolymer

The method employed was based on the ASTM D1638-74 procedure. A blank solution containing 25 ml of dried isopropanol and 6.25 ml of dried toluene was poured into a 50 ml Erlenmeyer flask. Then, 5 ml of a 2M solution of di-n-butylamine in toluene was added. Five drops of 0.04% w/v solution of bromophenol blue in dried methanol were added as indicator. Then, the reference solution (blank) was titrated using standardised 1N hydrochloric acid, so that the blue solution changed its colour to a permanent yellowish colour. Separately, 0.25 g of prepolymer was weighed in a 50 ml Erlenmeyer flask. Similarly, 25 ml of dried isopropanol, 6.25 ml of dried toluene and 5 ml of the 2M solution of di-n-butylamine were added to the sample flask. Five drops of colorant solution were added as indicator. The flask was placed on a hotplate at 50°C for 10 minutes to aid the solubilisation of the sample. It was similarly titrated using the standardised HCl solution.

The calculation of the NCO content was based on the following equation:

$$\%NCO = \frac{42.02 * (V_1 - V_2) * N}{1000 * W_s} * 100 \qquad \textbf{(3.4)}$$

where %NCO is the percentage of the NCO functional groups of the prepolymer in excess; V_1 is the volume of the HCL in ml added to the blank solution; V_2 is the volume of standard HCl solution in ml added to titrate the sample solution, N the normality (in this case 1) and W_s is the weight in grams of the sample added.

The value of the %NCO of the sample obtained by titration is then compared with the theoretical value $\%NCO_{theoretical}$, which is calculated based on equation 3.5:

$$\%NCO_{theorical} = \frac{42 * F * NCO_{excess}}{\left(MW_{diisocyanate} * NCO_{total}\right) + \left(MW_{polyol} * OH_{total}\right)} * 100 \qquad (3.5)$$

where F is the functionality of the diisocyanate, NCO_{excess} is the number of moles in excess, $MW_{diisocyanate}$ the molecular weight of the diisocyanate, NCO_{total} the total number of NCO moles added in the original formulation, MW_{polyol} the molecular weight of the polyol employed and OH_{total} the number of polyol moles added in the formulation.

3.3.1.2.3 *Different chain extender concentration: hard and soft PUs*

Based on the results of the prepolymer formulations explored, the formulation that was considered most suitable to use in the RIM and IJP systems was that with a NCO:OH ratio of 8:1. This prepolymer was synthesised using polypropylene glycol (PPG) of molecular weight 2000 g/mol. The next step taken in the design of a polyurethane formulation was to determine the composition of the second stream (e.g. polyol and chain extender mixture). A series of castings were prepared to determine the impact that the chain extender content had on the properties of the obtained polyurethane. Basically, only two different kinds of formulations were tested, one with a high hard-block content and a second with low hard-block content. The first one contained a molar ratio of NCO:OH:BDO of 6:1:5 and the second one a ratio of 6:5:1. The overall NCO/OH ratio was kept to 1. Only two formulations were chosen, as the purpose was only to determine the proportion of chain extender that should be mixed with the polyol that would be dispensed by the RIM experiments in Stream two, and also to be tested in the IJP system.

The castings were prepared in 250 ml paper cups. The calculated amounts of prepolymer, chain extender and polyol were weighed and mixed manually for 1 minute before pouring the reaction mixture into a 20 ml disposable aluminium dish.

The castings were placed in a vacuum oven at 10^{-4} mmHg and 80°C for 3 hours to cure. The polyurethanes formed were analysed using GPC following the same procedures described before. The samples were also characterised by DMA (Perkin Elmer Pyris Diamond) with cooling controller applying the compression sinusoidal oscillatory test. The PU sample was cut with specific dimensions; 7 mm thick x 11 mm long x 6 mm wide, placed in the holder of the instrument and the sample chamber was closed. The test started when the sample reached -100°C. The results were compared with the results from the analysis of the properties of a PU commercially available from RS (polyurethane potting compound for encapsulating electronic circuits and components). The procedure to make the casting of this sample was the same as described previously, following the manufacturer's formulation, which was a mixture of 5 parts of "hardener" and 2 parts of "resin" on a weight basis.

3.3.1.3 Reaction kinetics of un-catalysed PU reaction using DSC

The kinetics of two different PU formulations were studied. The first had a high hard-block content with 5:1:4 mol ratio of MDI, PPG 2000 and 1,4 butanediol, respectively. The second with low hard-block content had a ratio of 5:4:1 mol of MDI, PPG 2000 and 1,4 butanediol, respectively. The sample was prepared following the methodology described in section 3.3.1.2.1.

A base line was established in the range from 0°C to 250°C and experiments conducted in dynamic mode at 5, 20 and 30 °C/min. From these experiments it was possible to calculate the activation energy, Ea, for both formulations. The thermal behaviour showed that only one exotherm was observed for the polymerisation of high hard-block content formulation. Consequently, using this formulation isothermal experiments were undertaken for the determination of reaction conversion. Isothermal reaction was allowed at 30°C, 40°C and 50°C for 0, 5, 10, 15, 30, 60 and 180 minutes. The kinetic parameters and reaction progress were calculated using the methods described in section 3.2.1.1.

3.3.1.4 Study of alternative catalysts

The uncatalysed polymerisation reactions have been shown to be slow, (see section 3.4). Processes, such as RIM, require fast reactions which are achieved by using catalysts. There are a number of mercury, tin and amine catalysts available for

existing fast processing methods such as RIM but these are toxic and it is more desirable to seek new catalysts which are more environmentally friendly even for low output technologies such as IJP. A series of new titanium and zirconium catalysts (Johnson Matthey) were being explored elsewhere in the laboratories and these were tested. For commercial confidentiality reasons the structures of the catalysts can not be made available. As far as this work is concerned, a detailed knowledge of the catalyst chemistry is not needed as their only role is to speed up the reaction. The means by which this is done is not relevant. Four catalysts were under study, two were zirconium-based (Zr1 and Zr2) and two were titanium-based (Ti1 and Ti2). Preliminary experiments were undertaken using catalyst Zr1 at three concentrations: 0.05, 0.1 and 0.196 % w/w of polyol. These experiments demonstrated that the reaction rate was sufficiently low to be followed by DSC with a catalyst concentration of 0.1%. On that basis, the other catalysts Zr2, Ti1 and Ti2 were also studied at the same concentration. Apart from adding the small quantities of catalyst to the formulations, in all other respects, the reactions were carried out using the experimental procedure described in section 3.3.1.3.

3.3.2 RIM Experiments

Experiments were carried out using a mini-RIM machine which provides a good example of a large-scale process which embodies process intensification, notably in the mixing process. It was conducted in order to compare a well-established macro-scale technology with the proposed IJP methods which superficially embody the same concepts i.e. pumping of two reactive fluids which require mixing before reacting. The RIM experiments also allowed the processability of the designed prepolymer to be checked and the practicalities of scaling down to IJP levels to be explored.

The RIM machine employed has been developed over many years in-house. It employs four feed streams (Figure 3.4) each independently computer-controlled for precision dispensing of PU reactants. Only two streams were used.

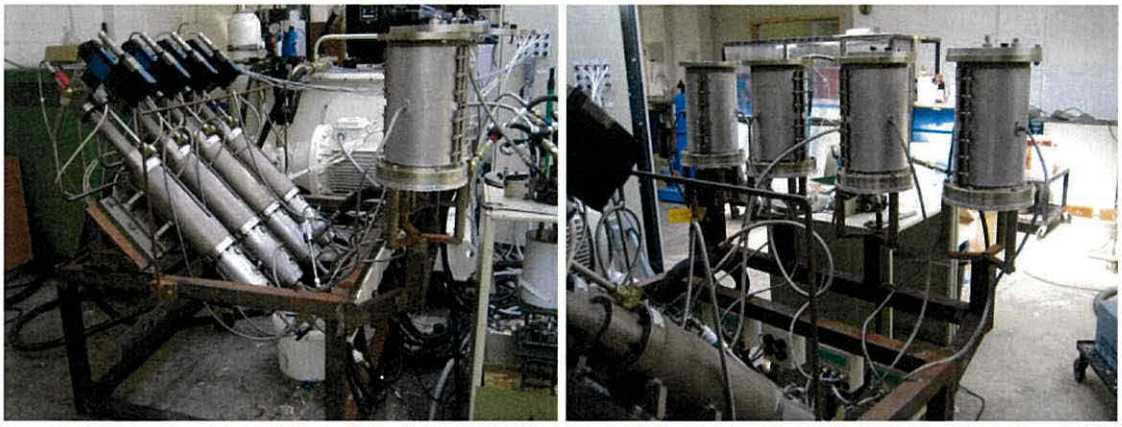

Figure 3.4 Four-stream mini-RIM machine.

Each stream was fitted with a 5 L reagent tank fitted with a lift-off lid which formed air-proof seals to protect the reactants from moisture i.e. to avoid the formation of polyureas. A mechanical stirrer was fitted to each storage tank. One stream was used for the storage of NCO-functionalised prepolymer and a second for the polyol. The tanks could be heated. All hoses were also heated (typically 60^0C). The reactants were dispensed from the storage tanks by lance pumps through a self-cleaning impingement mixhead (Krauss Maffei). A pressure of up to 150 bar could be safely handled (Ridley, 1996).

The synthesis of the prepolymer with a 8:1 NCO:OH ratio (1250 g of MDI (Desmodur 44M), 1250 g of PPG 2000 (previously dried in a rotavapour for 3 hours at 90°C) and 1.5 g of conventional dibutyltin dilaurate catalyst (Sigma Aldrich)) was carried out at 60°C using a storage tank as a batch reactor. The NCO content of the prepolymer was determined by the procedure described in section 3.3.1.2.2 to assess the extent of reaction. Once the %NCO in the prepolymer was known, the formulation of the polyurethane was calculated to give a molar ratio 6:1:5 of prepolymer:PPG 1000: 1,4 butanediol. Stream 2 was loaded with 3000 g of PPG 1000, 1350 g of 1,4 butanediol and 2.9 g of catalyst. The Krauss Maffei MK-6150 mixhead (Figure 3.5) served as a reactant flow control valve and also as a mixing device. By effective sequence control of the mixhead in conjunction with the displacement of the lance pumps, it was possible to achieve a wide range of reactant throughput rates at controlled stoichiometries.

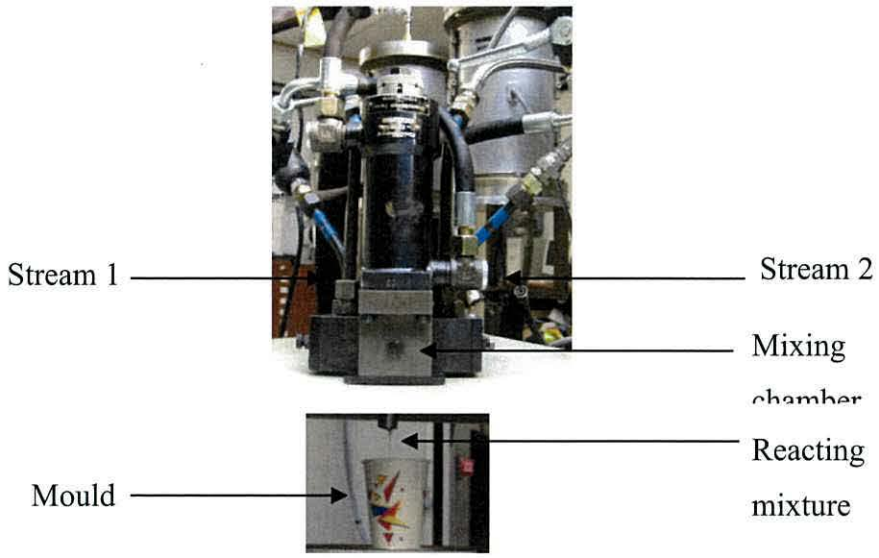

Figure 3.5 Krauss Maffei MK-6250 mixing head and an example of the dispensing of well-mixed reactants of controlled stoichiometry into a paper cup.

The machine settings and tank temperatures used are summarised in Table 3.1

Table 3.1 Machine settings and system parameters employed in the RIM experiments

	Stream 1	**Stream 2**
Reactant	Prepolymer 8:1 NCO/OH ratio	PPG 1000 + 1,4 butanediol + catalyst mixture
Tank temperature (°C)	60	Ambient
Orifice Diameter (mm)	0.1	0.1
Mix ratio	1	1

The reacting mixture was injected into a mould (paper cup) and placed in a vacuum oven at 80°C for 24 hours in order to cure. The molecular weight of the product was determined by GPC.

3.3.3 Reacting drops

As discussed in Chapter 2, mixing on the micro-scale should be considered carefully in order to miniaturise the RIM process for PU synthesis. Based on the findings by Wickert et al. (1987), it was of interest in this present research to study the reaction between two air-borne reactant droplets, with the purpose of simulating the

process that would occur (e.g. unassisted mixing) in the miniaturisation of PU synthesis using ink jet printing as the means for dispensing reactants. A series of uncatalysed and catalysed bulk polymerisation reactions between two droplets were followed by FTIR and Raman spectroscopy. One of the microdroplets was of prepolymer containing 21.5% NCO and the second droplet was formed from a mixture with a molar ratio 4:1 of PPG molecular weight 1000 g/mol and 1,4 butanediol (from now on referred to as the polyol mixture). The catalysed system comprised a droplet with the same polyol mixture, plus 0.1%w of Ti1, The droplets were produced using a Socorex micropipette in the range of 20 – 200 μl and placed in a 1mm deep cavity in an aluminium slide. The prepolymer drop weighed 12.81 mg while the polyol-mixture droplet had a mass of 11.3 mg.

To follow the reactions using FTIR spectroscopy, a drop of the polyol mixture was placed on top of the prepolymer droplet already in the cell of the Golden Gate accessory. A spectrum was obtained at time 0, 45, 90 and 160 min. When following the reaction using Raman microscopy, the laser was focused onto the surface of the prepolymer droplet, and subsequently a microdroplet of the polyol mixture was placed on top. With the laser focused on the same spot the reaction taking place at the interface of the two reactive droplets was monitored. In this case, a spectrum was scanned every 15 minutes during the first hour, and every hour thereafter for a further 4 hours.

3.3.3.1 Mass and energy balance in two droplets

The mass and energy balance of the reaction between two colliding drops was calculated using a simple model in which the following assumptions were made:

i. The model considered a batch reactor with constant volume.

ii. The properties of the droplets are constant with time and are used as approximated values.

iii. The reaction is considered homogeneous, e.g. mixing is considered to happen instantaneously through reaction and molecular diffusion

ULEDA software (a numerical integration package developed in-house for the solution of ODE and algebraic expressions (Gosden and Johnson, 1999) was employed to solve the model equations for the reaction. The equations and parameters used are described in detail in Appendix I.

3.4. Results and Discussion

3.4.1 Batch System

3.4.1.1 Solution Polymerisation and on-line monitoring of PU reaction

The reactant (poly(1,4 butanediol) 2000) was analysed as it was a key component in the model formulation used. The PU produced from this soft-block component should have a molecular weight much greater than 2000. When analysed by GPC, since the polymer should have a larger hydrodynamic volume than any of the reactants, it will have a shorter retention time. The poly(1,4 butanediol) 2000 elution time was 7.5 min. The elution time of the polymer produced vs reaction time changed little (see Figure 3.6) indicating that no significant polymerisation had taken place. This was also the cased when the reactants were left to react a further 22 hours.

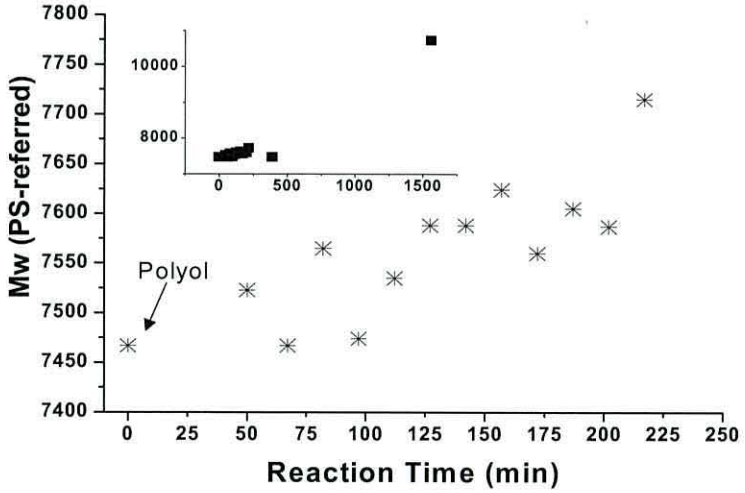

Figure 3.6 Change of weight average molecular weight M_w (PS-referred) of the polyurethane with reaction time for a formulation with molar ratio 1MDI: 0.5 poly(1,4 butanediol) 2000: 0.5 chain extender.

These findings show a small increase in molecular weight M_w of the polymer with reaction time. Either the reaction rate was very slow or that something else was contributing to the slow development of molecular weight. The model formulation was modified to 1 mol of MDI, 0.2 mol of poly(1,4 butanediol) 2000 and 0.8 mol of 1,4 butanediol. The reaction was followed for three hours, and the change of molecular weight M_w with time monitored. The results can be seen in Figure 3.7.

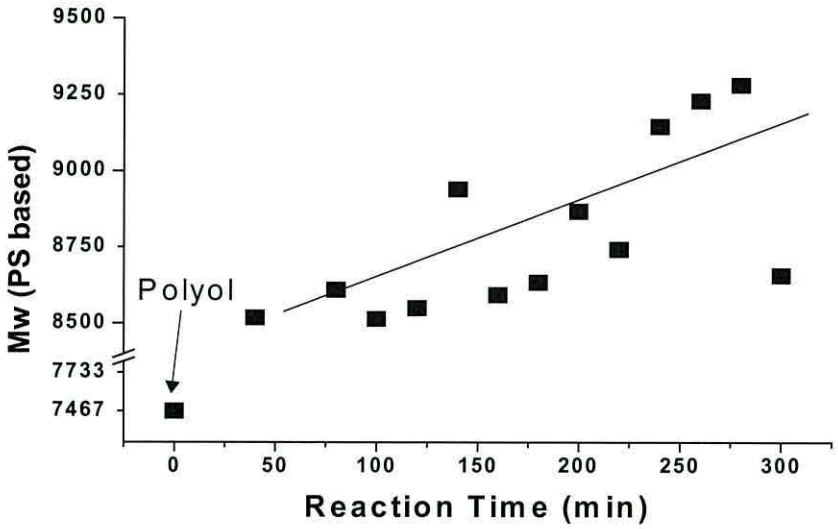

Figure 3.7 Change of M_w (PS-reference standard) of the polyurethane with reaction time for a formulation with molar ratio 1MDI: 0.2 Poly(1,4 butanediol) 2000: 0.8 chain extender.

Once again the GPC analysis showed that very little polymerisation had occurred. In the third synthetic approach, the new Process Monitoring System developed by Polymer Laboratories Ltd was tested, and the polymerisation of a mixture containting 1 mol of MDI, 0.2 mol of poly(1,4 butanediol) 2000 and 0.8 mol of 1,4 butanediol was monitored on-line. The reaction was followed during the first three hours.

Figure 3.8 shows the output of the light scattering detector at three angles, 35, 90 and 145°. In the plot shown, different stages of the reaction are shown including (i) the change in the scattering due to the extraction of the poly(1,4 butanediol) 2000, (ii) the addition of the MDI, and (iii) the start of the polymerisation. Each stage can be clearly seen. The signal levelled at ~6000 s, is the point in the process where the MDI was completely mixed with the polyol and polymerisation commenced. The signal from the three light scattering detectors at the different angles all showed a steady increase, suggesting that the properties of the reacting mixture were changing due to the growth of the polymer chains.

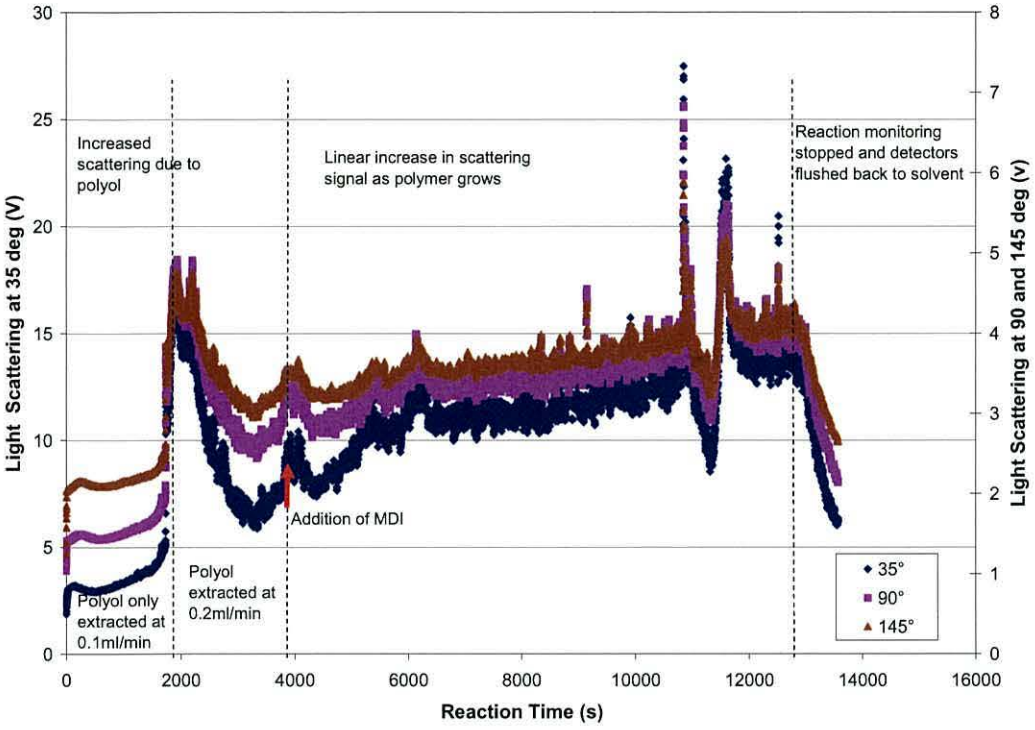

Figure 3.8 Online monitoring of polyurethane reaction: Light scattering detector signal.

However, the change was not sharp (e.g. from 11 to 13 V in 4500 s for the detector at 35°C), which suggests that only a small change in molecular weight was occurring in the time frame analysed (see Figure 3.7).

The signals obtained from the viscometer and refractive index detectors, shown in Figure 3.9, show and upward trend with time as might be expected if polymerisation is taking place.

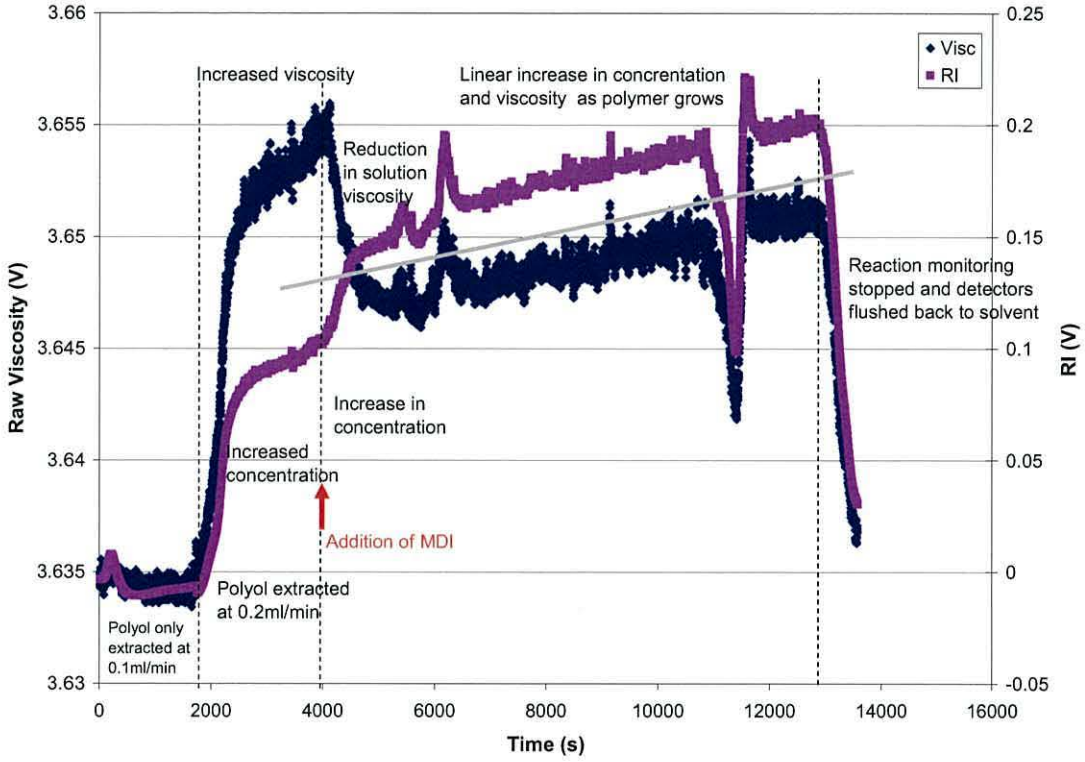

Figure 3.9 Online monitoring of polyurethane reaction: Viscometer and refractive index.

The results from the on-line monitoring of the polyurethane synthesis (Figure 3.8 and Figure 3.9) are similar to those published by Catalgil-Giz et al. (2001). Even though the formulation of the reaction mixture was substantially different in composition (e.g. different raw materials and composition employed), the results by these authors also showed that the signals from the refractive index detector and capillary viscosimeter fluctuated in a similar manner during stages (i) –(iii) of the process (i.e. reactant addition, mixing and polymerisation). The similarity between the trends reported by Catalgil-Giz and co-workers and those presented in this research indicate that polymerisation processes can be monitored on-line using the new technology developed by Polymer Laboratories Ltd. The main difference between the technological infrastructure of the systems employed is that the one tested in this work is significantly more sophisticated. The system employed by Catalgil-Giz, included only a single angle light scattering detector, a single capillary viscometer and no refractive index detector.

The results obtained here show that the first polyurethane synthesis monitored on-line by the technology developed by Polymer Laboratories Ltd is a robust technique that provided relevant information about this reactive process.

However, accurate monitoring of the reaction with this system is only possible during the first stages of the polymerisation. This is due to the increase of viscosity of the reacting mixture which can, potentially, block and destabilise the flow controller. The end-product from the on-line synthesis was characterised by GPC. An apparent molecular weight of 9,000 was obtained.

3.4.1.1.1 *Different NCO:OH ratios*

Stoichiometry imbalance will affect the development of molecular weight in step polymerisations. The impact of different stoichiometric ratios of reactants was explored using DSC.

The thermogram in Figure 3.10 clearly shows the exotherm due to polymerisation. In this experiment a stoichiometric ratio of NCO:OH < 1 was used. The endothermic peak at around 67 °C corresponds to the melting temperature of the PPG 2000, and as the temperature increases, the onset of polymerisation (~190 °C) leads to the polymerisation reaction exotherm which extends to ~ 225 °C.

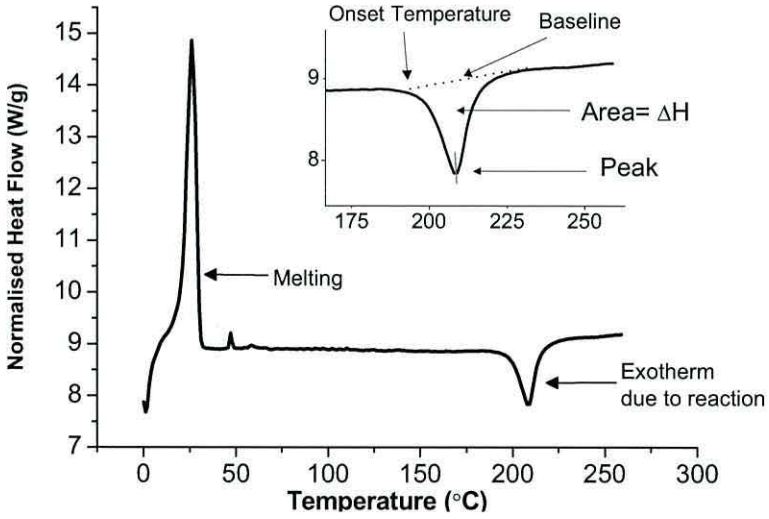

Figure 3.10 Thermogram of the polyurethane reaction with a NCO/OH ratio 0.4; (endothermic peak upwards and exothermic peak downwards).

It is shown in Table 3.2, that as the NCO:OH ratio increases, the onset polymerisation temperature also increases. These results can be explained by the fact that MDI molecules are not very flexible, and it is necessary to add more energy to the reactive mixture so that the NCO block can move and the reaction begins. Similarly, the exotherm peak is shifted to higher temperatures at higher NCO content. The area of the exotherm, ΔH, is related to the overall conversion of the reactants, which

suggest that at higher ΔH value, longer polymer chains are formed. These findings confirm the expectations that, as the NCO content increases, the molecular weight should increase. Molecular weight change with stoichimetry is analysed later in this section.

Table 3.2 Thermal data for the polymerisation reaction at NCO:OH ratios < 1.

NCO:OH ratio	Onset (°C)	-ΔH (kJ/g)	Peak (°C)
0.18	182	19	188
0.4	187	26	194
0.6	197	22	207

According to Figure 3.11, the polymerisation process with NCO:OH ratios ≥ 1 occurs in two stages, i.e. the thermogram shows two exotherm peaks. This is likely to be due to the fact that the MDI molecule has low flexibility (e.g. mobility) so it is easier for the BDO to diffuse, resulting in the formation of MDI-BDO hard-segment blocks first.

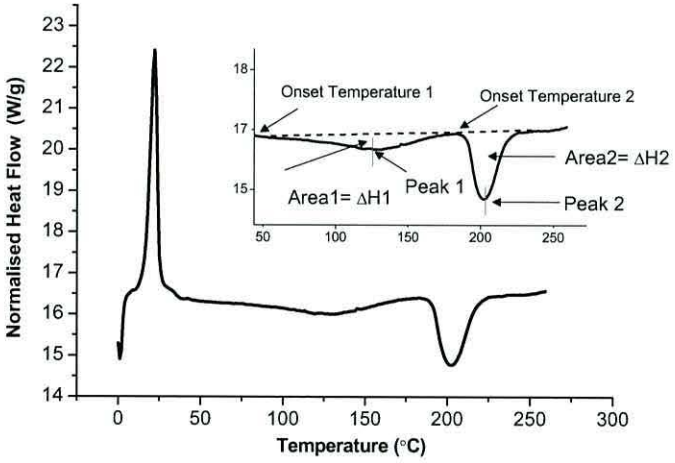

Figure 3.11 Thermogram of the polyurethane reaction at ratios NCO/OH>1; (endothermic peak upwards and exothermic peak downwards).

Consequently, the first exotherm peak observed is attributed to the reaction between NCO and BDO molecules that form the hard-block, and then at higher temperature a second wave of PU reaction is observed, where the chains are extended and the soft-block is formed. From Table 3.3 it can be seen that the onset and peak temperatures of the first exotherm decrease as the NCO content rises. However, extracting values for ΔH has to be done carefully, because it is likely that the two exotherms overlap resulting in information being masked. Therefore more

information is needed about this thermal behaviour and is discussed later in this section.

Table 3.3 Thermal data for the polymerisation reaction at NCO:OH ratios ≥ 1.

NCO:OH ratio	Onset (°C)		-ΔH (kJ/g)		Peak (°C)	
	Peak 1	Peak 2	Peak 1	Peak 2	Peak 1	Peak 2
1	123	193	3.9	5.30	154	209
2	108	201	24.5	4.30	140	216
3	97.0	189	20.4	58.2	129	200

Another indication of the effect of stoichiometry imbalance is the molecular weight of the polymer. The degree of polymerisation is calculated using Flory's equation (Equation 2.8), which indicates that the degree of polymerisation, and therefore the molecular weight of the polymer is affected by the stoichiometry of the reactants. It is evident that the highest molecular weight will be achieved when the NCO:OH ratio is ~1. As can be seen from Table 3.4, the results from GPC analysis are consistent with the described behaviour.

For the polyurethanes formed from a formulation with an excess of any of the functional groups (i.e. NCO or OH), it is clear that the molecular weight is lower than that obtained for the polyurethane with stoichiometric formulation. The increase in M_w observed when the NCO content is increased from ratios below 1 (i.e. OH groups in excess) can be explained on the basis that for larger NCO content, longer molecules can form until the limiting reactant (e.g. MDI) is completely consumed.

Table 3.4 Molecular weight and its distributions for PU with different NCO:OH ratios.

NCO:OH Ratio	M_w (Ps-referred)	MWD
0.18	9000	1.8
0.4	11500	1.9
0.6	18100	2.1
1	35000	2.3
2	22500	2.4
3	11400	1.9

On the other hand, when there is an excess of NCO groups (e.g. ratios >1) the molecular weight decreases because the degree of polymerisation (Equation 2.8) is lower than that corresponding to the polymer obtained from formulation of the ratio 1. Also, the polydispersity is reduced when functional groups are in excess as depicted in Figure 3.12.

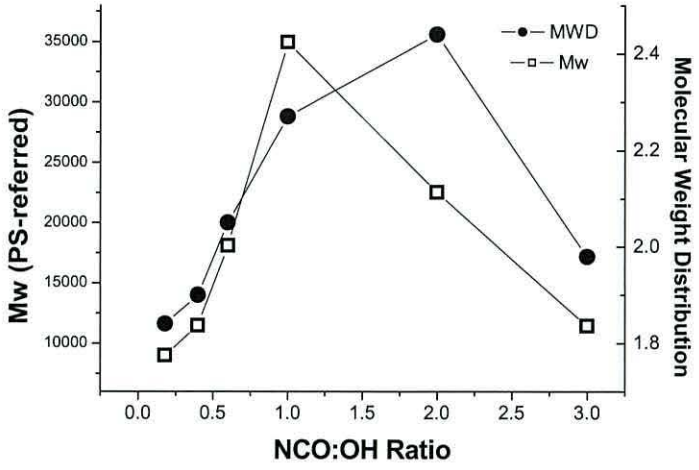

Figure 3.12 Change of M_w of final product with change in stoichiometry.

These findings are consistent with the earlier discussion made in this section, where an increase in molecular weight was expected for polymers synthesised with an NCO:OH ratio < 1. This is where the observation that at higher NCO contents, higher ΔH values were observed suggesting a molecular weight increment.

The prepolymer to be employed in RIM and IJP experiments was designed to have an excess of NCO groups. The primary parameter to be considered was that the prepolymer obtained should be liquid at a temperature of 60°C, because the RIM machine was able to heat Stream 1 up to that temperature. The prepolymers prepared using a PPG 1000 and with formulations with a molar ratio NCO:OH below 2 were all solids, and so not suitable for the RIM or ink jet printing systems. Prepolymers, Prep-4, Prep-10 and Prep-11, were synthesised using PPG 2000 and NCO:OH in the ratios 2:1, 3:1 and 4:1 respectively. These prepolymers did not melt, neither at 50 nor at 60 °C. As shown in Figure 3.13 these have similar chromatographic profiles.

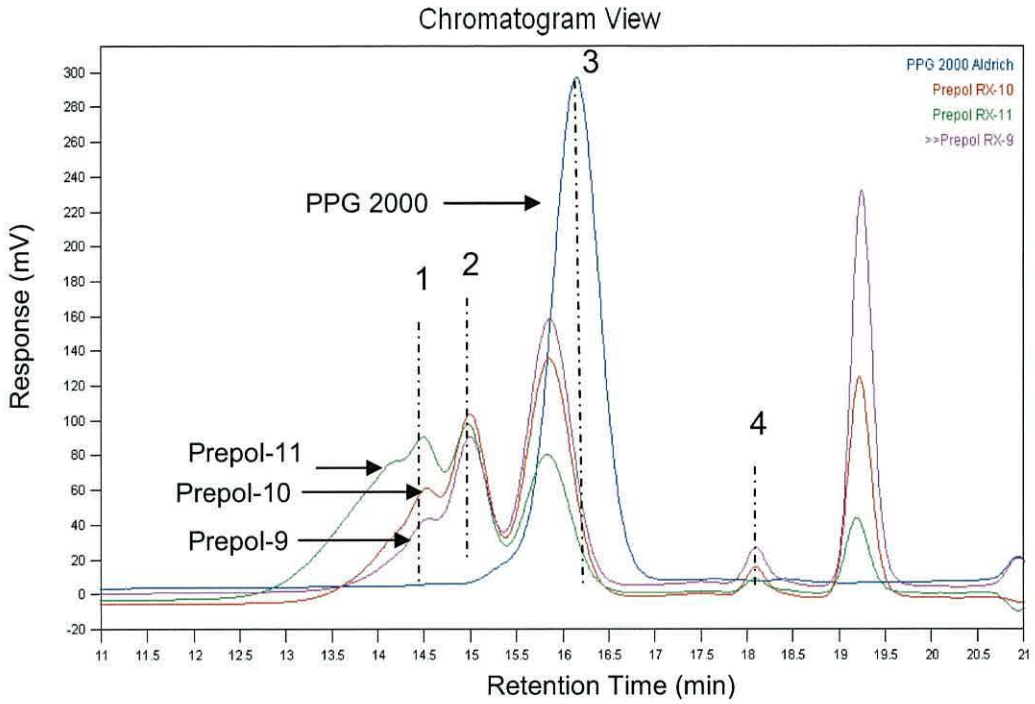

Figure 3.13 Overlay of chromatograms describing molecular weight profile for prepolymers Prep-9, Prep-10 and Prep-11 in contrast with the PPG 2000.

Four different peaks (marked from 1 to 4 in Figure 3.13) are visible within the calibration area. As the NCO content increased, the relative M_w of each peak increased in comparison with the starting polyol, whereas the polydispertity (PD) and peak area remained relatively constant ($1.0 < PD < 1.2$) in all formulations. The molecular weight of the prepolymers 9, 10 and 11 with NCO:OH ratios of 2, 3 and 4, respectively are shown in Table 3.5.

Table 3.5 Molecular weight values of the different peaks of prepolymers Prep-9, Prep-10 and Prep-11 in comparison with the initial PPG 2000.

PPG 2000				
	Mp	**Mn**	**M_w**	**PD**
Polyol	3100	3080	3200	1.1
Prep-9				
Peak No.				
1	8000	9100	10100	1.1
2	3900	3900	4000	1.0
3	561	540	550	1.0
4	180	177	180	1.0
Prepol-10				
Peak No.				
1	11700	14200	15300	1.1
2	7967	7846	8020	1.0
3	3973	3841	4000	1.0
4	560	540	550	1.0
Prepol-11				
Peak No.				
1	12200	16000	18500	1.2
2	8076	7804	8000	1.0
3	4030	3906	4000	1.0
4	560	530	540	1.0

The prepolymer that was fluid at 60°C was Prepol-12. The formulation used for its synthesis contained 8 mol of NCO and only 1 mol of OH (PPG 2000), so that it was the best candidate to be used in the RIM experiments. The chromatographic profile of the prepolymer Prepol-12 showed also four peaks as shown in Figure 3.14.

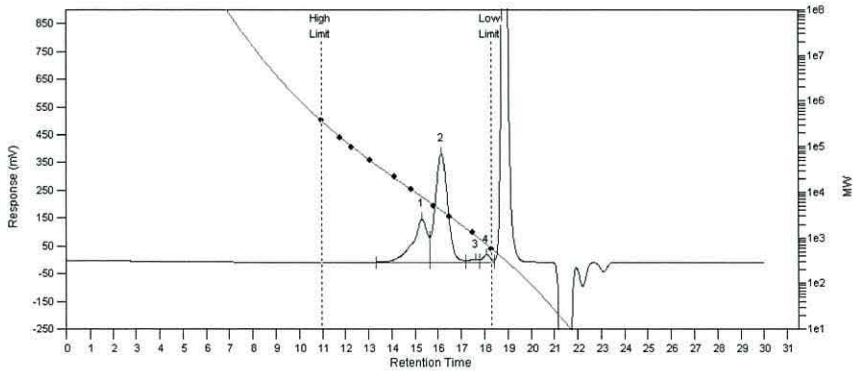

Figure 3.14 Chromatogram of the prepolymer Prepol-12.

The molecular weight of each peak of the Prepol-12 is shown in Table 3.6, which also shows that the polydispersity of the peaks is narrow (~1), making the peaks well-defined. It is evident that the largest polymer molecules (i.e. M_w = 9817) are present in relatively low proportion, whereas those with a molecular weight of 4000 are present in higher amount, as can be seen in Table 3.6.

Table 3.6 Apparent molecular weight of Prepol-12 after 60 min of reaction.

Prepoly-12					
Peak No.	**Mp**	**Mn**	**M_w**	**PD**	**% Area**
1	7900	8900	9800	1.1	31
2	4000	3800	4100	1.1	65
3	1100	1300	1200	1.0	1.3
4	720	710	730	1.0	2.8

The progress of the reaction to form prepolymer Prep-12 using the conventional catalyst dibutyltin dilaurate at a concentration of 0.1%w was followed for 60 minutes. The reaction went to completion after 10 minutes. Thereafter, the molecular weight remained constant, as shown in Figure 3.15.

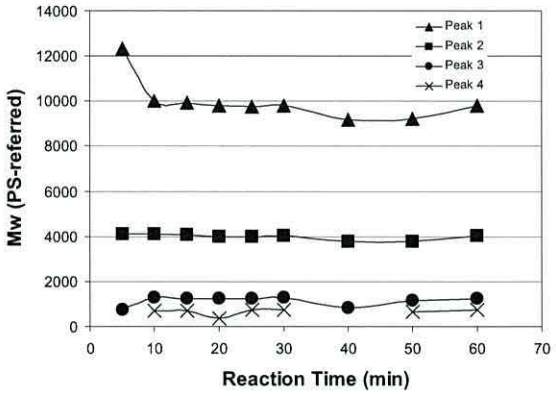

Figure 3.15 Change of the four molecular weight peaks of Prepol-12 with time.

Considering that the formulation for this prepolymer comprises 8 mol of MDI (with a functionality F=2) and 1 mol of PPG 2000, the theoretical %NCO is calculated from Equation 3.5, which yield %NCO=4.7 %. The average %NCO content determined experimentally was also 14.7%, as 12.5 ml and 11.6 ml of HCl solution were required to titrate the blank and 0.2567g of sample respectively. This %NCO determined by titration indicated that the experimental procedures were high-quality. (When the %NCO determined by titration is considerably less than the

theoretical value, this is an indication that there are contaminants in the reactants. In particular it can be an indication that the raw materials still contain water).

3.4.1.1.2 *Chain extender for hard and soft PUs formulations: DMA Results*

The impact of the concentration of 1,2 butanediol in the polyol mixture was examined by the effect on the molecular weight and glass transition temperature, Tg, of castings prepared using Prepol-12. The purpose was to the determine the appropriate concentration of chain extender to be added to the Polyol, Stream 2, in the RIM and IJP experiments. Two different formulations for the castings were tested, one containing a molar ratio of NCO:OH:BDO of 6:1:5 and the second one a ratio of 6:5:1. The overall NCO:OH ratio was kept to 1:1. The molecular weight and Tg of the polyurethanes obtained from the castings were obtained by GPC and DMA, respectively.

Figure 3.16 shows the temperatures at the first peak maxima in the plots of the tan δ of these materials which were taken as Tg temperatures.

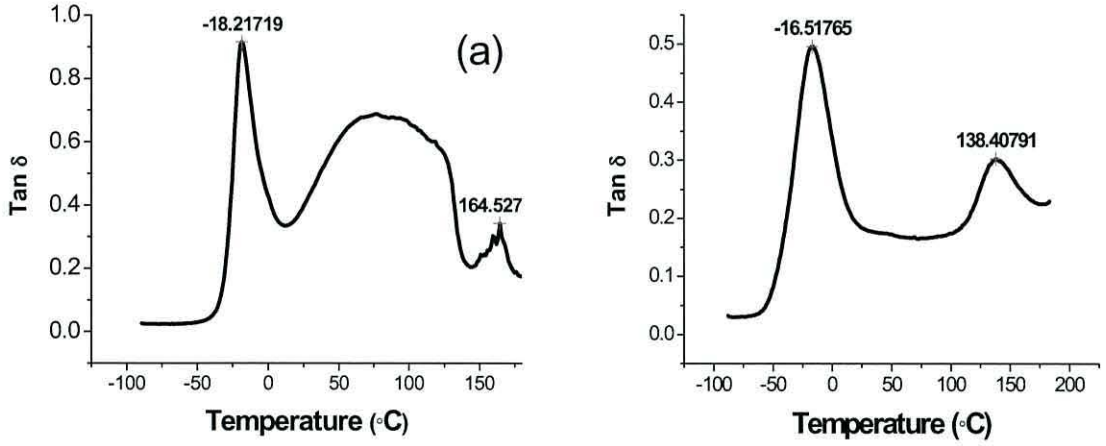

Figure 3.16 Glass Transition temperature, Tg, for (a) low and (b) high hard-block content.

The results are shown in Table 3.7 and it is clear that the polyurethane with more hard-block content had a higher Tg compared to the low hard-block content (i.e. soft).

Table 3.7 Formulations and properties of the different castings tested using in-house made prepolymers.

Sample Name	NCO:OH:BDO	Tg (°C)	M_w (Peak 1)	PD (Peak 1)
High hard-block content	6:1:5	-16.6	9500	1.49
Low hard-block content	6:5:1	-18.2	16150	1.16
Commertial PU	-	15	-	-
Poor mixing and OH excess	3:5:1	-23.9	13630	1.28

Furthermore, the molecular weight of the hard PU was lower than that of the soft polymer. These results are readily explained by the fact that the hard PU contains more hard-block units per unit mass. The additional crystallinity which this introduces in the polymer makes it stiffer and harder than the material with a low hard-block content. As a consequence the minimum temperature needed to allow crankshaft movement of the polymer chain in the amorphous domains (as manifest by Tg) will be higher than that needed with a polymer with a higher amorphous content. The results presented here agree with data reported in the literature (Hsu et al., 1999).

These results may be placed in context if the glass transition temperature is compared with products available commercially. For that purpose, a lyurethane was synthesised using a "polyurethane kit" from RS Components Ltd. and the product characterised. The product was not soluble in THF suggesting that it was crosslinked, which precluded determination of its molecular weight by GPC. The Tg of the commercial material was analysed using the DMA. As Figure 3.17a shows, a well defined peak is obtained yielding Tg ~15 °C. When the sample was examined, it became evident that this PU was much harder than that synthesised using Prepol-12 (Tg=-16.5°C).

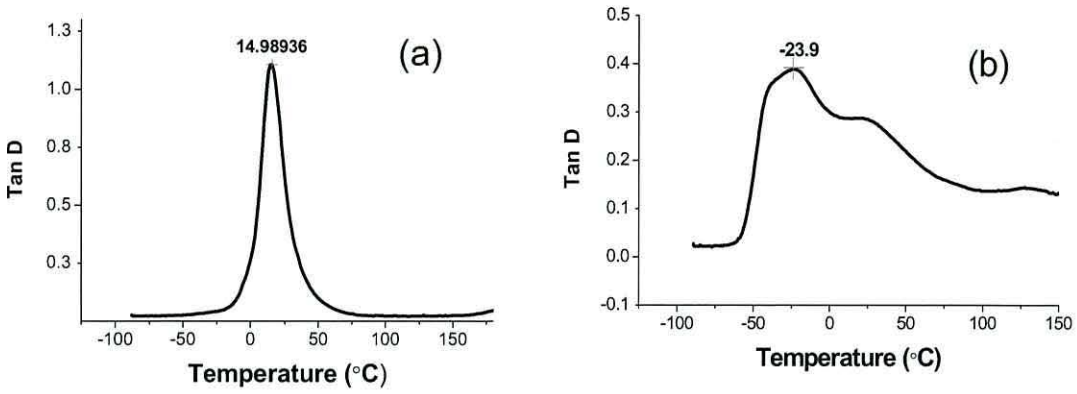

Figure 3.17 Glass Transition temperature, Tg, for (a) commercial PU and (b) PU with OH excess and poor mixing.

Also, the commercial PU showed a clear yellowish physical appearance, while the PU synthesised using Prepol-12 was a whitish solid. The difference in colour and opaqueness is derived from the molecular structure (aromatic PUs tend to yellow) and the phase separation of the hard and soft segments in the polymer chain.

In an additional test run to demonstrate that an overall stoichiometric imbalance would affect Tg, a PU casting was prepared with an excess of OH groups. It was expected that the insufficiency of NCO groups would lead to a PU with longer and more flexible chains and hence a lower Tg. The results in Figure 3.17b and the glass transition temperature of -23.0 °C can be clearly seen.

Rather than establishing a specific formulation, the aim of these findings was to serve as a simple guide for the design of PU formulations suitable for RIM and IJP studies. Clearly, the final formulation should be designed with the final properties of the product in mind, but the IJP technology might not be capable of handling the reagents required. The RIM technology is much less sensitive to the nature of the reactants but is not without its limitations. For the purposes of this investigation, the formulation chosen for use in the RIM and IJP experiments was that leading to a high hard-block content.

3.4.1.2 Kinetics of the un-catalysed PU reaction

There is the need to study the kinetics of the polymerisation reaction used with IJP and RIM technologies as the dynamics of the chemistry has to be comparable with the dynamics of the technologies, As a rule of thumb, the dynamics of the technology should be faster than the rate at which reaction occurs. In this section, the kinetic study of the hard and soft PU (e.g. high and low hard-block content respectively) is

presented. Using the DSC methods in the dynamic mode, heating rates of 5, 10, 20 and 30 °C/min, were employed and the Kissinger method used for the calculation of the kinetic parameters. As shown in Figure 3.18 there is a difference between the thermograms obtained for the hard and soft PU formulations. The formulation containing high hard-block content shows a single exotherm, (even though there is a perturbation in the exotherm which it is due to the hand mixing, it is considered to be single process). The low hard-block formation produces two peaks (Figure 3.18b) the first with a temperature in the range of 108 °C < T_f < 153 °C and the second exotherm between of 183 °C < T_f < 208 °C. This is discussed later on in this section.

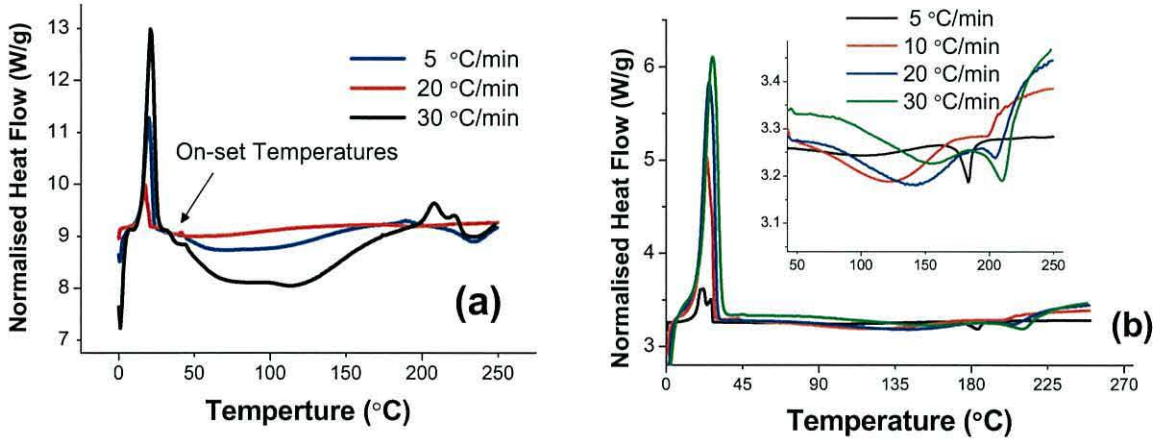

Figure 3.18 Dynamic experiments for non-catalysed reaction containing (a) high hard-block content at 5, 20 and 30° C/min; and (b) low hard-block content at 5, 10, 20, and 30° C/min.

The value of the parameters, on-set temperature, exotherm peak temperature and ΔH were determined using the Pyris Data Analysis software (Perkin Elmer).

The activation energy, E_a, for the polymerisation of the formulation with a high hard-block content product can be calculated by plotting the Kissinger parameters $\ln(\beta/T_f)$ vs $1/T_f$, and as shown in Figure 3.19.

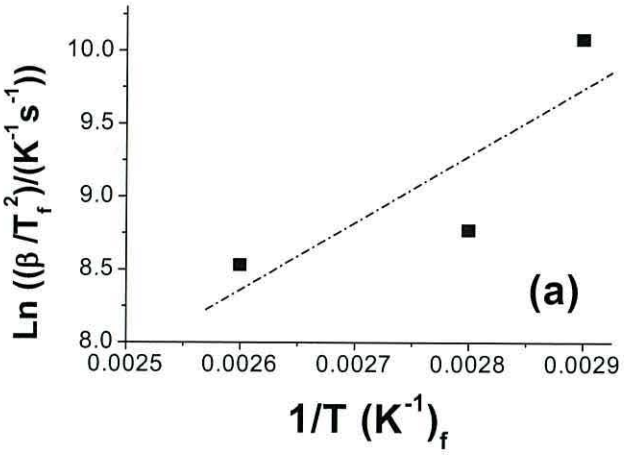

Figure 3.19 Plot of $\ln(\beta/T_f)$ vs $1/T_f$, used to determine the activation energy, E_a, using the Kissinger method for the non-catalysed reaction of a formulation with high block content PU.

Table 3.8 Thermal parameters obtained at different scan rates for the calculation of E_a for uncatalysed formulations with a high and a low hard-block content PU.

High Hard-block content			
Heating Rate (°C/min)	**5**	**20**	**30**
Onset Temperature (°C)	45.3	46.2	46.2
Exotherm Temperature Peak (°C)	71.7	86.5	117.7
ΔH (J/g)	17.9	70.0	121.2
R (J/ K mol)	8.314		
Activation Energy (kJ/mol)	**38.3 ± 8**		

It is clear that the onset temperature for this reaction was in the range 45 – 46 °C and is independent of the heating rate. However, the ΔH values increased as the heating rate increased which means that the scan rate directly affects the reaction rate and hence the temperature of the exothermic peak. It follows that it is important for comparison purposes that the total heat liberated due to the polymerisation be made when experiments are run at the same heating rate. However, the coefficient of regression of 0.84 in the calculation indicates that experimental errors were present. This may be explained by the fact that the reaction starts immediately on mixing and continues before loading the DSC pan and the stabilisation of the instrument, prior to data capture and the temperature is raised. The exothermic heat measured by the instrument will be slightly lower than it should be for this reason, so measuring T_f accurately is difficult. The precision of the measurements is lowered as it is almost

impossible to replicate the mixing, pan sealing, DSC stabilisation from experiment to experiment. The problem can be minimized by lowering the temperature of the reactants and the mixing process, but not in a significant way.

The parameter chosen to compare the kinetic behaviour of the reaction was the activation energy E_a. It quantifies the energy needed to activate the polymerisation; the lower the activation energy needing to be overcome to begin the reaction, the faster the reaction will occur at any given temperature. The activation energy of 38.3 kJ/mol obtained is within the range reported (Dimier et al, 2004). These authors found an activation energy value of 43.6 kJ/mol for a polyurethane formation comprising three components: prepolymer with NCO excess, a polyester and BDO using mercury as a catalyst.

The reaction containing low hard-block contents (e.g. soft PU) presented two exotherms. As a first approach, the activation energy of both stages of the reaction was calculated using the Kissinger method, using the method previously used for the hard PU formulation. The results are shown in Figure 3.20 and Table 3.9.

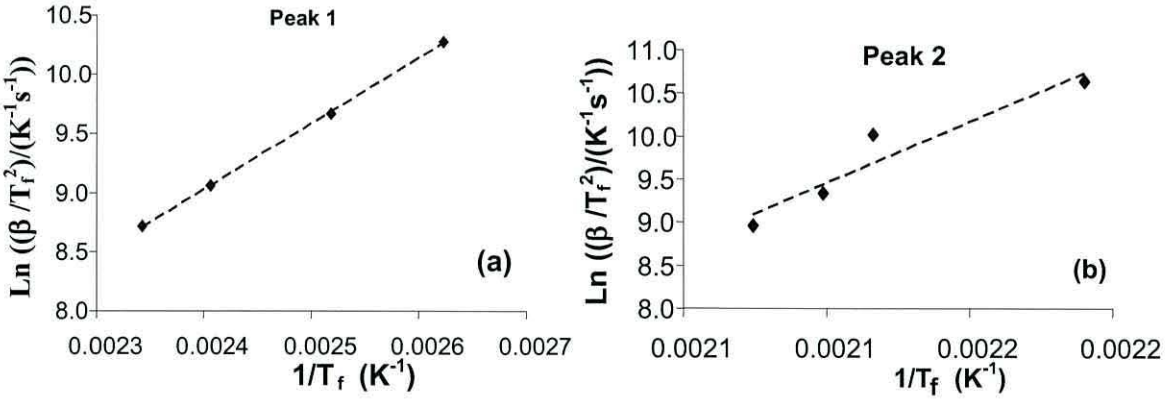

Figure 3.20 Kissinger plots for the non-catalysed reaction of low block content PUs. (a) The first, and (b) the second exotherm.

Table 3.9 Thermal parameters obtained at different scan rates for estimating E_a for the uncatalysed low hard-block content PU.

Low hard-block content: exotherm one				
Heating Rate (°C/min)	5	10	20	30
Onset Temperature (°C)	60.4	69.3	95.4	122.8
Exotherm Temperature Peak (°C)	108.2	124.1	142.7	154.0
ΔH (J/g)	26.3	23.3	11.4	3.8
R (J/ K mol)	8.314			
Activation Energy (kJ/mol)	**46.1 ± 1**			
Low hard-block content: exotherm two				
Heating Rate (°C/min)	5	10	20	30
Onset Temperature (°C)	174.0	193.9	196.3	193.4
Exotherm Temperature Peak (°C)	183.6	199.6	203.5	209.1
ΔH (J/g)	21.6	0.8	2.6	5.3
R (J/ K mol)	8.314			
Activation Energy (kJ/mol)	**118.2 ± 14**			

As mentioned earlier, it is clear that the first phase of the reaction is faster than the second because the activation energy E_a calculated for the first reaction stage was 46.1 kJ/mol whereas for the second it was 118.2 kJ/mol. This may be explained by the fact that the small molecules of the BDO diffuse more rapidly and the hard-block is formed first. As the temperature continues to rise, the polyol molecules start to react and the soft-segment is formed. The chain extender content affects the kinetics of the polymerisation as can be seen from Figure 3.21.

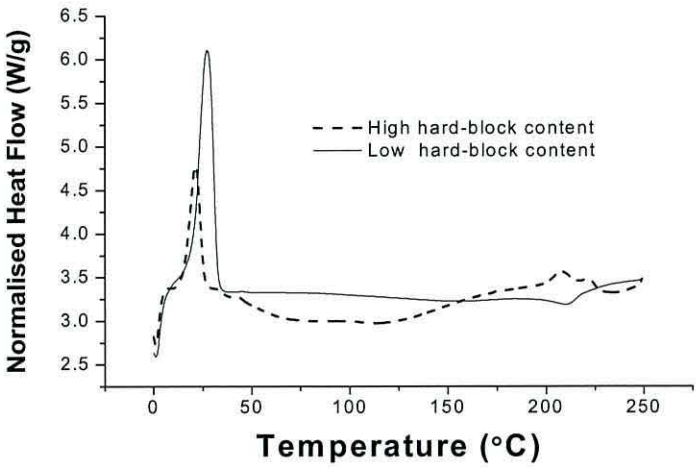

Figure 3.21 Comparison of the thermograms for the reaction of the hard and soft formulations at a heating rate of 10°C/min.

The reaction with more than one exotherm, perhaps should not be treated by the Kissinger method, since it is possible that the second exotherm is the result of an exothermic crystallisation process rather than polymerisation.

A series of isothermal kinetic experiments were carried out with the hard PU formulation. The temperatures chosen were 30, 40 and 50 °C. Firstly, it was necessary to calculate the total ΔH of the reaction, which is the heat developed in the process at full conversion. This was obtained by heating a weighed amount of reaction mixture from 0 to 250 °C at 10 °C/min and subsequently reheating as shown in Figure 3.22.

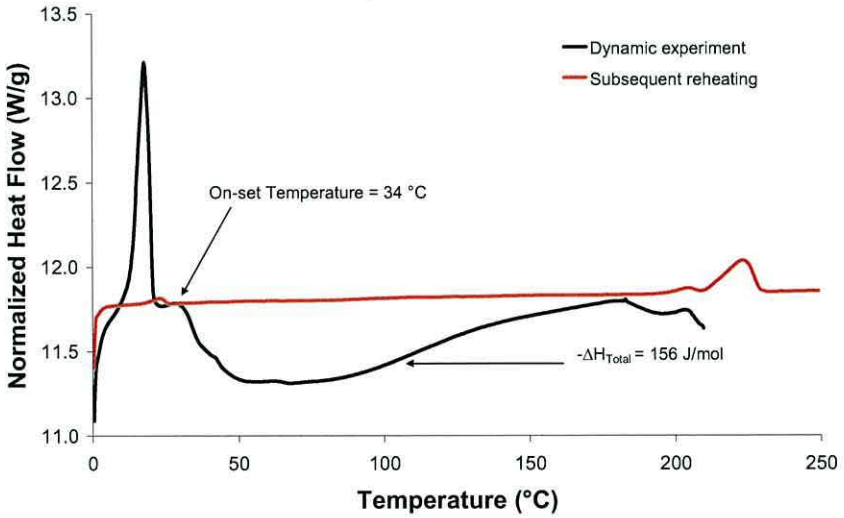

Figure 3.22 Dynamic run for determining the total ΔH for the uncatalysed polymerisation of a high hard-block content formulation.

Isothermal experiments were then undertaken at different temperatures to follow the conversion. After given times, dynamic experiments run at 10°C/min were carried out to determine the amount of unreacted material. For example, the reheating of the sample after isothermal reactions at 50°C for 5, 10, 15, 30, 60 and 180 min.

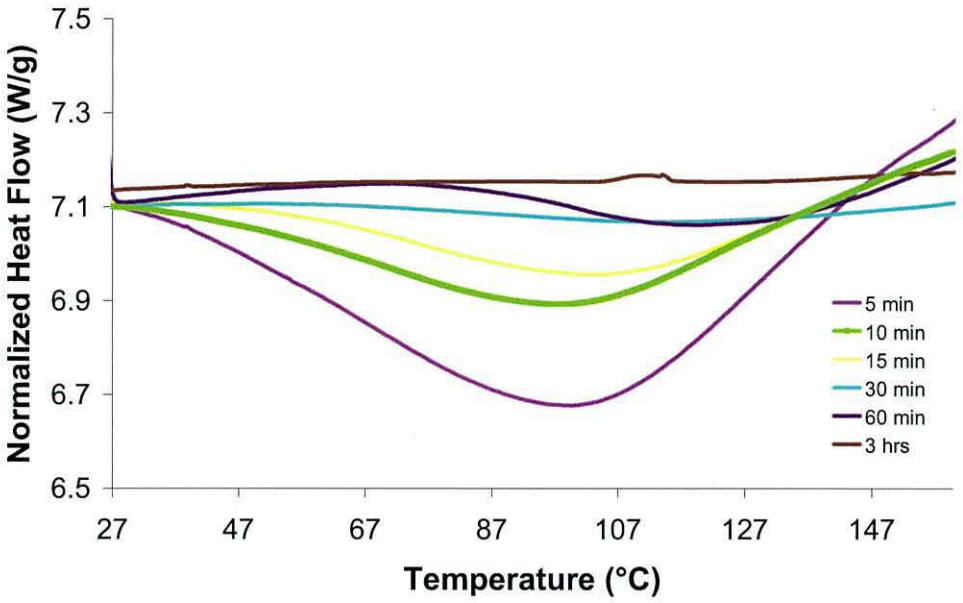

Figure 3.23 After reaction at 50 °C for the periods shown, the reaction exotherms obtained resulting from unreacted material (uncatalysed reaction of high hard-block content polyurethane).

From the thermograms in Figure 3.23, on-set temperature, exotherm peak temperature and ΔH were determined for each time interval using the Pyris Data Analysis software (Perkin Elmer) and are shown in Table 3.10. The fractional conversion α achieved after each time was calculated using equation 3.3.

Table 3.10 Reaction progress determined by isothermal experiments at 50 °C.

Reaction Time (min)	On-Set Temperature (°C)	Peak Temperature (°C)	ΔH (-J/mol)	α
0	34	68	160	-
5	48	103	64	0.59
10	61	102	34	0.78
15	62	106	34	0.78
30	83	121	26	0.83
60	90	132	19	0.88
180	118	134	2.7	0.98

The essential assumption for calculating the kinetic parameters was that the polymerisation reaction is second order with equimolar concentrations i.e. [NCO]=[OH] and a density of 1 kg/L (see Section 2.2). On this basis, the slope from a plot of $(1/[NCO])-(1/[NCO]_o)$ vs reaction time (Equation 2.6) should yield the value of the reaction rate constant k (Equation 3.3). A similar procedure was followed for the isothermal reactions carried at 30 and 40 °C. Figure 3.24 shows that the good linear fit to the data for reactions at 30, 40 and 50 °C confirms that the reaction follows second order reaction model.

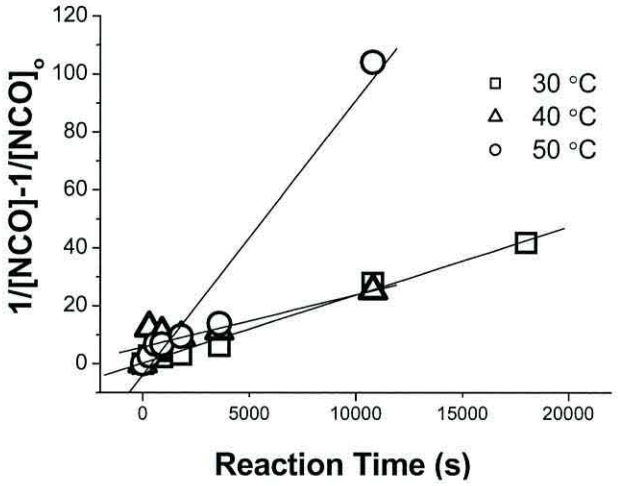

Figure 3.24 Plot $(1/[NCO])-(1/[NCO]_o)$ vs reaction time for the calculation of reaction rate constant at 30, 40 and 50 °C for the uncatalysed reaction of high hard-block content PU.

The calculated values for the reaction rate constant for the 3 temperatures tested are shown in Table 3.11 together with the coefficient of regression.

Table 3.11 Reaction rate constant at different temperatures calculated from a linear regression for a second order un-catalysed reaction for high hard-block content PU

Reaction Temperature	**30 °C**	**40 °C**	**50 °C**
k (kg/mol s)	0.0024	0.0018	0.0095
Coefficient of Regression R^2	0.99	0.87	0.98
Half-life time (s)	772	1028	195

The coefficient of regression points out the experimental errors. The small decrease in the reaction rate constant between 30 and 40 °C can be explained by the fact that the reaction mixtures were prepared by hand. It is evident that the mixing achieved during the 15s of manual stirring was probably not efficient enough to mix

all the reactants homogeneously. However, the half-life time value for temperatures between 30 and 50 °C was in the range of 17 – 3 min. This fact suggests that the reaction is slow for RIM and IJP experiments, as 95% of conversion was only achieved only after 5 hours of reaction (see Table 3.10). For that reason attention was given to the use of catalysts to speed up the reactions.

3.4.1.3 Catalyst Selection

Four commercial catalysts were studied, two zirconium-based (Zr1 and Zr2) and two titanium-based (Ti1 and Ti2). Preliminary experiments were undertaken using Zr1 at three concentrations: 0.05, 0.1 and 0.196 % w/w of polyol and the corresponding thermograms are shown in Figure 3.25.

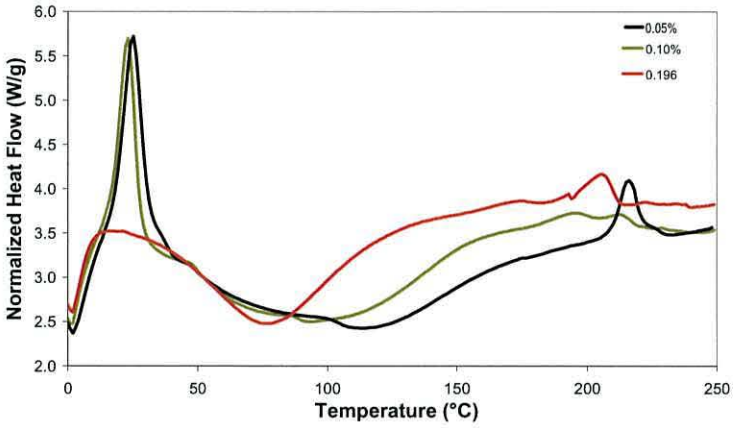

Figure 3.25 Comparison of the thermograms, at a heating rate of 30 °C/min, of the reactions using catalyst Zr1 at different concentrations for the formation of high hard-block polyurethane.

The thermograms show that at higher catalyst concentrations, T_f (the exotherm peak temperature maximum) shifted to lower temperatures suggesting that the catalyst lowers the activation energy and increases the reaction rate at any given temperature. In the case of Zr1 at the highest concentration used (0.196% w/w polyol), the onset temperature for the reaction was in the same range as the melting temperature of the polyol masking the onset of polymerisation. Hence the experiments using a high catalyst concentration are so fast that they can not be conducted in a way which allows the collection of essential low-conversion kinetic data. The DSC thermograms for reactions carried out employing only 0.05 and 0.1% w/w polyol, showed that polymerisation was sufficiently slow to collect reliable data to complete conversion. The reaction onset temperature was approximately 45 °C. The activation energy was

calculated for both concentrations using the Kissinger method which yielded values of 43.3 and 35.1 kJ/mol respectively at catalyst concentration of 0.05% and 0.1% w/w polyol. Similar experiments were then carried out with the other catalysts, Zr2, Ti1 and Ti2. The results are shown in Table 3.12 albeit at different concentrations, which nevertheless lie within the range of concentrations of Zr1 used.

Table 3.12 Activation Energy of the four new catalysts tested.

Catalyst	Concentration (%w/w)	Activation Energy (kJ/mol)	Coefficient of Regression ($R^{2)}$
Zr1	0.05	43.3	0.80
	0.1	35.1	0.94
	0.196	25.1	0.95
Zr2	0.05	46.8	0.99
Ti1	0.100	48.7	0.99
Ti2	0.130	53.4	0.83

From the results obtained, it can be seen that the zirconium-based catalyst demonstrated better performance that the titanium-based ones.

3.4.2 RIM Experiments

Experiments were carried out using a mini-RIM machine in order to (i) understand a well-established macro-scale technology (ii) check the processability of the designed prepolymer, and (iii) explore the practicalities of scaling down the pumping systems and mixing to IJP levels.

Several key steps of the process have been identified as important when scaling down. Firstly, when preparing the prepolymer, it became evident that adequate control of heating was needed in order to maintain a constant temperature of 60 °C in the day-tank and in the hoses through which the material was recirculated. The reduction of the prepolymer viscosity by using it at as high a temperature as possible assisted the recirculation, mixing and temperature stability. Also, the day-tank containing the prepolymer has to be completely closed to avoid any contamination with environmental moisture. It was observed that even a small orifice in the tank lid allowed sufficient moisture into the tank overnight to form a 1 cm thick layer of polyurea on top of the prepolymer. The theoretical value of the %NCO content of

prepolymer was 14.7% and it was compared to the value of the synthesised prepolymer determined by titration and the value for the latter was only 10%, a direct result of moisture ingress into the storage system.

The formulation was adjusted to account for this lower NCO concentration and appropriate quantities of PPG 1000, BDO and tin-based catalyst were loaded to the Stream 2 day-tank. The volumetric ratio of prepolymer/polyol mixture was set to 1.20 which was achieved by adjusting the duration for which Stream 1 and Stream 2 were pumped through the mixhead. In the experiments carried out these were 120 mm and 35 mm, respectively, the different rates being used to ensure that good mixing was achieved. These adjustments made possible the accurate dispensing of stoichiometric quantities of both chemical streams.

The mean apparent M_ws of the hard polymer synthesised using the RIM machine are shown in Table 3.13.

Table 3.13 Apparent molecular weights of PU obtained in the RIM experiments.

RIM EXP 1		
Peak No.	**M_w(PS-referred)**	**PD**
1	20400	1.6
2	5340	1.0
3	1780	1.1
4	700	1.0

The castings prepared manually gave samples with M_w=9507 and a polydispersity PD=1.49 for peak 1. For the RIM samples the corresponding figures were M_w=20,365 and PD=1.58. Although both are high hard-block content polyurethanes, the higher M_w obtained with RIM points to significantly better mixing, as was expected.

The mixing efficiency in the RIM experiments is due to the reactants being intensively mixed by impingement at the molecular level. Any striations which might form are very rapidly broken down by diffusion processes. The mixing process is significantly aided by the fact that the reaction is also taking place. The polymerisation is mixing activated, and in RIM processes operated effectively, the mixing is achieved within micro seconds. As a consequence polymerisation kinetics are independent of the diffusion of the reactants and entirely governed by the reaction kinetics until the viscosity of the reacting mass introduces diffusion control or phase

separation (molecular-weight driven or the result of crystallization) . Finally, an important observation made in these experiments was the fact that because the prepolymer stream was heated to 60 °C whereas the Krauss Maffei MK-6150 mixhead employed was not heated, after some time, the prepolymer phase separated blocking the mixing head. Even though the mixing head had a self-cleaning mechanism, the only possible way to unblock the feed stream was to manually disconnect all pipework and the mixhead.. The hoses in Stream 1 had to be replaced with new ones. From these observations it was clear that even at this macroscale, there were some practical issues that should be considered in order to achieve a successful process with the formulations selected.

In the case of IJP technology, when the droplets of a polyol and isocyanate stream impinge, the physical energetics of the impact are low. However, because the droplets are very small, it is possible that small physical forces such as hydrogen bonding, Brownian movement and the energetics of the chemical reaction will be sufficient to cause rapid mixing. The interaction between two air-borne droplets, reacting and non-reacting, is considered in Chapter 5.

3.4.3 Reacting drops

3.4.3.1 FTIR

The prepolymer and polyol mixtures used were examined by FTIR. The prepolymer was designed to contain 21.5 %NCO. The PPG 1000 and BDO was that used for the formation of a hard PU. The individual spectra of each are shown in Figure 3.26.

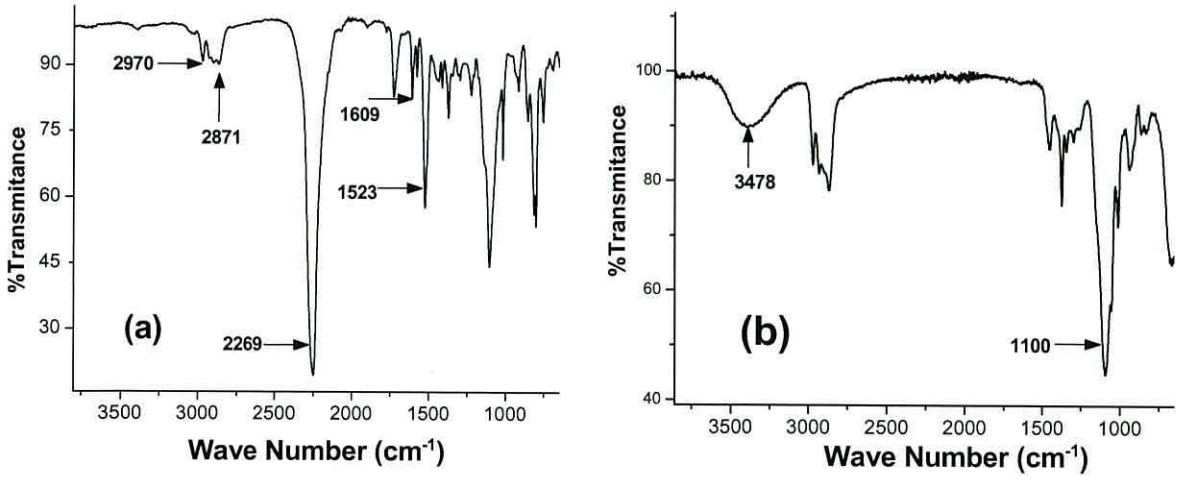

Figure 3.26 FTIR spectra of (a) prepolymer and (b) polyol.

Some of the characteristic bands observed are presented in Table 3.14.

Table 3.14 IR Characteristic Group Frequencies of PU reactive mixture.

Sample	Functional Group	Wave number* (cm^{-1})	Comments
Prepolymer with 21.5 %NCO excess (% w/w)	C-H	2970 - 2850	C-H stretch vibration
	N=C=O	2270 - 2240	Asymmetric stretch in aryl isocyanates
	C=C	1609	Aromatic ring stretching vibrations
	N-H	1523	Secondary amine deformation vibration
PPG 1000g/mol	O-H	3478	Stretching with prescence of intermolecular hydrogen bonding
	C-O	1100	Stretching vibration
Urethane	N-H	3323	Hydrogen bonded stretching vibration in secondary urethanes
	C=O	1710	Carbonyl stretching vibration

*Data based on (Socrates, 2001; Wilhelm et al., 1998; Recalde et al., 2005; Ferry and Jacobsson, 1996; Rajendran et al., 1982).

The finger-print region of the spectra is complex but only two peaks need to be considered in this study. The ν (C-H) band in the region of 2970 cm^{-1} is a suitable reference signal since it remains nearly constant with time during polyurethane formation and several authors have successfully used it for normalisation purposes in kinetic studies (Ferry and Jacobsson, 1996; Recalde et al., 2005). The NCO band at ~2270 cm^{-1} decreases when the –NCO group reacts and was used to follow the polymerisation progress. The spectra at reaction time t=0 min and at t = 162 min illustrating the constant nature of the 2970 cm^{-1} band and the change in the 2270 cm^{-1} are shown in Figure 3.27 a and 3.27b, respectively.

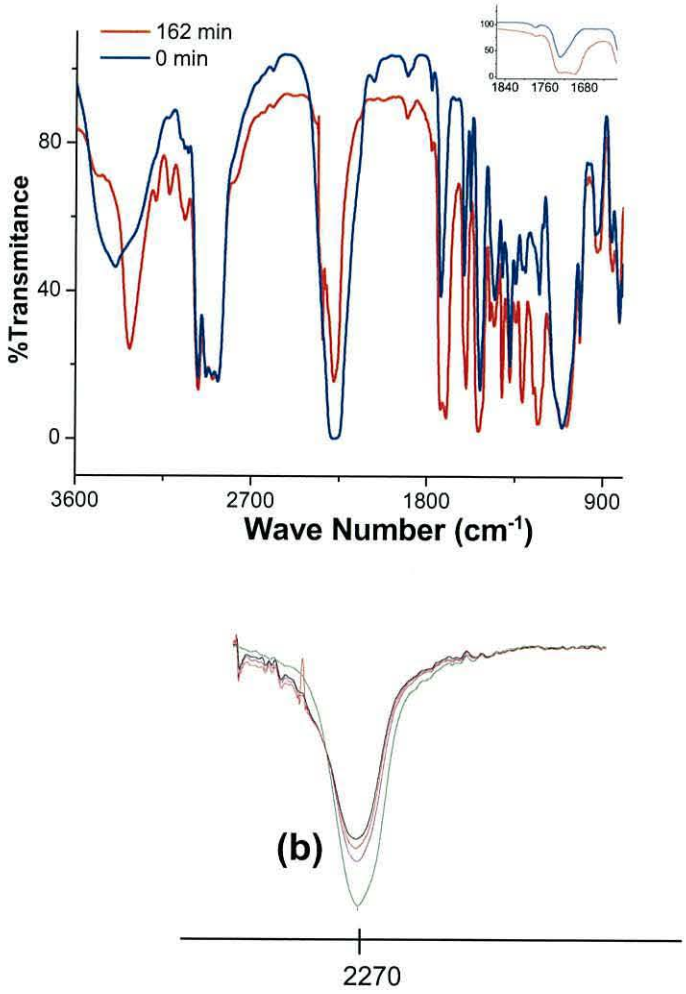

Figure 3.27 FTIR spectra of two reacting droplets normalised to the area of the transmission peak at 2970 cm^{-1} (a) at t=0 and t=162 min, and (b) showing the decreasing area of the peak at 2270 cm^{-1} with polymerisation time.

The fractional reaction conversion was calculated by assuming that the normalised areas of the NCO peak at time t was proportional to the NCO concentration at that time. If the concentration [NCO] is defined as (see Appendix 1):

$$[NCO] = [NCO]_o (1 - \alpha) \tag{3.6}$$

then, from equation 3.6, the fractional conversion α is:

$$\alpha = 1 - \frac{[NCO]}{[NCO]_o} \quad . \tag{3.7}$$

Where [NCO] is proportional to the area of peak at time t and $[NCO]_o$ proportional to the area at time 0. The data obtained was fitted to a second order

reaction model (equation 2.6). Figure 3.28 shows the plot of $1/\alpha$ vs 1/t, so that the slope of the straight line should yield the half-life ($1/k[NCO]_o$) .

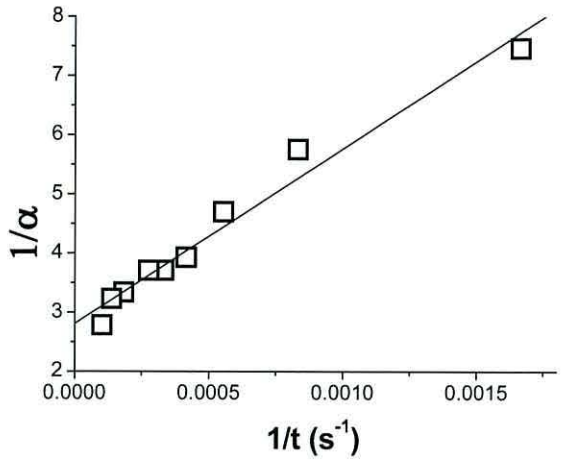

Figure 3.28 Variation of polyurethane conversion with polymerisation time for the reaction between two prepolymer and a diol mixture as obtained by FTIR.

The linear fit yielded a half-life of ~50 min at 20 °C with a coefficient of regression of 0.98. Even though this reaction contained 0.1 % of Ti1 catalyst, the half-life calculated from the spectra is longer than expected (see Table 3.11). Based on the activation energy (~38.3 kJ/mol) deduced from the DSC measurements, the half life is expected to double for every 10 °C, Thus based on the half life of a 770 s at 30 °C (Table 3.11) the half life at 20 °C is expected to be ~25 min. This could be caused by the fact that, instant reaction occurred when the two reactants were in contact and a polyurethane film was formed in the interfacial zone impeding the progress of the reaction. This was an important effect that was studied in more detail by Raman microscopy that facilitated the measurements in this interfacial zone and is discussed later in this section.

Similarly, the NCO peak did not disappear completely (Figure 3.27) probably because, as two droplets of the same size were put in contact and even though the volumetric ratio was 1, the molar ratio evidently was not stoichiometric. While the prepolymer droplet contained 2.24 $x10^{-5}$ mol of NCO groups, the OH mixture droplet only contained $1.1x10^{-5}$ mol. Hence, the molar ratio was 2 having an excess of NCO and having the OH as a limiting reactant.

From this information, complementary data was obtained by Raman spectroscopy which is described below.

3.4.3.2 Raman Spectroscopy

Raman spectroscopy was also employed to study the chemical structure of the reacting mixture. The individual spectra of each reactant are shown in Figure 3.29.

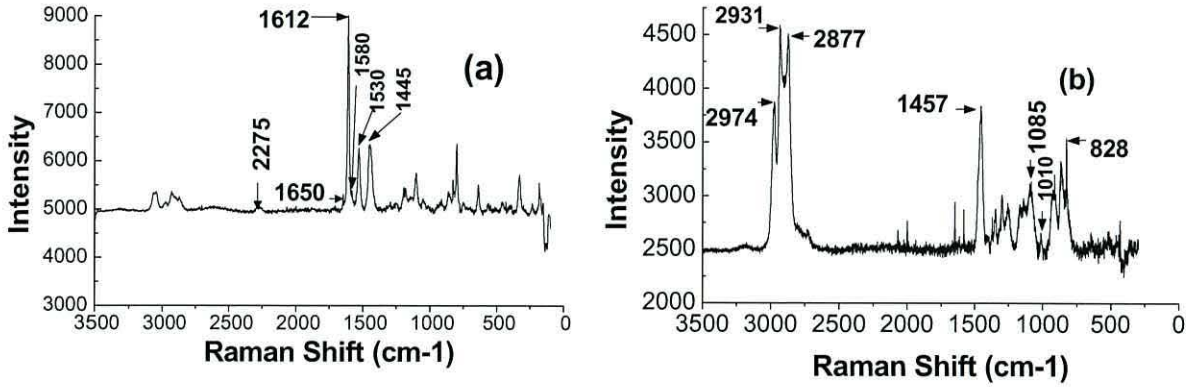

Figure 3.29 Raman spectra of (a) prepolymer; (b) polyol.

Some of the characteristic bands that can be identified in these spectra are summarised in Table 3.15.

Table 3.15 Raman Shifts of the characteristic groups in the PU reactive mixture.

Sample	Functional Group	Raman Shift* (cm^{-1})	Comments
Prepolymer with 20.65 %NCO excess (% w/w)	N=C=O	2275	Asymmetric stretch
	C=0	1650	Carbonyl present in carbamate, for N,N-disubstituted urethanes (amide I: stretching vibration)
	C=C	1612	Aromatic ring breathing/stretching vibrational modes
	N-H	1580	Secondary amine deformation vibration
	CHN	1530	Urethane amide II vibration
	N=C=O	1445	Symmetric stretch
PPG 1000g/mol	$-CH_3$	2974	Aliphatic C-H asymmetric stretching
	$-CH_2-$	2931	Acyclic asymmetric C-H stretching
	$-CH_3$	2877	Symmetric C-H stretching
	$-CH_3$	1457	Aliphatic asymmetric C-H deformation
	C-O	1085	Primary alcohol C-C-O stretching
	C-C	828	Stretching in branched alkanes

*Data based on (Parnell et al., 2003; Socrates, 2001).

It was expected that the prepolymer bands at 1530 and 1445 cm^{-1} would decrease in intensity as the reaction progressed. The intensity of bands at 1650 and 1580 cm^{-1} might be expected to decrease since the relevant functional groups stem from the polyurethane. For purposes of this study, the carbonyl band at 1650 cm^{-1} was selected as a reference band for normalisation purposes as this is attributable to the aromatic ring in the methyl diphenyl diisocyanate molecule which does not change during the reaction.

The laser was focused on the interface between the reactants and the reaction followed for 5 hours. The initial and final spectra are shown in Figure 3.30.

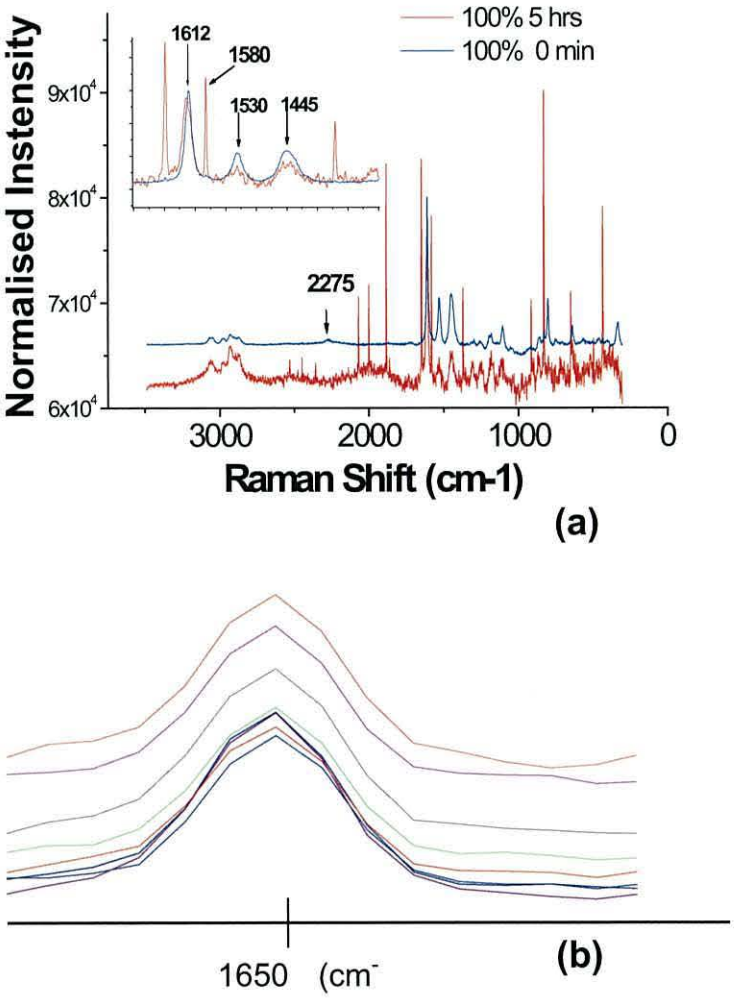

Figure 3.30 Raman spectra of two reacting droplets (a) at t= 0 and t=300 min, and (b) showing the increasing peak height at 1650 cm^{-1} with polymerisation time.

The fractional reaction conversion was calculated assuming that the normalised peak height of the carbonyl peak at time t was proportional to the PU concentration at that same time. Thus, the fraction α converted can be written as:

$$\alpha = \frac{(I_t - I_o)}{(I_{ref} - I_o)} \tag{3.8}$$

where I_t is the intensity of the 1650 cm^{-1} peak at time t, I_o is the intensity at time t=0 and I_{ref} is the intensity of the peak at 100% reaction completion. Unfortunately, in the spectra obtained it was not possible to achieve the intensity at full conversion due to the stoichiometric imbalance. Consequently, the reference peak conversion was taken from Figure 3.28, which suggests that 50% conversion was achieved in 2956 s. So, the conversion was determined from:

$$\alpha = \frac{(I_t - I_o)}{(I_{ref} - I_o)} * 0.5 \tag{3.9}$$

Figure 3.31 shows the the plot of $1/\alpha$ vs 1/t, where the slope of the straight line is therefore the half-life ($1/k[NCO]_o$) .

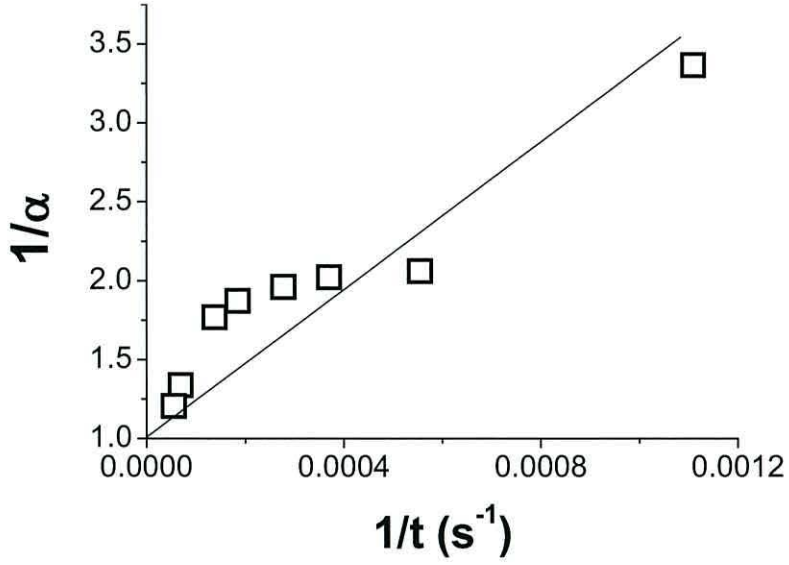

Figure 3.31 Variation of polyurethane conversion with polymerisation time for the reaction between two droplets based on FTIR data.

Again, the data obtained was fitted to a second order reaction model (equation 2.6) and the linear regression yielded a half-life of approximately 30 min with a coefficient of regression of 0.96. It is likely that in the interface where the two reactants meet, and where the laser was focused, instant mixing occurred giving rise to a reaction driven by the kinetics rather than by diffusion. This half-life of

approximately 30 min is similar to the kinetic behaviour studied for the uncatalysed system (Table 3.11), but the Raman study was conducted at room temperature (i.e. 20 °C).

The difference in results obtained from FTIR and Raman spectra could be explained by the fact that while FTIR gives information on the transmittance of the sample, which is an average of the whole reactive mixture, Raman microscopy looks at the interface of the reactants and more accurate results are obtained. As Raman is sensitive to the values of fractional conversion from FTIR data, the fact that the two half-life values calculated are within a factor of 2, suggest that the initial assumption from the FTIR data is reasonable.

If indeed rapid polymerisation occurred at the interface, the film formed here could have prevented further mixing of the remaining species, leading to a chemical reaction driven by diffusion. Such an interfacial product layer was also observed by Wickert and co-workers (1987). In their work, the authors reported that after 10 minutes the dispersion of MDI into polyether stopped as a tendency for the interface to be stable was noted. The authors called this film a "surf-product", which they suggested affected the stability of the dispersion. They observed that when this film was perturbed mechanically (i.e. manual mixing) the film was ruptured and the dispersion of the MDI in the polyether continued. This phenomenon also occurs in the RIM process, where impingement mixing causes the stretching of the "surf-product" and allows further dispersion.

In the results presented in the present study, it is speculated that when the reactants make contact, homogenous reaction occurs in the interface. Since it is assumed that at this scale the striation thickness is small, this reaction is kinetic driven with no time for diffusion to occur at the interface. In this case, the mixing rate is slower than the reaction rate giving rise to a fast reaction. However, after the formation of the polyurethane film at the interface, since it is not perturbed mechanically, the reaction slows down and it becomes diffusion driven.

From these findings, it is believed that at IJP scale, phenomena such as hydrogen bonding, Brownian movement, difference in chemical potential and the reaction itself would drive the mixing, and since the striation thickness between the two droplets is small enough, the species presumably would react virtually instantaneously upon contact.

3.4.3.3 Mass and energy balance in two droplets

The reaction between two reactant droplets one containing the NCO groups and the other the OH groups, was simulated on the scale of 100 μm and the mass and energy balance calculated. The kinetic parameters employed were those calculated from DSC experiments (see section 3.4.1.2) for a reaction occurring at 50°C.

The equations, assumptions and parameters used are described in detail in Appendix I. The mass balance was determined by considering a micro-reactor of perfect spherical shape and with a radius of 100 μm, according with the assumptions described in section 3.3.3. Three simulations were done, at an initial concentration $[NCO]_o$ of 1.59, 2 and 3 mol/L. The change in fractional conversion with time for the three cases is shown in Figure 3.32.

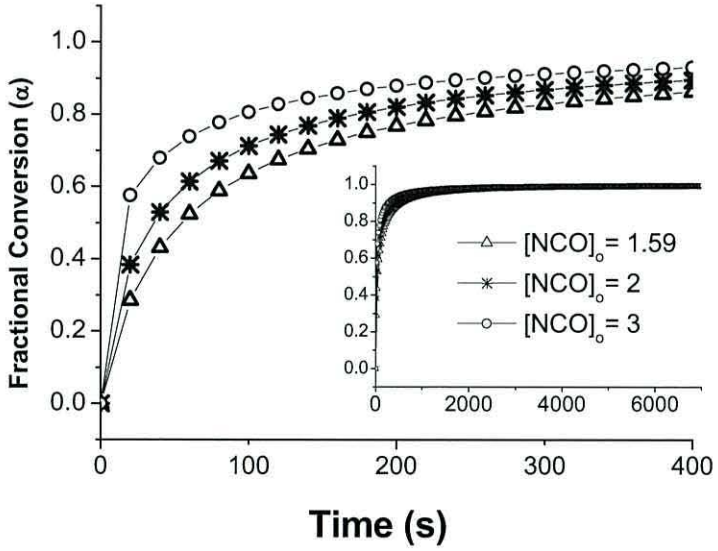

Figure 3.32 Change of the fractional conversion with time for a reaction occurring inside a droplet of diameter 100 μm.

As the figure shows, a conversion of 50% is achieved at 64 s and 99% at approximately 6900 s for a concentration of 1.59 mol/L. Evidently, if the starting concentration increases, the reaction is faster. For instance, if the concentration is doubled, the half-life decreases by about a half.

Also, a change in the micro-reactor temperature will have an effect on the reaction conversion, since the reaction rate is described by the Arrhenius equation (equation 3.2). Again, simulating the same at 30 °C the reaction is slightly slower as shown in Figure 3.33.

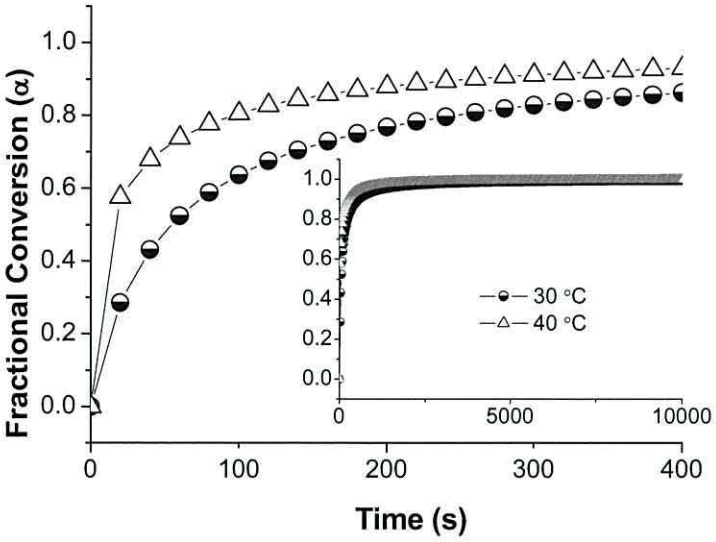

Figure 3.33 Effect of the temperature on fractional reaction conversion.

At 30°C achieving 50% conversion takes 55 s compared with 17 s at 50 °C. However, in addition to increasing the reaction rate, increasing the temperature will also reduce viscosity. Therefore, the operating temperature of an IJP system will directly affect the polymerisation process as well as the ease with which the materials can be handled.

These predictions are only based on mass balance and calculation of the heat exchange due to the exothermic nature of the reaction. Heat loss to the surroundings has not been considered either. For a more accurate prediction, an energy balance has been roughly calculated simultaneously with the mass balance, as explained in detail in Appendix I. Figure 3.34 shows the fractional reaction conversion and the temperature inside the droplet micro-reactor, plotted as a function of reaction time.

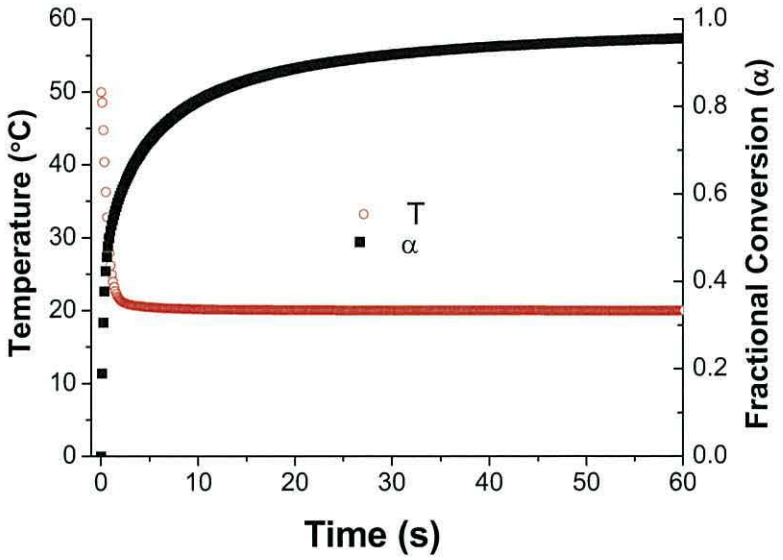

Figure 3.34 Fractional conversion and the temperature inside a droplet of diameter 100 μm plotted as a function of time for an exothermic reaction.

This model shows that at constant drop volume, the fractional conversion increases while temperature decreases with time. Using the current parameters, it can be seen that the temperature will drop from the starting temperature of 50 °C of the reactants down to 20 °C in about 5 s due to heat being transferred by convection to the surroundings. Also, 50% of conversion is achieved in the first 2 s and 98% in approximately 60 s.

Based on these simulations, it is seen that if accurate dispensing of stoichiometric quantities is achieved by IJP, then a practically instantaneous reaction will occur. Obviously, the process can be tailored to meet specific needs. Perhaps the use of a catalyst that decreases the activation energy, increasing the starting concentration of the reactant or increasing the system temperature will have a direct effect on the reaction rate constant. This may lead to a faster reaction which will directly affect the process inside the droplet. While a very fast reaction could yield the immediate formation of a hard-bouncing droplet, a slower one would give the opportunity for the reactants to move inside the drop and migrate to the surface and a different PU could be formed. However, a very fast reaction is not necessarily the best option, because the formation of a polyurethane film (i.e. "surf-product") could stop the mixing of remaining species in the droplets. Therefore the reaction should be slow enough to allow mixing to completion.

3.5. Conclusions

Achieving the desired PU properties relies on the mictrostructure achieved by a combination of both the product formulation and the process conditions. Conventional batch processes were characterised by means of analytical techniques such as GPC. It was found that the change of initial formulation from 2:1:1 of NCO:poly(1,4 butanediol) 2000: BDO to a ratio of 5:1:4 did give a faster reaction, from 24 hrs down to 4 hours respectively. It was also found that in these uncatalysed systems the final M_w (PS reference) was around 9,000. This system was also monitored by a state-of-the-art on-line monitoring system developed by Polymer Laboratories. In real time the properties of the reacting mixture were measured by detectors such as viscosimeter, light scattering and refractive index detector. While it was possible to monitor the reaction at low conversions, after 3 hours the mixture was too viscous to continue analysis.

Based on these initial findings it was evident that a change in formulation had an important impact on the end product and the process. Therefore the effect of stoichiometry imbalance on reaction process was assessed by DSC and GPC. In reactions with NCO:OH < 1 it was found that a higher ΔH value suggested that higher molecular weight polymer would form. On the other hand, reactions with NCO:OH ratios ≥ 1 showed two reaction exotherms, where the second one was possibly due to an exothermic crystallisation process rather than polymerisation. Also, in this range, as the NCO:OH ratio increased the onset temperature decreased suggesting a faster reaction mechanism. In terms of the molecular weight, it was found that when the initial formulation contains equimolar quantities, that is a ratio of 1:1 NCO:OH the highest molecular weight is obtained, while any imbalances yield a lower molecular weight in the final product.

From this information, a prepolymer was designed to be employed in the RIM experiments with the purpose of obtaining a liquid form of MDI and also to decrease its vapour pressure, making it safer to handle. The formulation contained 8 moles of MDI and 1 mol of PPG 2000 with a %NCO of 14.7. Subsequent reaction between the prepolymer and a mixture of PPG 1000 and chain extender was designed to form a final PU casting. It was found by means of DMA analysis that the higher the concentration of chain extender (e.g. BDO) employed, the harder the final product obtained. In other words, higher BDO concentrations resulted in a higher glass transition temperature Tg but lower molecular weight. The formulation designed for

the RIM experiments was 6:1:5 of MDI:PPG 1000:BDO. The manual casting gave a molecular weight of around 9,500.

After the formulations were designed, it was necessary to assess the reaction kinetics of the process. It was confirmed by DSC dynamic methods, for a second order reaction, that the reaction of the high hard-block content reaction was faster than that of the low hard-block content. Nevertheless, the half-life for temperatures between 30 to 50 °C was in the range of 13 – 3 min, which is still a slow reaction. Tin catalysts are conventionally used for RIM processes, however due to their toxic nature it was more desirable to seek new catalysts which are more environmentally friendly even for low output technologies such as IJP. Again by DSC dynamic experiments four new catalysts were studied: two zirconium-based and two titanium-based. It was found that at higher concentrations the reaction was faster. The concentrations employed were between 0.05 and 0.196%. It was found that catalyst Zr1 showed the best performance, but the Ti1 showed more compatibility for IJP systems, because it was completely soluble in the polyol mixture and did not alter the physical properties of the reactant (i.e. neither the colour changed, nor did small particles form a suspension). During these experiments it was demonstrated that poor mixing (e.g. hand-mixing) had an important impact on the polymerisation process, leading to slower reactions and lower molecular weight PUs.

The RIM experiments conducted demonstrated that the efficient mixing, which defines this technique, and the prepolymer formulation used have a remarkable impact on molecular weight of the final product. While the hand-made castings yielded a PU with a M_W of around 9,500, the castings made by the RIM machine gave a molecular weight of around 20,000. These experiments also highlighted the important similarities with the IJP systems: the basic principle of pumping two streams in into a space where impingement and chaotic mixing takes place. In the RIM process, mixing is achieved within seconds due to chaotic mixing and, of course, to the chemical reaction. This, as a consequence, makes the polymerisation kinetic driven inside the mixing head, which is independent of the diffusion of the reactants. Then, in the final stages of the reaction (i.e. in the mould) the reaction is diffusion driven. Observations made in the course of the RIM experiments demonstrated that practical issues, such as controlling the temperature of the reactants, the blockage of the prepolymer lines, and the water content within the system are potential risks to the

success of the process and should be considered for the implementation of a miniaturised process.

In order to simulate the reaction between two inkjet droplets, experiments were undertaken in which μL volumes of reactant were monitored spectroscopically. By following the changes in FTIR absortion bands at ~2270 cm^{-1} and Raman Shifts at 1650 cm^{-1}, the half-life for conversion was 30 to 40 min. It was found that when the reactants make contact, homogenous reaction occurs at the interface forming a polyurethane film. After the formation of such a film at the interface, the reaction slows down and becomes diffusion driven.

A simulation of the equimolar reaction between two droplets in the size range of 100 μm was undertaken employing the kinetic parameters calculated experimentally, and the results showed that 50% conversion can be achieved in the first 2 s and 98% in approximately 60 s.

In summary, if stoichiometric quantities can be accurately dispensed by IJP, it would appear that an instantaneous reaction should occur at the 100 μm scale, not only because the striation thickness at that scale is small enough, but also because the chemical energetics of the process will drive the mixing inside the micro-reactor. In the following sections the IJP technology is reviewed, studied and tested in order to assess whether or not the capabilities and limitations of the technology can lead to the miniaturisation the PU synthesis.

Chapter 4. Ink Jet Printing Technology

4.1 Microtechnology and Microengineering: Tools for Process Intensification

There are numerous starting points for the intensification (i.e. downscaling) of polyurethane synthesis, including the exploitation of nano and microscopic novel auxiliaries. A variety of materials and fabrication methods are now available for the construction of microreactors and microprocess components, as described in Chapter 1. One such technology is ink jet printing, and in attempting to adapt it for the handling of polyurethanes, based on the concept of PI, it is essential to understand the physical and chemical phenomena occurring when attempting to produce polymers on a surface. Down-scaling of processes is probably a greater challenge to a chemical engineer than scale-up, since scaling down is still in its infancy and there are no conventional approaches which might be adopted. Suppositions are common on the macro-scale. For example, momentum balance is typically neglected in reactor modelling and assumptions such as "perfectly mixed" are common practice with the purpose of simplification of calculations. On the micro-scale, such assumptions are not always right, and studies should be undertaken to confirm or neglect them. New developments require new thinking, and the strategies needed to go from the macro to the micro-scale present interesting challenges.

As an hypothesis it was believed that using micro-process technology, such as IJP, for the production of precision printed polymer films (including multi-layered functional products) should have some advantages including (a) the precision dispensing of reactants which spontaneously react on mixing, (b) the accuracy and precision of placement of polymer on a surface, and (c) the ability to build up multi-layered materials where each layer might have specific transport or electrical properties i.e. intelligent devices. There are numerous devices which might be produced using reactively processed films from bulk polymerisation reactions rather than the laying down of polymers from solution e.g. rapid prototyping, microdevice or tailored film structures for the active healing of wounds where individual layers play a different role in the overall healing process. It is not uncommon for it to be now thought that products and systems designed using scale-down logic, could potentially lead the

development of production tools that will enable innovations throughout all aspects of the chemical and materials industry. The benefits of micro-process technology for the processing and manufacture of solids with specific properties have already led to a number of process innovations such as miniaturised sensors and devices with added new functionality, as described in section 4.2.1. However, many of the broad generalisations now appearing in the literature need to be treated with some caution as the work of this thesis will demonstrate.

In this Chapter the principles of IJP technology are described together with an analysis of the benefits and limitations that this technology offers as a tool for the mini-synthesis of polyurethanes.

4.2 Ink Jet Printing Technology for printing of functional materials

Since the 1970's innumerable and contrasting applications of IJP technology have been reported all based on the accuracy of the dispensing system for any given individual fluid. The most typical and known application of this tool has been directed towards the printing of images. A good example is the printing of plain text or digital-coloured images at high speed and with very high resolution. The imaging industry has applied this technology in different formats ranging from narrow to wide formats such as advertising posters. Furthermore, printing appliances have been built not just for printing onto paper but onto diverse substrates such as bottles, boards and even cans. However, IJP technology has also had an important technological impact in areas outside graphic arts printing (Gans et al., 2004; Calvert, 2001a).

An IJP system has the ability to deliver small quantities of liquid to very-specific locations, it has become a robust and versatile tool for printing functional materials to manufacture a wide variety of electronic and optical devices. The areas benefiting most are electronics and optics, with fabrication processes being enhanced and improved using inkjet printing systems. For instance, polymer-based electronic parts such as solar cells, transistors, sensors, multicolour polyLED displays, microfluidic devices amongst others, have been successfully fabricated using inkjet printing systems (Pede et al., 1998; Kawasea et al., 2003; Paul et al., 2003). Organic LEDs formed using IJP are being incorporated in flexible displays. Also under active development is the low-temperature fabrication of passive (conductor, capacitor) and active (field effect transistor) electrical components (Ko et al., 2007). It has proved possible to print gold

nano-particles, PVP (poly-4-vinylphenol) and semiconductor polymer (modified polythiophene) onto flexible polymer substrate.

It is possible also to fabricate thin film circuits, semiconductors and capacitors based on three-dimensional ceramics (successive layers of ceramic powder). The printing of nano-particle inks comprising of gold or other metal suspensions to form electrodes for photovoltaic cells was reported in 2003 (Burns et al., 2003). Xue (2006) reported the use of IJP for printing silver tracks to act as source/drain electrodes in low-cost polymer thin film transistors (TFTs). More recently, Wei et al (2007) showed that a stable carbon nanotube (CNT) based ink (0.3% w) could be printed onto an acetate film. Likewise, the fabrication by IJP of composite TFTs comprised of organic semiconducting material and nanostructured conductors was demonstrated (Hsieh et al., 2008).

Ink Jet Printing technology has contributed to the optical component industry as well. The manufacturing of transparent and coloured micro-lenses was reported by Dansebrink and Aegert (1999). It was achieved by printing hybrid organic sols onto glass substrates followed by ultra violet (UV) initiated polymerization. Such microlenses can be used to focus light onto a detector array, optical fibres and sensors, for illumination in flat panel displays, computers and for imaging in photocopiers and lithography. Additionally, the manufacture of a colour filter with monochrome green was developed (Koo et al., 2006). This was achieved by inkjet printing a colour filter using a greenish nano-particle ink. The chromatic characteristics of the filter were compatible with a commercial specification for the green colour. The light transmittance of the greenish subpixel patterns was measured to be nearly 80%.

The growth in the use of inkjet printing systems has been rapid. Successful applications in micro-scale biological science included the manufacture of biochips and bio-related microelectomechanical systems (BioMEMs) (Cooley et al., 2001). The process of chip manufacture in biological science is similar to that in electronics, the main difference being that the active element is biological matter (Zaugg and Wagner, 2003). Advanced IJP applications have been described, including developments in scaffold-aided tissue regeneration. Direct printing of cells and proteins within 3D hydrogel structures has been reported (Boland et al., 2007). Many layers of cells and hydrogels were printed into 3D structures using a fast gelling hydrogel system. Cell printing opens the possibility of controlling the type of tissue that can be regenerated

within the scaffold. In the same manner, Xu et al. (2006) developed a method creating 3D cellular structures. These consisted of sheets of neural cells prepared by alternate inkjet printing of neuronal precursor cells and fibrin gels in a layer-by-layer process. Automated and direct inkjet printing of primary embryonic hippocampal and cortical neurons created complex cellular patterns and structures.

In 1996, Blanchard et al (1996) reported the use of inkjet printing technology to deliver small drops of reagents to a chemically modified silicon dioxide surface, where they reacted to synthesize DNA, allowing the formation of high-density oligonucleotide arrays. The basic scheme for the in-situ DNA was to covalently attach an organic linker molecule to a surface, followed by the building of the DNA molecule off the end of the linker through a series of coupling and deprotection steps. Similar research and results have been reported since then (Cooley et al., 2001). In a similar manner, peptide arrays can be synthesized using IJP and are commonly used for drug and expression screening studies (Rowe et al., 2000a). Such technology can be used in clinical diagnosis and drug release applications, particularly in the preparation of monodisperse polymer microspheres for the preparation of tablets with graded pharmaceutical contents (Rowe et al., 2000b; Katstra et al., 2000).

According to Zhang et al. (2007), combinatorial methods are crucial for drug discovery and are also now used for the screening of new materials in the materials science field, the latter application fuelled by the current interest in finding new superconductors, catalysts, fuel cell anode and dielectric materials. In their work, the authors indicate that the approaches to ceramic library preparation include the use of ink jet printing. Similarly, inkjet printing technology has been used for combinatorial polymeric materials research as an alternative to the typical combinatorial approach (Gans and Schubert, 2003). Moreover, the contribution of IJP to polymer characterization has become considerable with its implementation in the automated multiple-layered MALDI-TOFMS sample preparation of synthetic polymers, allowing the deposition of matrix, additive and analytical solutions (Meier et al., 2003). This sample preparation technique has the benefit of high speed and accuracy that allows the optimization of the sample shape to an extent impossible when placing polymers on surfaces (spotting) by hand.

The textile industry is interested in IJP for example, as a tool for pigment printing (Yang and Naarani, 2007). El-Molla (2007) has reported the synthesis of acrylate

oligomers as aqueous, UV-curable binders for inks used for ink jet printing onto textiles.

In an investigation of the printability of a diluted PU dispersion, Berg et al (2007), using a piezoelectric system successfully printed a PU dispersion containing 40% w of polymer with an average molecular weight of 1600 g/mol. Using 96 V pulses of duration 28 ms at a repetition frequency of 200 Hz, they were able to produce layered structures with a solution that had a viscosity of 20 mPa s. Ink jet printing is even beginning to be applied in polymer synthesis; however, there is no report of its application in the miniaturisation of a step-growth polymerisation process e.g. polyurethane synthesis.

4.2.1 Sensors and Devices fabricated using Ink Jet Printing

There is growing interest in micro devices for applications in electronics, optics, biomaterials and drug delivery as reviewed in Chapter 1. The successful printing of micro device structures will rely on methods to deposit fuctionalised materials. Many different materials have been successfully printed in both single and multiple layers.

Single layers are often printed as part of a device that was previously formed by other methods such as spin coating or evaporation. For example, Mabrook and co-workers (2005a) fabricated a fuse that was based on films of conducting polymers. The ultra thin films were fabricated by printing water soluble conductive polymer poly(3,4-ethylenedioxythiophene) doped with poly(styrenesulphonate) (PEDOT:PSS) onto polyester film. They were exposed to alcohol atmospheres, and as a result a non-reversible change was observed in the morphology of the organic layer which disrupted the current flow. This principle is also the basis for vapour sensors (Mabrook et al., 2005b). Carter (2006) demonstrated the feasibility of fabricating imaging sensors. A solution of photo-polymerisable sensing elements containing 0.6% w/w of pH sensitive dye was printed onto an optical fibre image guide. The sensing ability of the reported fluorescein-doped printed device was in the range of pH between 6 and 9.

In multilayer devices, the first material is printed (for example gold) and further treatment is done (e.g. sintering the metal) before the second layer is deposited on the top. Evidently, not only dots were printed, but continuous lines also. At room

temperature, the drop-to-drop spacing was about 100 μm (Ko et al., 2007). In 1998, Pede et al described a technique based on IJP and stereo-lithography to fabricate conducting polymer devices. Neutral and conducting polymers were printed on an alumina surface. The solvent evaporated quickly as the droplets fell. In total, 10 drops were deposited at the same point. The solidified material gave a thick, wide and homogeneous polymer deposition. Subsequent exposure to iodine vapour induced both polymerisation and doping of the material pattern. Deposition of conjugated polymers was possible due to the absence of chemical reaction between the printed solution and the substrate.

Similarly, a biosensor was engineered (Setti et al., 2005) by printing PEDOT:PSS on ITO coated glass. The deposition was repeated 10 times over the same surface. Subsequently, a biological ink containing 6 mg/mL of the enzyme glucose oxidase (GOD) was then printed, repeating the deposition twice. Finally, the inkjet printed area was dip-coated in a solution of cellulose acetate to encapsulate it with a semi-permeable membrane. The prototype is depicted in Figure 4.1.

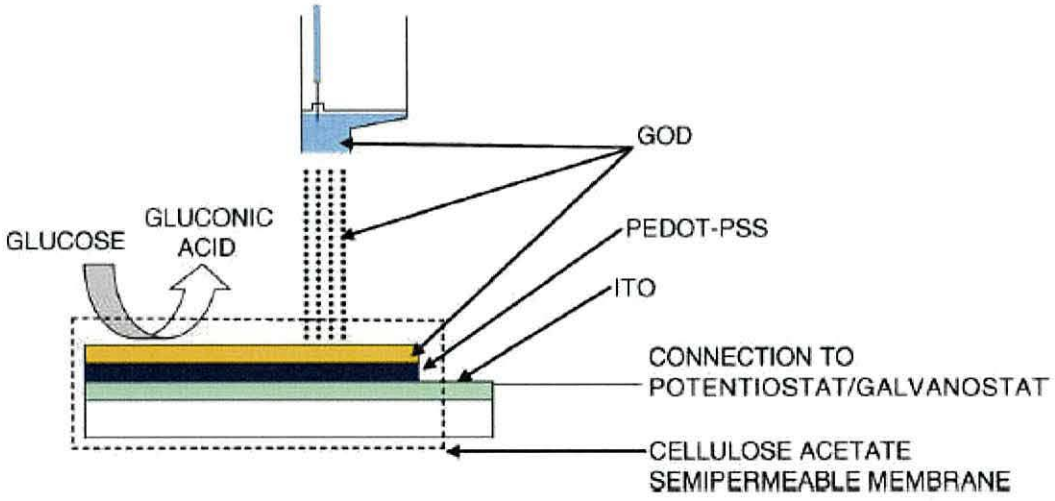

Figure 4.1 Schematic diagram of the prototype of the complete GOD inkjet printed electrode reproduced from Setti et al. .

In all these multilayered devices, no chemical reaction occurred between layers. It was assumed in each case that the trajectory followed by the printed material allowed the droplet to reach the substrate at the desired location.

In the case where a reaction takes place between printed layers, it was suggested by Calvert et al (2006) that a model for the multilayer process might be that shown in Figure 4.2 in which two possible paths are possible depending on the relative diffusion and reaction rates. The resulting structure is either a single mixed layer or two separated layers.

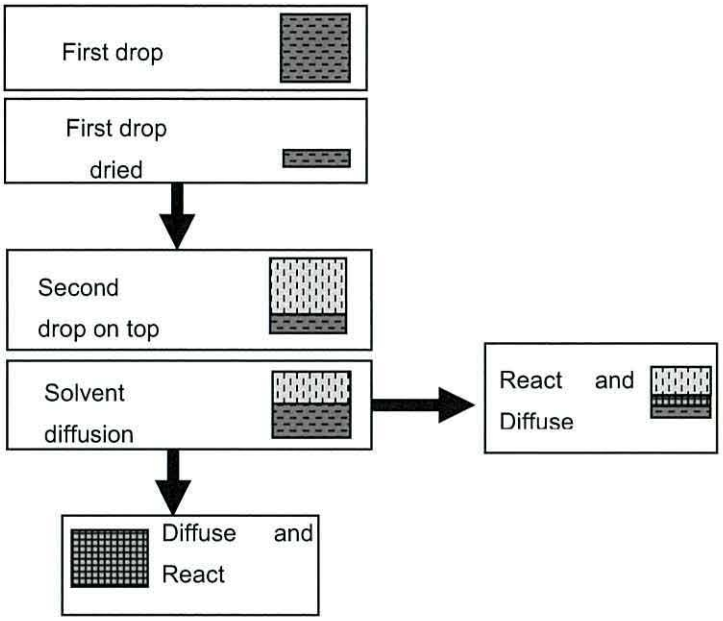

Figure 4.2 Multilayer process suggested by Calvert. A first drop is printed and dried. Then the second droplet is deposited on top and re-dissolves the first one. Two paths are possible: diffuse and react to form a single layer, or react and diffuse giving two divided layers (Calvert, 2001a).

Clearly, printing complete devices by means of IJP using multiple layers and the interaction between them opens an interesting opportunity for research. However as the direct fabrication of micro devices raises many questions, the real possibilities and constraints remain relatively unexplored. As recognised by many authors, a current limitation is the lack of a simple robust IJP system capable of handling a wide range of liquids, notably, those with a high viscosity.

There are no reports in the literature of any studies related to the use of IJP technology in the process intensification of PU synthesis. Since this would involve the printing of functionalised liquids never tested before, the feasibility of using IJP with reactive low molecular weight reactants is unknown. The work of this thesis is devoted to the IJP of reactants which lead to polyurethanes, a large and versatile class of polymers which have not previously been made using this technology before. Hence, it is important to understand the process of IJP to compare it to methods such

as reaction injection moulding, which is a relatively macroscopic compared with IJP methods. Hence, the identification of the key factors is needed to implement the miniaturisation.

4.3 Mechanisms of IJP systems

There is a diverse range of technologies that fall into the ink jet printing category. The basis of IJP technology is to push an inviscid liquid (inertial forces are large in comparison to viscous forces so the latter are neglected) through a small nozzle or array of nozzles onto a substrate (Mittal, 1987). The technology employed to dispense inks has been implemented in many different designs which can be found elsewhere (Le, 1998; Basaran, 2002). It is usually divided into the continuous and the drop-on-demand ink-jet methods, where the main difference is in the principle of drop generation.

In continuous IJP, pressurized fluid is forced through an orifice or nozzle (typically 50-80 μm in diameter), to form a liquid jet. Surface tension acts to amplify even minute variations in the jet diameter, causing the jet to break up into drops (Raleigh breakup). If a single frequency disturbance, in the correct frequency range is applied to the jet, this disturbance will be amplified and drops of extremely repeatable size and velocity will be generated at the applied disturbance frequency. The disturbance is usually generated by an electromechanical device (a piezoelectric transducer for example), that creates pressure oscillations in the fluid. To control the uniformity of the droplets generated by Raleigh breakup, electrostatic forces are employed. The drops break off from the jet in the presence of an electrostatic field, referred to as the charging field and hence acquire a charge. This creates a steady stream of charged ink droplets that are ejected forwards. The charged drops are directed to their desired location, either the catcher or one of several locations on the substrate, by a fixed electrostatic field. The charge is varied by changing the voltage applied, thus supplying data to the drop as to its desired printing location. This type of IJP is used to print relatively volatile inks (Mittal, 1987). Droplet generation rates for commercially available continuous mode ink-jet systems are usually in the 80-100 kHz range, and produce droplets that are approximately twice the orifice diameter of the droplet generator.

In the impulse or drop-on-demand (DOD) IJP, droplets are formed only when needed. The mechanisms of commercially available DOD printers, and most common designs used for printing functional materials are piezoelectric and thermal (Figure 4.3). However, solenoid and acoustic dispensers have been used for that purpose as well (Rose, 1999; Paul et al., 2003).

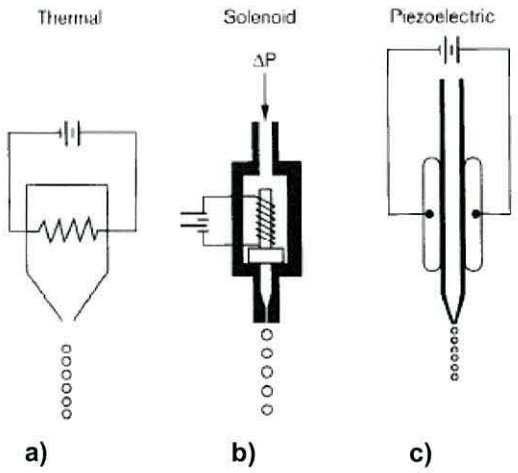

Figure 4.3 Three types of IJP dispenser: a) thermal, b) solenoid, c) piezoelectric. Reproduced from (Lemmo et al., 1998).

The transducer in a thermal printer is a thin film resistor. A current is passed through this resistor, causing a sharp rise in the liquid temperature. The ink in contact with the resistor is vaporized, forming a vapour bubble over the resistor. This bubble creates a volume displacement in the fluid forcing an ink droplet through the orifice. Several authors have successfully used the thermal IJP (Setti et al., 2005; Boland et al., 2007; Xu et al., 2005; Yoshioka and Jabbour, 2006; Xu et al., 2006) by modifying commercial printers, usually HP DeskJet model 550 and DJ500C. Olivetti I-Jet has been used as well. The pattern is usually outlined by power point (Microsoft) software, and printed on flexible films. The concentration of the reactants (layer thickness) can be controlled by changing the HSL (hue, saturation and luminosity) print settings. The quantity of red, green and blue (RGB) are usually controlled by the saturation, the composition of each colour is identified by the hue, and the darkness of the colour (and therefore the amount of printed ink) is related to the luminosity.

For this type of commercial printer, the print head has two rows of 25 nozzles (with a diameter close to 50 μm) separated from each other by 170 mm. The offset of the rows are 85 mm. These cartridges are able to fire all 50 nozzles with a print speed

of up to 250,000 drops per second or at 80 ml at 85 mm resolution (Xu et al., 2006). However, there are concerns about the high temperature (about 300 °C) reached inside the nozzles for a period of about 5 μs. It is possible that the high thermal stress on the ink could cause damage to the biological and/or synthetic organic ink components

The piezoelectric technology is usually preferred because it applies no thermal load to the ink. Basically, a pressure wave is generated in the ink reservoir when a voltage pulse is applied to a piezoelectric material (Sirringhaus and Shimoda, 2003). This mode of operation has been described by several authors who provide a complete understanding of the whole printing process (Calvert, 2001a). This type of IJP has been used effectively (Danzebrink and Aegert, 1999; Kawasea et al., 2003; Pede et al., 1998; Natori et al., 2005). Typically the modification of office printers, such as the Epson Stylus 400 takes place or the use of equipment specially designed to print functional materials. It has been reported that the characteristics of the electric pulse used (e.g. voltage and pulse width) is a function of the liquid properties. For that reason, each printer has to be calibrated in order to print a specific ink. Normally, droplet volume ranges from 2 to 40 pL depending on nozzle size and the driving waveform (Kawasea et al., 2003).

Another type of inkjet dispensing technology combines the high-speed actuation of a micro-solenoid valve with other equipment, such as syringe pumps, to create a steady state hydraulic pressure upstream from the micro-solenoid valve. A stream of liquid which is driven by the pressure created by an external component (such as a syringe pump) moves rapidly towards the orifice of the nozzle. After the valve is triggered, a drop is ejected due to the movement of the valve that opens and closes periodically, dispensing the fluid in a continuous mode (Rose, 1999). This technology can dispense droplets over a broad range of volumes from nano to micro-litres, and also hundreds of microliters as a stream of fluid. Its positive displacement nature means that air bubbles and fluid surface tension have minimal effects on precision and accuracy. The reported standard error is 2–3% with a coefficient of variation of 3–10% depending on the volume (Tisone, 1998).

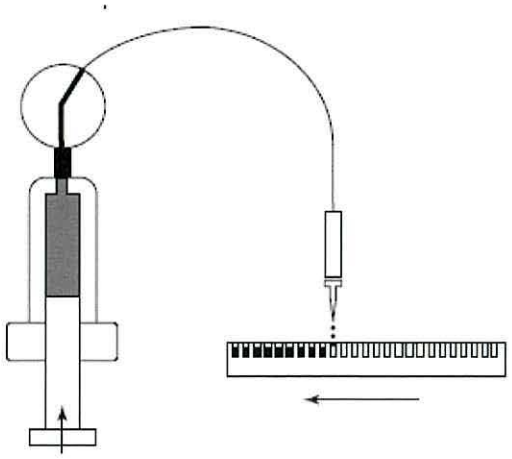

Figure 4.4. Syringe–solenoid inkjet dispensing reproduced from (Rose, 1999).

4.4 Fundamental concepts in IJP

All fluid handling systems, including microdevices such as the IJP involve mass, energy and momentum transfer. The physical processes occurring may be described by mathematical models. For the microtechnology of IJP it is important to understand whether the typical models used for macro-scale are still applicable. All models will involve assumptions and these may not hold when scaling down e.g. unconventional effects, such as slip, compressibility, intermolecular forces, viscous dissipation to mention some (Gad-el-Hak, 2001). In particular, surface effects may become dominant in micro-devices. The surface/volume ratio for a length scale of 1m (as in macro scale equipment) the ratio is around 1 m^{-1}, whereas in the case of micro-devices (e.g. length scale of 1μm) is around $1x10^{6}$ m^{-1}. This substantial difference indicates that the magnitude of the surface is much larger than the volume contained in it. This condition will definitely affect mass, energy and momentum transfer over the surface.

4.4.1 Mass, energy and momentum balance models used for IJP

It has been recognised that the results of some experiments conducted using micro-devices could not be explained or predicted by traditional flow models (Gad-el-Hak, 2001). However, it cannot be generalised whether a model will be applicable to a specific system without a specific assessment being made. For that reason, before any assumptions are made, it is necessary to establish which approximations can be used in the modelling.

The conventional macroscopic approach to study liquid-fluid mechanics, assumes that the fluid is an incompressible continuum (Sabersky and Acosta, 1964; Deen, 1998). This model presumes that the local properties, including density, velocity and pressure can be defined in space as average values. Also, the model assumes that these properties change continuously from one point to the other within a flow (Nguyen and Werely, 2002). On this basis, the mass, energy and momentum balances are described by a set of partial differential equations, known as the Navier-Stokes Equations (Bird et al., 1997)). This model can be applied to the IJP system where liquid drops are regarded as being completely immersed in a large expanse of air.

As an approximation, liquids with point and transport quantities with a length scale L = 10 nm, can be considered as continuous (Nguyen and Werely, 2002). This length scale is sufficient to have at least 10^4 molecules in a sample consisting of a cubic volume of side 8 nm. This amount of matter will give less than 1% statistical variation when computing an average value of kinematic (e.g. velocity and acceleration) and thermodynamic (such as pressure and density) properties. Similarly, for continuous transport quantities, the molecules in the fluid are assumed to interact more often with each other than with the boundaries constraining the flow. This continuous model ignores the molecular nature of the fluid. If the fluid is studied as a collection of molecules, deterministic and statistical models can be employed to describe the fluid mechanics (Gad-el-Hak, 2001).

As described in Section 4.6, the length-scale of the IJP system employed in this research, allows the fluid to be considered as a continuum i.e. the conservation of mass and momentum can be described using the Navier-Stokes model. This approach is presented, in detail in Appendix II. The final mathematical expressions that describe the motion of an incompressible, Newtonian, non-reacting and isothermal fluid including surface tension effects are:

$$\nabla \cdot v = 0 \tag{4.1}$$

and

$$\rho\left(\frac{\partial v}{\partial t} + v\nabla v\right) = -\nabla p + \mu\nabla^2 v + F_{st} \tag{4.2}$$

where v is the velocity vector, ρ constant density, p the fluid pressure, μ the constant viscosity and F_{st} the body force acting of the fluid e.g. surface tension and electrostatics.

The trajectory followed by a droplet has been modelled in detail and the work published on the kinetics of droplets in flight (Lee, 1974; Fromm, 1984) is considered to be fundamental to the understanding of such processes.

4.4.2 Fluid dynamics of Drop-on-Demand Ink Jet Printers

The fluid dynamics of DOD inkjet printers was studied by Fromm (1984) who solved numerically the dimensionless Navier-Stokes equations using the radius of the nozzle as the reference unit of length. The single parameter, where in all fluid properties are contained, is the ratio between the dimensionless Reynolds (Re) and the Weber (We) numbers where the Reynolds Number is given by equation 2.10 (Chapter 2). The physical meaning of a low Re number for example is that, for an incompressible fluid, viscous forces predominate. The We number is given by:

$$We = \frac{Dv^2\rho}{\sigma} \tag{4.3}$$

where σ is the surface tension of the fluid and D is the nozzle diameter. This dimensionless number is a general measure of the relative magnitude of surface effects. This is important because the tendency of the flow to increase the surface area will bring molecular forces into play which may sensibly modify the basic distribution of velocity and pressure. The smaller the Weber number, the larger the relative influence of the molecular attraction should be and vice versa. On this basis, the dimensionless ratio reported by Fromm is:

$$\frac{\mathrm{Re}}{We} = \left(\frac{\sigma r}{\rho\eta^2}\right)^{1/2} \tag{4.4}$$

where r is the radius of the nozzle and η the kinematic velocity, defined as the ratio of the absolute viscosity μ divided by the density ρ of the fluid. This ratio relates viscous and inertial forces and the flow influenced by surface tension. Several authors (Zhao et al., 2003; Derby and Reis, 2003) have used the same ratio, but expressed somewhat differently by:

$$\frac{\mathrm{Re}}{\sqrt{We}} = \frac{(\sigma\rho D)^{\frac{1}{2}}}{\mu} \quad . \tag{4.5}$$

In this equation, all terms are defined as before. It was found that in most commercial DOD printers, the ratio falls between 1 and 10 (Derby and Reis, 2003). If the value is small, it means that the viscosity predominates and a larger pulse is needed to print a drop of liquid (as a consequence, the drop has lower velocity). If the parameter value is high, an extended liquid column is formed before the droplet is created, leading to the appearance of satellite drops. The influence of liquid properties on printing is shown in the plot of We vs Re in Figure 4.5

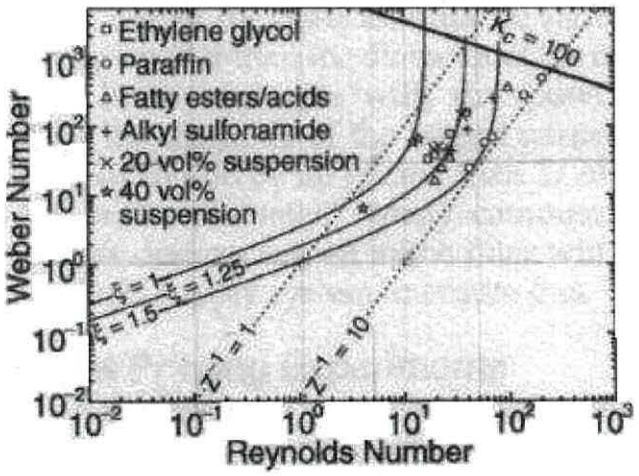

Figure 4.5 The influence of fluid properties on printing conditions. Reproduced from Derby and Nuno (2003).

The dotted lines defined by $Z^{-1}=1$ and $Z^{-1}=10$ indicate the limits of fluid properties that are typical for inkjet printers. The parameter Z^{-1} is the Ohnesorge (Oh) number, which is expressed as:

$$Z^{-1} = \frac{\mathrm{Re}}{(We)^{\frac{1}{2}}} = \frac{(\sigma\rho D)^{\frac{1}{2}}}{\mu} \quad . \tag{4.6}$$

4.4.3 Drop Formation Mechanism in a Piezoelectric IJP

Drop formation is the combined result of jet dynamics and fluid properties (Chou and Faeth, 1998; Guo et al., 2004). A typical ink jet system comprises the ink reservoir, a voltage-gated orifice and a two or three dimensional translation

mechanism. A piezoelectric IJP has a capillary system filled with liquid which is pressurised by an electrically pulsed piezo-electric actuator which generates short pressure pulses that propagate through the liquid and are transformed into motion at the nozzle i.e. in the time frame of a pulse, the liquid reaches sufficient velocity to cause a liquid jet to emerge from the nozzle. Once free of the nozzle, the liquid decelerates due to pressure loss through the nozzle and expansion of the actuator. Inertia forces and surface tension then lead to a drop being formed. Figure 4.6 shows actual drop formation for different time delays i.e. the time between the initial voltage rise and the appearance of an outward moving meniscus from the orifice.

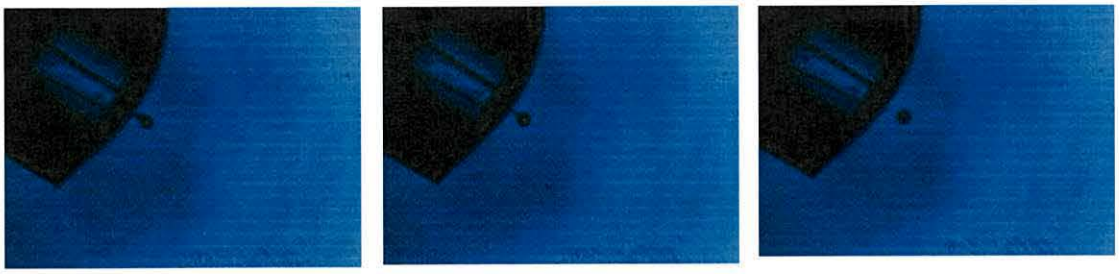

Figure 4.6 Drop formation mechanism. Photographs by Yara Almanza.

Fluid properties and other conditions, such as pulse amplitude, pulse width, pulse frequency and driving voltage affect the drop formation process. The pulse width affects the volume (size) whereas the driving voltage determines the velocity of the emerging droplet. This is mainly because the voltage controls the magnitude of the pressure applied to the liquid, whereas the pulse width sets the time that this pressure will last. Thus the outputs will be the drop volume and drop velocity. It is important to note that these two variables are interdependent and cannot be individually adjusted.

The effects of liquid dynamic viscosity upon the surface tension driven instabilities were investigated by Wong and by Nomura et al (2001). Wong reported that four different break-up modes (M1-M4) can be predicted from a plot of Reynolds number against Weber number (Table 4.1, Figure 4.7). The ranges used in this experimental study were: $1 \leq Re \leq 1000$, $0.5 \leq We \leq 25$ and $0.005 \leq Oh \leq 0.4$. These modes correspond to different combinations of liquid inertia, liquid viscosity and surface tension acting on the jet.

Table 4.1 Description of Four Break-up Modes Observed by Wong (2003).

Mode	Description
M1	Rapid formation of main drops close to the orifice and with few or absence of satellite droplets
M2	Drop formation is due to capillary pinch off, and satellites are formed in between the primary drops
M3	Rayleigh type mode with the jet breaking up simultaneously at several places along the jet into a continuous stream of droplets. Satellite droplets are formed from the contraction of liquid threads connecting the primary drops
M4	Nonlinear disintegration, the jet first elongates and a swell develops at its end

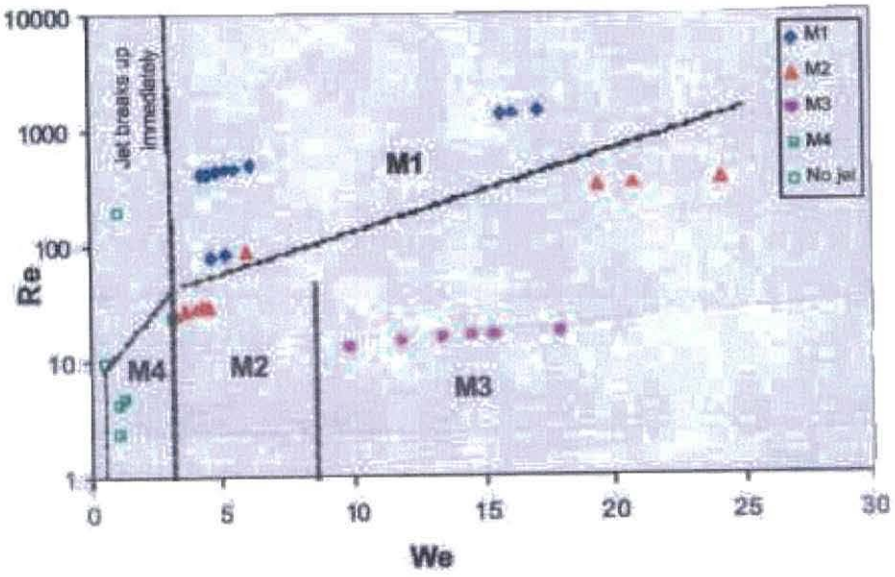

Figure 4.7 Map of the four break-up modes by Wong (2003).

On the other hand Nomura et al used a numerical method (Moving Particle Semi-implicit model) to describe the droplet break-up behaviour. By comparing the numerical model with experimental observations in a gas-liquid system, this study suggested that there are five distinct modes of break-up (Table 4.2) determined by the initial Weber number.

Table 4.2 Break up modes in terms of Weber according to Nomura.

Break up mode	**Weber number**
Vibrational	$We \leq 12$
Bag	$12 < We \leq 50$
Bag and stamen	$50 < We \leq 100$
Sheet stripping	$100 < We \leq 350$
Wave crest stripping followed by catastrophic break up	$We > 350$

4.4.4 Relevance of Surface Tension

When a liquid of density ρ issues steadily from an orifice into the air, drops may form at the orifice or at the end of a disintegrating cylindrical jet. At low flow rates, formation occurs close to the orifice; as the flow increases a jet forms, and at higher flow rates, drops form by jet breakup at surface perturbations. This is where surface tension plays its part in the process, since it amplifies minute variations in the jet diameter. The surface tension is the force that holds the molecules of a liquid together. The definition of this force is in terms of force per unit length. It can also be thought of as the work required to change the interfacial area between the liquid and vapour phases.

The stronger the intermolecular attractions in a liquid, the greater the work needed to bring the molecules from the bulk liquid to the surface and therefore the greater the value of the surface tension. For a drop to separate from a nozzle of radius r, it is necessary that in the inlet of the nozzle, the pressure is high enough to at least overcome the surface tension σ (Zhao et al., 2003). The pressure difference ΔP needed can be expressed by:

$$\Delta P = 2\sigma / r \quad . \quad (4.7)$$

So, the pressure difference will be proportional to the ratio of the unit surface energy to the radius of curvature of the surface. This is a special case of a more general relationship that is the basic equation of capillarity and was given by Young and Laplace. In effect, equation 4.7 indicates that a change in surface area of a droplet must be balanced by a surface pressure difference ΔP. The change in surface free energy is then equal to the work done against this pressure difference. Typically, surface tensions of the inks used in commercial printers range from 40-70 mN/m, and the drop sizes are between 30 and 150 μm (Mittal, 1987; Shimoda, 2003). It has been

demonstrated that for liquids under identical pressure conditions, the ejected liquid column becomes longer as the surface tension decreases (Wu et al., 2004).

4.4.5 Viscosity

Viscosity has a pronounced effect on droplet volume. At lower viscosity values, the droplet volume is higher (Blazdell and Evans, 2000). It has been demonstrated that for liquids under identical pressure conditions, the ejected liquid column becomes shorter as the viscosity increases and the flight velocity decreases (Wu et al., 2004). The effect of high viscosity on break-up time is not obvious. Surprisingly perhaps it has been found that at higher viscosities the droplets are more stable and give better printing quality. However, since pressures within piezoelectrically-diven printers are very low, typically falling in the range between 100 – 500 kPa (Derby and Reis, 2003), the maximum viscosities that commercially available piezoelectric printers can handle is very limited. Several systems are equipped with integrated heaters so as to increase the temperature of the fluid and hence decrease its viscosity thus enabling a wider range of fluids to be dispensed.

4.4.6 Fluid properties necessary for printing

It is clear from the previous sections that the physical and rheological properties of a fluid are very important in controlling its behaviour during droplet generation (Lee, 1974). For the successful application of IJP as a manufacturing tool for the micro synthesis of polymers, the correct fluid properties are essential. Studies by Derby's group (Derby and Reis, 2003) indicated that physical properties such as the viscosity and surface tension of a fluid strongly influence the drop size and velocity for a given pressure pulse when using a piezoelectric DOD system. To be able to use commercial inkjet methods in a process, the working fluid must be free of particles on the order of the orifice diameter and have the following properties (Guo et al., 2003; Shimoda, 2003; Mittal, 1987):

- Low viscosity from 1mPa s to 30 mPa s
- Surface tension between 20 and 70 mN/m
- Newtonian behaviour
- Spherical droplets formed without disturbances such as satellite drops

4.5 Experimental Procedure

As described in Chapter 2, linear polyurethanes of the type studied are usually obtained by the reaction of at least two materials, a diisocyanate and a polyol. In order to control the physical properties of the polymer, a second low molecular weight diol is usually used and this is commonly called a chain extender. Indeed, many different combinations of difunctional coreactants can be used to achieve the desired product properties. The stoichiometry of the reactants is important as well as the chemical type of diol. Isocyanates react with both primary and secondary alcohol groups spontaneously; the former being much more reactive than the latter. The rate of reaction can be controlled through the use of catalysts which are usually incorporated into the diols used. In order to use IJP as a tool for the miniaturisation of the synthetic process of PU, several methodologies were developed and are described in the following sections.

4.5.1 Printing polyol solution onto a diisocyanate film

Polyurethanes are typically formed from di-isocyanates and polyfunctional compounds containing two or more functional group, commonly hydroxyl-groups (see Chapter 2 for more details). The diisocyanate employed in this work was 4,4'-methylene diphenyl diisocyanate (MDI) which has a lower vapour pressure than other diisocyanates frequently used e.g. TDI and HDI. This reduces the hazards when handling it and makes MDI the least hazardous of the commercially available diisocyanates. MDI is a solid at ambient temperature (melting point = 47^0C), so it is necessary to dissolve it in a suitable solvent for IJP purposes or to make a pre-polymer which is a liquid as explained in Chapter 2.

4.5.1.1 Pre-polymer Synthesis

The pre-polymer employed was synthesised using 8 mols of MDI (Desmodur 44M, Industrial Copolymers Ltd) and 1 mol of polypropylene glycol with a mean molecular weight of 2000 g/mol (PPG 2000, Sigma Aldrich). The tin dibutyl octoate catalyst (Sigma Aldrich) was used as received and added to the reactants at 0.1% of the mass of polyol. MDI was used as received from the supplier with no further treatment but was stored at -20°C to avoid dimerisation. The PPG 2000 was first dried in a vacuum oven at 60°C for two hours. It was further dried using a rotary

evaporator (Büchi Model R-114) at 95° C for four hours. The PPG 2000 was finally poured into a tin with 70 grams of molecular sieve drying agent (Sigma Aldrich) for every 250 g of PPG 2000. Before closing the can, nitrogen gas was bubbled into the polyol to create an inert atmosphere and to eliminate atmospheric moisture. The material was left over the molecular sieve to dry for at least 24 hrs before using.

To prepare the pre-polymer the MDI flakes, the dried PPG 2000 and catalyst were weighed and placed in a 500 ml five-neck glass reactor. The reactor was put on an electromantel (Electrothermal, Model MB) at 50° C for 15 minutes. After the MDI flakes melted, the mechanical stirrer (Eurostar Basic Kika, Labor Technike) was turned on, nitrogen gas was bubbled into the reactor and temperature monitored using a thermocouple (Type K) linked into a computer for data capture. Figure 4.8 shows the reactor set up for the synthesis of the PU pre-polymer.

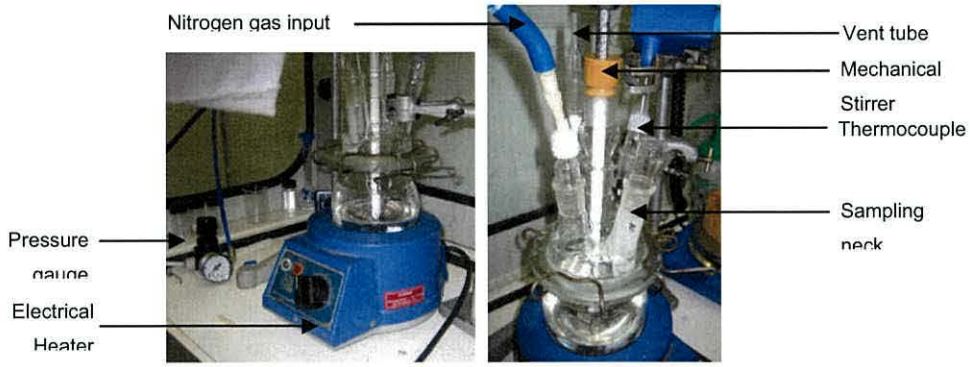

Figure 4.8 Reactor set-up for the synthesis of pre-polymer

The mixture was left to react for one hour after which the pre-polymer was poured into a glass jar, nitrogen was injected and the lid sealed with a thermoplastic film. The pre-polymer was liquid at 50 °C but at room temperature it solidified. In order to make it printable, it would be necessary to add a solvent, such as tetrahydrofuran (THF). As the IJP head is not suitable for handling this type of organic solvent, it was decided to layer the pre-polymer on a glass substrate and inkjet dispense the polyol mixture.

Although a spin coater technique device was available for creating a thin film of prepolymer on a glass substrate, it was decided to use the doctor blade technique instead, since it was a simpler means of handling the prepolymer. Glass slides were cleaned following the procedure described in Appendix III. Scotch® Magic™ Tape

was placed on the glass substrate to define an area of 25mm x 25mm. On the free surface of the glass, liquid pre-polymer (at 50° C) was poured and a glass roller drawn over it to form a 5μm-thick film.

4.5.1.2 Preparation of polyol mixtures

Polypropylene glycol with a mean molecular weight of 1000 g/mol (PPG 1000) was dried following the same procedure as that used for the PPG 2000. 1,4 Butanediol was used as a chain- xtender. Three different PPG1000-chain extender-catalyst mixtures were prepared in order to generate a set of functionalised reactants mixtures (also referred as functionalised inks) be tested. Their compositions are given in Table 4.3.

Table 4.3 Polyol formulations employed.

Mixture Number	PPG 1000 molar content	1,4 butanediol molar content	Catalyst content %w
1	5	1	0.1
2	4	2	0.1
3	3	1	0.1

The purpose of making such mixtures was to modify the viscosity of the reactants and to prepare polymers with different physical properties (controlled by the hard-block content i.e. molar ratio of iisocyanate to chain extender).

4.5.1.3 Determination of viscosity of PPG 1000 and 1,4 butanediol

Rheological measurements on the PPG 1000 and 1,4 butanediol mixtures were determined using an Advanced Rheometer AR550 (TA Instruments). With this instrument, sample materials are placed within standard-size double concentric cylinders which were maintained at a constant temperature of 25 °C. The automatically controlled instrument was run under the following conditions:

1. Pre-shear from 0.10 Pa for 40 seconds
2. Oscillation (sweep step) at a frequency of 0.1 to 10 Hz
3. Conditioning: 0.1 Pa for 2:00 minutes
4. Stepped flow: shear rate ramp from 0.1 to 500/s for a constant time of 30 seconds.

The instrument was then set to auto-zero after which the measurement was initiated. From the viscosity of the initial materials, i.e. PPG 1000 and 1,4 butanediol and 2-propanol, it was possible to estimate the solution viscosities by an empirical method. It is generally true that the viscosity of a liquid mixture is not a linear function of composition i.e. the mole or mass fraction. Often some exponential type dependence is observed in practical situations. Arrhenius (Viswanath et al., 2007) suggested the equation:

$$\log\eta_m = x_1 \log\eta_1 + x_2 \log\eta_2 \quad \textbf{(4.8)}$$

where x_1 and x_2 are the mole fractions and η_1 and η_2 the viscosities of the pure components respectively. For this equation to be applicable, it is necessary that the liquids in the mixture have a similar structure and one of the components should be present in a dominant excess in the mixture.

4.5.1.4 Preparation of polyol mixture for use with an IJP

All the mixtures proved to be so viscous that the IJP system was not capable of handling them. To reduce their viscosity, and improve conductivity (which is discussed in Chapter 6) anhydrous 2-propanol was used as a solvent to dilute the polyol mixtures. Solutions of different concentrations were prepared, by adding a known amount of polyol mixture (Table 4.4) to the solvent in a 10 ml volumetric flask.

Table 4.4 Solutions prepared with different mass content of polyol mixtures in 10 ml of 2-propanol anhydrous.

Mixture 1		**Mixture 2**		**Mixture 3**	
Solution No.	%Weight	Solution No.	%Weight	Solution No	%Weight
M1-15	15	M2-15	15	M3-15	15
M1-20	20	M2-20	20	M3-20	20
M1-25	25	M2-25	25	M3-25	25
M1-30	30	M2-30	30	M3-30	30
M1-35	35	M2-35	35	M3-35	35
M1-40	40	M2-40	40	M3-40	40
M1-45	45	M2-45	45	M3-45	45
M1-50	50	M2-50	50	M3-50	50

The solutions were agitated to ensure good mixing before filtering using a 0.2 μm PTFE syringe filter and pouring in 4 ml vials for use into the Microdrop IJP system.

4.5.1.5 Determining the surface tension of polyol solutions used in IJP

The experimental determination of the surface tension of functionalised inks (i.e. polyol mixture and prepolymer) was undertaken using the capillary rise method. Glass capillary tubes with nominal diameter of 1.60 mm were immersed into a 20 ml crystallising dish containing the samples. As the tendency of liquids to rise up in capillary tubes is a consequence of the surface tension, the height h reached by the liquid was measured and the surface tension σ calculated by:

$$\sigma = \frac{\rho g h r}{2} \tag{4.9}$$

where g is the acceleration due to gravity (9.81 m/s^2), ρ the density of the fluid and r the diameter of the capillary. In this calculation it is assumed that the contact angle of the meniscus in the capillary tube is cero.

The surface tensions of the mixtures were then calculated using the equation suggested by Freundlich (1926), where linear dependency on concentration is assumed, i.e.

$$\sigma = \sigma_1 x_1 + \sigma_2 (1 - x_1) \tag{4.10}$$

where x_1 and x_2 and σ_1 and σ_2 are the molar fractions and surface tensions of components 1 and 2 respectively.

4.5.2 Materials handling

The IJP system which was used as the basis of the work described in the thesis was designed and built by Morris (2004). This micron-resolution system was built for the printing of micro-dots typically used for the construction of electronic devices using commercially formulated polymer solutions such as PEDOT:PSS (Bayer).

The IJP system comprised the now classical three main sections:

(i) A computer controlled motorised x-y stage that allowed a guaranteed substrate printable area of 25 mm x 25 mm. It also allowed fast movement of the stage to avoid nozzle clogging and to control droplet to droplet solvent interaction. The stage movement resolution was 1μm. The stepper motors were controlled by sending commands from the computer via a RS232 serial connection. The command language employed was EASI. The commands turned on the driver motors, controlled their speed, moved the x-y stage and triggered the inkjet printer head.

(ii) A piezoelectric IJP head with a 50 μm nozzle (Microdrop model MD-K-130) that was mounted on a z micrometer. The distance between nozzle and the substrate was kept short (0.5 mm) to keep the airflow around the nozzle to a minimum in order to avoid droplet flight deviation. The functionalised ink was fed from a 4 ml glass vial through a PTFE tube. The nozzle comprised a glass capillary and piezoelectric crystal. The former allowed the use of a range of organic fluids due to its inert nature. The print head was controlled by the Microdrop controller, which generated square wave pulses to the piezoelectric actuator. It was possible to vary the pulse voltage and duration to give appropriate conditions to form spherical droplets without disturbances. The pulse was measured with an oscilloscope using an external output from the Microdrop controller. The continuous mode was employed to calibrate the equipment and characterise the droplet ejection and the external trigger mode used for printing the functionalised

materials. The print head specification are: permissible liquid viscosity from 0.4 to 20 mPas; maximum liquid throughput 1 μL/s; variation of dispensed volume < 1 %; maximum drop rate 2,000 /s; drop range of flight < 20 mm depending on drop size and drop velocity < 2.5 m/s.

(iii) An optical system comprising a microscope objective and a digital video camera device which were fixed on a vertical support parallel to the nozzle. The position was selected to capture images of the deposited droplets on a substrate. More details can be found in Morris (2004). For the present study, the original system was modified and the webcam mechanisms were updated to a new model, Logitech QuickCam. Also, a new microscope objective (4x objective, focal length 31.04 mm from Edmund Optics) was included. The variable length tube was refabricated, with a coarse and fine movement focusing feature. A second optical system was placed in a horizontal position in order to see simultaneously the falling droplet and its deposition on the substrate. The pictures of the falling droplets were taken using the stroboscopic light included in the Microdrop controller box. It was possible to control the delay between the ejection of the droplet and the triggering of the LED strobe light, in order to observe the different stages of drop formation. Figure 4.9 depicts the IJP system components.

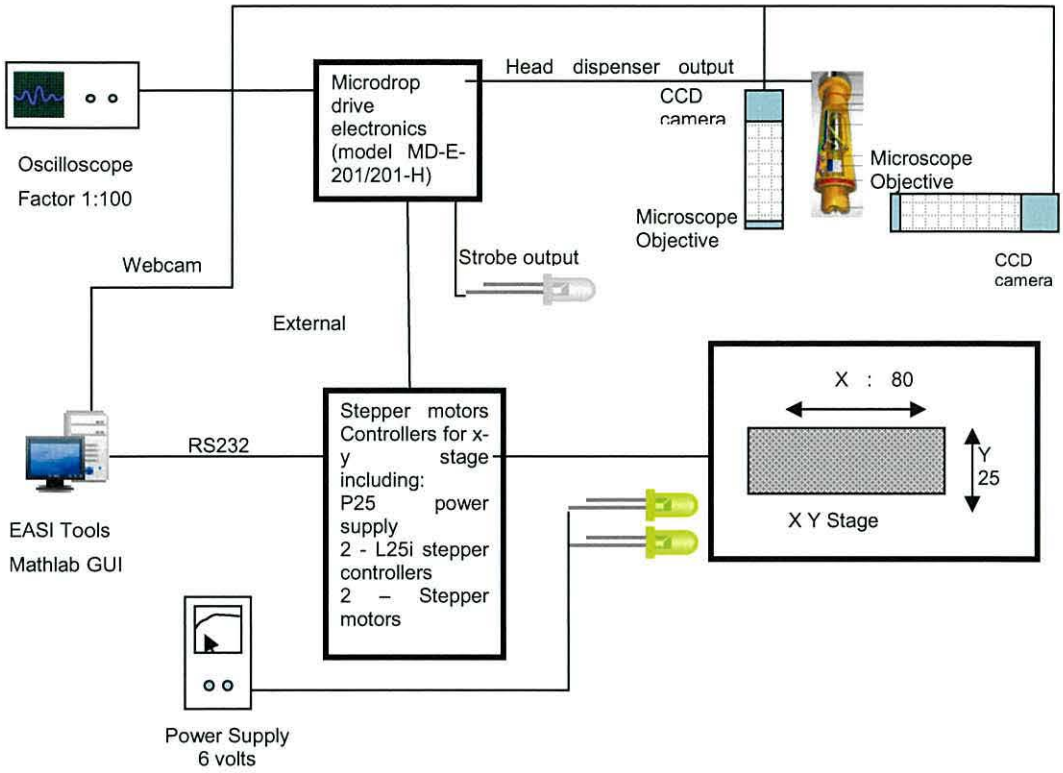

Figure 4.9 Diagram of IJP System designed by Morris (2004).

The whole system was controlled by a Matlab Graphical User Interface (GUI), which permitted the control of the stages and nozzle head in order to generate lines of printed material in the desired locations automatically. For more details the reader is referred to Morris (2004).

Moisture affects the polymerisation, dust and particulate matter could potentially block the IJP nozzle. For these reasons, an inert clean environment for the handling of reactants and the IJP was essential. Initially, an inflatable polyethylene glove box filled with nitrogen gas was used. However, it was observed that any perturbation of the inflated bag created air movement inside it, affecting the direction of the droplet flight. As an alternative, the system was placed inside a fume cabinet, protected by plastic screens. It helped to protect the system from the dust and at the same time it provided a safe environment for the handling of the diisocyanate, a necessary precaution. The fume cabinet was located in a class 1000 clean room operating at a controlled humidity of 45%.

4.5.3 Calibration of the IJP head using a Taguchi experimental design

In order to identify the limits of the IJP device, it was necessary to identify the voltage and pulse width conditions that allow spherical droplet formation without disturbances. The fluids used in the exploratory experiments were (i) a 2% PEDOT PSS solution in methanol (Avecia (Morris, 2004)), and (ii) a pure 2-propanol solvent. The solutions were filtered using a 50 μm PTFE syringe filter. Methanol (99% purity) was used to flush the nozzle head. All reagents were used as supplied.

So as to maximize the data obtained from a moderate number of experiments, an experimental design was undertaken based on the Taguchi model (Taguchi, 1986). To obtain adequate droplet formation, the variation of two factors (F = 2), e.g. voltage and pulse width were considered, each with five levels (L = 5). These five different values of the two variables were established based on literature information (Morris, 2004; Derby and Reis, 2003). The orthogonal design was done using the SPSS software (SPSS Inc.), which yielded the experimental conditions for 25 runs ($L^F = 5^2$). The factor levels are shown in Table 4.5.

Table 4.5 Voltage and Pulse levels used for the initial experiments.

Voltage (Volts)	Pulse width (μs)
50	20
110	50
150	90
200	130
250	160

Before using the IJP device, solvent (methanol) was flushed through the pipes and nozzle several times to ensure that there was no dried polymer inside the pipe system. Then, the PEDOT:PSS solution was placed in the vial of the apparatus. A syringe was connected to the pipe attached to the top of the vial with the polymer solution. Some air was then introduced to let the fluid run through the pipe towards the dispenser head, until a small meniscus was observed coming out from the nozzle. For further details check the Microdrop manual[(1)]. Next, the drop formation process was observed using the microscope objective attached to the IJP and images were captured with the webcam. After completing the experiments, the vial containing the remnants of the polymer solution was replaced by a vial containing pure solvent, and the entire pipe system was flushed clean again.

(1) User Manual for Standard Microdispenser systems with dispenser heads models MD-K-130, MD-K-130SP, MD-K-140 H with drive electronics MD-E-201, MD-E-201H and Strobe diode MD-0-501, as available for 2002.

4.5.3.1 Testing printability of the prepared functionalised inks

Solutions with the potential for being dispensed by IJP were identified in trial runs. To determine the optimum values of pulse width and voltage, the method used for initial calibration of the system was again used. This entailed using the webcam to observe droplet formation for a matrix of values and the experimental conditions for droplet formation recorded for each solution.

4.6 Results and Discussion

4.6.1 Calibration of the IJP for PEDOT:PSS and anhydrous 2-propanol

The optimum pulse width and voltage settings for successful inkjetting of the PEDOT:PSS solution were determined following the Taguchi-designed experiments described in section 4.5.2. The quality of the droplets obtained was graded on a three level scale. Level one was assigned to no droplets coming out from the nozzle or to the appearance of a fluid meniscus, as shown in Figure 4.10.

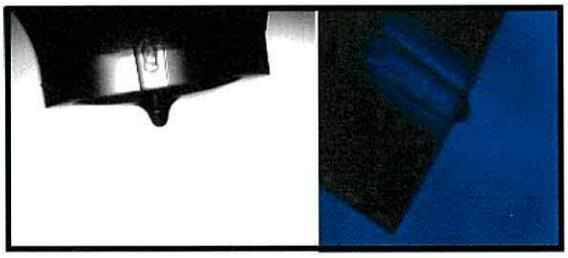

Figure 4.10 Quality of droplet Level 1 is assigned to no droplets coming out from the nozzle or just the appearance of a meniscus. Photographs by Yara Almanza.

Level two was the classification used to describe droplets with anomalies such as long jets that did not break, the appearance of satellite drops, trajectory deviation, broad droplet size distribution, or the accumulation of liquid outside the nozzle (big droplet). Cases that fall into level-two category are shown in Figure 4.11 and Figure 4.12. The break-up modes in this category are similar to models M2 and M3 suggested by Wong (2006). In the first case satellite droplets were formed between primary drops due to capillary pinch off. In the second case, the jet broke up simultaneously at several places along the jet into a continuous stream of droplets.

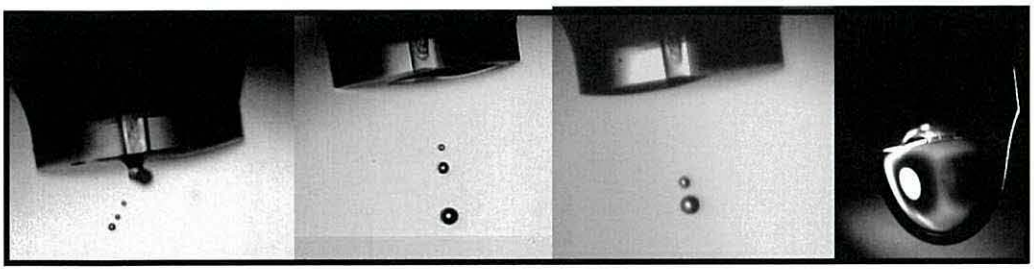

Figure 4.11 Anomalies present in droplets. From left to right: deviated trajectory, different droplet sizes, satellite droplets appearance and adhesion of liquid on nozzle surface. Photographs by Yara Almanza.

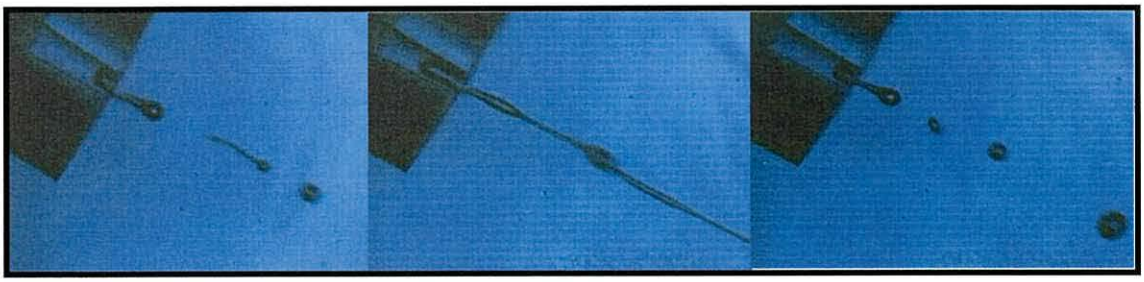

Figure 4.12 Quality of droplet Level 2 assigned to droplets with anomalies. From left to right, irregular jet break up, no breakup of jets and irregular size droplets. Photographs by Yara Almanza.

Level three was the classification into which very good droplet formation took place i.e. where the break up of the jet occurred within a short distance of the orifice so that a reproducible droplet was formed without satellite droplet formation and with no deviation of the trajectory. This behaviour is illustrated in Figure 4.13.

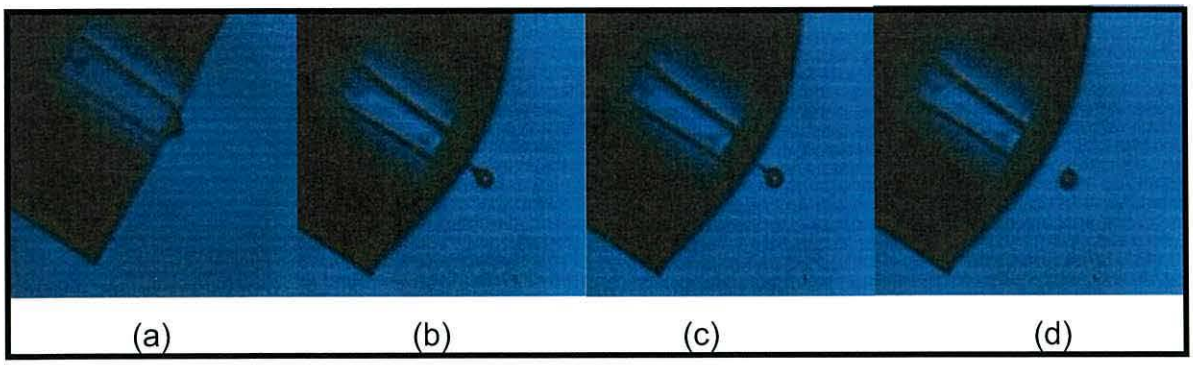

Figure 4.13 Example of good drop formation assigned as Level 3. (a) Meniscus appearance, (b) jet ejection, (c) jet break down, (d) falling homogeneous droplet. Photographs by Yara Almanza.

The results for the drop formation of PEDOT:PSS solution in methanol are shown in Figure 4.14 where the droplet quality is plotted as a function of experimental conditions: voltage and pulse width.

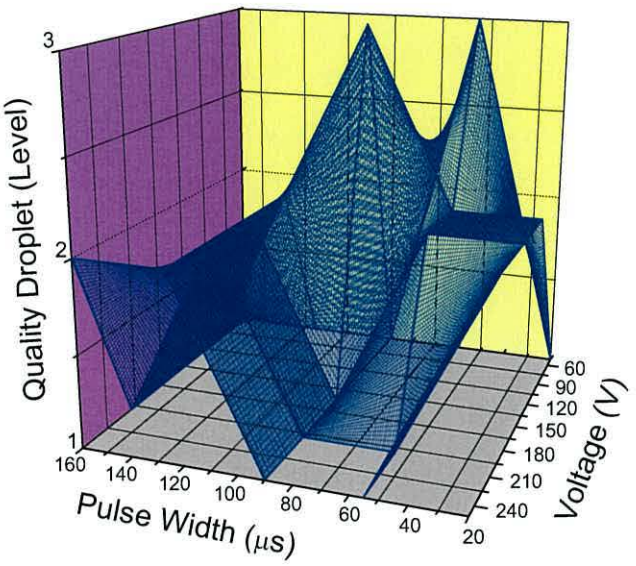

Figure 4.14 Droplet quality for PEDOT PSS solution in methanol as a function of voltage at different pulse widths.

The plot shows that the only combination of conditions that allowed good drop formation of PEDOT:PSS (i.e. level 3) were 50 V for 50 μs, and 110 V for 90 μs. The limited combination of conditions yielding good droplets, may be due to the fact that the driving voltage and the duration of the pulse were not in the required proportion. In other words, when there is no drop formation, the pulse is not strong enough to eject a drop from the nozzle and/or the time that the pulse is present (pulse width) is shorter than required.

The conditions for good drop formation of anhydrous 2-propanol were similarly determined. Only one set of conditions was found to be successful, normally 110 V for 90 μs, as shown in Figure 4.15.

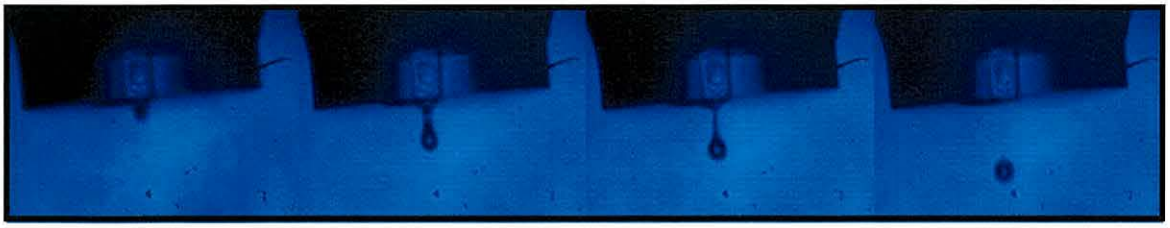

Figure 4.15 Good drop formation of anhydrous 2-propanol at 110 V for 90 μs. Photographs by Yara Almanza.

Thus conditions for printing good quality droplets of these two conventional fluids, PEDOT:PSS solution and 2-propanol, were the same: 110 V for 90 μs. This is reasonable since both solutions have similar viscosities (~20 mPa s) and surface tension (~23 mN/m). The velocity of the droplet, ~2.5 m/s, was calculated by measuring the distance travelled by the drop in sequential images and dividing it by the time delay between the ejection pulse and the strobe flash. This result lies within the specifications of the Microdrop IJP head, which suggests that expected droplet velocities lie between 2 and 4 m/s.

From such data Re, We and Z^{-1} were calculated, and the value of Z^{-1}=5.4 placed the operating point in the zone for good droplet formation when plotted on the Derby and Nuno plot in Figure 4.5.

4.6.2 Polyol solution deposition on diisocyanate films

Experiments with 24 polyol mixtures demonstrated that only mixtures with a very low polyol content (%w) could be jetted using the Microdrop IJP system. In the case of Mixture 1, none could be dispensed successfully. Of the Mixture 2 systems only M2-10, M2-20 and M2-30 could be dispensed and when the conditions for obtaining good droplets were explored only deformed droplets were produced (i.e. Level 2 quality). Figure 4.16 shows that at 110 V and a pulse width of 80 μs, mixture M2-10 could be dispensed but, instead of a falling droplet, the liquid accumulated on the external side of the nozzle. (The dotted curves in the figure have been superimposed on the meniscus to highlight this effect).

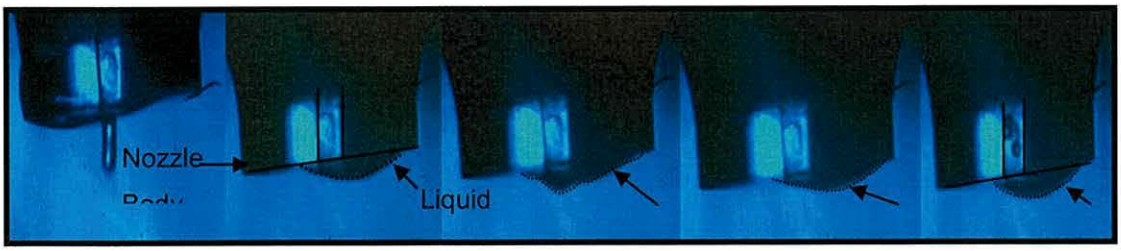

Figure 4.16 Printing of the mixture M2-10 containing 10% of polyol Mixture 2 using 110 V pulses 80 μs in duration. Photographs by Yara Almanza.

In contrast, Figure 4.17 shows that mixture M2-20 was dispensed as small and irregular droplets at 150 V using a pulse width of 90 μs. The droplets were so small, that their trajectory was not completely vertical.

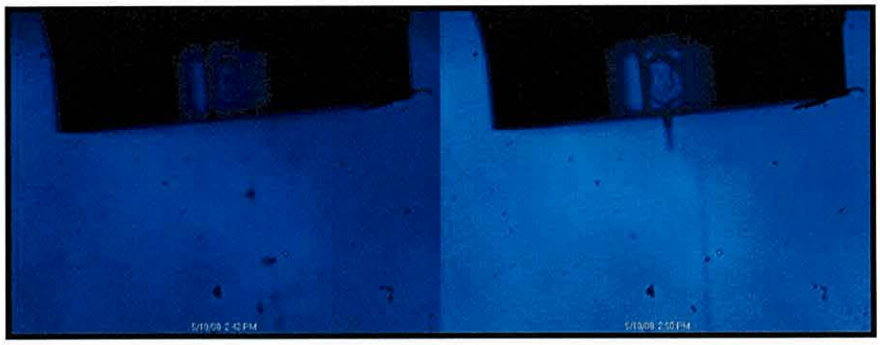

Figure 4.17 Ejection of mixture M2-20 containing 20% of polyol Mixture 2 using 150 V pulses of 90 μs duration. Photographs by Yara Almanza.

Solution M2-30 formed very well-defined droplets at 250 V with a pulse width of 120 μs. However, the droplets emerging from the nozzle did not fall under the influence of gravity onto the substrate but accumulated on the outer surface of the nozzle forming one large droplet as shown in Figure 4.18. It is possible to see from the images that the smaller droplets (delineated by dotted lines) are exiting the nozzle orifice but staying within the big droplets.

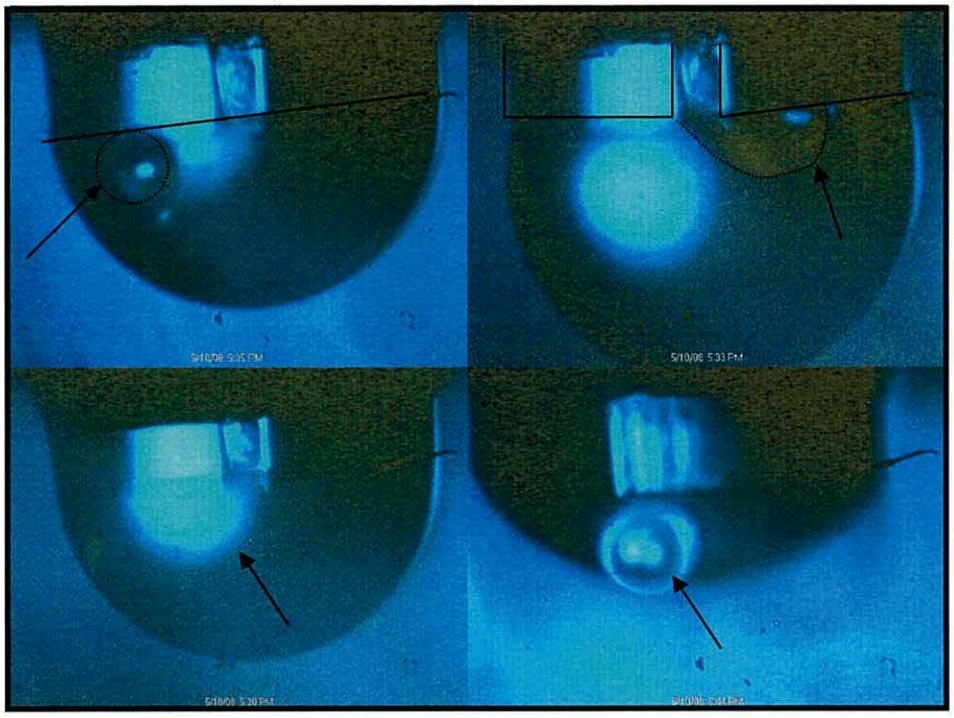

Figure 4.18 Ejection of mixture M2-30 containing 30% of polyol Mixture 2 using 250 V pulses of 120 μs duration. It is assumed that due to the evaporation of some of the solvent, the difference in concentrations allows the small drops to be seen by the camera. Photographs by Yara Almanza.

This phenomenon is likely to be produced by the relatively high viscosity and adhesion force of the ink, that overcomes gravity, and attract the droplets to the outside surface of the nozzle body.

It is important to emphasise the extreme susceptibility of the inks to clog the nozzle. Once the nozzle was blocked, an elaborate procedure was conducted to unblock it, including the application of hot air, ultrasound and pack pressure. These procedures were risky, because they could damage the nozzle head permanently.

Finally, from the set of mixtures in the class Mixture 3, only M3-10 was able to flow out from the 50μm nozzle. With a 50 V pulse lasting 20μs or 50 μs, satellite droplets were formed whereas at 60 V for 20 μs or 50 μs duration, droplets and jets emerged in different directions from the nozzle, as shown in Figure 4.19.

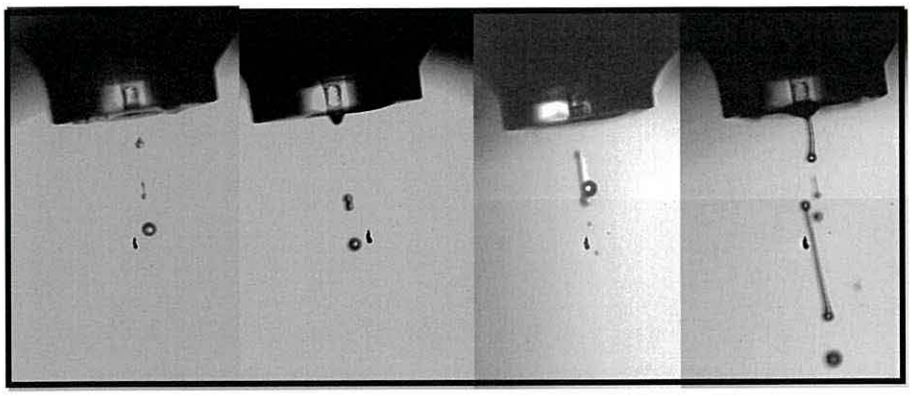

(a) (b) (c) (d)

Figure 4.19 Printing of mixture M3-10 at (a) 50 V and 20μs (b) 50 V and 50 μs (c) 60 V and 20 μs (d) 60 V and 50 μs. Photographs by Yara Almanza.

Figure 4.20 shows the rheological properties of polyol PPG 1000. The linear dependency of shear stress on shear rate which yields a constant viscosity of ~180 mPa s confirms that the fluid follows Newtonian behaviour. The viscoelastic properties are given in (b) where G' and G" are the elastic and viscous moduli respectively and n* is the dynamic viscosity. The storage modulus G' measures the amount of stored energy and it is related to the elastic properties of the sample. The viscous properties of the fluid are related to the amount of energy dissipated by the material, which is indicated by the loss modulus G''. Since G'' is much larger than G' the liquid is more elastic and has a non-viscoelastic behaviour.

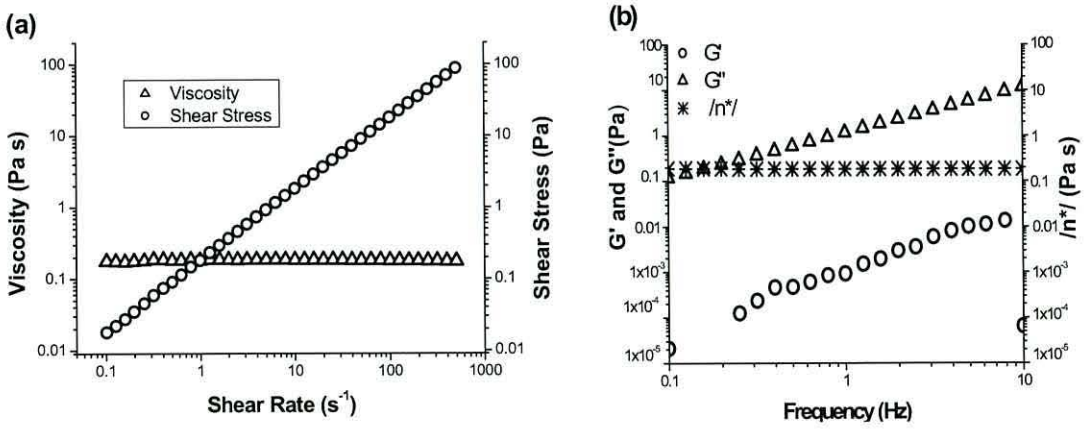

Figure 4.20 Rheological properties of PPG 1000. (a) Viscosity and shear stress as a function of shear rate, and (b) elastic modulus G', viscous modulus G" and dynamic viscosity n* as a function of frequency.

The rheological properties of 1,4 butanediol are shown in Figure 4.21, and is also seen to behave as a Newtonian fluid, with a constant viscosity ~ 79 mPa s over the shear rate range used. Again, from Figure 4.21(b) we see that it is a non-viscoelastic fluid.

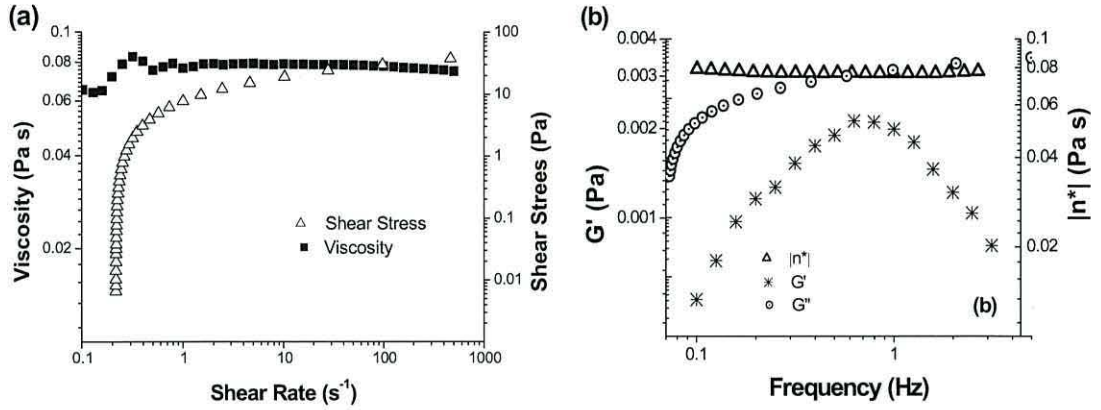

Figure 4.21 Rheological properties of 1,4 butanediol. (a) Viscosity and shear stress as a function of shear rate, and (b) elastic modulus G', viscous modulus G" and dynamic viscosity as a function of frequency.

The surface tension of the polyol mixture was 25.5 mN/m, a value which is in the range of desired fluid properties. However, the pure polyol mixture was too viscous to be handled by a conventional IJP system. Dilutions were prepared by volumetric methods, which are standard and known to be very precise. The viscosity and surface tension of the dilutions were estimated using equations 4.8 and 4.10 respectively and results are shown in Table 4.6. Again, assuming that the resulting velocities of the droplets would be between 2 and 4 m/s, the range of Re, We and Z^{-1} was estimated and shown in Table 4.6.

Table 4.6 Estimated properties of the 24 functionalised fluids.

Parameter	Mixture 1	Mixture 2	Mixture 3
Viscosity (m Pa s)	$2.21 \leq \mu \leq 2.79$	$2.24 \leq \mu \leq 2.95$	$2.22 \leq \mu \leq 2.85$
Surface Tension (mN/m)	23	23	23
Re	$35.79 \leq Re \leq 90.30$	$33.95 \leq Re \leq 89.33$	$35.05 \leq Re \leq 89.92$
We	$8.7 \leq We \leq 34.74$	$8.62 \leq We \leq 34.72$	$8.63 \leq We \leq 34.73$
Z^{-1}	$12 \leq Z^{-1} \leq 15$	$11 \leq Z^{-1} \leq 15$	$11.93 \leq Z^{-1} \leq 15.26$

Assuming that the mathematical models employed for the prediction of the viscosity and surface tension of the mixtures are valid, the range of the non-dimensional numbers Re, We

and Z^{-1} indicate that, according to Wong, the break-up mode of all the functionalised inks would be mainly M2 and M3 type (i.e. Level 2 quality droplets) with a very limited possibility that Inks prepared from Mixture 2 would break-up following mode M1 (i.e. Level 1 quality droplets). Similarly, based on the Derby and Nuno plot, the functionalised inks prepared from Mixture 2 only a the slight possibility of being printed since the Z^{-1} number ($\geq$ 11) was just about the upper limit (Z^{-1}=10). It is not surprising then that none of the 24 different solutions were printable.

It is possible that the calculated values of viscosities and surface tensions did not reflect the actual values (that should be determined experimentally for each ink). However, any differences are unlikely to be large since the experimental observations match the predictions based on these values.

4.7 Conclusions

The methodology used here was similar to the one used by Danzebrink and Aagert (1999), where the functionalised fluid was diluted in solvent to obtain a 30% w solution. Then, using a Microdrop IJP system with a nozzle diameter also of 50 μm, spherical droplets were deposited onto coated glass slides in a dust-free environment.

In this study the process was designed to place a 5 μm thick layer of pre-polymer on a glass surface and subsequently coated by printing of polyol solution. However, it was experimentally demonstrated that it was not a feasible methodology for the current polyurethane system. Firstly it was not possible to print the desired amount of polyol mixtures using the conventional IJP system. The mixture of polyol PPG1000, 1,4 - butanediol and 0.1% of catalyst was diluted in anhydrous 2-propanol to reduce the viscosity. Even this was insufficient to tailor the ink properties. Secondly, the technique also leads to a large surface/volume ratio of the iso-cyanate terminated pre-polymer i.e. the area of exposure of the reactant to ambient moisture (even inside a clean room) is large and the reaction of the NCO groups with moisture is likely. Such a reaction will lead to NH_2 terminated prepolymer chains which are very reactive to NCO groups yielding urea groups within the surface layer and an imbalance in the stoichiometry with respect to the OH functionalised reactants. This is not good for the synthesis of good quality polyurethanes of the type desired.

The nature of the 24 functionalised inks, therefore, did not allow the use of the available piezoelectric IJP system and so the synthesis could not proceed.

An alternative methodology was considered, analogous the one employed by others (Setti et al., 2005; Boland et al., 2007; Xu et al., 2006), in which a commercial printer was adapted to print fuctionalised inks. As the cartridges employed worked with the thermal printing mechanism, the chemistry of the inks was susceptible of modification. Also, the nature of the inks was not suitable for printing, especially for the poor compatibility of the cartridges with the chemicals employed. On the one hand a pre-designed printing head can be operated with high accuracy and reproducibility, and in addition all the driving electronics and positioning software are easy to tailor to a specific application. On the other hand, it also has its disadvantages. For instance, the limitation in the liquids suitable to print (e.g. very low viscosity), the formation of satellite dtoplets, the complication of maintenance and prevention of nozzle clogging. The properties of a core functional material dissolved in a solvent can create unwanted lumps of material that block the printhead's nozzle and create gaps in the lines of the printed material. Therefore, a balance should be made between the benefits and constraints when considering the use of IJP technology in the implementation of the micro synthesis of polyurethanes. The possibility of construction of a stainless steel nozzle and a whole IJP system was also considered. However, exploratory test using laser micromachining of apertures in a stainless steel sheet gave poor quality nozzles. It was concluded that a different approach was needed in order to print the desired chemicals. The alternative methodology studied is described in Chapter 5.

Chapter 5. Construction and Testing of a new IJP System

5.1 Process Intensification: an Ink Jet Printing System suitable for micro-synthesis of polyurethanes

Process Intensification normally comprises the development of new technologies that have the capability of decreasing the size of a chemical plant whilst maintaining or improving the output level. There are many advantages in down-scaling as has been described in Chapter 1. However, down-scaling itself has many virtues when the product is of a complex nature and special techniques are needed for its manufacture. Attempts to miniaturise the synthesis of polyurethanes using Ink Jet Printing technology was described in Chapter 4. Unfortunately, the approach gave rise to many problems. The rheological characteristics of the diol were such that they were too viscous to be pumped by the available piezoelectric IJP system. Even solutions of the diol in isopropanol proved difficult to pump. The study showed that the maximum content of functionalised material in solvent that could be made to flow through a 50 μm nozzle was 30% w/v. Even at this concentration, though, poor droplet formation was observed. Alternative methodologies were considered and tested, but none were successful. It was concluded, therefore, that a completely new IJP system was required, specifically designed for handling the reactants commonly used for polyurethane synthesis. The new system should be capable of withstanding the high pressures generated when handling viscous fluids and should comprise materials of construction which are inert to the functionalised reactants. Unfortunately, a bid for the funding needed for such a system which could handle the key reactants failed and this had an impact on what was possible from an experimental standpoint in the rest of the programme.

In this Chapter, then, is presented the outcome of studies carried out towards the synthesis of polyurethanes using modified IJP technology. The novelty of the approach lay in the attempt to make two droplets collide in mid-air. The droplets were to be of defined size (stoichiometry) and each containing the necessary reactants for the reaction (i.e. one droplet containing –NCO groups and the second containing –OH groups). From lessons learned in the first attempt to miniaturise the PU synthesis reported in Chapter 4, a high voltage facility was incorporated in the IJP system in an effort to

prevent the fluid from sticking to the exterior of the nozzle. This was thought to be one of the primary reasons preventing good droplet formation. The colliding droplets, once co-mingled, would form a micro-reactor which is the most extreme example of down sizing. It would also remove the need for intensive mixing if the reactants spontaneously mixed on this scale i.e. it would be a good example of PI.

5.1.1 Mini-synthesis of polyurethanes and related methodologies

No reports have been published on the synthesis of polyurethanes in micro-droplets. However, there is literature available related to the synthesis of polyurethane microspheres (Ramanathan et al., 1998) with particle size in the range of 0.1 to 100 μm when reactions are carried out by dispersion, suspension or cryogenic grinding of thermoplastic polyurethanes (Saunders, 1965). These processes though, are on a conventional macroscopic scale.

Piezoelectric Ink Jet Printing technology has been used to print effectively aqueous polyurethane colloidal suspensions with a maximum content of 40% wt (Berg et al., 2007). Also El-Molla (2007) reported the successful printing of the aqueous UV-curable binder of polyurethane acrylate at a maximum concentration of 20% w/w in deionised water. In both cases, the already formed polyurethanes were printed, and their synthesis was not conducted *in-situ*.

The design of a new polymerisation reactor system based on IJP technology is reported in the following sections and in the context of process intensification.

5.1.2 Basis of the new equipment design

The results reported in Chapter 4 are the starting point for the design of the new IJP reaction system. The main limitations of the standard MicroDrop piezoelectric IJP technology for micro-reactor applications were:

i) the pre-designed piezoelectric printing head was not capable of pumping fluids with a viscosity higher than 20 mPa s;

ii) the chemical resistance of the materials used in the printing-head was poor;

iii) some of the functionalised liquids ejected from the nozzle did form droplets but these aggregated on the exterior of the nozzle rather than falling onto the substrate;

iv) nozzle clogging and head maintenance were a problem when dispensing reactive fluids.

The technique, which involved the reaction of a layer of pre-polymer on a glass substrate with a dispensed diol, was not a good option. After deposition, the pre-polymer was likely to react with atmospheric moisture unless the entire system was housed in a controlled atmosphere.

An alternative to building a complete new pumping system for the reactants, would have been the addition of a second micro-dosing head to the existing IJP system. Such a system might be used to print one dot of diisocyanate, and immediately after a drop of polyol on the top, or even to get the two droplets to coalesce prior to reacting on the substrate. The latter situation leads to the interesting problem of matching the reaction dynamics to the flight time of the droplet. However, the approach would only be feasible provided the pumping system and head could deliver discrete droplets of the right size in order to achieve the necessary stoichiometry of reactants for polyurethane formation. This approach was not attempted because of the high cost of developing an extended IJP system, using the existing hardware and software platforms.

The challenge of building a new pumping system on the IJP scale which would be capable of fulfilling the requirements needed for the mini-reactor synthesis of polyurethanes envisaged and on a limited budget was considerable. Two main elements guided the design: the process of polyurethane chemistry and the technology which had to be capable of producing droplets from standard reactants. Furthermore, the new system had to be capable of minimizing the frequently encountered problems of the nozzles becoming clogged and the formation of satellite droplets. The system should be capable also of withstanding aggressive cleaning methods.

There have been a few studies of microreactor design and fabrication that inspired the design of the new IJP system and the development of a polyurethane mini-synthesis technique. Okamoto and co-workers (2004) created a new method to increase the productivity of continuous flow micro-reactors by incorporating two thin tubes with an OD of 300 μm into a straight tube of 1 mm inner diameter and 500 mm long. The procedure followed was to alternately pump two liquids at a constant rate of 120 μl/min using a piezoelectric pump in the frequency range 0.5 to 20 Hz automatically and from of 0.01 up to 1.53 Hz manually. A second system comprised a mechanical pumping system, e.g. syringes with piston displacement controlled by a stepper motor. The micro-reactor used in this second set up was a channel of 2 mm width. The kinematic viscosity of the fluids pumped was the same as that of water. The authors' finding was

that in order to achieve complete homogeneous mixing for liquid-liquid reactions, it is necessary to increase the area of the interface.

Chen (2007) studied the collisions of diesel-diesel drops and diesel-ethanol drops, an area of study relevant in the field of spray combustion. The methodology employed involved the concept of two droplets colliding in mid-air, which is particularly pertinent to the micro-reactor concept envisaged for polyurethanes. Chen's experimental set up is shown in Figure 5.1.

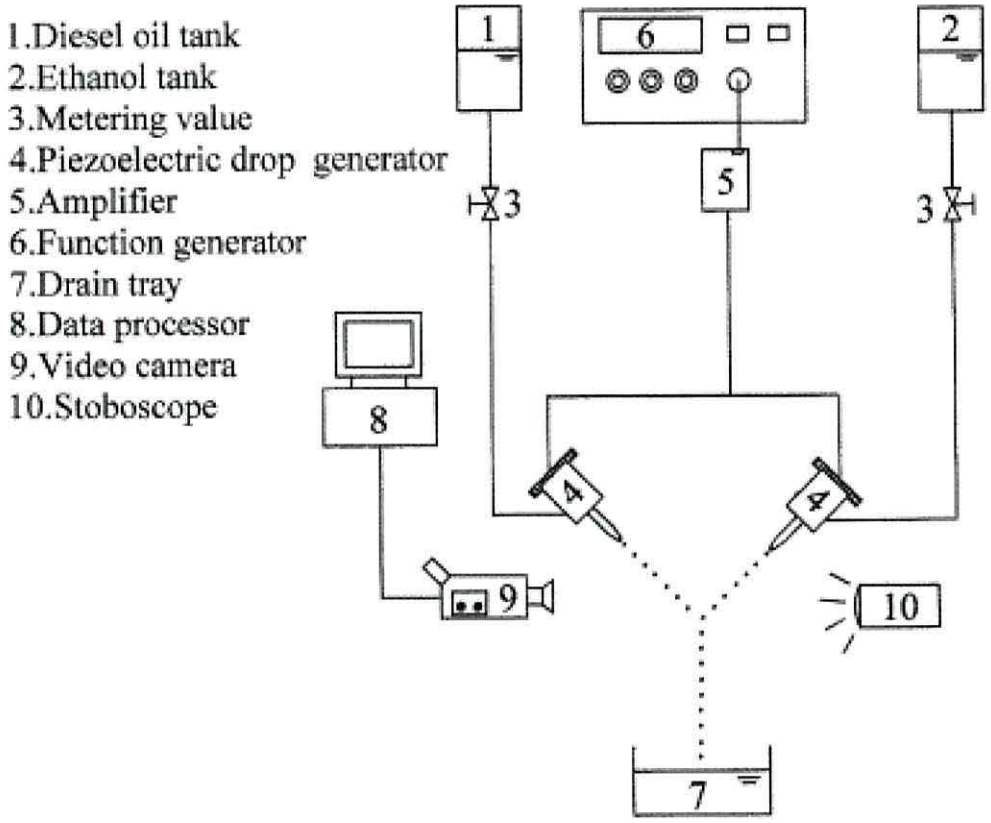

Figure 5.1 Experimental set-up published by Chen (2007).

The system consisted of two piezoelectric drop generators of equal size (in the range of 700 – 800 μm) which were driven by only one function generator. Ethanol and diesel oil, were delivered through two separate pressurised containers. A stroboscopic light was placed in front of the colliding droplets, and was synchronised with the pulse generator. This allowed the collision of droplets to be recorded by a video camera.

There are many similarities in the Chen approach to the design of the new micro-urethane reactor system developed here. The pumping system adopted was that based on available IJP technology (despite the known weaknesses) but other parts of the system, such as the optical and image capture sub-systems, had to be developed and integrated. This is also the case for the high voltage system needed for the electrostatic enhancement of droplet formation.

The use of electrostatics to assist droplet formation has been known for some time. Blazdell and Evans, (2000) used a charging electrode surrounding the liquid jet coming out from the nozzle at the point where the drops started to separate. The metallic body of the nozzle assembly was at 0 V, and the ink employed was conductive. The droplets acquired charge as they were formed and separated from the main stream. The deflection of the droplets was determined by the level of charge obtained by varying the voltage. The trajectories of the droplets and landing position were established by high voltage (18 kV) plates. The basic principles of the system adopted in the present work are described in Section 5.1.3.

5.1.3 Electrostatics in Ink Jet Printing

Droplets can acquire an induced electrical charge when emerging from a nozzle in the presence of an electric field. In Figure 5.2 the electric field is created by applying a voltage, V, to a metal plate situated under a grounded metal nozzle. If the emerging liquid has sufficient conductivity, it acts essentially as an extension of the grounded nozzle. Thus positive charges on the metal plate induce negative charges at the surface of the droplet (Taylor and Secker, 1994).

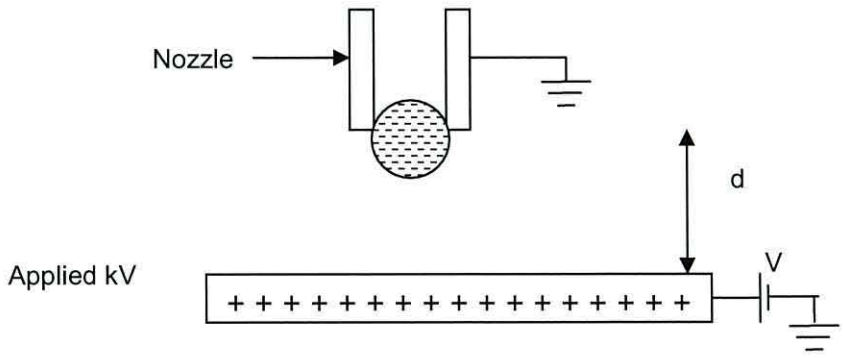

Figure 5.2. Electric field created between parallel plates.

The charge, Q that is acquired by a drop of radius R is given by:

$$Q = 4\pi\varepsilon_o RV \tag{5.1}$$

where ε_o is the permittivity of free space (8.85×10^{-12} F/m) and V the voltage applied between electrodes (Taylor and Secker, 1994). There is a maximum charge that a droplet can attain which is limited by two phenomena:

(i) Atomisation which occurs when electrostatic repulsion forces in the droplet exceed its surface tension. The resulting droplet breakup into a fine mist reduces the total energy of the system.

(ii) Corona onset caused by electrical breakdown of the air surrounding the droplet. A corona discharge is associated with a highly non-uniform electric field, and usually occurs at the boundaries of conductors with small radii e.g. edges and points (Figure 5.3). In such systems, if the electric field at such boundaries exceeds the breakdown field of the gas, a partial breakdown occurs (recognised by a weak glow). Full breakdown is prevented by the rapid decrease in field away from the edge or point.

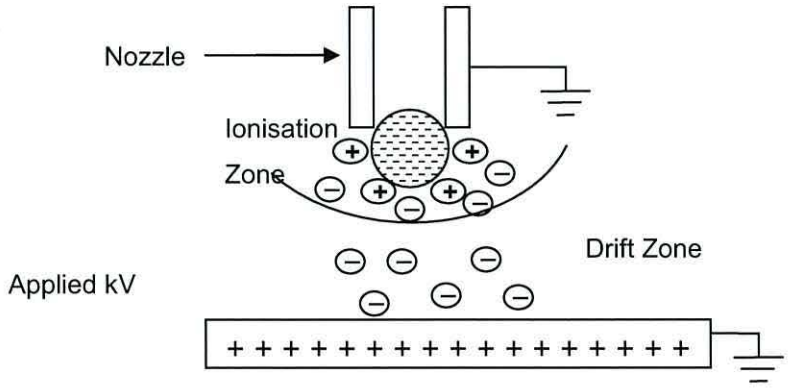

Figure 5.3 Two main zones in a corona discharge.

Based on these facts, the new IJP system was designed to charge the droplets to encourage ejection from the nozzle and to drive them while keeping the voltage low enough to avoid both the onset of corona and atomisation.

5.1.4 Droplet collision

The aim of the new concept was to make two droplets of functionalised reactants collide in mid-air, giving rise to a rapid mixing of the droplets. The coalesced droplets would then form a free surface micro-reactor.

The collision between two liquid droplets has been identified by others as being of importance e.g. for understanding atmospheric rain processes, in spraying processes, emulsion polymerisation and fuel sprays. Also, the phenomena within colliding droplets provide information for the implementation of blended fuels in diesel engines to increase efficiency and to replace fossil fuels. It is relevant to this research to review what behaviour has been observed in two droplet collisions in order to understand what can be expected.

Typically, there are four categories which describe the outcome of a drop collision: a) coalescence, b) bouncing, c) separation and d) shattering. The first one takes place at low Weber numbers (equation 4.3) or low velocities, and is when both drops combine to form a single drop. The second occurs when the drops are prevented from coalescing by the surface tensions so that they suffer deformation with no mass exchange. The last two categories are collisions with higher impact energy (Mashayek et al., 2003). Chen (2007) studied the collision of diesel-diesel and diesel-ethanol drops. In the first case the collision of two diesel droplets with identical properties and dimensions was explored.

In this research the viscous effects were ignored, and also it was assumed that there was no appreciable size effect on drop collision data for droplets with diameter in the range of 200 – 1000 μm. Therefore, the data presented were described in terms of the Weber number and impact parameter X. The latter term, was defined as the distance between the relative velocity vector (located at the centre of one drop) and the centre of the other drop and was of the form X

$$X = \frac{b \sin|\beta - \alpha|}{d} \tag{5.2}$$

where the variables are related to the geometry of the colliding droplets, as shown in Figure 5.4. Table 5.1 shows the dimensionless groups used and their values.

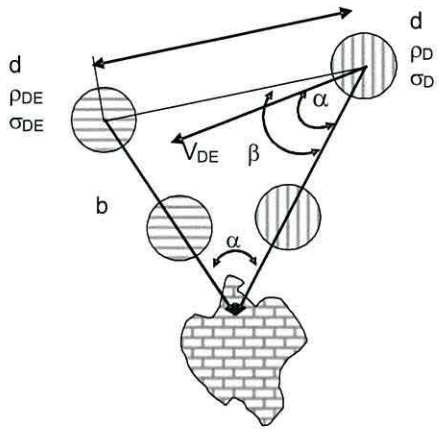

Figure 5.4 Geometry for calculating of the impact parameter X (Chen, 2007).

Table 5.1 Dimensionless groups and their value used in studies conducted by Chen (2007).

Dimensionless Variable	Definition	Value or Range
Diameter ratio	d_D/d_E	0.98–1
Weber number	Eq. 5.2	$0.6 < We < 100$
Reynolds number	Eq. 5.1	$30 < Re < 450$
Impact Parameter	Eq. 6.1	$0 < X < 1$
Density ratio	ρ_D/ρ_E	1.02
Surface tension ratio	σ_D/σ_E	1.27
Viscosity ratio	μ_D/μ_E	2.63

Subscript: D = diesel oil; E = ethanol

The phenomena observed in the diesel-diesel droplet collisions included coalescence and different types of separation.

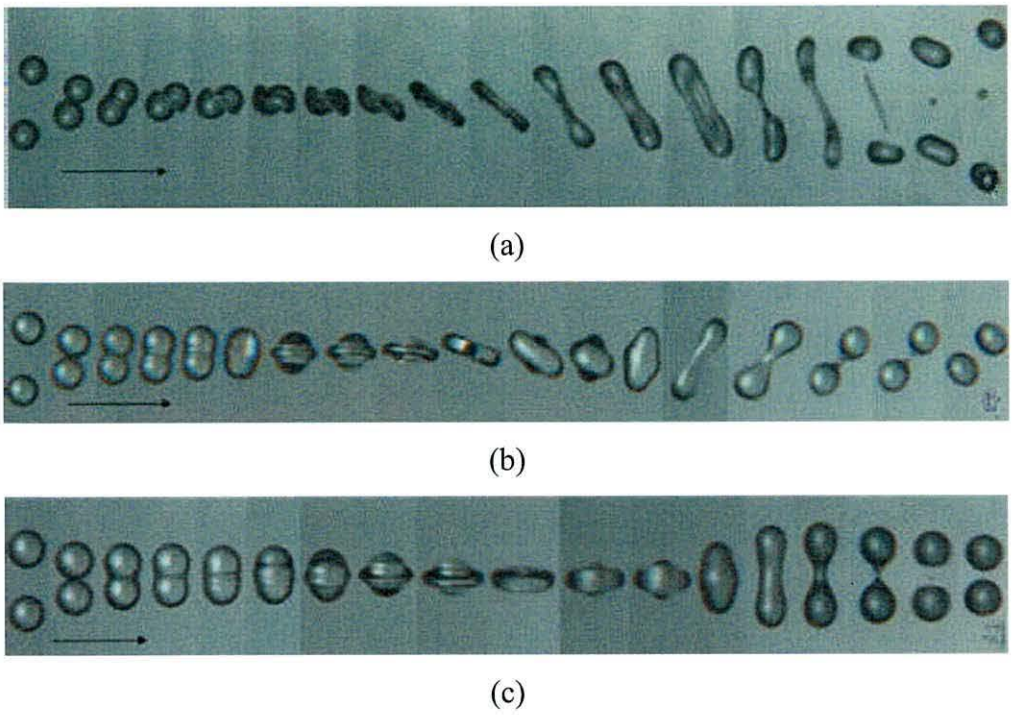

(a)

(b)

(c)

Figure 5.5 Phenomena observed by Chen in diesel-diesel droplet collisions. (a) Stretching separation at We ≈ 71 and X ≈ 0.41, (b) oblique reflex separation at We ≈ 40 and X ≈ 0.15 and (c) reflex separation at We ≈ 35.

The images presented in Figure 5.5 show stretching, oblique and reflex separation. The author considers that these collisions are quite symmetric because both were diesel drops. It was found that the phenomena occuring after a two-drop collision depend on the strength of the liquid bridge formed and is determined by the nature of the fluids involved.

On the other hand, the collision between ethanol and diesel droplets showed that the ethanol spread onto the surface of the diesel drop just after touching the interface. The phenomenon lasted about 0.1 ms from the moment of impact to the other end of the diesel droplet. The droplets had a diameter of 780 μm at very low Weber number (Figure 5.6a).

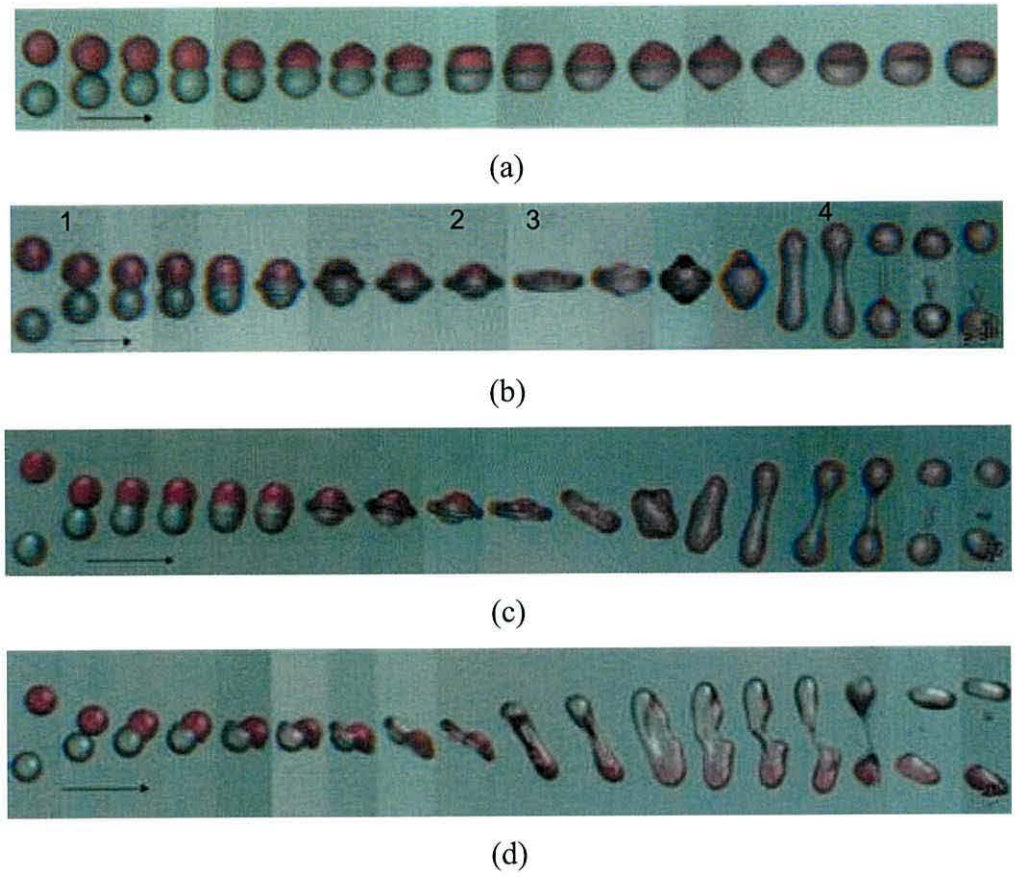

Figure 5.6 Phenomena observed by Chen in Diesel-ethanol droplet collisions. (a) Drop collision at We ≈ 2 ethanol droplet is on top (red droplet), (b) head-on reflex separation, (c) Oblique reflex separation, (d) Stretching separation.

The liquid bridge in the reflex separation observed in Figure 5.6b, broke at the upper end (step 4) because more ethanol was present in the cross section at that point causing weakness. In the oblique reflex separation (Figure 5.6c) the break-up area was again near the weaker end (top). This is different to the case for diesel-diesel drops (Figure 5.5(a)), where the break-up is more in the centre of the liquid bridge, because both droplets are of the same species. Similarly, the liquid bridge shown in Figure 5.6(d) is thicker than the one presented in figure Figure 5.5(a) because the spread of ethanol over the diesel increases the thickness of the liquid bridge.

In all the experiments conducted by Chen, no chemical reaction occurred and all the viscosity effects were neglected. Furthermore, the results were valid for liquid drops with the same dimensionless parameters, which involved similar droplet dimensions and physical properties.

Other authors have developed mathematical models for liquid drop collisions which include pressure and viscous effects. For example, Mashayek et al (2003) reported the mathematical simulation of the coalescence collision of liquid droplets and studied the effects of the Reynolds number (equation 2.10), impact velocity, drop size ratio, and internal circulation. The mathematical model was based on the Navier Stokes equations (see Appendix II) for incompressible viscous Newtonian fluid with constant properties (Mashayek and Ashgriz, 1995). The simulation was executed using the following liquid properties: density 10^3 kg/m^3; kinematic viscosity 10^{-6} m^2/s; surface tension 0.0067 N/m; $3 \leq Re \leq 60$, where the drop radius of 54 μm corresponds to Re = 60 and initial relative velocity of 2.23 m/s. The authors reported that the effect of increasing the Reynolds number on the collision of drops of the same size was to yield thinner drops during the coalescence. It was found as well, that in the collision of drops of different size, the smaller drop goes through considerably larger deformation in the early stages of the process. However, at longer times a spherical shape is achieved. Mashayek (2003) also found that in the collision of two different size droplets, "there is a larger penetration into the larger drop at smaller size ratios". In addition, it was concluded that the major portion of such penetration occurred in a short interval as the coalescence occurred.

The complex nature of the free surface flow problem is difficult to simulate accurately and the existing mathematical models are limited by the simplifying assumptions that are made. Hence, more experimental data is needed to guide and develop better models.

5.1.5 Mixing

There are two ways to induce mixing on the micro scale: active and passive mixing. The first one involves the use of external energy sources such as ultrasound, electrokinetic instabilities, and piezoelectric vibrating membranes to mention some. Electrowetting-induced merging of droplets has been studied in the past (Hessel et al., 2005). In one such experiment where two 1.75 μL droplets, one containing fluorescein, KCl and KOH and the second only the salts, were placed between two planar electrodes surrounded by silicone oil. One of the droplets was actuated towards the other by applying 30 V across the plates, in order to change the interfacial tension. It was found that this did not lead to sufficient turbulence for effective mixing, so the process was

diffusion limited. Nevertheless, it was found that mixing in droplets with very different surface tensions was faster than with liquids with similar properties. Passive mixing, in contrast, involves the modification of a flow by changing the flow energy, for example by using a hydrostatic potential or making different streams flow into contact.

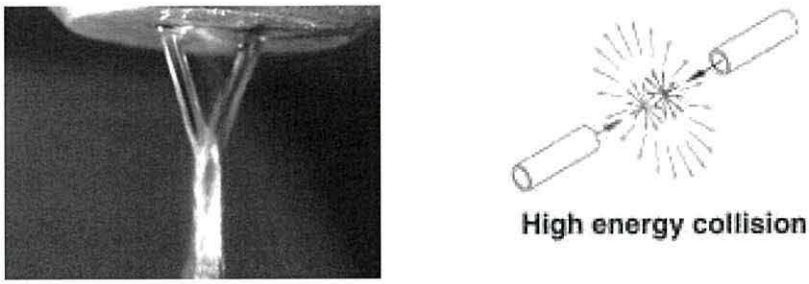

(a) (b)

Figure 5.7 (a) Y-type jet generated by a jet micromixer. (b) High energy collision to induce mixing. Source: Hessel et al (2005).

This concept includes the collision of high velocity jets (Figure 5.7) to provide turbulent mixing, and can be used even at lower velocity, if there is no other micro-mixer alternative.

The extent of mixing is an important topic in the study of drop collisions. If the synthesis of polyurethanes is to take place inside a droplet, mixing is the key to performing the reaction efficiently. If the energy is not enough to induce turbulence, then the mixing will be driven by means of molecular interdiffusion (Graveson et al., 1993). The diffusive flux ϕ of a solute is given by:

$$\phi = D \bullet A \bullet \nabla c \qquad (5.3)$$

where D is the diffusion coefficient, A the interfacial surface area and ∇c the concentration gradient of the species (Hessel et al., 2005). If the diffusion coefficient and species concentration are determined by the chemistry of the polyurethanes, e.g. by the stoichimetry, then this is one way the interfacial surface area can be manipulated in order to maximise the mixing.

5.2 Building a Tailored Ink Jet Printing System

5.2.1 Overview

For this part of the study, a new pumping system with two nozzles was built. The working principle of the nozzles is based on two solenoid valves that open and close in response to an electronic signal thus controlling the ejection of fluid from the nozzles. This system was set up taking into account that it would require the development of several independent parts; the positioning, lighting, pumping, control, pulse generation systems, and the electronic circuits for each nozzle.

The fact that every single component of the system was built to suit the specific applications of the current study helped make the system cost effective. It also enabled accurate monitoring and modification as required. On the other hand, there were limitations such as a reduced robustness and a shorter lifetime (up to 200 million actuations) of the instrument compared to the Microdrop System.

5.2.2 Basis of system design and restrictions

The requirements that were taken into consideration when designing the new IJP system included:

1. Maximum diameter of the nozzle housing to fit in the tubing coming from the different pumping systems.
2. Easy maintenance and cleaning.
3. Sealing and tightness.
4. Appropriate building materials to support high pressure and to be chemically resistant.
5. Tools required for the construction.
6. Possibility of adjusting to different pumping systems (interchangeable parts).
7. Relative low-cost spare parts.
8. Prospect of adding a series of nozzles.
9. Possibility of expanding the design to include external components, such as a computer-control system.
10. Integrated optical system in order to visualise falling droplets.
11. Incorporation of high-voltage parts and connections to earth to avoid risks.

The design of the new system led to the construction of a prototype system which was modified constantly on an on-going basis in order to improve its performance.

5.2.3 Micro dispensing system

The key components employed to build this instrument were two micro-dispense VHS solenoid valves, model M/VJ from The Lee Company Ltd with an internal nozzle diameter of 0.08 mm. The 062 Minstac port in each valve allowed simple leak-proof connections to a 0.031" nominal diameter Teflon tubing and nominal wall thickness 16 (drawings and specifications can be found in the Appendix III). The fittings on each side of the tubing were assembled with aluminium and stainless steel. To prevent any clogging particle from passing through the tubing, a 35 μm in-line filter was incorporated into each streamline. At the end of the Teflon tubing a 062 Bulkhead union was used to connect the liquid reservoir. The latter was built in cylindrical form using stainless steel giving a capacity of 4 ml. The cylinder was built to fit between the Teflon tubing and the entrance of the pumping system, as shown in Figure 5.8.

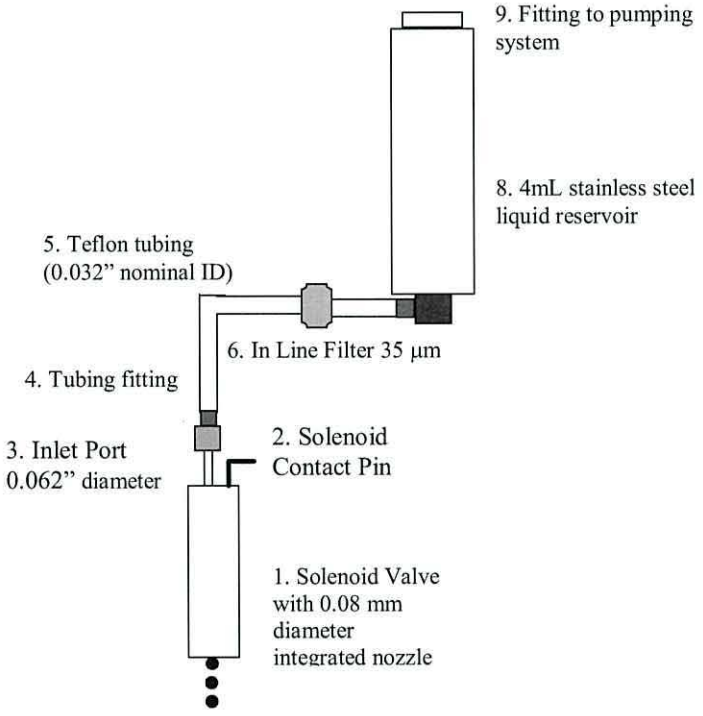

Figure 5.8 Microdispensing system components.

The solenoid valves each required a spike-and-hold driver for proper operation. These were driven by pre-packed circuits from The Lee Company Ltd. The circuit housing was furnished with six terminals to which all the components (e.g. power supplies, pulse generator, valves) were connected as shown in Table 5.2. and Figure 5.9.

Table 5.2 Spike and Hold Driver Terminals

Terminal No.	Description	Equipment Connected	Wire Colour
1	System Ground	Negative (-) lead from power supplies and TTL (pulse generator) firing signals	Black
2	Hold Voltage (5 V)	Positive (+) lead from the Hold Voltage power supply	Purple
3	Control Signal (0 or 5 V)	Positive (+) lead from the TTL control signal (pulse generator)	Yellow
4	Spike Voltage (24 V)	Positive (+) lead from spike voltage power supply	Red
5	Valve connection	Either lead of the solenoid valve (coil not polarised)	Orange
6	Valve connection	Either lead of the solenoid valve (coil not polarised)	Blue

Figure 5.9 Spike-and-Hold Driver Electronics Terminals.

The principle that governs these solenoid valves demands a spike voltage to open them up. This voltage can be applied for a maximum of 0.35 ms, otherwise at this high power level more heat will be generated than the valve can safely dissipate. If a longer on-time is required, the solenoid voltage must be reduced to +5 V (hold voltage) in order to prevent irreversible damage to it. To operate the valves for optimising fluid dispensing and reducing the risk of overheating, a fully assembled spike and hold driver was connected. The driving circuitry was pre-tuned to apply precise power pulses to the

valves and offered the facility to vary the valve actuation time (from 0.35 to 2 ms) as well as the frequency (max. 1000 Hz). In this specific case, the minimum spike voltage was 24 V, the hold voltage was 5 V and a maximum spike time of 0.35 ms at 1000 Hz.

A Thandar TG503 5 MHz pulse/fuction generator was connected to the drive circuit via its TTL output. This function generator output acts as the control (or trigger) voltage. The "on" time, duty cycle and operating frequency of the valves are determined by this input signal. The drive electronics were capable of converting a control signal into a spike and hold voltage. Two separate power supplies were required, one for 24 V and the other for 5 V.

When the control signal is 0 V, the circuit is not energized. When the signal goes high, that is 5 V, the circuit energizes the spike timer and the hold voltages to the valve. After the spike period, the circuit turns off the spike voltage and leaves the hold voltage energized for as long as the control signal remains high. When the control signal goes low, the voltage to the valve is turned off regardless of the spike timer status.

The pulse width and the spike-and-hold voltages, were monitored using a 20 MHz oscilloscope (HAMEG, model HM205). In order to avoid permanent damage to the valves, it was necessary to hook up each of the positive leads from the two channels of the scope using the differential method. It was suggested by the manufacturer that direct connection of the oscilloscope to the valves must be avoided at all times. The complete system was connected as shown in Figure 5.10.

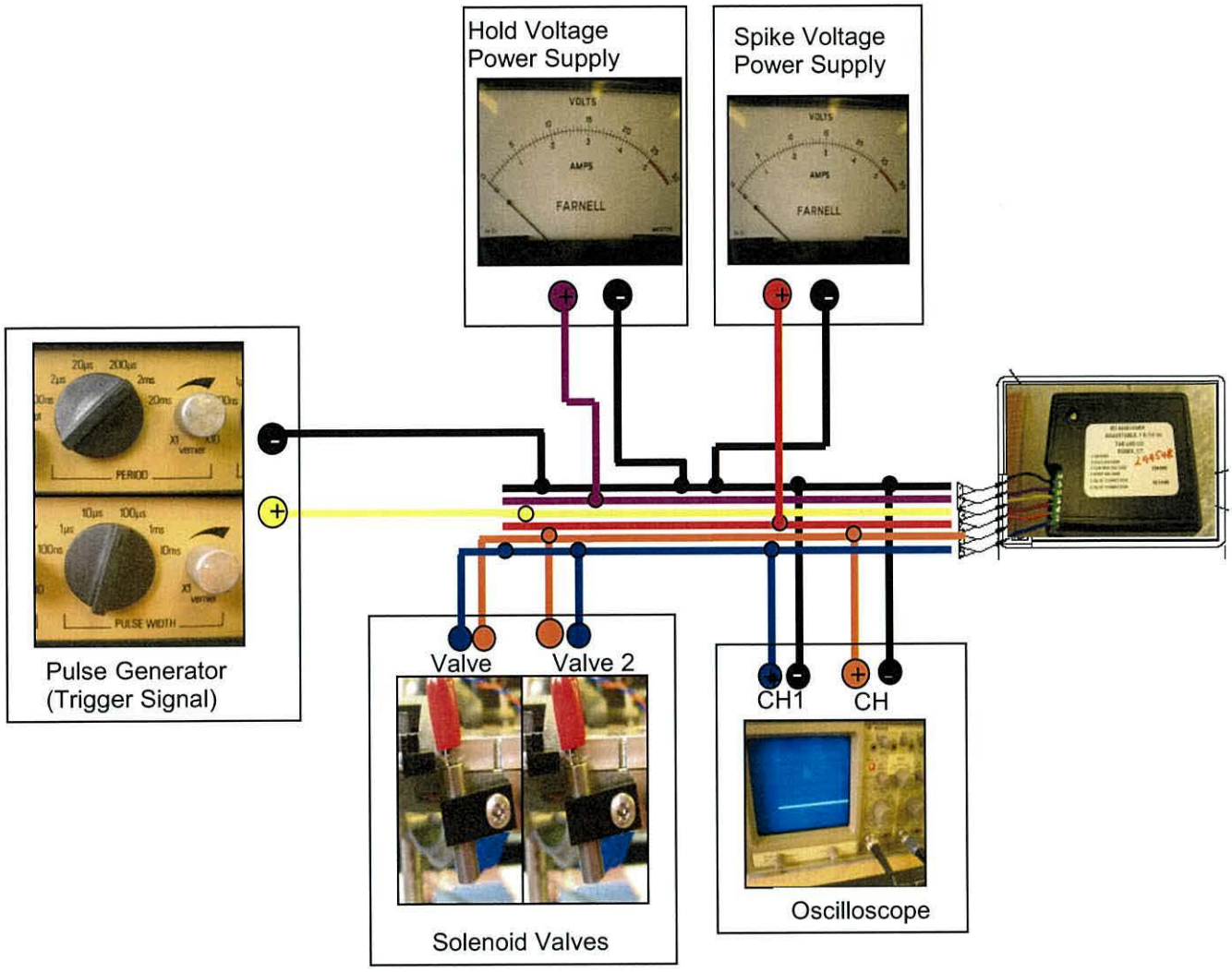

Figure 5.10 Wiring the IJP-Solenoid Valves System.

The coil resistance R of the solenoid valve was 110 Ω nominal at room temperature. The power P dissipated in this resistor is given by

$$P = I^2 \cdot R = \frac{V^2}{R} \tag{5.4}$$

where I is the current flowing through it, and V the voltage across it. Thus at a working voltage of 5 V, the power dissipated is 0.272 W. The maximum power dissipation with convective air-cooling was 0.5 W. To avoid permanent damage to the valves, the timings should always be within the specified safe limits, which are shown in Table 5.3. Also shown are the set values of the various parameters.

Table 5.3 Solenoid valve safe settings and limits.

Variable	Minimum Value	Maximum Value	Set Value
Spike Voltage (V)	24	24	24
Hold Voltage (V)	5	24	5
Spike Time (ms)	0.35	2	0.35
Control (Trigger) Voltage (V)	0	5	5
Frequency (Hz)	1	1000	100
Period (ms)	1	1000	10
Power Disipation (W)		0.5 (@1000 Hz, 24 V and 0.35 ms)	

The actual signal registered by the oscilloscope using the above parameters is shown in Figure 5.11. It was observed that a negative voltage (~-100V) was present after each pulse. This is the back-electromotive-force (BMF) and provides an indication of the proper operation of the valves.

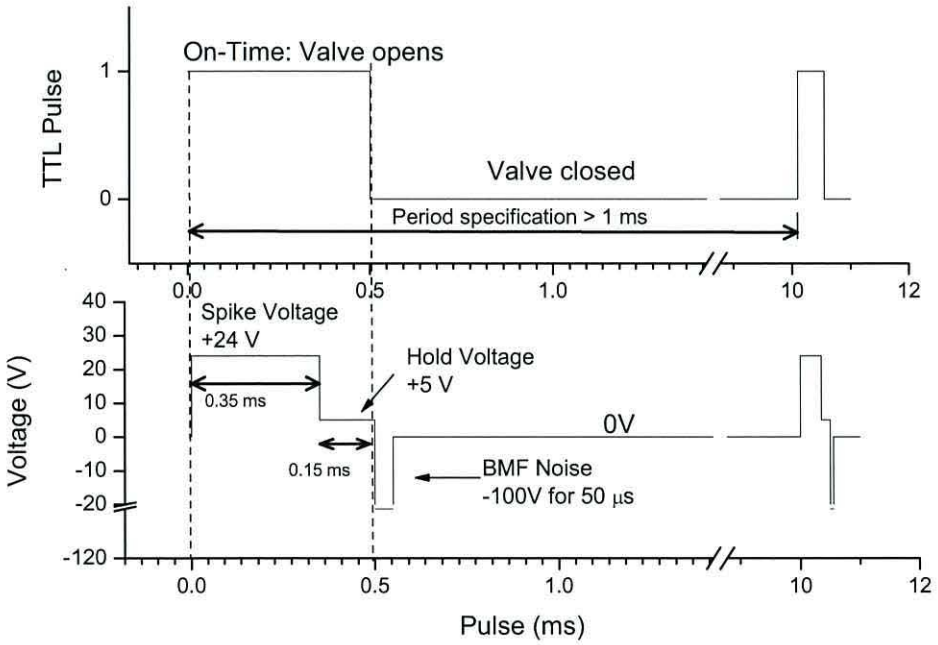

Figure 5.11. Pulse generation and valve response as seen on the oscilloscope. The upper plot shows the signal out by the pulse generator while the lower plot shows the spike-and-hold voltage signal that is sent to the solenoid valves. (BMF noise pulse confirms proper operation of the valve).

5.2.4 Pressure System

There was a variety of options of pumping systems available, which included the adaptation of syringe pumps, pumps used in chromatography and a compressed nitrogen cylinder. For simplicity, it was decided to use the nitrogen gas, but the system allows interchanging of the pumping system if required.

Nitrogen gas compressed at 230 bar (oxygen free) was employed to push the liquid towards the solenoid valves. A two-stage regulator from Freshford Ltd was used to control the pressure of the outgoing gas in the range 0 to 690 kPa . The outlet connection of the regulator was a 5/8" BSP female right-hand cone to which 6 mm tubing was fitted. At the other end of the tubing, a G 1/8 pneumatic miniature regulator and a 40 mm diameter pressure gauge were incorporated. The working pressure for the gauge ranged from 0 to 248 kPa. The pressure applied to the micro dispensing system was limited by the specifications of the Teflon tubing and solenoid valves, which could not exceed 830 kPa. Figure 5.12 shows the configuration of the pressure system.

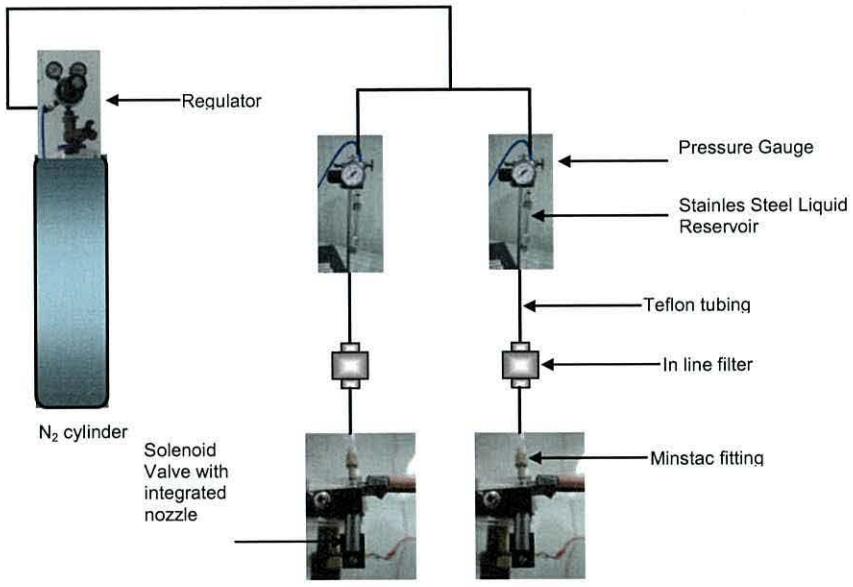

Figure 5.12 Diagram showing the pressure system connected to the dispensing system.

5.2.5 Electrostatic System

The IJP system was equipped with a high-voltage setup in order to charge the droplets coming out from the nozzle and attracting them to the substrate.

In order to provide a conducting ground "plane", the outer body of the nozzle was coated in a gold film, deposited using the Edwards Auto 306 evaporator. Before placing the solenoid valve inside the chamber, the nozzle orifice was protected with kapton tape to avoid any blockage. The solenoid valve was placed on the substrate using a probe and tape to create an angle of 70 degrees between the valve and the substrate holder. The valve was orientated so that the nozzle pointed towards the outside of the chamber. The area surrounding the nozzle was coated in that position once, and then a second evaporation took place by changing the position of the valve. The second time, the orifice pointed to the centre of the chamber in order to ensure that all the inside part of the solenoid valve was covered with gold without blocking the nozzle.

Subsequently, the valve was connected to earth (0 V). A 5 cm metal disc, which was connected to a high-voltage power supply, was placed 1.6 cm under the solenoid valve. The voltage supply used was a Brandenburg Alpha Series II model 2707. The potential between the two metal surfaces, was set within the range 0 to 15 kV, in order to establish a high-field at the nozzle.

Working with a high-voltage system requires important safety measures. The potential hazard is not the high-voltage itself, but the current derived from it, which should be < 50 μA. Hence, a chain of 3 x 5 MΩ resistors was placed between the high-voltage power supply and the metal disc as shown in Figure 5.13, which limited the maximum current to 33 μA at 5kV.

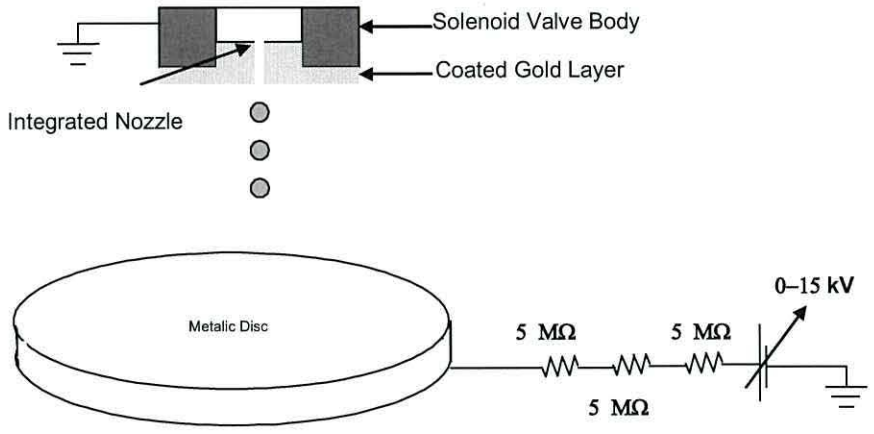

Figure 5.13 The high-voltage system comprising a gold coated solenoid valve and a metal disc with three 5 MΩ resistors incorporated to limit the current to 30 μA.

The resistors were placed in an acrylic tube to avoid contact with other parts of the system. All the metallic components of the IJP system were connected to earth and an earth wand was added to the housing structure (which is described in section 5.2.7), to make sure that after the experimental work was done, all parts were free of electrostatic charge.

5.2.6 Optical System

Observing the ejected droplets was an important task that the new IJP system should be capable of a high-speed video camera system was available to use for short period of time, (EPSRC loan pool). As this sophisticated equipment was not always available, an optical system was also built.

5.2.6.1 Stroboscopic System

In order to obtain images of the droplets ejected from the nozzles of the solenoid valves, it was necessary to integrate a webcam mechanism to a microscope objective and build a stroboscopic light arrangement. This system (similar to that described in section 5.5.1), gave the effect of freezing the motion of the droplet and the possibility of taking photographs and even calculating the falling velocities. The light source used was a 3 mm, 10 mA ultra-bright red Light Emitting Diode (LED) and the driving circuit was built based on the following components:

i. Trigger Circuit: to trigger the LED using a signal synchronised with the pulse that controls the solenoid valves. Its function is to produce the trigger signal for the Delay and Pulse LED circuits connected in series (See Figure 5.14).
ii. Delay Circuit: works as a timer that establishes the time delay after which the LED will turn on and can be varied from 90 μs to 1.2 ms.
iii. Pulse LED Circuit: sets the flash duration i.e. the time for which the LED is on. This can be varied from 90 μs to 1.2 ms.

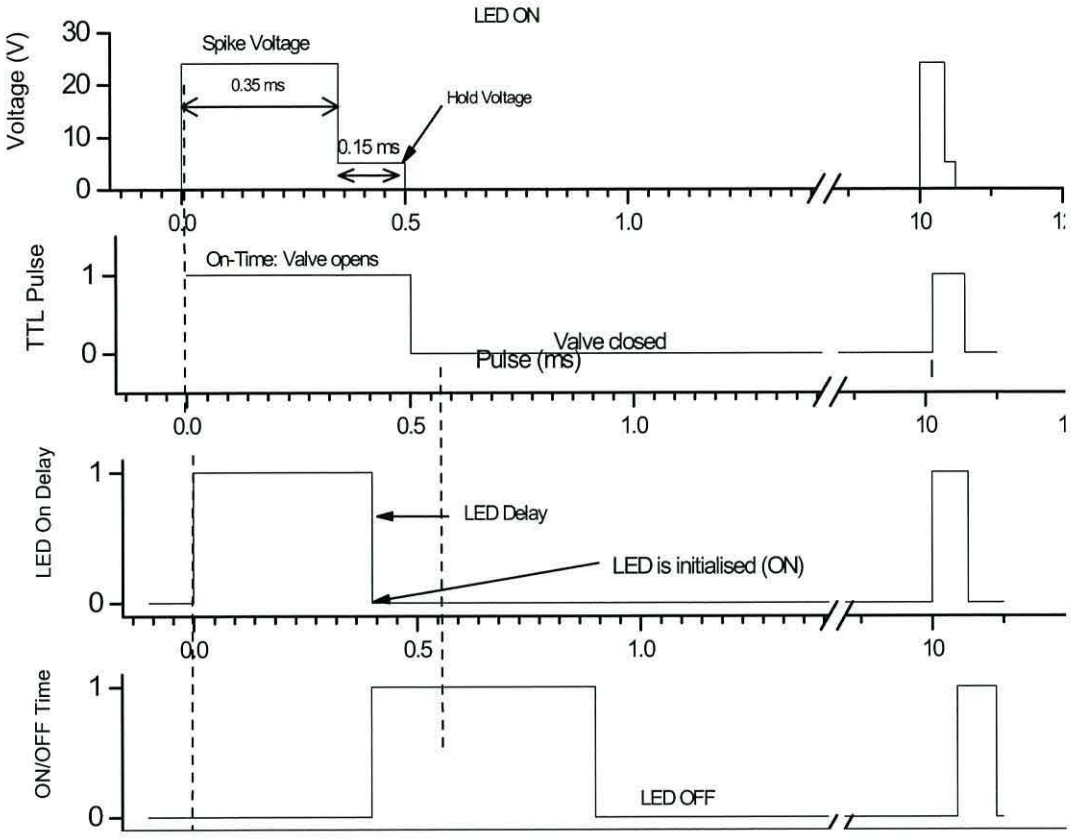

Figure 5.14 Synchronisation of the valve open pulse and the LED initialisation pulse and ON-time pulse. Once the pulse from TTL rises from 0 to 1 the valve opens, at the same time the LED is triggered and after a set time delay, it turns on for a period of time.

Figure 5.15 shows the circuit arrangement. The full circuit diagram can be found in Appendix III.

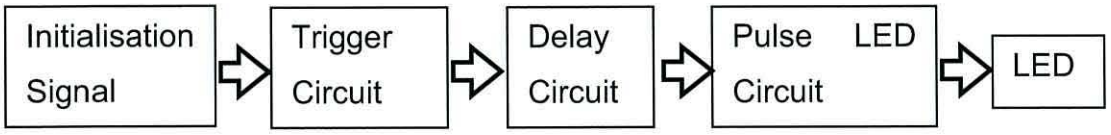

Figure 5.15 Stroboscopic System Design.

5.2.6.2 High Speed Camera System

The Photo-Sonics Phantom V7 monochrome high-speed camera has a maximum resolution of 800 x 600 pixels at a speed of 4800 frames per second giving 1.2 seconds of recording time. The images were analysed using Vision Research Inc. software version 1992-2005. The system included an Everest VIT ELSV-60 light

source from Solarc and a 1x lens model 312977 from Leica to observe the microdroplets. Also, tripods, triggering switch and PC processor were included for the installation of the high-speed camera system. In order to observe the falling droplets different variables, such as sample rate, exposure time, resolution, post-trigger value had to be set to relevant values. For instance, if the droplet velocity is high, a high frame rate and short exposure should be chosen but this compromises the resolution and brightness of the image. If the image observed is blurred, a shorter exposure time and brighter lighting was needed to improve the image. The parameters were adjusted depending on the lighting available, and the speed of the observed phenomena. The maximum sample rate e.g. frames per second that was possible to obtain depended on the resolution of the image, and is presented in Table 5.4.

Table 5.4 High-speed camera parameters: value ranges depend on resolution

Resolution	Maximum Sample Rate (fps)	Video Duration (secs)	Images Captured
800 x 600	4,700	0.6	2,938
640 x 480	7,207	0.6	4,622
512 x 512	8,213	0.7	5,749
512 x 384	10,000	0.7	7,223
512 x 256	15,037	0.7	10,834
512 x 128	29,197	0.7	21,669
512 x 64	51,282	0.8	43,339
384 x 512	10,000	0.7	7,223
320 x 240	2,4096	0.8	18,248
256 x 512	14,035	0.8	10,834
256 x 256	26,143	0.8	21,669
256 x 128	47,058	0.9	4,339
256 x 64	75,471	1.1	86,678
160 x 120	63,492	1.1	69,342
128 x 512	22,099	1	21,669
128 x 256	40,000	1.1	43,339
128 x 128	67,796	1.3	86,678
128 x 64	100,000	1.7	173,356
64 x 64	121,212	2.9	346,712
32 x 32	160,000	2.2	346,712

5.2.7 Complete IJP System Description

As detailed in previous sections, the complete IJP comprised, of i) microdispensing system, ii) pressure system, iii) electrostatic system and iv) optical system. The IJP layout is shown in Figure 5.16 and Figure 5.17. A stainless steel housing structure was built, which had a mobile rail onto which the microscope objective and webcam tube were clamped, and an adjustable z-stage holding a plate to which the solenoid valves were fixed. The ultra bright LEDs were fasten to the solenoid valves body just below the nozzle exit. The bodies of the solenoid valves were fixed on the plate but their angular and horizontal position were manually adjusted. The metal disc providing the high-voltage was placed on top of a manual x-y stage just below the nozzles (Figure 5.16). All parts mentioned above were connected to earth, except the high-voltage disc. The IJP system was placed inside a fume cupboard to extract all vapours generated by the chemicals used in experiments. The drive electronics of the dispensing system, the pressure system and high-voltage power supply were connected and placed just outside the cabinet so that any manual modification could be carried out from the exterior. This prevented the user from coming into direct contact with the chemicals and high field.

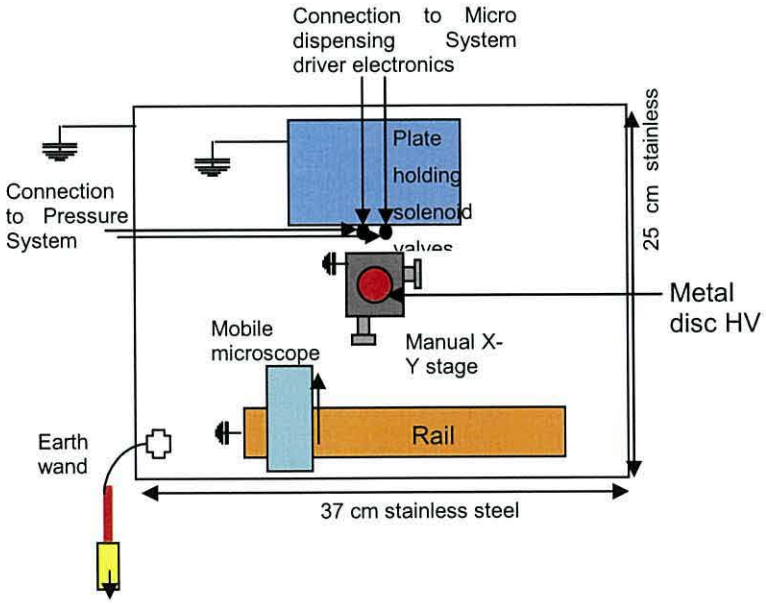

Figure 5.16 IJP System top sight, showing the component layout.

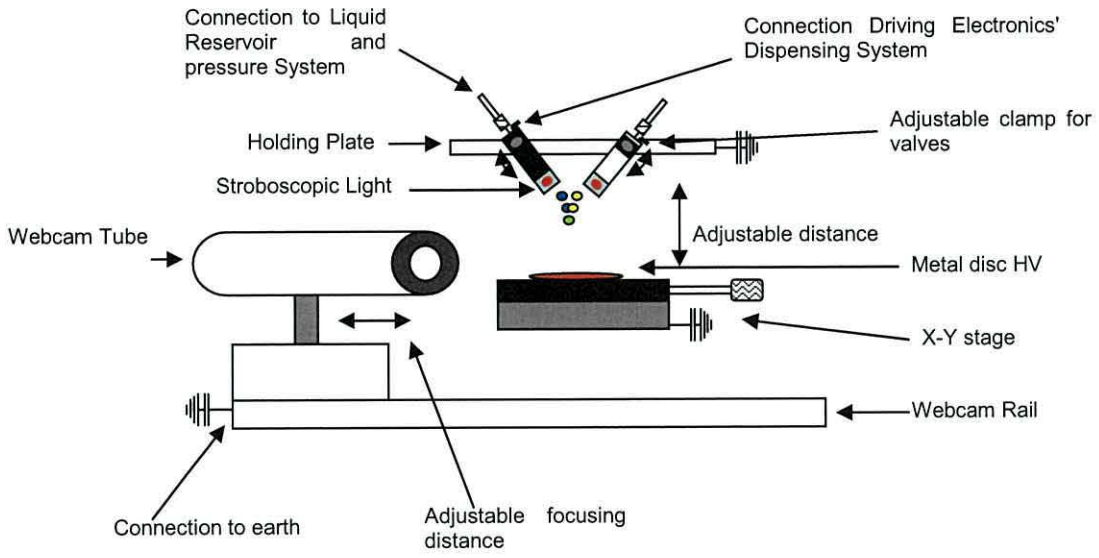

Figure 5.17 IJP System side view, showing the component layout.

5.3 Experimental procedure

5.3.1 Exploratory Experiments

The first set of experiments conducted with the new IJP pumping system did not include the use high-voltage to enhance droplet formation. The value of these initial experiments was that they led to the identification of the variables which needed to be controlled for droplet formation. Also, the limitations in the equipment design were addressed. In these preliminary studies, a series of experiments which employed a high purity grade of water normally used for liquid chromatography (HPLC) was carried out using the optical systems together with stroboscopic lighting and a high-speed camera for observing droplet formation.

5.3.1.1 System set up and samples preparation

HPLC grade water was filtered using a syringe filter fitted with PTFE filters (0.2 μm). Before introducing the water into the reservoirs of the IJP system, these were carefully cleaned following the process described elsewhere (Sayers, 2006). The reservoirs were positioned above the nozzles and connected by Teflon tubing to disposable 5 ml syringes. A pressure gauge was connected to the filled liquid reservoir. Each reservoir was pressurised from a nitrogen gas cylinder fitted with a pressure regulator. The regulator was initially set to 69 kPa and kept constant until further

evidence suggested that this variable needed to be changed. The pressure set in the second regulator, i.e. the pressure that controlled the flow of liquid into the solenoid valves, and could be varied from 0 – 241 kPa.

The micro dispensing system was activated by a pulse generator and this had two independent variables, one the so-called master pulse width (MP), set from the TTL output from the pulse generator. The master pulse generator could control the number of droplets per second and was capable of providing maximum pulse width of 0.35 ms at 1000 Hz beyond which the solenoid valve might sustain damage. Since the aim of the experiment was to study the quality of the droplets rather than the speed at which they were dispensed, the master pulse was initially set to a value of 0.5 ms at a frequency of 100 Hz. The spike voltage time (SVT), that is the time during which a voltage was applied to initiate the valve opening, could also be varied from a minimum of 0.35 ms up to 0.5 ms at a frequency of 100 Hz. This value sets the hold voltage time (HVT) to 0.15 ms, which is the time during which a lower voltage is applied just to keep open the valve. The initial identification experiments were designed to establish the values of the master pulse and spike times which would be suitable for dispensing the test fluid (water).

The stroboscopic optical system had four variables which required adjustment for the system to be effective. The first was the sample rate at which the image sensor (from the webcam) captured the images. Two levels were available, 15 and 30 frames per second (fpm). The preset value chosen was 30 fpm and was kept constant because this allowed the acquisition of more information about the droplet formation mechanism. A second variable was the shutter speed i.e the time during which the shutter was held open during the taking of a photograph. This could be controlled in the range of 1/10000 s to 1/15 s. At the higher shutter speeds, the shutter is held open for shorter time and the frequency at which the images are captured is higher, so the light reaching the image sensor is small. The other two adjustable variables were the delay pulse and the ON/OFF time, each being in the range from 90 μs to 1.2 ms. Both of these variables were initially set at the minimum value of 90 μs.

In order to find the optimal values of the nine variables, three were initially held constant i.e. the pressure in the first controller (69 kPa), the sample rate of the image

sensor (30 fps) and the master pulse period (10 ms for a constant frequency of 100Hz). The other six variables were initially set at the values shown in Table 5.5.

Table 5.5 New IJP system adjustable variables: range and preset values using the stroboscopic optical system.

Variable	Range	Preset Value
Gauge pressure	0 – 241 kPa	69 kPa
Master Pulse width (TTL)	MP ≥ 0.5 ms	0.5 ms
Spike voltage time	0.35 ms ≥SVT ≤ MP	0.35 ms
Shutter Speed	1/10000 - 1/15 sec.	1/100 sec
LED delay	96 μs – 1.2 ms	96 μs.
LED on/off time	96 μs – 1.2 ms	96 μs.

The use of the high-speed video camera required four parameters to be adjusted, namely: sample rate, exposure time, resolution, and post trigger values. The resolution was set to a value of 336 x 600 pixels because at that setting the image size was sufficiently large to observe the droplets emerging from the nozzle. The dynamics of droplet formation determines the value of the sampling rate. The rate of droplet formation depends on the nature of the fluid, so the sampling rate is specific for any given liquid and temperature. In the exploratory experiments with water, the sampling rate was set at 10,000 frames per second. The exposure time could be set in 1 μs increments from a minimum value of 2 μs. This variable depended on the lighting system employed (because it works similarly to the shutter speed time described above) and the optimal setting was experimentally determined to be 17 μs. Once the quality of the image was satisfactory, the setting was kept constant. Finally, as the post trigger value is dependent on the number of images recorded and therefore the sampling rate, it was decided to keep this value constant at the maximum value, which is equal to the number of frames captured by the high-speed camera. For instance, at a sampling rate of 10,000 the post trigger value is 13,929. This means that all the pictures taken after triggering the camera could be recorded in the camera's internal memory.

5.3.1.2 Parameter setup

An initial test of the new IJP pumping system was conducted using HPLC-grade water and the preset values of the variables described in the previous section. The stroboscopic optical system and high-speed video camera were tested separately. First

the stroboscopic system was used to observe the liquid coming from the nozzle and this experiment showed that the values of the parameters set (see Table 6.1) for the master pulse width, spike voltage time and gauge pressure were appropriate. However, the images recorded from the stroboscopic system were not clear, and the shutter speed had to be changed to 1/50 s. The setup of the stroboscopic light was not effective so the parameters of the LED delay and LED on/off time had to be adjusted. Using a Taguchi experimental design as detailed in section 5.5.2 these two parameters (F=2) were tested at five levels (L= 5). These experiments showed that the best value of the LED delay time was 400 μs with an ON time of 500 μs. The exploratory experiments using the stroboscopic optical system showed that the best settings of the adjustable parameter are those shown in Table 5.6.

Table 5.6 New IJP system variables for water dispensing.

	Variable	Value
	Gauge pressure	69 kPa
	Master Pulse width (TTL)	0.5 ms
	Spike voltage time	0.35 ms
Stroboscopic System	Shutter Speed	1/50 sec
	LED delay	400 μs.
	LED on/off time	500 μs.
High-speed video camera	Resolution	336 x 600
	Sample rate	1000 fps
	Exposure time	17 μs

The IJP pumping system was tested using the high-speed video camera. The parameters of the camera were initially set at the values described in section 5.3.1.1. It was confirmed that the dispensing and pressure setup found for water using the stroboscope were correct.

5.3.2 Polyurethane Synthesis

The feasibility of down-scaling the synthesis of polyurethanes using the IJP pumps has been explored. The experimental procedure followed is described in the following sections.

5.3.2.1 Calibration

The performance of the IJP pumps was assessed over as wide a range of input conditions as possible. The two fluids used in the initial experiments were water and isopropanol. The sample preparation procedure carried out for both liquids also followed the procedures presented in section 5.3.1.1. The properties of water and isopropanol are shown in Table 5.7.

Table 5.7 Properties of fluids employed for the IJP System Calibration.

Properties	HPLC-grade water	Isopropanol
Viscosity @ 20°C (mPa s)	1	2.4
Surface Tension (mN/m)	73.9	23
Density @ 20°C (g/ml)	1	0.786
Electrical Conductivity @ 25°C (μS/m)	5.5	6

The experiments for studying the impact on pressure, master pulse, and frequency on the dispensing of isopronanol were designed using a Taguchi orthogonal array, comprised of three parameters (F=3) and five levels each (L=5). The experimental conditions were obtained using SPSS software and are shown in Table 5.8.

The variables measured for water and isopropanol were drop diameter, drop velocity, and drop quality (using the scale defined in section 5.6.1.). The first two variables were obtained from image analysis, using the software included in the high-speed video camera system (Vision Research Inc. software version 1992-2005).

From the calibration results, it was possible to determine the parameter sensitivity for drop quality which made it possible to estimate the conditions which might be required when using the reactive liquids (prepolymer and the polyol) for polyurethane synthesis.

Table 5.8 Experimental conditions for the calibration of the IJP System, using Taguchi orthogonal array with three parameters (F=3) and five levels (L=5).

Experiment	Pressure (kPa)	Pulse Width (ms)	Pulse Frequency (Hz)
1	14	0.35	500
2	14	0.4	400
3	14	0.5	300
4	14	0.6	200
5	14	0.7	100
6	28	0.35	300
7	28	0.4	200
8	28	0.5	100
9	28	0.6	500
10	28	0.7	400
11	41	0.35	100
12	41	0.4	500
13	41	0.5	400
14	41	0.6	300
15	41	0.7	200
16	55	0.35	400
17	55	0.4	300
18	55	0.5	200
19	55	0.6	100
20	55	0.7	500
21	55	0.35	200
22	55	0.4	100
23	55	0.5	500
24	55	0.6	400
25	55	0.7	300

5.3.2.2 Formulations of reactants

Polyurethanes are formed from the reaction between diisocyanates and polyols, as described in Chapter 2. For the synthesis of polyurethanes using the IJP micro dispensing system, a typical two-stream urethane formulation was prepared one being the prepolymer stream and the second a polyol stream.

The prepolymer was designed to be isocyanate end-terminated (20.5 % excess of NCO used in its synthesis). The viscosity of the prepolymer was determined using the same method described in section 4.5.1.3. It was predicted from the results (shown in section 5.4.2.1), that the viscous reactant could not be dispensed unless diluted. A series of prepolymer solutions in tetrahydrofurane (THF) were prepared, named with

the prefix P, and their ease of dispensing checked. The THF (Fischer Scientific, density = 0.888 g/ml) was dried using a molecular sieve. The prepolymer was weighed into a 5 ml volumetric flask, and the THF added to the graduation mark. After the solutions were prepared, a micro magnetic stirrer was used to agitate the mixture for 24 hours. The different solutions prepared are shown in Table 5.9.

Table 5.9 Solutions of different concentrations prepared of prepolymer in THF.

Sample	Prepolymer content (g)	% w/w
P1	0.5945	13.39
P2	0.7887	17.76
P3	0.9838	22.16
P4	1.1897	26.80
P5	1.2838	28.92
P6	1.5519	34.95
P7	1.9147	43.12
P8	1.9907	44.84
P9	2.2343	50.32
P10	2.6645	60.01
P11	3.1110	70.07
P12	3.5630	80.25
P13	4.0038	90.18

After 24 hours of mixing, the solutions were filtered and prepared as described in section 5.3.1.1.

Similarly, the second reactive liquid prepared, was a polyol mixture that contained 78.91 % w/w of PPG with a molecular weight 1000 g/mol, 21.09 % w/w of 1,4 butanediol as a chain extender and 0.03% w/polyol w of a Ti-based catalyst. The viscosity of the mixture components were those determined before (as previously discussed in Chapter 3). A series of polyol mixture solutions in isopropanol, named with the prefix MIX-, was prepared and experiments undertaken to determine if they were capable of being dispensed by the new IJP system. The solutions were prepared using isopropanol (density = 0.786 g/ml) because of the possible solvents available, this had the relatively highest electrical conductivity coefficient (6 μS/m at 20°C) which was expected to benefit the performance of the high-field system of the IJP apparatus. The solvent was obtained from Sigma Aldrich and was used as received. The

corresponding amount of polyol mixture was weighed in 5 ml volumetric flask, and the isopropanol was added until the meniscus reached the level of the ring graduation mark. The stopper was placed into the top of the flask and the solution swirled gently for 24 hours using a micro magnetic stirrer. The different solutions prepared are shown in Table 5.10.

Table 5.10 Solutions of polyol of different concentrations prepared in Isopropanol.

Sample	Polyol mixture content (g)	% w/w
MIX1	0.3966	10.09
MIX2	0.5875	14.95
MIX3	0.7890	20.08
MIX4	0.9860	25.09
MIX5	1.1826	30.09
MIX6	1.3755	35.00
MIX7	1.5740	40.05
MIX8	1.6991	43.23
MIX9	1.7711	45.07
MIX10	1.9667	50.04
MIX11	2.3545	59.91
MIX12	2.7670	70.41
MIX13	3.1390	79.87
MIX14	3.5334	89.90

After 24 hours of mixing, the solutions were filtered and prepared as described in section 5.3.1.1.

5.3.2.3 Dispensing of reactants for polyurethane synthesis

The high voltage supplied by the Brandenburg instrument was implemented and verified using a Field Mill (prototype field mill voltmeter produced in-house by IDB at the School of Electronic Engineering, Bangor University). The actual maximum values of the positive and negative voltages applied were +9.8 kV and -9.2 kV, respectively. Preliminary experiments suggested that a negative polarity improved droplet formation.

A series of reactive liquid solutions (P1 to P13 and MIX1 to MIX14 were prepared and each of the P series reacted in turn with each of the M series paying

particular attention to the reproducibility of the droplets formed for each stream. The dispensing was aided by the application of high voltage only when this seemed appropriate. For more dilute solutions, the fluids dispensed unaided, i.e. without the high voltage. In the case where no proper droplets were formed, the variables pressure, master pulse width and voltage were also changed from those shown in Table 5.2 to those shown to be more pertinent from the calibration studies. After each experiment, the liquid reservoirs, Teflon tubing and solenoid valves were flushed with solvent: THF for the solenoid valve printing prepolymer solutions and isopropanol for the valve handling polyol mixture solutions.

Clogging of the nozzles occurred in the case of the more concentrated solutions tested, especially the prepolymer solutions. The solenoid valves and tubing were cleaned in an ultrasound bath containing water at 40°C for 15 minutes. After reassembly, dry nitrogen gas was flushed through the system followed by flushing with the appropriate solvent. The solenoid valves were again connected and initiated. Once the valves were working, they were immersed in an ultrasound bath for a second time, but on this occasion only for two minutes. To check that the valves were not damaged by this cleaning process, the valves' coil was measured with a multimeter. If the resistance value of the coil remained 110 Ω, the solenoid mechanism was not damaged.

The most readily pumped of the P and M series reactants were used in an attempt to synthesise polyurethanes on a substrate by impingement mixing of two droplets. The alignment of the nozzles in order to make the two droplets collide in mid air was done manually with the aid of the mechanical positioning device which embodied a screw adjustment that allowed the angular movement of the nozzles relative to each other. Once the position of the nozzles was established, the IJP pumps were initiated simultaneously, and the flight of the droplets observed using the high-speed video camera. A stainless steel plate fabricated with six semi-spherical holes with a capacity of 17 μl was used as the substrate to collect the falling reactive droplets.

5.3.2.4 Effect of Isopropanol on Polyurethane chemistry

The polyurethane reaction between two reacting droplets was studied and reported in Chapter 2. In the study, one droplet of polyol mixture and one droplet of prepolymer were added together simulating the phenomena that could occur on the

smaller scale using the IJP system. In that study, bulk polymerisation took place and no solvents were present. In the IJP system experiments, the addition of isopropanol was needed for two reasons: firstly to dilute the polyol mixture, assuming that it will behave as a solvent and hence be non-reactive. Secondly, to increase the conductivity of the reactive liquid.

In order to asses the impact of the isopropanol on the reaction and obtain evidence to support the hypothesis that the isopropanol was acting merely as a solvent, a series of FTIR spectroscopy and GPC experiments were conducted. A stoichiometric formulation was employed in order to assess the reaction rate and compare it with that corresponding to a reaction between a primary alcohol and the NCO. The stoichiometry ratio was then 1 mol of prepolymer and 2 moles of isopropanol. On the one hand, the reaction was followed by FTIR during the first 3 hours. On the other hand, a series of castings were prepared using the different polyol solutions in methanol, as shown in Table 5.11.

Table 5.11 Effect of isopropanol in polyurethane synthesis: sample composition.

Sample Name	**Concentration (% w polyol mixture / Isopropanol w)**
PUI-1	40
PUI-2	60
PUI-3	80
PUI-4	100
PUI-5	0 (stoichiometric quantities of prepolymer and pure isopropanol)

5.4 Results and Discussion

5.4.1 IJP Characterisation: calibration of the system

The performance of the new IJP system was examined in some detail. The impact of key variables such as pressure applied to pump the fluid (from hereon referred to simply as pressure), master pulse width, and frequency on the quality of droplets formed was studied. Two known liquids (water and isopropanol) were used for this purpose. The variables measured were drop diameter, drop velocity, and drop quality. The reason for calibrating the IJP system with water was to study the impact of its large surface tension on the drop formation mechanism and compare it with a lower surface tension liquid, such as isopropanol. A Taguchi experimental design was developed and the effect of the pressure on droplet size, velocity and quality is shown in Table 5.12.

Table 5.12 Calibration data for water: Output variables as a function of pressure.

Pressure (kPa)		Drop Diameter (microns)	Drop Velocity (m/s)	Drops Quality	Jet Length (mm)
14	Mean	253	2.93	3	.342
	Std. Deviation	35	.31	.00	.765
28	Mean	169	4.60	2	1.55
	Std. Deviation	67	.19	.00	.204
61	Mean	161	5.67	2	1.78
	Std. Deviation	35	.79	.00	.336
55	Mean	147	7.19	2	3.43
	Std. Deviation	20	.30	.00	.80
69	Mean	158	7.42	2	3.70
	Std. Deviation	23	.66	.0	1.24

The jet length recorded in the table is the distance measured from the solenoid external edge to the point where the liquid jet was observed to break into droplets. From Table 5.12, it is seen that the jet length increases with increased pressure. At the highest pressures (i.e. 55 and 69 kPa), the jet breakup occurred below the field-of-view of the camera and so could not be measured. The five measurements conducted for each pressure were made under the conditions presented in Table 5.8. In every set of

experiments the master pulse width and frequency were varied in order to identify which variables were dominant in the drop formation process. The results for the experiments conducted as a function of master pulse width and frequency are illustrated Figure 5.18.

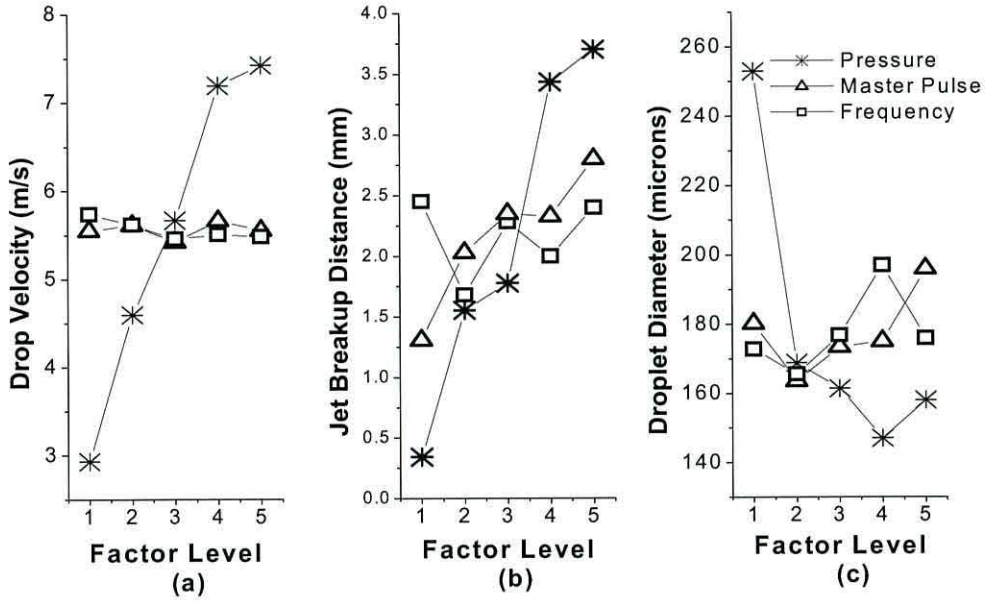

Figure 5.18 Effect of pressure, master pulse width, and frequency on (a) drop velocity; (b) jet break up distance and (c) drop diameter using water as the calibration fluid.

Figure 5.18 shows that the effect of the master pulse width and frequency are not significant over the range explored; it can be considered that the drop velocity does not change as the level of these two variables changes. Also the impact of changes in these two variables on the jet break up distance and drop diameter is not strong. In contrast, the change in pressure affects considerably the velocity, jet breakup distance and diameter of the falling droplets i.e., the slopes of the plots shown in Figure 6.19 are sharp. In the case of water, the velocity of the dispensed droplet ranged from 2.9 m/s up to 7.42 m/s depending on pressure. The recorded dimensions of the water droplets varied from 147 μm to 253 μm. Figure 5.19 shows the change in (a) drop velocity and (b) drop diameter plotted as a function of the actual pressure employed.

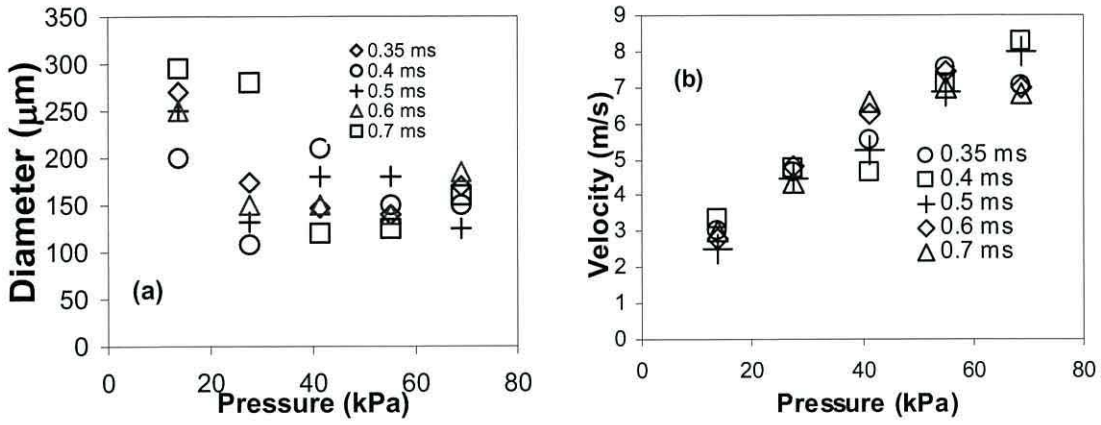

Figure 5.19 (a) Water-droplet velocity and (b) water-droplet diameter as a function of pressure for different master pulse widths.

One of the most important parameters to be considered is droplet diameter, because it defines the volume of liquid that will be dispensed. For a reactive process such as the formation of polyurethanes, the volume of the dispensed droplet will determine the amount of functionalised matter and hence the stoichiometry of the reaction. The results show that as the pressure increases a gradual reduction of the drop diameter is observed. This behaviour is an interesting finding because this pattern differs from the findings published by (Blazdell and Evans, 2000) where the average drop diameter increased with reservoir pressure. This difference in trend can be explained by considering the range of the applied pressure. It can be seen from Figure 5.19(a) that a decreasing trend in droplet size is observed in the range from 10 to 80 kPa, whereas the results reported by Blazdell and Evans (2000) were at higher pressures (200 – 500 kPa).

It is possible that, as shown in Figure 5.19(a), above a pressure of 60 kPa the drop diameter could start to increase. The device employed for the production of the droplets in the Blazdell and Evans work was also significantly different to that developed here. They employed a continuous electrostatic printer. This kind of IJP generates individual droplets by inducing a break-up of the continuous liquid stream using a piezoelectric drive rod. Hence, it is possible that the assumption that all the liquid dispensed formed droplets was applicable.

In the IJP system reported in this thesis, the solenoid valves dispensed the fluid in a discontinuous manner. The fixed amount of liquid ejected is a function of the time

for which the solenoid valve was open (determined by the master pulse width) and the pressure applied. It was experimentally observed that level-3-quality droplets were not formed in all situations. For many sets of conditions, a portion of liquid did not form drops but remained as a jet. It is likely then that the observed change in droplet diameter with pressure is due to an inherent limitation of this type of microdispensing technology.

From Figure 5.20 it can be inferred that droplet diameters decreased as the concomitant exit velocity increased. These results agree with those reported by Wong et al (2004) in which it was observed that as the velocity increases, the inertial forces become more important and enhance the growth rate of jet disturbance. Therefore, at higher jet velocities a more rapid convection of the disturbance takes place via the flow, fast enough to sweep them away by breaking the jet and therefore producing smaller droplets.

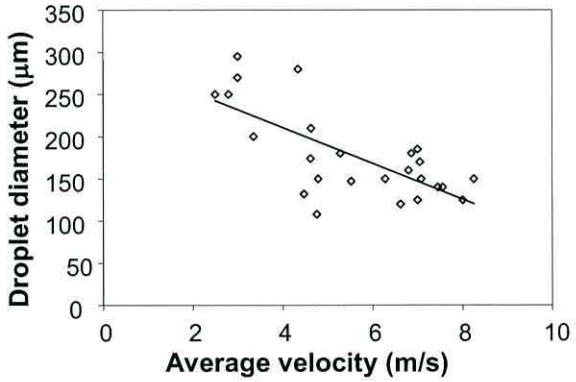

Figure 5.20 Relation between droplet diameter and jet velocity as the fluid pressure increases. Trend line drawn has a crrelation coefficient of 0.50.

In the current study the most important factor is the quality of the droplet. This was evaluated following the same scale as reported in Chapter 4. Level 3 corresponded to the best quality droplets which are not accompanied by satellite droplets, where the shape of the droplets was spherical, and where the size of the dispensed droplets was uniform. For calibrations conducted with water, only the drops injected at a pressure of 14 kPa yielded level 3 quality droplets. In the 3D plot depicted in Figure 5.21 the higher region of the surface represents the experimental conditions of pressure and pulse width needed to achieve a good quality (level 3) water drop. As the change in frequency did not significantly influence droplet quality, and since the dispensing rate was not

relevant to the study, the frequency was kept constant at 100 Hz to ease the process of image capture.

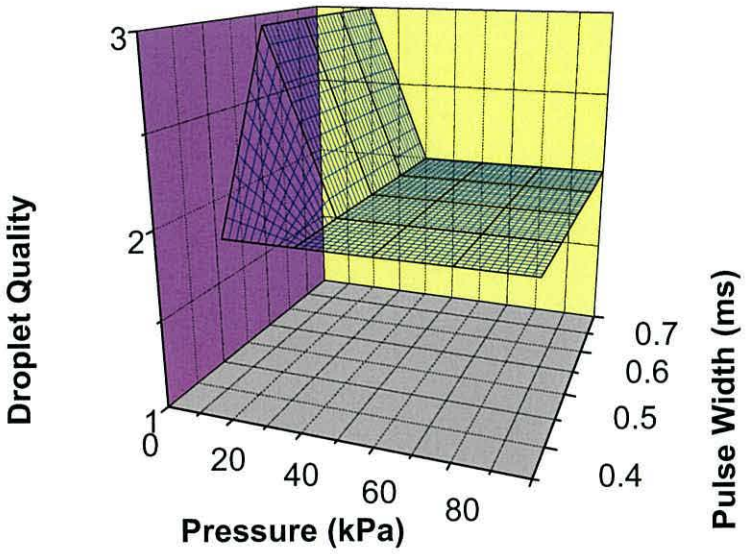

Figure 5.21 Set of experimental conditions for the calibration of the IJP using water,and the quality of the droplets produced.

The results obtained when calibration was carried out using isopropanol were similar to those reported for water above i.e. the trends seen when changing the main variables were similar. The effect of the frequency and the master pulse width changes on the droplet formation were minimal. However from Table 5.13, it is seen that the pressure at which the isopropanol was injected had a marked influence on the droplet diameter, velocity and quality.

The quality of the isopropanol droplets ejected did not reach level 3 under any conditions employed, presumably due to the different intrinsic properties of this fluid. The surface tension of isopropanol is 23 mN/m, approximately three times smaller than that for water. Furthermore, this value lies at the lowest limit of the surface tension range known to be needed for printable fluids (Mittal, 1987; Guo et al., 2003; Shimoda, 2003).

Table 5.13. Calibration data for Isopropanol: Output Variables as a function of Pressure.

Pressure (kPa)		Drop Diameter (microns)	Drop Velocity (m/s)	Drops Quality	Jet Length (mm)
14	Mean	175	2.77	2	1.03
	Std. Deviation	15.00	.35	.00	.64
28	Mean	179	4.43	2.	2.09
	Std. Deviation	20.12	.15	.00	.47
41	Mean	187	5.67	2	1.67
	Std. Deviation	22.63	.96	.00	.43
55	Mean	152	6.48	2	2.36
	Std. Deviation	20.26	.64	.00	.77
69	Mean	177	4.76	2	1.68
	Std. Deviation	43.39	2.49	.00	.59

From these initial studies on water and isopropanol, it is evident that the pressure used for ejecting the fluid is the most sensitive variable and has significant effect on all three output parameters (Figure 5.22). Consequently, in all subsequent experiments the frequency and master pulse width were held constant at 100 Hz and 6 ms respectively. Pressure was then adjusted according to the properties of the fluid to be dispensed by the IJP system.

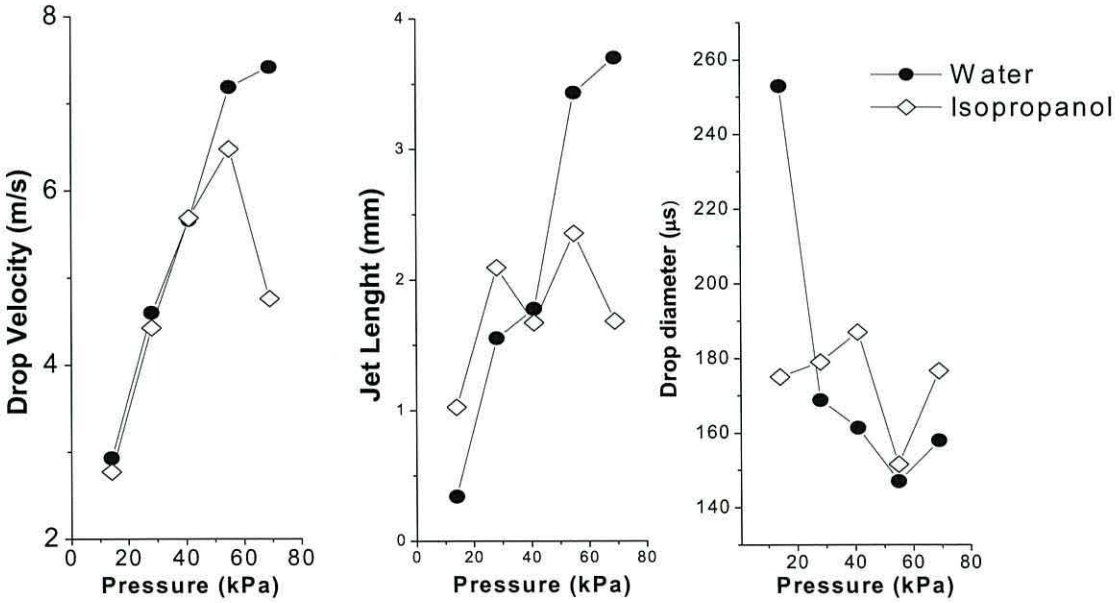

Figure 5.22 Effect of the pressure at which the calibration fluids were pumped on (a) drop velocity; (b) jet length and (c) droplet diameter.

5.4.2 Dispensing of reactive fluids for polyurethane formation

A series of polyol mixtures was prepared in isopropanol as a solvent and the capability of the IJP system for dispensing them as droplets was explored. Also prepolymer (oligomeric polyurethanes) solutions in tetrahydrofurane (THF) were also prepared and similarly tested. The prepolymer was synthesised so that the polymer chains were isocyanate end-terminated (20.6 % excess of NCO used in its synthesis). The viscoelasticity (elastic G' and viscous modulus, G") as a function of frequency (time) of these materials were examined and the data obtained is illustrated in Figure 5.23. The loss modulus G'' is smaller than that corresponding to the storage modulus G', indicative of an fluid with no viscoelastic behaviour.

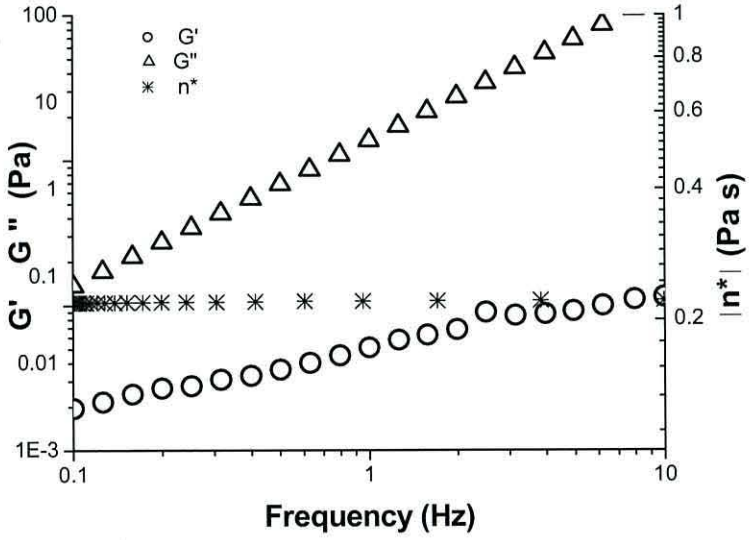

Figure 5.23 Dynamic measurement of the elastic modulus G' and the viscous modulus G" for the prepolymer with a 20.6% NCO content.

The decrease in the viscosity of the prepolymer with increasing shear rate (Figure 5.24) indicates a shear-thinning behaviour. Such a property should benefit the printing of prepolymer solutions since it increases the possibility of being able to dispense highly concentrated solutions.

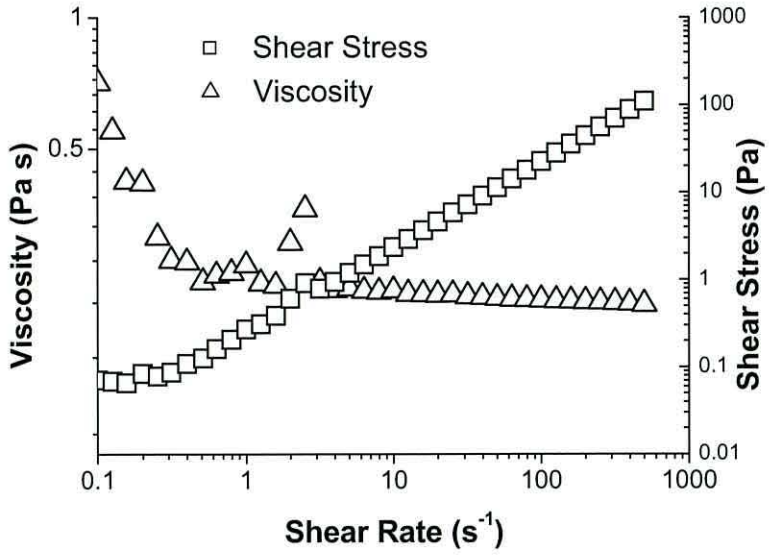

Figure 5.24 Static measurement of viscosity and shear stress for prepolymer with a 20.6 %NCO content.

Although 13 different concentrations of both the prepolymer (P-series) and polyol mixture (Mix series) were evaluated, only 6 solutions from each series were dispensed successfully (see Table 5.14).

Table 5.14 Reactive liquids successfully dispensed by the IJP system. Master Pulse Width was kept constant at 6 ms; frequency was kept constant at 100 Hz; high-voltage was held constant at -5 kV in the data illustrated.

Reactive Component	Sample	Pressure applied for dispensing (kPa)	Drop Diameter (microns)	Drop Velocity (m/s)
Prepolymer with 20.6 %NCO excess (% w/w)	P4 (26.80)	21	200	3.00
	P7 (43.12)	35	250	5.52
	P8 (44.84)	12	174	3.36
	P9 (50.32)	21	172	3.42
	P11 (70.07)	21	177	2.59
	P12 (80.25)	35	190	2.50
Polyol 1000g/mol + 1,4 butanediol + Ti-based catalyst (% w/w)	MIX5 (30.09)	21	230	3.22
	MIX6 (35.00)	28	225	1.86
	MIX7 (40.05)	35	250	2.58
	MIX9 (45.07)	41	263	2.92
	MIX10 (50.04)	41	225	1.36
	MIX11 (59.91)	41	228	1.44

To achieve successful droplet formation it was essential to apply a minimum voltage of -5 kV to the substrate. The electrostatic forces within the jet aid the jet breakup by helping to overcome surface tension. The applied voltage also ensures that the charged droplet is attracted to the substrate. It was observed that once that a stream of level-3-quality droplets started to emerged from the nozzle, the high-voltage could be turned off. A possible explanation is that, once the surface tension has been overcome, the inertial forces from the stream of falling droplets govern the movement of the falling droplets.

From the experimental data, it was found that the maximum concentration at which the functional liquids formed level-3-quality droplets was 70% w/w for the prepolymer solution (P12) and 60% w/w for the polyol mixture (M11). Occasionally, it proved possible to dispense an 80% w/w prepolymer solution with a few level-3-quality droplets but not reproducibly and satellite droplets were also observed.

These findings lend support to the initial assumption that because of the shear thinning a high concentration of prepolymer solution could be dispensed even though the dynamic viscosity of the prepolymer was high (~ 230 mPa.s). That such high concentrations of both the prepolymer and polyol could be dispensed by the new IJP system is a significant achievement.

These encouraging findings suggest that further improvement and refinement of the technique could lead to future developments of reactively processed 3D polyurethane structures using IJP micro devices similar to the layered structures using polyurethane colloidal suspensions (Berg et al. (2007). The significant additional feature of the present work over that of Berg et al. is the fact that the properties of the polyurethane materials fabricated can be more readily tailored through control of the reactant stoichiometries and chemical composition and therefore the final product properties.

Having determined the maximum concentrations of prepolymer and polyol solutions that could be microdispensed, attempts were then made to react one droplet of each solution (70& w/w, 60% w/w polyol mixture) by simultaneous ejection from adjacent jets. Both streams were triggered using the same electrical signal.

At the high concentrations used, the prepolymer droplet was ~30% smaller in diameter than the polyol droplet. As seen earlier, the velocity of smaller droplets tends to be higher. In this experiment, the prepolymer droplet velocity at 2.59 m/s was almost

twice that of the polyol droplet (Table 5.14). This difference in velocity meant that the two droplets arrived at different times at the intersection of their trajectories (Figure 5.25), which was located 3 mm downstream for each nozzle.

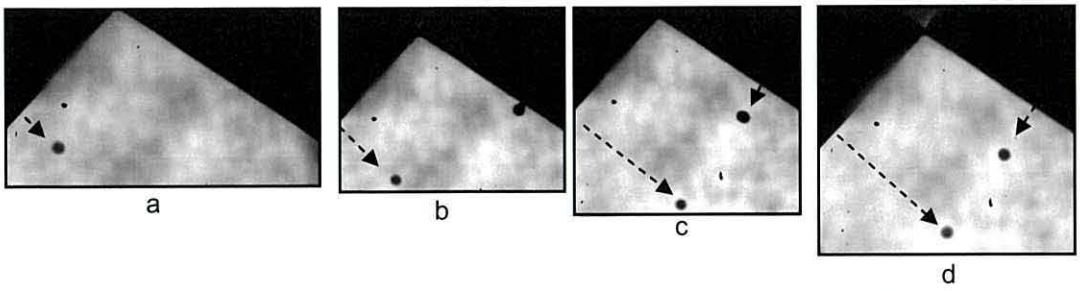

Figure 5.25 70% Prepolymer P11 droplet (left) and 60% polyol MIX11 droplet (right) triggered simultaneously with the purpose of making them collide in mid-air. (a) The prepolymer droplet is the first to appear; (b) after 545 μs the polyol droplet becomes visible; (c) both drops fly at different velocities; (d) the minimum gap between drops is 1.3 mm. Pothographs by Yara Almanza.

Once the stream of droplets was initiated, the high voltage was turned off before the high-speed camera was turned on. This was a precautionary measure since the focal length of the camera lens was only 1 cm, making it vulnerable to spark-over from the high-voltage plate. This is the reason why the droplet trajectories are not vertically downwards as would be expected in the presence of a voltage.

In the images in Figure 5.25, it appears that the droplets emerge at different times, even though they are triggered simultaneously. This apparent difference is because the nozzle aperture is set back in the body of the solenoid valve (Figure 5.13) so that the droplets are already well in flight before they emerge into the field view.

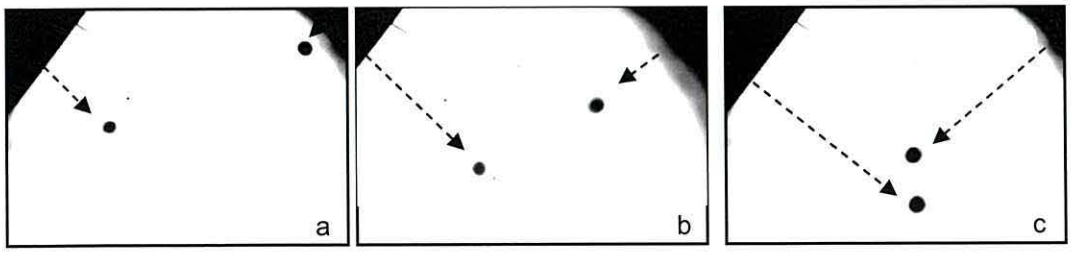

Figure 5.26. 27% Prepolymer P4 droplet and 30% polyol MIX5 droplet triggered simultaneously. a) The prepolymer droplets is the first to appear; b) with a delay of 363 μs the polyol droplet becomes visible; c) the gap between drops is 210 μm. Photographs by Yara Almanza.

Since phased triggered of the two droplets streams would have required new electronic circuitry to be built, an attempt at improving the probability of collision was made by choosing solutions of lower concentration. For example, the P4 and MIX5 solutions gave droplets of almost the same size (prepolymer 200 μm; polyol mixture 230 μm). However, the velocity of the polyol droplet was now higher (3.22 m/s vs 3.00 m/s), and by manually adjusting the angles of the nozzles the distance of closest-approach achieved was reduced from 1.33 to 0.21 mm.

With a similar set-up and simultaneous triggering, Chen (2007) was able to achieve the collision of two droplets. However, Chen employed fluids with similar rheological properties, unlike the situation here. The effects of viscosity and non-Newtonian behaviour of the prepolymer are important and are likely to be the origin of the final lag between the emergence of the two different droplets.

By incorporating additional electronic circuitry, staggered firing of the solenoids should ensure droplet collision. The required time delay is readily estimated from the velocity data in Table 5.14 and images such as those in Figures 5.25 and 5.26. In these cases, the prepolymer emerges first and travels at a different velocity. Therefore, the delay, t_D, between triggering the polyol and prepolymer solenoids will be given by:

$$t_D = \Delta t + \left(\frac{1}{v_2} - \frac{1}{v_1} \right) \cdot d \qquad \textbf{(5.5)}$$

where Δt is the observed time lag between the emergence of the prepolymer and polyol with simultaneously triggering, d is the distance downstream from the nozzle at which the collision is to occur (assumed identical and equal to 3 mm in the present case) and v_1 and v_2 are the velocities of the prepolymer and polyol droplets respectively.

For the highest concentration solutions Δt = 545 μs, v_1=2.59 m/s and v_2 = 1.44 m/s so that t_D = 1.47 ms. For the more dilute solution used in Figure 5.26, the corresponding values are Δt= 363 μs, v_1 = 3.00 m/s and v_2 = 3.22 m/s, so that now t_D = 295 μs.

Probably, the most important limitation inherent in the present system is the fact that the collision of the reactive droplets occurred in an open environment. Even in a clean room environment there is a controlled amount of humidity, so the possibility of interaction (i.e. reaction) between room-moisture and the reactive droplets is possible.

This is not good for the synthesis of high quality polyurethanes as discussed in Chapter 3. This is confirmed by the fact that, after the IJP experiments, even though all the parts in contact with the reactive materials had been cleaned and flushed with solvents, some days later the presence of solidified material blocked the whole system. Eventually, the Teflon tubing and the solenoid valves were replaced since it proved impossible to remove the polymer formed in them.

A further limitation is the need to use solvents such as THF and isopropanol for achieving good droplet dispensing. This presence could affect the development of the reaction. In particular, the use of isopropanol that contains a secondary OH group could react and endcap the NCO groups in the prepolymer, leading to a stoichiometric imbalance, as discussed in the following section.

5.4.3 Effect of the presence of isopropanol in polyurethane synthesis

Isopropanol was used to dilute the polyol mixture and to aid the electrostatic system. It was employed on the basis that it would act only as a solvent. It is recognised in this study that since there is one hydroxyl group in the isopropanol molecule there is a small possibility that this functional group could participate in the reactive process. Hence GPC was employed to determine the molecular weight of polyurethanes formed from the solutions containing isopropanol. Again, the synthesis of these polyurethanes was carried out by reacting a droplet of prepolymer (20.6 % NCO) with a droplet of polyol mixture in isopropanol so as to simulate the IJP process. The results obtained are shown in Table 5.15. Since the molecular weight distribution of the polymers formed was trimodal (as in Chapter 3), comparison is based on the mean molecular weight of the heaviest peak in the distribution. (This is valid since the relative areas of the 3 peaks remain constant for all mixtures).

Table 5.15 Weight average molecular weight M_w of the PU synthesised from different polyol-isopropanol solutions.

Polyol Mixture (%w/w) in isopropanol	**M_w (PS-referred)**
0	555
40	5396
60	5929
80	6778
100	7698

The results show a trend to decreasing M_w. However, in the absence of solvent and for two identical size droplets the ratio of NCO to OH groups should be 1:1. However, when isopropanol is added, while retaining the same droplet volume, the concentration of OH groups associated with the primary alcohol (polyol) decreases. Consequently, the ratio of NCO groups to the primary alcohol OH groups will increase with increasing dilution, as shown in Table 5.16. Interestingly, in view of the large difference in molecular weight between isopropanol (60 g/mol) and the primary alcohol (1000 g/mol) the concentration of OH from the secondary alcohol (0.33 mol fraction) is significantly in excess of NCO (0.08 mol fraction) even in the 80% polyol mixture. This confirms that in these experiments isopropanol is ineffective in endcapping the prepolymer.

Table 5.16 Calculated ratios of NCO groups to OH polyol groups at different dilutions in isopropanol.

Polyol Mixture (%w/w) in isopropanol	NCO/OH ratio
40	2.58
60	1.5
80	1.13
100	0.9

An extreme scenario was analysed, where stoichiometric quantities of dried isopropanol and the prepolymer were manually mixed and studied using FTIR spectroscopy immediately after the reactive mixture was prepared. The bands listed in Table 3.15 in Chapter 3 (page 89) are characteristic of the present reactive system and only the band at 2250 cm^{-1} (i.e. NCO band) was selected to facilitate identification of changes in the reactive mixture. Following the same procedure as in section 3.4.3, the decrease of NCO concentration with polymerisation time was calculated by assuming that the area under the selected peak was proportional to the NCO concentration in the reacting mixture. The results in Figure 5.27 showed that the half-life of the NCO groups reacting with isopropanol is approximately 7200 s, which is about 9 times slower than the reaction for the primary alcohol (i.e. polyol $t_{1/2}$~800 s).

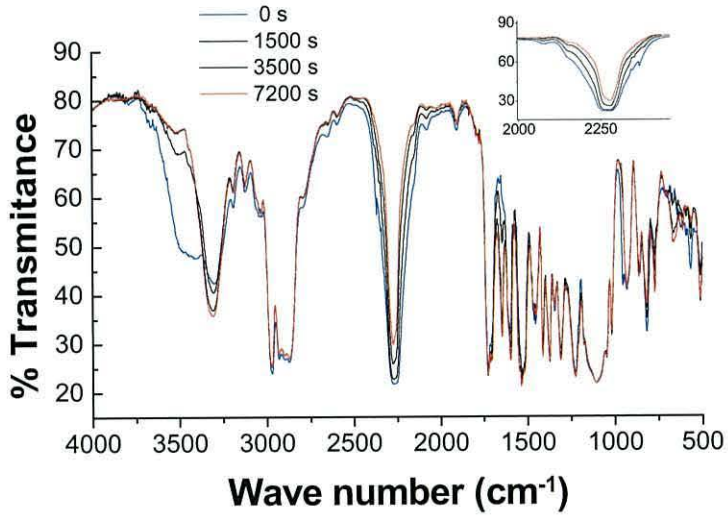

Figure 5.27 FTIR spectra of the reacting mixture of isopropanol and prepolymer. The decrease of 50% of NCO groups was achieved in ~7200 s.

From Figure 5.27 it is concluded that stoichiometric mixtures of isopropanol and prepolymer do react, albeit slowly as evidenced by the decrease in the NCO group (~ 2250 cm^{-1}). It is suggested that the reaction is slow enough to allow the evaporation of the solvent before the isopropanol endcaps the NCO groups. The GPC analysis of the mixture after 3 days showed that the molecular weight of the material formed is only slightly higher than that of the prepolymer (Figure 5.28) consistent with endcapping of the NCO groups by isopropanol.

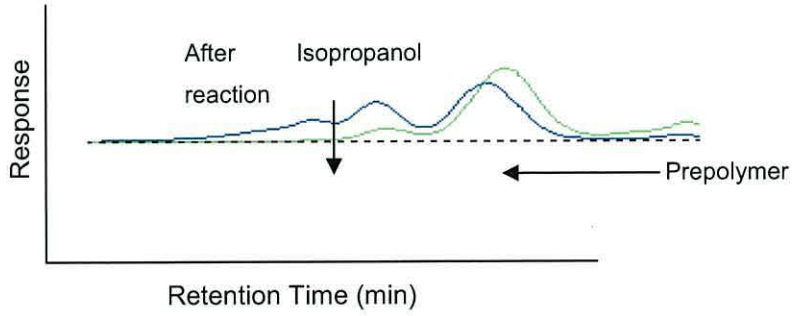

Figure 5.28 Overlay of chromatograms from the prepolymer and the material formed after the reaction of the prepolymer and isopropanol.

In summary, although the presence of primary and secondary alcohols leads to competing reactions, the reaction with the primary alcohol dominates.

5.5 Conclusions

A modified IJP-type micro-dispensing system based on solenoid valves was designed and built. A series of polyol mixture solutions in isopropanol was prepared. These contained 78.91 % w/w of PPG (MW= 1000 g/mol), 21.09 % w/w of 1,4 butanediol as a chain extender and 0.03% w/polyol w of a Ti-based catalyst. Also prepared was a series of shear-thinning isocyanate end-terminated prepolymer solutions (20.6 % excess of NCO). Experiments were undertaken to determine the conditions, if any, under which these fluids could be dispensed with the new system.

Exploratory studies with the in-house-built IJP system confirmed that the incorporation of the high-voltage mechanism was effective for preventing fluid from adhering to the outside part of the nozzle so that good droplet formation and ejection was achieved. It was possible to direct the formed droplets to the substrate with only 5 kV applied to the collection plate.

The maximum concentrations at which the functionalised liquids could be dispensed through the nozzle to form level-3-quality droplets were 70% w/w for the prepolymer solution (P12) and 60% w/w for the polyol mixture (MIX11). These were encouraging findings so attempts were then made at the microscale synthesis of polyurethanes by directing two droplet streams (70% w/w prepolymer and 60% w/w polyol) on a collision path. Under simultaneous triggering the polyol droplet was some

30% larger than the prepolymer droplet. It also had a smaller velocity and its emergence from the nozzle was delayed, so that droplet collision was not achieved. Changing to more dilute solutions reduced the distance of nearest approach to ~200 μm. These results suggest that further experiments in the IJP system are warranted, in particular, the introduction of a controlled time delay between the triggering of the individual solenoids, to counter the delayed emergence of the droplet and the differences in velocity.

In an attempt to understand the chemical reactions that are likely to occur when successful droplet collision is achieved, a supplementary set of experiments were undertaken, similar to those presented and discussed in Chapter 3. In these experiments the molecular weight was determined of polyurethanes formed by the reaction between two droplets, and was achieved by adding one drop of prepolymer to one drop of polyol solution in isopropanol. The resulting polymers were analysed by GPC, and the results suggested an 'isopropanol effect', because the molecular weight of the resulting polymer decreased with increasing isopropanol concentration. However, the reduction was not large and was attributed to the increasing mole fraction of the prepolymer. A further experiment was conducted by mixing stoichiometric quantities of prepolymer and isopropanol without any polyol. The results showed that the molecular weight of the product formed was slightly higher than that of the polyol. FTIR results showed that there is a reduction in the amount of free NCO groups, but the rate of this is so low that evaporation of the isopropanol is likely to have occured before it could endcap the NCO groups. Evidently, in the presence of the primary alcohol, reaction with the isopropanol is not particularly competitive, so that the isopropanol can be regarded simply as a solvent in the IJP experiments.

In summary, this chapter described a novel approach to downscaling the synthesis of polyurethanes using IJP technology. The technique was tested and evidence obtained that the technique could be successful once additional improvements had been made to the experimental setup. These include modifying the electrical system to achieve proper synchronisation in the dispensing of the reactive droplets. Also, it is necessary to operate under low humidity conditions to avoid stoichiometric imbalances which could also lead to the formation of polyureas that can potentially cause clogging of the IJP system. This study has taken a preliminary step towards understanding the basic requirements for the intensification of polyurethane synthesis.

Chapter 6. Conclusions

Process Intensification is a concept based on the design and creation of new techniques to reduce the size of a process by reconsidering the basis of such processes. This concept has already been applied in polymerisation reaction engineering, especially in the reaction injection moulding of polyurethanes. This efficient technique has led to the development of high added-value products.

This thesis reports the study undertaken to assess the feasibility of taking a further step, and move from the current RIM technology to the microscale to fabricate PU-based microdevices. This interest is driven by the fact that the progress and innovation achieved in the polyurethane field has already led to the development of smart multi-layered micro-sensors composed of functionalized polyurethane (PU) layers.

Ink Jet Printing (IJP) technology is a micro fabrication technique that has been employed for the construction of microdevices. The literature survey showed that there are several cases in which IJP has been employed to print functionalised materials, though the present research is the first one to study the application of IJP for the *in-situ* synthesis of polyurethanes. Therefore, within the concept of Process Intensification, there was strong justification for undertaking research to explore the feasibility of miniaturising the synthesis of PU using IJP technology.

In this study, the traditional polyurethane chemistry was characterised using state-of-the-art analytical instruments, which included DSC, DMA, GPC, FTIR and Raman techniques. The purpose of this part of the study was to understand the relevance of both the product formulation and the process conditions on the microstructure of the final PU -achieving the desired properties relies on it. As a first stage, conventional uncatalysed batch processes were characterised by GPC. It was learnt that a change in formulation of NCO:poly(1,4 butanediol) 2000: BDO ratio from 2:1:1 to 5:1:4 had an important impact on the reaction time which decreased from 24 hrs down to 4 hours respectively. The molecular weight M_w (PS reference) of the PU obtained in this system was around 9000. Also, an on-line monitoring system developed by Polymer Laboratories was employed to monitor the polymerisation in

real time. The change in properties of the reacting mixture including light scattering, refractive index and viscosity was monitored on-line for 3 hours.

The effect of stoichiometry imbalance on the polymerisation process was studied by DSC. It was found that formulations with ratios NCO:OH < 1 had a higher ΔH value, that suggests a higher molecular weight polymer is formed. Also, DSC results indicated that formulations with ratios NCO:OH ≥ 1 showed two reaction exotherms, where the second one was possibly due to an exothermic crystallisation process. Moreover, it was found that in this range, as the NCO:OH content increased, the onset temperature decreased yielding a faster reaction. GPC results indicated that it is desirable that the initial formulation should contain equimolar quantities, that is a ratio of 1:1 NCO:OH in order to achieve the highest molecular weight. Furthermore, any stoichiometry imbalances should be avoided, including that caused by reaction with atmospheric moisture, since it would lead to lower molecular weight in the final product.

From these results a prepolymer containing 8 moles of MDI and 1 mol of PPG 2000 was designed to be employed in the RIM experiments. This prepolymer contained 14.7% NCO and was employed to form a series of PU castings, by reacting it with different mixtures containing PPG 1000 and BDO as chain extender. Results of DMA analysis demonstrated that the higher concentration of the BDO employed in the castings formulation, the higher the glass transition temperature Tg and the lower molecular weight of the polyurethane obtained. Therefore it was concluded that the formulation to be employed in the RIM experiments was 6:1:5 of MDI:PPG 1000:BDO.

If the miniaturisation of PU synthesis is to succeed, then two essential factors will determine the reaction rate: the mixing and the reaction kinetics. On the one hand a fast reaction is needed. Therefore, the reaction kinetics of conventional formulations was studied by DSC and the data computed using the Kissinger method. The polymerisation followed a second order reaction model, showing that the reaction of high hard-block content was faster than that of the low hard-block content. The half-life was in the range of 13 to 3 min for temperatures between 30 and 50 °C, which can be considered a slow reaction for IJP processes. So it was concluded that a catalyst was needed in the initial formulation to speed up the reaction. These experiments also showed that poor mixing (i.e. hand-mixing) led to slower reactions and lower

molecular weight PUs. Similarly, DSC was employed to study four new alternative catalysts: two were zirconium-based and two titanium-based. The concentrations tested were between 0.05 and 0.196 %w. It was found that the higher the concentration of the catalysts employed, the lower the activation energy E_a of the polymerisation and therefore the faster the reaction. While the zirconium-based catalyst Zr1 showed the best performance, it was concluded that the most suitable catalyst to be employed for IJP experiments was the Ti1 due to its compatibility with the polyol mixture.

The traditional batch reactor system was compared with the RIM process. This showed that the molecular weight of the final polyurethane obtained using the RIM process was approximately twice that obtained from the batch process. While the hand-made castings yielded a PU with a M_w of around 9,500, the castings made by the RIM machine gave a molecular weight of around 20,000. It was observed that the production of higher molecular weight PU was achieved when accurate stoichiometric quantities were dispensed and when the mixing was efficient. The polymerisation process in RIM achieves homogeneous mixing within seconds due to the impingement mixing which makes the reaction kinetic driven and independent of the diffusion of reactants. Once in the mould, the final stage of the process is diffusion driven due to the high viscosity of the reacting mixture. Then, better properties may be achieved in the RIM process. RIM experiments allowed the identification of similarities between RIM and IJP processes. Both systems have the same principle of pumping two streams into a space where impingement and chaotic mixing takes place. Also both systems present similar issues: the need for accurate control of the temperature and dispensing of the reactants, to avoid contact with environmental moisture and the potential risk of blockage in the prepolymer lines.

Based on the kinetic data obtained, a simulation of the reaction between two droplets ~100μm in diameter was undertaken which showed that at such small scale, 50% conversion should be achieved in the first 2 s and 98% conversion in approximately 60 s. On the other hand, the mixing of the two droplets on the IJP scale, should be as efficient as it is in the RIM process. This may be due to the fact that striation thickness on that scale is sufficiently small to allow molecular mixing. Furthermore, the nature of the reacting droplets would enhance Brownian movement, would create hydrogen bonding and of course, the difference in chemical potential and

the reaction of polymerisation will drive the mixing inside the printed drops (acting as a surface free micro batch reactor).

By monitoring a reaction between two droplets by following the changes in FTIR absorption bands at ~2270 cm^{-1} and Raman Shifts at 1650 cm^{-1}, it was found that the half-life was 30 to 40 min. It was concluded that in the interface where the two reactants meet, molecular mixing occurred and instantaneous reaction took place yielding a PU film. In this site, the reaction was kinetic driven. After some time, the formed PU film acted as a barrier and slowed down the reaction. At this second stage of the process the reaction became diffusion driven. The same phenomena have been observed to occur in the RIM process, although in this process the PU film at the interface is mechanically ruptured by the impingement mixing.

On this basis, synthesis of PUs by using a conventional piezoelectric IJP system was attempted following a similar methodology to the one used by Danzebrink and Aagert (1999). In the present study, the experimental procedure involved the dilution of the mixture of polyol PPG 1000, 1,4 - butanediol and 0.1% of catalyst in anhydrous 2-propanol to reduce the viscosity. The main strategies tested were designed to place a 5 μm thick layer of pre-polymer on a glass surface and subsequent printing of 30% w polyol solution by a Microdrop IJP system with a nozzle diameter of 50 μm in a dust-free environment. However it was demonstrated experimentally that this was not a feasible methodology. Also, the nature of the 24 functionalised solutions tested was such that the available piezoelectric IJP system could not be used for dispensing them. In order to achieve the miniaturisation of PU synthesis by using IJP technology it is required to match physical and chemical properties of the reactants, which is a very challenging task.

It was demonstrated that the IJP systems available commercially, analogous to the one employed by other authors (Setti et al., 2005; Boland et al., 2007; Xu et al., 2006) were not suitable for use in the current research. This is due to the use of cartridges that are not chemically resistant and because they usually work with a thermal printing mechanism that can potentially modify the nature of the reactants. The advantages of a pre-designed printing head include the accuracy and reproducibility of the droplets formed. However the limitation is that only very low viscosity liquids can be dispensed. For that reason, the possibility of fabricating a stainless steel nozzle was

explored. However, the laser micromachining of apertures in stainless steel sheet gave poor quality nozzles.

On this basis, it was concluded that new equipment had to be built and tested. Therefore, a modified IJP system, based around solenoid valves and the application of an electric field, was designed and built. The novelty of the approach taken in this second attempt to miniaturise the PU synthesis sought to make two droplets collide in mid-air. Each droplet contained the necessary reactants for the reaction i.e. one droplet containing –NCO groups while the second contained –OH groups. Exploratory studies with the in-house-built IJP system confirmed that the incorporation of the high-voltage mechanism effectively prevented the fluid from adhering to the outside part of the nozzle and ejection of droplets was achieved. It was possible to direct the formed droplets to the substrate with only 5 kV applied to the collection plate.

A series of polyol mixture solutions in isopropanol were prepared, these contained 78.91 % w/w of PPG (MW= 1000 g/mol), 21.09 % w/w of 1,4 butanediol as a chain extender and 0.03% w/polyol w of a Ti-based catalyst. Also prepared was a series of shear-thinning isocyanate end-terminated prepolymer solutions (20.6 % excess of NCO). The conditions, under which these fluids could be dispensed, if any, were determined experimentally. The maximum concentrations for which the functionalised liquids could be passed through the nozzle to form level-3-quality droplets were found to be 70% w/w for the prepolymer solution and 60% w/w for the polyol mixture. Under simultaneous triggering the polyol droplet was some 30% larger than the polymer droplet. Although it also had a larger velocity its emergence from the nozzle was delayed, so that droplet collision was not achieved. The distance between the droplets was ~200 μm. These findings suggest that if further experiments are undertaken, including the introduction of a controlled time delay between the triggering of each individual solenoid valves in order to counter the delayed emergence of the droplet, a collision is warranted.

In an attempt to hypothesize the chemical reactions that are likely to occur if droplet collision is achieved, the molecular weight of polyurethanes formed by the reaction between two droplets, one drop of prepolymer to one drop of polyol solution in isopropanol, using a micropipette was determined by GPC.

The results suggested an 'isopropanol effect', a stoichiometric imbalance shown by the decrease in molecular weight of the resulting polymer with increasing

isopropanol concentration. However, the reduction was not large and was attributed to the increasing mole fraction of the prepolymer. FTIR results showed that there is a reduction in the amount of free NCO groups, but the rate of this is so low that evaporation of the isopropanol is likely to have occurred before it could endcap the NCO groups. Evidently, in the presence of the primary alcohol, reaction with the isopropanol is not particularly competitive, so that the isopropanol can be regarded simply as a solvent in the IJP experiments.

From these findings, it is concluded that at this stage of the study it was not possible to adapt a specific formulation suitable for IJP process since it was not possible to dispense the viscous reactive components and the use of a solvent was necessary. However, the formulations explored can be used in the future as an outline in the design of new PU formulations suitable for IJP studies.

Nevertheless, this study represents significant progress in the process intensification of PU synthesis. With relative little further work the collision and reaction of two functionalised droplets should be achieved as discussed in the following section.

Further work

As an immediate improvement of the present experimental set up, the adaptation of an independent electronic driving circuit for each solenoid valve is suggested. With data obtained in this research it is possible to calculate the time delay required between the triggering of the nozzles. The incorporation of the necessary electronics would allow the impact of two colliding droplets to be studied so as to confirm the hypothesis that they would actually form a spherical micro-batch reactor. Subsequently, attempts could be made to build single and multiple layer PU films by these process. To achieve this goal, it would be necessary to adapt a computer controlled motorised x-y stage so as to allow the accurate positioning of the reacting drops onto the substrate.

More sophisticated developments would see the solenoid valves replaced by a stainless-steel nozzle that would allow different pumping systems to be attached to enable the processing of more viscous fluids. The pumps that could be explored include those commonly used successfully for other purposes including high-pressure syringe pumps, or even a capillary-bore rheometer (Rosand) capable of dispensing polymer melts and the reaction injection moulding lance pumps which were also capable of quantitatively dispensing viscous fluids and slurries. The major challenges would be to establish an effective design for the stainless steel nozzle that would be able to resist high pressure, be capable of heating so as to reduce the viscosity of the fluid. Also, building a mechanism to create pulses in order to control the droplet formation using continuous-flow pumping systems and the incorporation of the overall assembly would be a challenge.

In addition the implementation of a self-cleaning system should be considered in order to remove any contamination and blockages in the nozzle (e.g. the incorporation of an ultrasound system).

References

Acharya, V., Prabha, C. R. and Narayanamurthy, C. (2004) *Biomaterials,* **25,** 4555-4562.

Ahmed, A., Bonner, C. and Desai, T. A. (2002) *Journal of Controlled Release,* **81,** 291-306.

Allen, G. (1987) *Polymer Journal,* **19,** 1-10.

Aref, H. (1994) *Chaos, Sohtons & Fractals,* **4,** 745 748.

Aref, H. (2002) *Phys. Fluids,* **14,** 1315-1325.

Atkins, P. W. (1994) *Physical Chemistry,* Oxford University Press, Oxford.

Basaran, O. A. (2002) *AIChE Journal,* **48,** 1842-1847.

Bayer (2003) *Reinforced Plastics,* **47,** 7.

Becker, H. and Locascio, L. E. (2002) *Talanta,* **56,** 267-287.

Berg, A. M. J. v. d., et al. (2007) *Soft Matter,* **3,** 238 - 243.

Bhadeshia, H. K. D. H. (2002) *Materials Science & Metallurgy* University of Cambridge, Cambridge.

Billmeyer, F. (1984) *Textbook of Polymer Science,* John Wiley & Sons, Inc., USA.

Bird, R. B., Stewart, W. E. and Lightfoot, E. N. (1997) *Fenomenos de Transporte,* Editorial Reverte, S.A., Mexico.

Biswal, D. and Hilt, J. Z. (2006) *Polymer,* **47,** 7355-7360.

Blanchard, A. P., Kaiser, R. J. and Hood, L. E. (1996) *Biosensors & Bioelectronics,* **11,** 687-690.

Blazdell, P. F. and Evans, J. R. G. (2000) *Journal of Materials Processing Technology,* **99,** 94 -102.

Boland, T., et al. (2007) *Materials Science and Engineering: C. Next Generation Biomaterials,* **27,** 372-376.

Boodhoo, K. V. K., Jachuck, R. J. and Ramshaw, C. (1995) *1st. International Conference on Process Intensification for the Chemical Industry*, Vol. 18 (Ed, Ramshaw, C.) BHR Group Conference Series, Antwerp, Belgium.

Brookes, A., et al. (1997) *Spectrochimica Acta Part A: Molecular and Biomolecular Spectroscopy Applications of Fourier Transform Raman Spectroscopy - VII,* **53,** 2303-2311.

Brown, M. E., et al. (2000) *Thermochimica Acta,* **355,** 125-143.

Burgess, T., et al. (2002) *European Management Journal,* **20,** 199-212.

Burns, S. E., et al. (2003) *MRS Bulletin,* **28,** 829-834.

Burt, J. P. H., et al. (2007) *Journal of Micromechanics and Microengineering,* **17,** 250-257.

Calvert, P. (2001a) *Chem. Mater.,* **13,** 3299-3305.

Calvert, P. (2001b) *Chem. Mater.,* **13,** 3299-3305.

Calvert, P., Jabbour, G. and Yoshioka, Y. (2006) Department of Materials Science and Engineeering and Optical Sciences Center, University of Arizona, Tucson AZ.

Carter, J. C., et al. (2006) *Biosensors & Bioelectronics,* **21,** 1359-1364.

Catalgil-Giz, H., et al. (2001) *Journal of Applied Polymer Science,* **82,** 2070-2077.

Chen, D., Gao, X. and Dollimore, D. (1993) *Thermochimica Acta,* **215,** 133-141.

Chen, R.-H. (2007) *Applied Thermal Engineering,* **27,** 604-610.

Cheung, K. C. and Renaud, P. (2006) *Solid-State Electronics, Papers Selected from the 35th European Solid-State Device Research Conference - ESSDERC'05,* **50,** 551-557.

Chou, W. H. and Faeth, G. M. (1998) *International Journal of Multiphase Flow,* **24,** 889-912.

Chou, W.-Y., et al. (2007) *Thin Solid Films,* **515,** 3718-3723.

Chovan, T. and Guttman, A. (2002) *Trends in Biotechnology,* **20,** 116-122.

Cooley, P., Wallace, D. and Antohe, B. (2001) *SPIE Conference on Microfluidics and BioMEMS*MicroFab Technologies.

Cowie, J. M. G. (1991) *Polymers: Chemistry and physics of modern materials,* Chapman & Hall, New York.

Danzebrink, R. and Aegert, M. A. (1999) *Thin Solid Films,* **351,** 115-118.

Dawood, I. (1994) *IRC Polymer Science and Technology,*University of Bradford, Bradford, pp. 116.

Deen, W. M. (1998) *An Analysis of Transport Phenomena,* Oxford University Press, Oxford, UK.

Derby, B. and Reis, N. (2003) *MRS Bulletin,* **28,** 815-818.

Deshmukh, S. A. R. K., et al. (2007) *Chemical Engineering Science, Fluidized Bed Applications,* **62,** 416-436.

Dimier, F., et al. (2004) *Polymer Engineering and Science,* **44,** 518-527.

Edwards, M. F. (2006) *Chemical Engineering Research and Design*

Special Issue In Honour of Professor Jack Richardson on the Occasion of his 85th Birthday, **84,** 255-260.

Elman, N. M., et al. (2008) *Biosensors and Bioelectronics,* **23,** 1631-1636.

El-Molla, M. M. (2007) *Dyes and Pigments,* **74,** 371-379.

Erkoc, E., et al. (2007) *Chemical Engineering Science,* **62,** 5276-5281.

Etchells, J. C. (2005) *Process Safety and Environmental Protection, Trans IChemE, Part B,* **83,** 85–89.

Fan, L. H., et al. (1997) *Polymer,* **38,** 3609-3616.

Ferry, A. and Jacobsson, P. (1996) *Polymer,* **37,** 737-744.

Flory, P. J. (1971) *Principles of Polymer Chemistry,* Cornell University Press Ltd, London.

Freundlich, H. (1926) *Colloid and Capillary Chemistry,* Menthuen & Co Ltd., London.

Fromm, J. E. (1984) *IBM J. Res. Develop.,* **28,** 322-333.

Fu, Y., et al. (2004) *Sensors and Actuators A: Physical,* **112,** 395-408.

Gad-el-Hak, M. (2001) *Mécanique & Industries,* **2,** 313-341.

Gans, B.-J. d., Duineveld, P. C. and Schubert, U. S. (2004) *Advanced Materials,* **16,** 203-213.

Gans, B.-J. d. and Schubert, U. S. (2003) *Macromol. Rapid Comun.,* **24,** 659-666.

Ghafar-Zadeh, E., Sawan, M. and Therriault, D. (2008) *Sensors and Actuators A: Physical,* **141,** 454-462.

Gogate, P. R. (2008) *Chemical Engineering and Processing: Process Intensification,* **47,** 515-527.

Górski, L. and Malinowska, E. (2005) *Analytica Chimica Acta,* **540,** 159-165.

Graveson, P., Branebjerg, J. and Jensen, O. S. (1993) *J. Micromech. Microeng.,* **3,** 168-182.

Grieve, R. L. (2003) SynUthane International Inc., www.sinopu.com.

Guo, R., et al. (2003) *Journal of the European Ceramic Society,* **23,** 115-122.

Guo, R., et al. (2004) *Ceramics International,* **30,** 2259-2267.

Hessel, V., Löwe, H. and Schönfeld, F. (2005) *Chemical Engineering Science,* **60,** 2470.2501.

Hilt, J. Z. and Peppas, N. A. (2005) *International Journal of Pharmaceutics,* **306,** 15-23.

Hsieh, G. W., et al. (2008) *Physica E: Low-dimensional Systems and Nanostructures,* **40,** 2406-2413.

Hsu, J.-M., Yang, D.-L. and Huang, S. K. (1999) *Journal of Polymer Research,* **6,** 67-78.

Hugo, P., Wagner, S. and Gnewikow, T. (1993) *Thermochimica Acta,* **225,** 143-151.

Hwang, S. and Meyerhoff, M. E. (2008) *Biomaterials,* **29,** 2443-2452.

Jachuck, R. J., et al. (1997) *Applied Thermal Engineering,* **17,** 861-867.

Jensen, K. F. (2001) *Chemical Engineering Science,* **56,** 293-303.

Jensen, K. F. (2003) *Microreactor Technology and Process Intensification. 226th American Chemical Society National Meeting*American Chemical Society, New York.

John, R., Neelakantan, N. R. and Subramanian, N. (1991) *Thermochimica Acta,* **179,** 281-293.

Joung, K. I., et al. (2001) *Microchemical Journal,* **68,** 115-120.

Katstra, W. E., et al. (2000) *Journal of Controlled Release,* **66,** 1-9.

Kawasea, T., et al. (2003) *Thin Solid Films,* **438 –439,** 279–287.

Keil, F. J. (2007) *Modelling of Process Intensification,* Wiley-VCH, Weinheim.

Kendagannaswamy, D. K. and Siddaramaiah (2002) *Journal of Applied Polymer Science,* **84,** 359-369.

Kenny, J. M., et al. (1995) *Thermochimica Acta,* **269/270,** 201-211.

Kip, B. J., et al. (2000) *Vibrational Spectroscopy,* **24,** 75-92.

Kissinger, H. E. (1956) *J. Res. Nat. Bur. Stand.,* **57**.

Ko, S. H., et al. (2007) *Sensors and Actuators A,* **134,** 161–168.

Kock, M. V., KVandenBussche, K. M. and Chrisman, R. W. (2007) *Micro Instrumentation for High Throughput Experimentation and Process Intensification - a Tool for PAT,* Wiley-VCH GmbH, Weinheim.

Kolodziej, P., Macosko, C. W. and Ranz, W. E. (1982) *Polymer Engineering and Science,* **22,** 388-392.

Koo, H. S., et al. (2006) *Displays,* **27,** 124-129.

Król, P. and Pilch-Pitera, B. (2001) *European Polymer Journal,* **37,** 251-266.

Król, P. and Pilch-Pitera, B. (2003a) *European Polymer Journal,* **39,** 1229-1241.

Król, P. and Pilch-Pitera, B. (2003b) *Polymer,* **44,** 5075-5101.

Lan, P. N., et al. (1996) *Biomaterials,* **17,** 2273-2280.

Le, H. P. (1998) *Journal of Imaging Science and Technology,* **42,** 49-62.

Lee, H. C. (1974) *IBM J. Res. Develop.*, 364-369.

Lee, L. J., et al. (1980) *Polymer Engineering and Science,* **20,** 868-874.

Lemmo, A. V., Rose, D. J. and Tisone, T. C. (1998) *Current Opinion in Biotechnology,* **9,** 615-617.

Liu, Z., et al. (2005) *Biomacromolecules,* **6,** 1713-1721.

Mabrook, M. F., Pearson, C. and Petty, M. C. (2005a) *Sensors & their Applications XIII,* **15,** 39-44.

Mabrook, M. F., Pearson, C. and Petty, M. C. (2005b) *Sensors and Actuators B-Chemical,* **115,** 547-551.

Mashayek, F. and Ashgriz, N. (1995) *Journal of Computational Physics,* **122,** 367-379.

Mashayek, F., et al. (2003) *International Journal of Heat and Mass Transfer,* **46,** 77-89.

McCreedy, T. (2000) *TrAC Trends in Analytical Chemistry,* **19,** 396-401.

Meier, M., et al. (2003) *Rapid Communications in Mass Spectrometry,* **17,** 2349-2353.

Mestl, G. (2000) *Journal of Molecular Catalysis A: Chemical,* **158,** 45-65.

Meyer, J.-U. (2002) *Sensors and Actuators A: Physical,* **97-98,** 1-9.

Mills, P. L., Quiram, D. J. and Ryley, J. F. (2007) *Chemical Engineering Science,* **62,** 6992 – 7010.

Mittal, K. L. (1987) In *Surface and Colloid Science in Computer Technology* Plenum Press, New York, pp. 409-427.

Moggridge, G. D. and Cussler, E. L. (2000) *Chemical Engineering Research and Design Materials Processing,* **78,** 5-11.

Mohr, W. D., Saxton, R. L. and Jepson, C. H. (1957) *Industrial and Engineering Chemistry Fundamentals,* **49,** 1855-1856.

Moreno, J., Arregui, F. J. and Matias, I. R. (2005) *Sensors & Actuators B,* **105,** 419-424.

Morris, D. J. (2004) *PhD Thesis University of Wales,* Bangor.

Moulijn, J. A., et al. (2008) *Computers & Chemical Engineering, Process Systems Engineering: Contributions on the State-of-the-Art - Selected extended Papers from ESCAPE '16/PSE 2006.,* **32,** 3-11.

Natori, A. Y., et al. (2005) *Materials Science and Engineering B,* **122,** 231–235.

Nguyen, N.-T. and Werely, S. T. (2002) *Fundamentals and Applications of Microfluidics,* Arthec House, Boston.

Nicholson, J. W. (1991) In *The Chemistry of polymers*Royal Society of Chemistry Paperbacks, Great Britain, pp. 69-71.

Nisar, A., et al. (2008) *Sensors and Actuators B: Chemical,* **130,** 917-942.

Nomura, K., et al. (2001) *Journal of Nuclear Science and Technology,* **38,** 1057-1064.

Odian, G. (1970) *Principles of Polimerization,* Mc Graw Hill Book Company, New York.

Okamoto, H., Ushijima, T. and Kitoh, O. (2004) *Chemical Engineering Journal,* **101,** 57-63.

Ou, J.-J. and Ranz, W. E. (1983) **38,** 1005-1013.

Parnell, S., Min, K. and Cakmak, M. (2003) *Polymer,* **44,** 5137-5144.

Paul, K. E., et al. (2003) *Applied Physics Letters,* **83**.

Pede, D., Serra, G. and Rossi, D. D. (1998) *Materials Science and Engineering,* **C 5,** 289-291.

Rajendran, G. P., V.Mahadevan and Srinivasan, M. (1982) *European Polymer Journal,* **18,** 953-956.

Ramanathan, L. S., Shukla, P. G. and Sivaram, S. (1998) *Pure & Appl. Chem.,* **70,** 1295-1299.

Ramshaw, C. (1983) *The Chemical Engineer***,** 13-14.

Ramshaw, C. (1995) *1st. International Conference on Process Intensification for the Chemical Industry*, Vol. 18 BHR Group Conferences Series Publications, Antwerp, Belgium.

Ramshaw, C. and Cook, S. (2006) *Chemical Engineer***,** 42-44.

Rauwendaal, C. (1991) *Mixing in Polymer Processing,* Marcel Dekker, New York.

Recalde, I. B., et al. (2005) *European Polymer Journal,* **41,** 2635-2643.

Reisch, M. (1999) *Chemical and Engineering News,* **77,** 70.

Reynolds, M. M., Frost, M. C. and Meyerhoff, M. E. (2004) *Free Radical Biology & Medicine,* **37,** 926-936.

Ridley, M. B. (1996) *Interdisciplinary Research Centre in Polymer Science and Technology* University of Bradford, Bradford, England, pp. 198.

Rodrigues, J. M. E., et al. (2005) *Thermochimica Acta,* **427,** 31-36.

Rose, D. (1999) *Drug Discovery Today,* **4,** 411–419.

Rowe, C. W., et al. (2000a) *Journal of Controlled Release,* **66,** 11-17.

Rowe, C. W., et al. (2000b) *Journal of Controlled Release,* **66,** 11-17.

Sabersky, R. H. and Acosta, A. J. (1964) *Fluid Flow: a First Course in Fluid Mechanics,* The Macmillan Company, USA.

Saliterman, S. S. (2006) *Fundamentals of BioMEMS and Medical Microdevices,* SPIE Press, Bellingham.

Saunders, J. H., Pigott, Kenneth A. (1965) MOBAY CHEMICAL CORP 3214411, United States.

Sayers, P. (2006), Vol. 2008 Cleanroom Protocols: Substrate Cleaning Method. Bangor University website, http://cleanroom.eng.bangor.ac.uk/files/Glasscleanproc.pdf, September 2008.

Schwartz, C. J. and Bahadur, S. (2007) *Wear,* **262,** 331-339.

Setti, L., et al. (2005) *Biosensors & Bioelectronics,* **20,** 2019-2026.

Shimoda, T., Morii K., Katsuyuki, Seki S., and Kiguchi H. (2003) *MRS Bulletin*, Vol. 28, pp. 821-827.

Sirringhaus, H. and Shimoda, T. (2003) *MRS Bulletin*, Vol. 28, pp. 802-806.

Socrates, G. (2001) *Infrared and Raman Characteristic Group Frequencies. Tables and Charts,* John Wiley & Sonts Ltd, England.

Stankiewicz, A. I. M., Jacob A. (2000) *Chemical Engineering Progress,* **96**.

Starink, M. J. (2003) *Thermochimica Acta,* **404,** 163-176.

Stieglitz, T. (2001) *Sensors and Actuators A: Physical,* **90,** 203-211.

Stremler, M. A., Haselton, F. R. and Aref, H. (2004) *Phil. Trans. R. Soc. Lond. A,* **362,** 1019–1036.

Tadmor, Z. and Gogos, C. G. (1979) *Principles of Polymer Processing,* Wiley-Interscince, New York.

Taguchi, G. (1986) *Introduction to Quality Engineering: Designing quality into products and processes,* Asian Productivity Organization, Hong Kong.

Tanaka, Y., et al. (2007) *Biosensors and Bioelectronics,* **23,** 449-458.

Taylor, D. M. and Secker, P. E. (1994) *Industrial Electrostatics- fundamentals and measurements,* Research Studies Press Ltd., Somerset, England.

Taylor, S. M. and Fryer, P. J. (1992) *Thermochimica Acta,* **209,** 111-125.

Tisone, T. C. (1998) United States BIO DOT INC (US) 5741554, Orange, CA, USA.

Tuominen, J., et al. (2007) Controlled Therapeutics (Scotland) Ltd., http://www.ctscotland.com/.

Viswanath, D. S., et al. (2007) *Viscosity of Liquids: Theory, Estimation, Experiment and Data,* Springer, The Netherlads.

Vo-Dinh, T., Cullum, B. M. and Stokes, D. L. (2001) *Sensors and Actuators B: Chemical,* **74,** 2-11.

Wagner, S., Hugo, P. and Gnewikow, T. (1993) *Thermochimica Acta,* **225,** 153-163.

Wei, T., et al. (2007) *Carbon,* **45,** 2712-2716.

Wickert, P. D., Ranz, W. E. and Macosko, C. W. (1987) *Polymer,* **28,** 1105-1110.

Wilhelm, C., Rivaton, A. and Gardette, J.-L. (1998) *Polymer,* **39,** 1223-1232.

Willner, I., Willner, B. and Katz, E. (2007) *Bioelectrochemistry, Bioelectrochemistry 2005, Selection of papers from the 18th International Symposium, Coimbra, Portugal, 19 - 24 June 2005,* **70,** 2-11.

Wong, D. C. Y., et al. (2004) *International Journal of Multiphase Flow,* **30,** 499–520.

Woods, G. (1990) *The ICI Polyurethanes book,* ICI Polyurethanes, The Netherlands.

Wu, H.-C., Hwang, W.-S. and Lin, H.-J. (2004) *Materials Science and Engineering A,* **373,** 268-278.

Xu, T., et al. (2006) *Biomaterials,* **27,** 3580-3588.

Xu, T., et al. (2005) *Biomaterials,* **26,** 93-99.

Xue, F., et al. (2006) *Microelectronic Engineering,* **83,** 298-302.

Yang, C.-C., et al. (2007) *Sensors and Actuators A: Physical, 25th Anniversary of Sensors and Actuators A: Physical,* **136,** 398-402.

Yang, Y. and Naarani, V. (2007) *Dyes and Pigments,* **74,** 154-160.

Yoshioka, Y. and Jabbour, G. E. (2006) *Synthetic Metals,* **156,** 779-783.

Zaugg, F. G. and Wagner, P. (2003) *MRS Bulletin*, Vol. 28, pp. 837-842.

Zhang, Y., et al. (2007) *Journal of the European Ceramic Society,* **27,** 2229-2235.

Zhao, X., et al. (2003) *Ceramics International,* **29,** 887-892.

Zia, K. M., et al. (2008) *Carbohydrate Polymers,* **74,** 149-158.

Ziaie, B., et al. (2004) *Advanced Drug Delivery Reviews, Biosensing and Drug Delivery at the Microscale,* **56,** 145-172.

Appendix I. Mass and Energy Balance for a Reaction in a Drop

AI.1 Mass Balance for reaction between two droplets

The mass balance model for a reaction between two droplets ejected from an IJP system is based on the following simplifications:

1. One prepolymer droplet of diameter d ~100 μm containing NCO functional groups is ejected from an IJP nozzle and reacts with a droplet containing the OH functional groups (polyol + chain extender) of identical size.
2. Both droplets collide with each other forming a spherical drop twice the volume of the initial ones.
3. Due to the small scale of the droplets, the striation thickness is small enough to consider perfect mixing inside the droplet.
4. The new formed drop is considered to be a batch reactor.
5. It is assumed that properties of the drop, such as density and volume remain constant throughout the process.
6. The stoichiometry of the reaction is equimolar (i.e. molar ratio = 1), so that the concentration of the NCO groups is equal to that of the OH groups.
7. The reaction follows a second order kinetic model.

The volume for each of the reactant droplets V_r is given by:

$$V_r = \frac{4}{3}\pi\left(\frac{d}{2}\right)^3 \qquad \textbf{(A.1)}$$

so that for a droplet of diameter 100 μm, $V_r = 5.24\text{x}10^{-10}$ L.

The mass balance for a batch reactor considers that there are neither input nor output streams, only that generation equals the accumulation. Accumulation is expressed by:

$$Accumulation = \frac{dN_{NCO}}{dt} \qquad \textbf{(A.2)}$$

where N_{NCO} is the number of moles of species NCO present at time t. If the amount of initial NCO is N_{NCOo} , then the progress of the reaction in terms of the fractional conversion α can be expressed by:

$$\alpha = \frac{N_{NCOo} - N_{NCO}}{N_{NCOo}} \quad . \tag{A.3}$$

Generation is expressed by:

$$Generation = r \ * V_{total} \tag{A.4}$$

where r is the reaction rate and V_{total} the total volume of the reactor.

For the second order equimolar reaction of polyurethanes, [NCO] and [OH] are the concentration of the respective functional groups at time t and defined as:

$$[NCO] = [OH] = \frac{N_{NCO}}{V_{total}} \tag{A.5}$$

where it is assumed that the total volume of the reactor remains constant. When:

$$Accumulation = Generation$$

$$\frac{d[NCO]}{dt} = -[NCO]_o \frac{d\alpha}{dt} \tag{A.6}$$

$$\frac{d\alpha}{dt} = -\frac{1}{[NCO]_o} \frac{d[NCO]}{dt} \tag{A.7}$$

where $[NCO]_o$ is the initial concentration of the diisocyanate .

For a second order reaction and for a stoichiometric ratio of 1, then the reaction rate is expressed as:

$$-\frac{d[NCO]}{dt} = k([NCO]_o(1-\alpha))^2 \quad . \qquad \textbf{(A.8)}$$

Substituting equation A.8 to A.7 then:

$$\frac{d\alpha}{dt} = \frac{k}{[NCO]_o}([NCO]_o(1-\alpha))^2 \quad . \qquad \textbf{(A.9)}$$

The reaction rate constant considered for modelling purposes was that calculated at 30 °C by DSC experiments (see section 3.4.1.2) k = 422 L/mol s.

On the basis that in a total volume V_{total}:

$$V_{total} = 2 * V_r = 2 * \left(5.2x10^{-10} L\right) = 1.0x10^{-9} L \qquad \textbf{(A.10)}$$

the initial concentration $[NCO]_o$ in the spherical batch microreactor was calculated considering that the prepolymer had a %NCO = 21.5 (i.e molecular weight of 390.7 g/mol) and a constant density ρ of approximately 1.2 g/mol:

$$[NCO]_o = \frac{\left(\rho * V_r / Mw\right)}{V_{total}} = 1.59 \frac{mol}{L} \quad . \qquad \textbf{(A.6)}$$

Employing ULEDA software, equation A.9 was resolved and the results shown in section 3.4.3.3.

AI.2. Energy Balance for reaction between two droplets

Similarly, the energy balance for a batch reactor considers that the energy accumulated in the system equals the energy transferred from the surroundings, i.e.

$$\Delta U = Q - W \tag{A.12}$$

where ΔU is the change in the internal energy, Q is the energy transferred and W the work produced. When W = 0, then

$$dU = dQ = dH \tag{A.13}$$

where dH is the change in the system's enthalpy due to heat generated by the reaction plus heat absorbed by the system given by:

$$dH = mC_p dT + \Delta H_R (rV) dt \tag{A.14}$$

where m is the mass of the droplet microreactor, C_p is the heat capacity, and ΔH_R is the heat of reaction. The heat exchange with the surroundings can be included in a general term such as:

$$dQ = h_o * A_h * (T_s - T) dt \tag{A.15}$$

where h_o is known as the total convection heat transfer coefficient, A_h the area of heat transfer and Ts the temperature of the surroundings. Finally, the energy balance for the batch reactor is:

$$h_o * A_h * (T_s - T) dt = \Delta H_R * (rV) + mC_p \frac{dT}{dt} \quad . \tag{A.16}$$

Then, at a constant volume, the reaction rate equation is expressed by:

$$r = k([NCO]_o(1-\alpha))^2 \qquad \textbf{(A.17)}$$

and the dependence of k on temperature T follows the Arrhenius equation:

$$k(T) = A_o \cdot \exp\left(\frac{-E_a}{RT}\right) \qquad \textbf{(A.18)}$$

where A_o is the Arrhenius frequency factor, E_a the activation energy, R the ideal gas constant and T the absolute temperature.

The values of the constants needed for modelling are calculated from the kinetic data obtained in section 3.4.3.3 and from typical values for PU synthesis. These constants are shown in Table A.1.

Table A.17 Values of constants employed for the modelling of energy balance in a reacting drop

Constant	Value
A_o (L/mol s)	1.89×10^{9}
A_h (m^2)	12.57×10^{-8}
$[NCO]_o$ (mol/L)	1.59
Cp (J/kg K)	2500
$-\Delta H_R$ (J/mol)	60 000
h_o (J/s m^2 K)	50
R (J/mol K)	8.314
ρ (kg/m^3)	1
T_s (°C)	20
V (L)	1.047×10^{-9}

From the set of equations A.16, A.17 and A.18, together with the mass balance equation A.6 the energy balance was solved using ULEDA software and the results are shown in section 3.4.3.3.

Appendix II. Mass and Momentum balance for fluid Transport: Navier-Stokes equations

AII.1 Mass Transport

The mass balance model for the transport of a fluid is based on the following simplifications:

8. There is no chemical reaction taking place.
9. It is assumed that the properties of the fluid, such as density and volume remain constant throughout the transport.
10. There is no generation of material.

If ∇ is defined as:

$$\nabla = \partial_1 \frac{\partial}{\partial x_1} + \partial_2 \frac{\partial}{\partial x_2} + \partial_3 \frac{\partial}{\partial x_3} \qquad \textbf{(AII.1)}$$

where ∂_i is the unit vector and x_i the variables corresponding to axes 1, 2 and 3 respectively (i.e. coordinates of position usually designed as x,y,z), then accumulation is described by the change of fluid density ρ with time i.e.

$$\frac{\partial \rho}{\partial t} = -\nabla \cdot \rho v \qquad \textbf{(AII.2)}$$

where v is the velocity vector and ρv is the mass flow vector. Hence, if the fluid is incompressible (e.g. constant density) then the mass balance is:

$$\nabla \cdot v = 0 \qquad . \qquad \textbf{(AII.7)}$$

AII.2 Linear momentum transport

Linear momentum is defined by Newton's second law:

Force = Mass x acceleration .

The balance of linear momentum is defined by:

Acceleration or Inertia = Surface forces + Body forces

which can be redefined as:

$$\rho\left(\frac{\partial v}{\partial t} + v\nabla v\right) = -\nabla p + \mu\nabla^2 v + F_{st} \qquad \textbf{(AII.4)}$$

where the left-hand side of the equation expresses the rate of change of momentum for an incompressible fluid. The terms on the right-hand side of the equation are the pressure p change, viscous forces change for a Newtonian fluid, and the body forces F_{st} acting on the fluid (i.e. surface tension and electrostatic forces), respectively.

The term expressing the change in the viscous forces comes from the change in the shear stress which is given by:

$$\nabla\tau \qquad \textbf{(AII.5)}$$

where τ is the shear stress defined by:

$$\tau = -\mu\nabla v \qquad \textbf{(AII.6)}$$

For a Newtonian fluid, e.g. with constant viscosity coefficient μ, combining equations AII.5 and AII.6:

$$\nabla\tau = \mu\nabla^2 v \qquad \textbf{(AII.7)}$$

Equations AII.3 and AII.4 are the Navier-Stokes equations commonly employed for the description of mass and momentum transport in microscale processes, such as Ink Jet Printing.

Appendix III. New IJP System: Diagrams of the Solenoid Valves and Circuitry Employed

Diagram 1 Solenoid valve specification sheet

Diagram 2 Integrated circuit for driving solenoid valves

Diagram 3 Stroboscopic light driver integrated circuits

DWG. NO.	PROPRIETARY ITEM
INKX0508800A	This document contains proprietary information and is submitted upon the express conditions that the information contained herein will not be used directly or indirectly in any way detrimental to the interests of the Lee Company, and/or in violation of regulation DAR 7-104.9 (a) (1 JULY 1974), et seq.

ALT.	DATE	BY	DESCRIPTION
A	06-03-2005	RJC	INITIAL RELEASE

ACTUAL SIZE

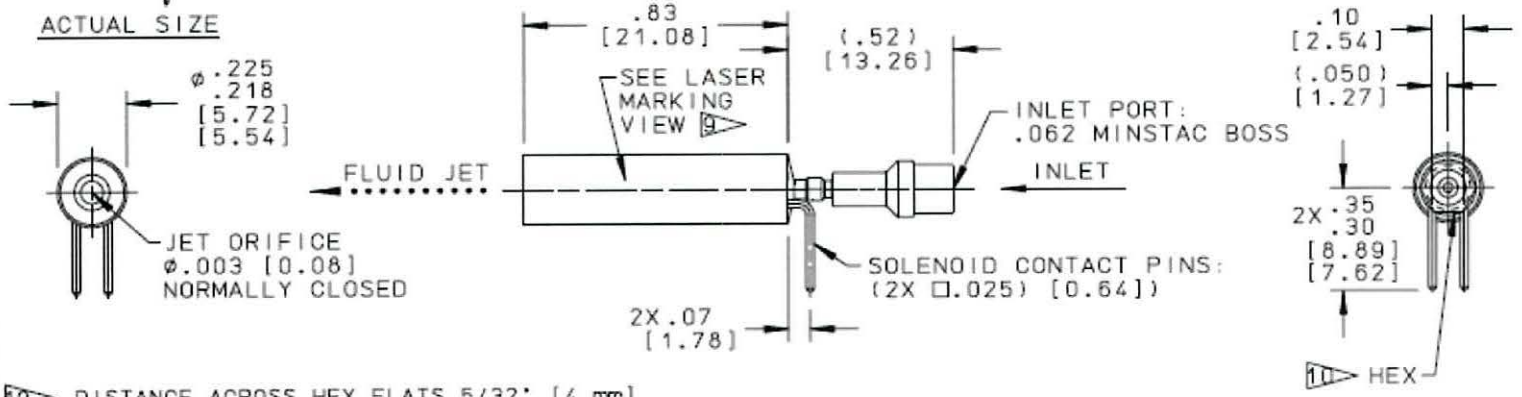

10 DISTANCE ACROSS HEX FLATS 5/32" [4 mm].
9 DIRECTION AND ORIENTATION OF LASER MARKING IS RANDOM.
8. MINSTAC FITTINGS MUST BE TIGHTENED TO 5-10 oz-in (0.035-0.07 N-m) WHILE BACKING UP THE BOSS FITTINGS ON THE VALVE. APPLICATION OF THE FITTING TORQUE TO THE VALVE BODY WILL RESULT IN DAMAGE TO THE VALVE.
7. OPERATING PRESSURE: 0-120 PSIG [0-827 kPag]
6. MAXIMUM OPERATING FREQUENCY: 1,000 Hz AT 24 VDC PULSE VOLTAGE FOR 0.35 MILLISECONDS AND 51 VOLT ZENER VOLTAGE SUPRESSION DIODE.
5. LOHM RATE: 110,000 LOHMS NOMINAL.
4. COIL RESISTANCE: 110 OHMS NOMINAL AT ROOM TEMPERATURE.
3. POWER DISSIPATION: 0.5 WATTS MAXIMUM WITH NORMAL CONVECTION AIR COOLING AND NO FLOW. ALLOWABLE POWER IS GREATER WITH FLOW.
2. ACTUATING VOLTAGE: 24 VDC PULSE. VOLTAGE PULSE DURATION SHOULD BE BETWEEN 0.35 AND 2 ms. FOR LONGER ON TIMES REDUCE THE VOLTAGE TO 5.0 VDC
1. WETTED MATERIALS: 430, 302 SS, PPS, PEEK, EPDM, SAPPHIRE & EPOXY.

NOTES:

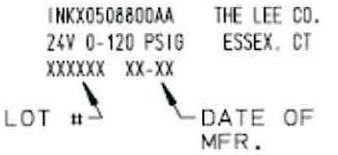

LASER MARKING VIEW

-FMF-
THE LEE CO.
ESSEX, CT

NOTES AND DIMENSIONS SHOWN HEREON ARE FOR INSPECTION IDENTIFICATION ONLY. ALL MANUFACTURING RIGHTS ARE RESERVED.

REF. NO.
INKD0508800

UNLESS OTHERWISE SPECIFIED DIMENSIONS ARE IN INCHES [mm]
TOLERANCES:
.XX ±.015 [0.38]
.XXX ±.005 [0.13]
ANGLES ±2°
INT CORNER R .01 [0.25] MAX
SURFACE FINISH 63 √
DO NOT SCALE DRAWING

THIRD ANGLE PROJECTION

DRAWN	RJC	06-03-2005
CHK'D	Digitally signed by Leslie Galczynski Reason: This copy is accurate	
APP'D	Date: 2006.08.03 14:23:55 -04'00'	
MAT.	SEE NOTE 1	
H.T.		
FINISH		

TITLE VHS-M/VJ-EPDM-ø.003-24V

THE LEE COMPANY
ESSEX, CT

SIZE	CODE IDENT. NO.	DWG. NO.	REV.
A	ONZR4	INKX0508800A	A

SCALE: 2/1 SHEET 1 OF 1

DWG. NO.
IECX0501350

PROPRIETARY ITEM
This document contains proprietary information and is submitted upon the express conditions that the information contained herein will not be used directly or indirectly in any way detrimental to the interests of the Lee Company, and/or in violation of regulation DAR 7-104.9 (a) (1 JULY 1974) et seq.

ALT.	DATE	BY	DESCRIPTION
A	02-13-2001	BFF	INITIAL RELEASE
2	05-15-2001	BFF	MODIFY DWG VIEWS
3	04-19-2002	RJC	ADDED .1 to 5 TO TITLE, & REVISED LABEL TEXT
4	05-13-2002	RJC	REVISED LABEL MARKING

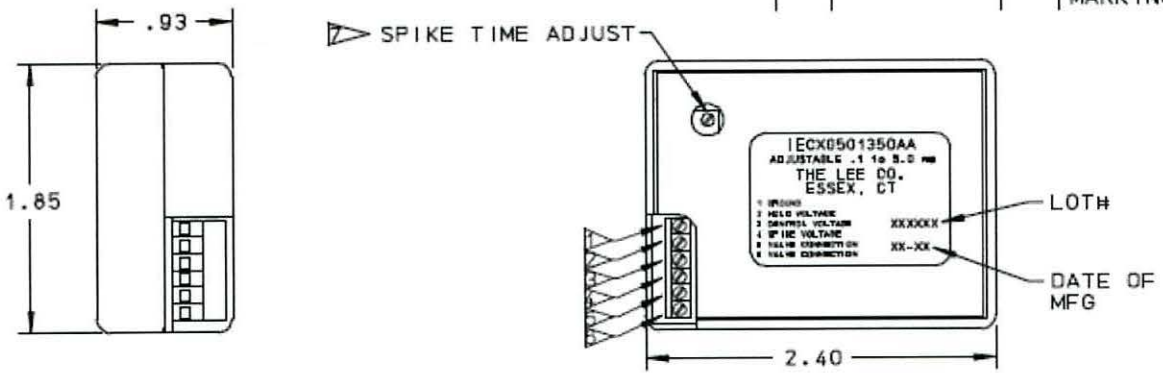

SPIKE TIME ADJUSTABLE FROM .1 ms TO 5.0 ms. (FACTORY PRESET IS .30 ms. USE OSCILLOSCOPE WITH A DIFFERENTIAL PROBE TO MEASURE THE FIRING SIGNAL. NEVER GROUND EITHER VALVE CONNECTION).
VALVE CONNECTION (POWER SIDE).
VALVE CONNECTION (OPEN COLLECTOR).
SPIKE VOLTAGE (9.5 TO 40V).
CONTROL VOLTAGE (0-5 VOLTS TTL).
HOLD VOLTAGE (MAXIMUM-SPIKE VOLTAGE).
GROUND.

NOTES:

-FMF-
THE LEE CO.
ESSEX, CT

NOTES AND DIMENSIONS SHOWN HEREON ARE FOR INSPECTION IDENTIFICATION ONLY. ALL MANUFACTURING RIGHTS ARE RESERVED.

REF. NO.
IECD0501350

UNLESS OTHERWISE SPECIFIED DIMENSIONS ARE IN INCHES [mm]
TOLERANCES
.XX ±.015 [0.38]
.XXX ±.005 [0.13]
ANGLES ±2°
INT CORNER R .01 [0.25] MAX
SURFACE FINISH 63 ✓
DO NOT SCALE DRAWING

THIRD ANGLE PROJECTION

DRAWN	BFF	02-13-2001
CHK'D		
APP'D		
MAT.		
H.T.		
FINISH		

TITLE SPIKE & HOLD DRIVER-.1 to 5 ms

THE LEE COMPANY
ESSEX, CT

SIZE	CODE IDENT. NO.	DWG. NO.	REV.
A	ONZR4	IECX0501350A	A

SCALE 1/1 SHEET 1 OF 1

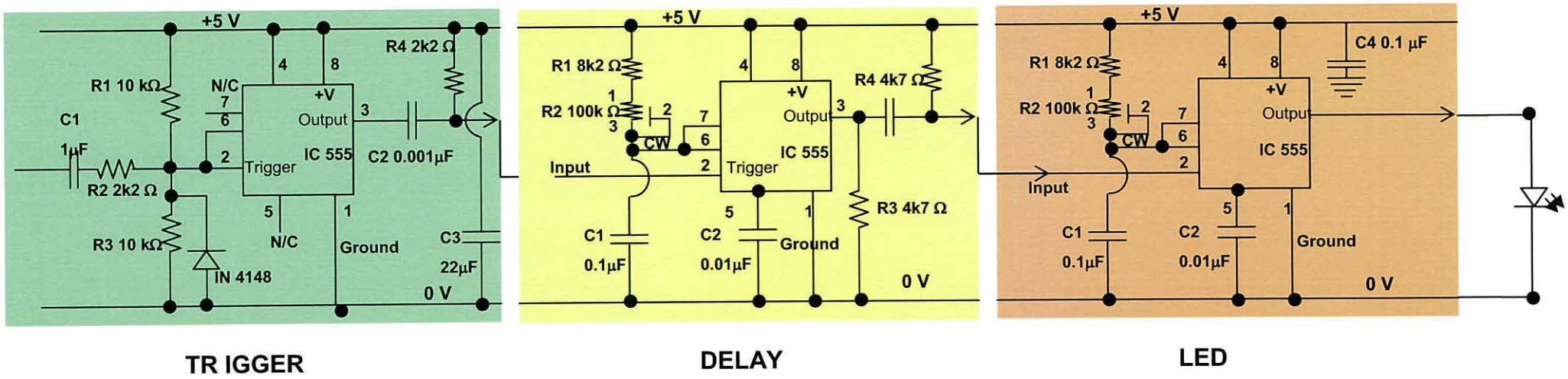

Figure AIII-1 Stroboscopic Light Driver Integrated Circuits.

Conferences and Meetings

Bangor University: "Beyond Boundaries 2008 Conference". Bangor, UK. January 2008. Oral Presentation: *Process Intensification for the Miniaturisation of Polyurethane Synthesis.* Yara Almanza, A.F Johnson and D.M. Taylor.

Royal Society of Chemistry: "The Young Scientist" Symposium. St. Asaph, UK. 27 June 2007. Oral Presentation: *Miniaturisation of Polyurethane Synthesis.* Yara Almanza, A.F Johnson and D.M. Taylor

Royal Society of Chemistry: "Ink Jet Printing of Functional Materials: Fundamental Chemistry and Materials Science". Manchester, UK. 12–14 June 2006. Oral presentation*: Microscale Synthesis of Polyurethane Polymers by Inkjet Printing: Initial Studies.* Yara Almanza, A.F Johnson and D.M. Taylor

Institution of Engineering and Technology (IET): "Younger Members' Section Papers Evening". St. Asaph, UK, January 2006. Awarded with the first prize for best oral presentation: *Ink Jet Printing of Functionalised Materials.* Yara Almanza, A.F Johnson and D.M. Taylor